PNEUMATIC VARIABLE STIFFNESS SOFT ROBOT END EFFECTORS

Loai Ali Talib Al Abeach

Autonomous Systems and Robotics Centre
School of Computing, Science & Engineering
University of Salford, Salford, UK

Submitted in Partial Fulfilment of the Requirements
of the Degree of Doctor of Philosophy
June, 2017

Publications

1- A journal paper is published in the Soft Robotics journal (current impact factor is **8.649**).

Al Abeach Loai A.T., Nefti-Meziani Samia, and Davis Steve. Soft Robotics. June 2017. Design of a variable stiffness soft dexterous gripper. Ahead of print. https://doi.org/10.1089/soro.2016.0044

2- A journal paper is submitted to the journal of Bionic Engineering.

Al Abeach, Loai A. T., Nefti-Meziani, Samia, & Davis, Steve (2017). "A Variable Stiffness Soft Gripper Using Granular Jamming". Bionic Engineering.

3- A poster in the 1st UK Manipulation Workshop, Birmingham.

Al Abeach, Loai A. T., Davis, Steven, & Nefti-Meziani, Samia. (2016). "A Computer Controlled Soft Robot Manipulator for Safe Human-Robot Interaction". 1st UK Manipulation Workshop, Birmingham.

4- A poster in the College of Science and Technology Research and Innovation Showcase 2015, University of Salford.

Al Abeach, Loai A. T., Davis, Steven, & Nefti-Meziani, Samia. (2015). "Continuum Soft Gripper". College of Science and Technology Research and Innovation Showcase 2015, University of Salford.

Contents

List of Figures

Acknowledgements

I would like to take this opportunity to extend my heartfelt thanks to those who gave me assistance and corporation in the successful completion of this thesis.

First and foremost, I wish to express my sincere thanks to my supervisor, Dr. Steven T. Davis, for his constructive feedback, guidance and the freedom given to me in research matters. Also, I would like to convey my gratitude to the director of the Autonomous Systems and Robotics Centre at the School of Computing, Science and Engineering, Prof. Samia Nefti-Meziani for her support and kindness.

During the course of my work, I had the pleasure of collaborating with many colleagues for whom I have great regard, and I wish to extend my warmest thanks to all those who have helped me with my work. I am grateful to all the technical staff for their assistance and support in fabricating the various components for the robot end effectors.

Further, I am indebted to my family members; my parents, my loving wife, Mrs H. Al-Abdulaziz, and my little angles (Hasan, Fatimah, Ali and Zainab) for their understanding and support, my brother, my sisters and siblings for their constant encouragement and their nice wishes. Finally, the financial support of the Iraqi Ministry of Higher Education and Scientific Research (as a sponsor) during the research period, is gratefully acknowledged.

Abbreviations

Abbreviation	Description
3D	Three dimensions
AMADEUS	Advanced MAnipulator for DEep Underwater Sampling
AwSA	Actuator with Stiffness Adjustable
CAD	Computer-Aided Design
cRSEA	compact Rotary Series Elastic Actuator
DC	Direct Current
DOF	Degree Of Freedom
FMA	Flexible Micro-Actuator
GND	Ground
MACCEPA	Mechanical Adjustable Compliance and Controllable Equilibrium Position Actuator
PC	Personal Computer
PID	Proportional-Integral-Derivative
PD	Proportional-Derivative
PMA	Pneumatic Muscle Actuator
PWM	Pulse Width Modulation
SEA	Series Elastic Actuator
VSA	Variable Stiffness Actuator

Abstract

Traditionally, robots have been formed from heavy rigid materials and have used stiff actuator technologies. This means they are not well suited to operation near humans due to the associated high risk of injury, should a collision occur. Additionally, rigid robots are not well suited to operation in an unstructured environment where they may come into contact with obstacles. Furthermore, traditional stiff robots can struggle to grasp delicate objects as high localised forces can damage the item being held.

The relatively new field of soft robotics is inspired by nature, particularly animals which do not have skeletons but which still have the ability to move and grasp in a skilful manner. Soft robotics seeks to replicate this ability through the use of new actuation technologies and materials.

This research presents the design of a variable stiffness, soft, three-fingered dexterous gripper. The gripper uses contractor pneumatic muscles to control the motion of soft fingers. The soft nature of the gripper means it can deform if it collides with obstacles, and because grasping forces are spread over a larger area the chance of damaging the object being held is reduced. The gripper has the ability to vary its stiffness depending upon how it is to be used, and in this regard two methods of varying the stiffness are explored. In the first method, the finger is formed from an extensor muscle which acts antagonistically against the contractor muscles. Increasing the total pressure in the system increases the stiffness of the fingers. The second approach uses granular jamming to vary the stiffness of the actual finger structure.

This thesis explores the behaviour of both extensor and contractor pneumatic muscles and develops a new simplified mathematical model of the actuator's behaviour. The two methods of stiffness variation are then assessed experimentally. A number of multi-fingered grippers are then designed and their kinematics determined before prototypes are presented. Control of the grippers was then explored, along with the ability to adjust the stiffness of the grasp.

Chapter One

1 General Introduction

1.1 Introduction

Recently, there has been increased interest in a new field of robotics systems to produce a new type of robot called a “Soft Robot”; see, for example, (Lipson H., 2014). The soft robot, as the name implies, is made from soft materials, principally to allow for the possibility of safe interaction with humans. There are, though, a range of new applications that could become possible with the use of soft robots. In contrast, rigid robots, which are currently the most popular design worldwide, are made using rigid materials like copper, aluminium and steel with inflexible joints (Kim, S., Laschi, C., & Trimmer, B., 2013). Nevertheless, rigid robots clearly have many applications and benefits. Moreover, the techniques used to design, implement, and control rigid robots are well understood.

The characteristics of rigid robots can be summarised as follows: they are rigid, strong, easily controlled, widely used in manufacturing, and move in a very precise and rapid fashion. However, due to their rigidity, this type of robot does not have the elasticity or ability to deform in order to interact with an unstructured or congested environment (Majidi C., 2014). Hence, there are certain limitations to the use of the rigid robots in new application areas such as dangerous area exploration, rescue operations and while interacting with humans. However rigid robot can be made to be safe through the use of software. Haddadin demonstrated how an industrial robot could use sensors and software to make safe human-robot interaction possible (Haddadin, S., Albu-Schäffer, A., & Hirzinger, G., 2009).

By contrast, soft robots are soft, lightweight, can safely interact with humans, have the ability to work in an unspecified environment and can be constructed using low-cost materials. According to (Lipson H., 2014), these characteristics could lead to a new range of applications within robotics where the use of stiff/rigid robots is impractical.

As a new field, there will clearly be many challenges to the design and implementation of soft robotics (Trivedi, D., et al., 2008). Many soft robot prototypes have been built around the world. Developers are being inspired by natural creatures and biological appendages in the design and implementation of soft robots (Kim, S., Laschi, C., & Trimmer, B., 2013). Indeed, some soft robot prototypes even emulate the behaviour of the animals in their operation. However, researchers have faced real challenges in controlling the performance of such robots; see (Trivedi, D., et al., 2008). The biggest control problem arises from the fact of there is no specific mathematical model to describe the exact behaviour or kinematics of soft robots; all the current, well-known control techniques do not give the required quality of performance.

Another challenge in soft robotics design and construction is the design of their end effectors (Robinson, G., Davies, J., & Jones, J., 1998). The end effector is an important part in any robot whose purpose is to achieve object grasping or processing. A soft robot's end effector may be required to be soft in order to interact safely with humans or to deform around the object it is grasping. Clearly, soft robots and their end effectors should have the ability to grasp, handle and process objects in close proximity to humans without any possibility of causing them any harm.

1.2 Aim and Objectives

The concept of continuum manipulators will be used in this research to develop a variable stiffness soft robot and soft end effectors. The use of pneumatic muscle actuators to power the suggested end effectors should lead to continuum, variable stiffness end effectors that are physically soft. Hence, these variable stiffness soft robot end effectors could be safely used around humans in an unstructured environment, in contrast to traditional rigid/stiff and large-scale robots.

The objectives of this research are:

- Investigate soft robotics, including any benefits and critical success factors.
- Design and construct a pneumatic variable stiffness soft robot manipulator and its end effectors.
- Develop computer control hardware for the proposed manipulator.
- Investigate the variable stiffness capabilities for the proposed end effectors experimentally.
- Test and analyse the designed system and compare performance with expectations from theoretical analysis.
- Identify and discuss the novel capabilities of the pneumatic variable stiffness soft robotic system.

1.3 Research Methodology

Throughout this research, many tasks have been conducted, such as the design of a pneumatic variable stiffness end effector, a granular jamming-based variable stiffness end effector, an appropriate controller, a four-fingered soft robot end effector and a variable stiffness soft robot manipulator. Additionally performance analysis and evaluation of the above prototypes has been conducted. The overall research methodology during the various stages of this research can be illustrated as follows:

1- Conduct a literature review of compliant actuators, continuum manipulators, robot end effectors and soft robotics to understand current research efforts.

2- Study the characteristics of pneumatic muscle actuators to develop a mathematical model for operation of these actuators.

3- Design and construct pneumatic variable stiffness continuum soft robot end effectors using pneumatic muscle actuators.

4- Analyse the kinematics of the new design.

5- Develop a procedure to determine the stiffness of the new actuator design.

6- Analyse the performance of the new variable stiffness pneumatic muscle continuum arm and its end effectors experimentally.

7- Analyse the behaviour of the new manipulator from a theoretical perspective and compare this with experimental results.

8- Explore different methods of achieving variable stiffness such as the use of granular materials in the development of granular jamming variable stiffness continuum actuators.

9- Design and construct a variable stiffness granular jamming variable stiffness soft robot end effector using granular jamming variable stiffness continuum actuators.

10- Use sensors (pressure, force and displacement) to allow the soft robot and end effectors to be closed loop pressure, force and position controlled.

11- Design a Proportional-Integral-Derivative (PID) controller to control the performance of either the variable stiffness continuum soft robot arm or its end effectors.

1.4 List of Contributions

- Experimental development of a mathematical model for contractor and extensor pneumatic muscle actuators.
- Analysis of the variable stiffness capabilities of pneumatic muscle actuators.
- Development of a fully compliant continuum, variable stiffness, soft robot end effector using only pneumatic muscle actuators.
- Development of an enhanced continuum variable stiffness soft robot end effector by increasing the number of fingers and reducing the number of contractor muscle actuators which are used to control finger bending.
- Development of a granular jamming variable stiffness soft robot end effector based on continuum manipulation.
- Development of a continuum pneumatic soft robot arm and its end effector using only soft materials, both of which are actuated by contractor and extensor pneumatic muscle actuators only.

1.5 Organisation of Thesis

This thesis is divided into six chapters, which are organised as follows:

The second chapter discusses safe human-robot interaction principles through the use of compliant and variable stiffness actuation strategies. This chapter will illustrate many types of actuators and discuss their compliance and suitability in the construction of soft robots capable of interacting safely with humans. This chapter specifies how the use of series elastic actuators, variable stiffness actuators and pneumatic muscles actuators can result in performance advantages over traditional actuators (electric motors and hydraulic actuators). Pneumatic muscle actuators design and implementation methods, are taken into consideration in this chapter. Pneumatic muscle actuators will be the main actuator used in this research. Hence, a literature survey of this type of actuator will be given in considerable detail in this chapter. The literature will answer the most important questions about what a pneumatic muscle actually is, how it works, how it is made and how it can be used. Furthermore, details of the mathematical models used for pneumatic muscles and the methods used to control pneumatic muscle actuators will also be introduced.

Chapter two will also give a general overview of continuum robotic manipulators. The definition and the various classifications of continuum arms will also be given. Pneumatic continuum arms are defined in this chapter. The main types of pneumatic continuum arms, such as the Walker expansive and contractile continuum arms, will also be introduced. The Air-Octor continuum arm and Single latex tube continuum soft robot arm will be discussed as forms of continuum arms that use cable tendons and air pressure to control their performance. The implementation and performance evaluation of granular jamming continuum soft robot arms will also be illustrated in chapter two. The mathematical models currently used to represent the behaviour of these continuum arms will be described. The use of pneumatic continuum actuators in developing a soft gripper will also be discussed.

In addition, chapter two will give an overview of continuum and soft robot end-effectors. Whole arm grasping and multi-fingered grippers as soft robot end-effectors will be illustrated. The benefits and critical success factors when using either type will be given. Recently developed granular jamming universal grippers will also be discussed in detail in this chapter.

In chapter three, the mathematical model used for the contractor and the extensor pneumatic muscle actuators will be developed theoretically, and will then be investigated by conducting a set of experiments. These experiments will investigate the force/displacement and pressure/displacement characteristics of both types of pneumatic muscle actuator. The variable stiffness capabilities of pneumatic muscle actuators and the granular jamming continuum finger will also be determined experimentally. The experimental results thus determined will be analysed and discussed in detail.

Chapter four will give an overview of safe human-robot interaction design requirements. A complete guide to designing, implementing and controlling the pneumatic variable stiffness soft robot end-effector will be given in detail. The development will start with an analysis of basic continuum soft robot end effector prototypes. The design steps will then be illustrated using graphical and pictorial representations of the proposed pneumatic variable stiffness soft robot end-effector. This will include the design of the soft robot end effector using the SolidWorks

Computer Aided Design (CAD) software application, the construction of the driving circuit, using an Arduino microcontroller and Pulse Width Modulation (PWM) expansion boards. The kinematics of the proposed pneumatic variable stiffness soft robot end effector will be analysed mathematically. In addition, a practical demonstration of the operation and a performance evaluation of the proposed pneumatic end-effector will be undertaken to show its grasping capabilities. Another variable stiffness soft robot end effector will be built using the same framework as the previous end effector. However, it will use granular jamming materials in its construction to have the ability to change its stiffness during operation. Three granular jamming continuum fingers will be used instead of the extensor pneumatic muscle actuators (fingers) of the previous design. The same experimental settings will be used to evaluate the performance of the granular jamming variable stiffness soft robot end effector.

Chapter five will give the design, implementation and a performance evaluation for two other pneumatic variable stiffness soft robot end effectors. The first soft robot variable stiffness end effector will be a modified version of the three-fingered pneumatic variable stiffness end effector illustrated in chapter four. The second soft robot end effector proposed in this chapter (which is the fourth gripper developed during this work) will be designed as a complete soft robot with its end effector. It will have the ability to grasp an object and move it to another location by bending the continuum arm to the required position. All these prototypes will be evaluated practically to assess their capabilities in interacting safely with humans. The performance of these prototypes will be controlled using a closed-loop control strategy.

Finally, in chapter six, a conclusion to the thesis will be given. The overall contributions from this work will also be illustrated in detail in this chapter. Finally, the limitations of the current study and suggestions for future work will be given at the end of the chapter.

Chapter Two

2 Literature Review

2.1 Introduction

Most of the machines around us depend on some form of actuator to perform their required tasks. An actuator is a device used to change stored energy to mechanical motion, with the form of actuation depending on the type and function of the machine (Davis, S., et al., 2003). Research within the field of actuators is continuous, and is intended to find reliable, efficient and powerful means of actuation; recently, the development of softer and more pliant actuators has also seen increased interest.

Robots are one such type of machine, developed with the intention of making our lives easier. Actuators represent a central and important part of a robot. They are responsible

for the movement of parts of, or even the entire, robot. Through this movement of the joints and links of the robot, the tasks required of the robot are accomplished.

Nowadays, manufacturers have adopted an automated response to improving productivity, and have become increasingly dependent on robots in their production lines (Huber, M., et al., 2008). The use of robots in industry has resulted in huge improvements in terms of accuracy, efficiency, and reducing production costs. Although these robots are rigid in their structures with inflexible links, they are nevertheless useful in the performance of repetitive and dangerous tasks. However, rigid robots are not always a best choice for close interactions with humans because of their rigidity from the use of solid, stiff materials in their construction. Hence, new types of robots, as well as actuators, have recently begun to see development.

To allow safe human-robot interaction, soft robots have been developed (Pfeifer, R., Marques, H., & Iida, F., 2013). The use of soft materials in the construction of soft robotics allows these robots to interact closely with humans with a minimised possibility of inflicting physical harm (Bainbridge, W., et al., 2008). This allows for the possibility of a new range of applications for soft robots such as rescue operations, medical surgery, safe industrial robots and robot assistants to help elderly and disabled people.

This chapter will illustrate the most popular compliant and variable stiffness actuators. Compliant actuators are designed specifically to reduce the rigidity of robot actuators to minimise the possibility of inflicting any injuries on humans during human-robot interactions. A new compliant soft actuator will be illustrated in this chapter. Moreover, an overview of soft continuum arms and their classification will be given. Then, some examples of the most well-known pneumatic continuum soft robot arms will be illustrated. Finally, in this chapter, different grasping techniques and end effector designs which are soft will be examined.

2.2 Actuators with an Elastic Element

As introduced in the above section, traditional actuators are not suitable for use in applications where robots interact directly with humans because of the rigidity, and the

high stiffness, of materials used in their construction. Researchers, especially those interested in human assistance robots, such as (Hurst, J., & Rizzi, A., 2008), began to introduce new types of actuators with an acceptable range of compliance, adaptability, and ability to work closely with humans in a safe manner.

In some special types of robots, for example, those that are used to help disabled people to walk, walking robots, or robots that experience high peak forces (e.g., when catching things) the force control of actuators is a particularly important requirement (Sergi, F., et al., 2012). Hence, the proposed actuator should be force controllable and have low output impedance, and there are a number of solutions that have been proposed by researchers to achieve these goals. In the following sub-sections, examples of these types of actuators will be illustrated.

2.2.1 Series Elastic Actuator

Pratt proposed the Series Elastic Actuator (SEA) for the first time (Pratt, G., & Williamson, M., 1995). They added a series elastic element, spring, to a rigid actuator construction. The proposed actuator was used in the MIT humanoid robot "Cog" (Brooks, R., & Stein, L., 1994), and for a small planetary rover. The construction of the SEA is shown in figure (2-1) below.

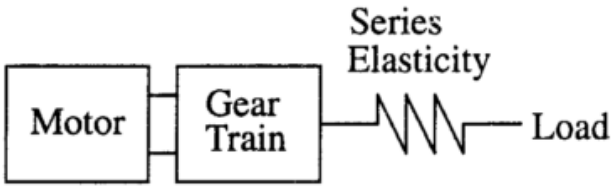

Figure 2-1: Block diagram for the series elastic actuator (Pratt, G., & Williamson, M., 1995).

The basic working principle of an SEA can be explained as follows: the force in the output of an actuator is dependent on the deviation of the series elastic element position multiplied by the spring constant.

The SEA can provide many benefits compared to the traditional stiff/rigid actuators. For example, a SEA has greater shock tolerance, lower reflected inertia and less

inadvertent damage to the environment. However, use of an electrical motor and gear train reduces the efficiency of the actuator and in addition, this actuator is big and heavy.

2.2.2 Hydro-Elastic Actuator

Robinson (Robinson, D., & Pratt, G., 2000) developed a Hydro-Elastic Actuator. It is a series elastic actuator, but it uses a hydraulic piston instead of an electrical motor. The series spring is placed between the hydraulic piston and the actuator output. Figure (2-2) below shows the structure of the Hydro-Elastic Actuator.

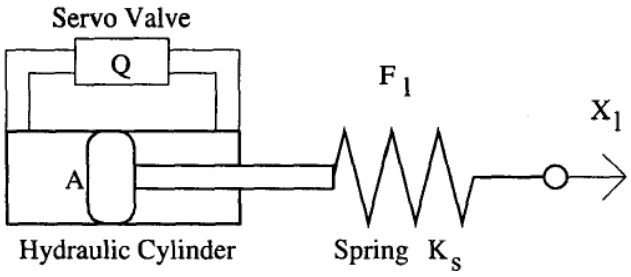

Figure 2-2: Hydro-Elastic Actuator structure (Robinson, D., & Pratt, G., 2000).

The use of a hydraulic cylinder instead of an electric motor will give a high power density to the actuator, especially if it is working at low speed. On the other hand, this will add an extra weight for the actuator, which reduces the compactness and mobile capabilities of the system.

2.2.3 Series Elastic Actuator for a Biomimetic Walking Robot

Robinson (Robinson, D., et al., 1999) proposed a technique to use an SEA for a biomimetic walking robot. This actuator consists of a brushless DC motor connected directly to a ball screw, which generates linear motion. The ball screw nut is joined by four compression springs to the output. A potentiometer is used to measure the compression of the spring. Figure (2-3) shows the structure of the actuator.

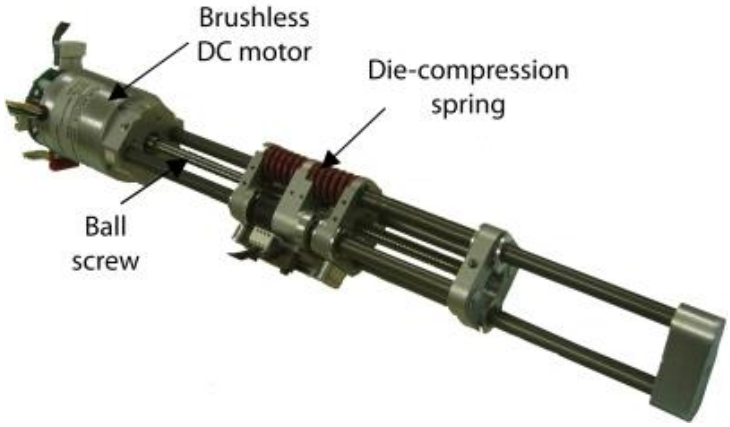

Figure 2-3: SEA for a biomimetic walking robot (Robinson, D., et al., 1999).

Special attention should be paid to the choice of spring constant of the elastic element. A high spring constant is required for large force bandwidth, while minimising the nonlinear friction and impedance requires a low spring constant. Therefore, during the physical actuator design process, a spring constant must be selected that represents the compromise between these two constraints. Another drawback is the size and the weight of the actuator.

2.2.4 Compact Soft Actuator

All the previously illustrated actuators produce a linear motion. However, Tsagarakis identified a compact soft actuator unit to use in multi-DOF and small-scale robotic systems (Tsagarakis, N., et al., 2009). The proposed actuator uses an arrangement of linear springs and a traditional electric motor to form a rotary compliant actuator. Figure (2-4) below shows the proposed compact soft actuator.

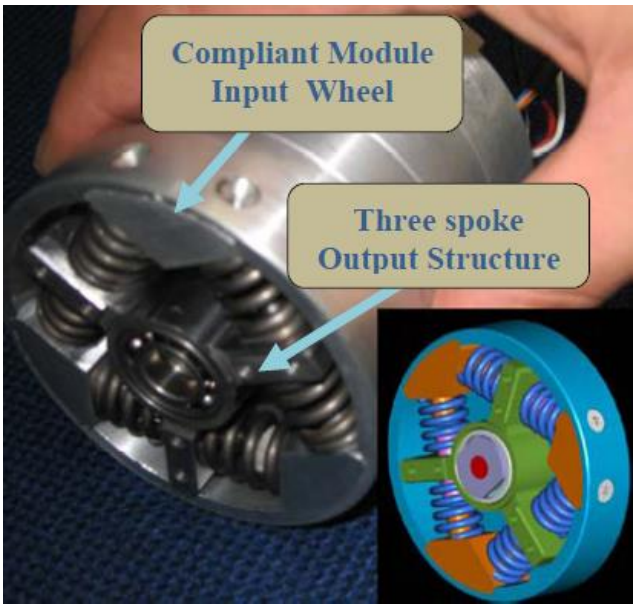

Figure 2-4: Compact Soft Actuator (Tsagarakis, N., et al., 2009).

In the construction of this actuator, six linear springs were placed as shown. The main function of them is to constrain the motion of the three spoke structures. These spoke structures are rotated about the motor shaft and act as a base on which to mount the output link. Two groups of position sensors are located in the actuator construction. Some of these sensors are used to measure the mechanical angle of the motor at all times; others are used to measure the deflection angle of the compliant module. Another function of these groups of sensors was to allow for evaluation of the joint torque.

Whilst the benefit of the actuator is its compactness, this actuator suffers from backlash, friction, limited performance at low output impedance and high positional errors.

2.2.5 Compact Rotary Series Elastic Actuator

Kong produced a compact Rotary Serial Elastic Actuator (cRSEA) (Kong, K., Bae, J., & Tomizuka, M., 2012). This actuator is used in human assistive robots. The cRSEA was designed to provide knee joint assistance. Figure (2-5) shows the construction of cRSEA.

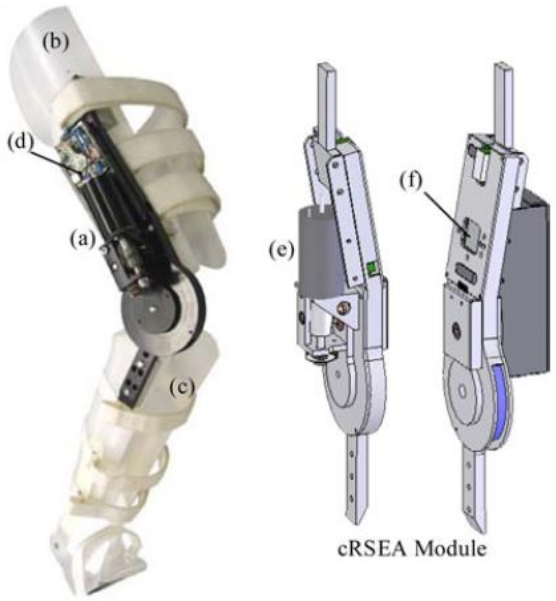

Figure 2-5: Compact series elastic actuator, which consists of: (a) proposed cRSEA module; (b) thigh brace; (c) calf brace; (d) motor driver; (e) dc motor; and (f) embedded controller(Kong, K., Bae, J., & Tomizuka, M., 2012).

A significant advantage of this actuator was the ability to isolate the load from the motor using the spring. This would mean that if there is some unexpected reaction on the load side, it will not affect the driving motor. However, the large size and the complicated nature of the structure are the main drawbacks of this actuator.

2.3 Variable Stiffness Actuators

To overcome the performance drawbacks and limitations of the SEAs, researchers, especially those interested in biped robots, developed new kinds of actuators that have the ability to change their stiffness or compliance during operation. The shape of walking robots is typically human inspired, however, their actuators are often constructed of stiff and rigid parts such as motors and pulleys. Robots actuated by stiff joints can be position controlled easily. However, these robots are not safe enough to directly interact with humans and additionally are not suitable for use in an unspecified environment.

Human's bodies, with their joint flexibility, have the ability to do a vast range of tasks in a very effective and precise manner. Tasks are achieved under different conditions in

different environments with high flexibility. Inspired by humans, researchers have proposed a variety of types of actuators. The Variable Stiffness Actuator (VSA) is one of the most promising actuator designs for use with walking robots. The VSA operates by controlling both the actuator compliance and its equilibrium position independently. Hence, many human-like motions can be achieved using only a small amount of energy at the input of the actuator.

In the following sub-sections the most promising VSAs will be described, along with their main design concepts and any enhancements that help overcome the drawbacks and limitations of the previously described SEAs.

2.3.1 Selective Compliant Actuator

The selective compliant actuator was constructed by Sugar (Sugar, T., 2002). Figure (2-6) shows the spring system for the actuator.

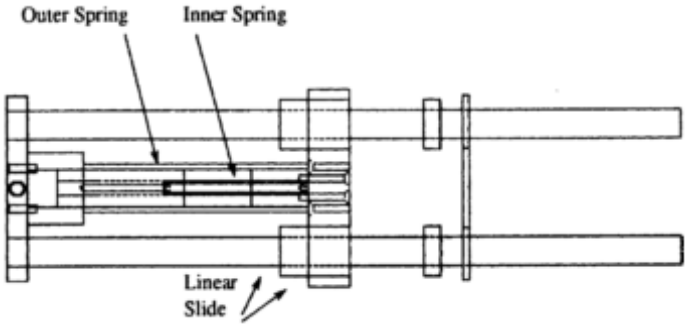

Figure 2-6: The spring system for the selective compliant actuator (Sugar, T., 2002).

The selective compliant actuator is constructed using a DC servomotor and a ball screw that is used to create linear motion, and then connected in series with the linear spring. The output force of the actuator will be applied through the spring.

The stiffness of the springs cannot change, but the equilibrium position of the springs can change by changing the position of the ball screw. The motor allows this to be performed at high speed, and has the capability of adjusting the effective stiffness of the actuator. The output force generated by the actuator is determined by the deflection of

the spring. However, this actuator is constructed from heavy and large components and this was found to reduce the compliance of the system.

2.3.2 Safe and Fast Physical Human-Robot Interaction Actuator

Tonietti proposed a VSA that can be used in a robot or any other machine that may physically interact with humans (Tonietti, G., Schiavi, R. & Bicchi, A., 2005). Figure (2-7) shows the conceptual design and the actual shape of the proposed actuator.

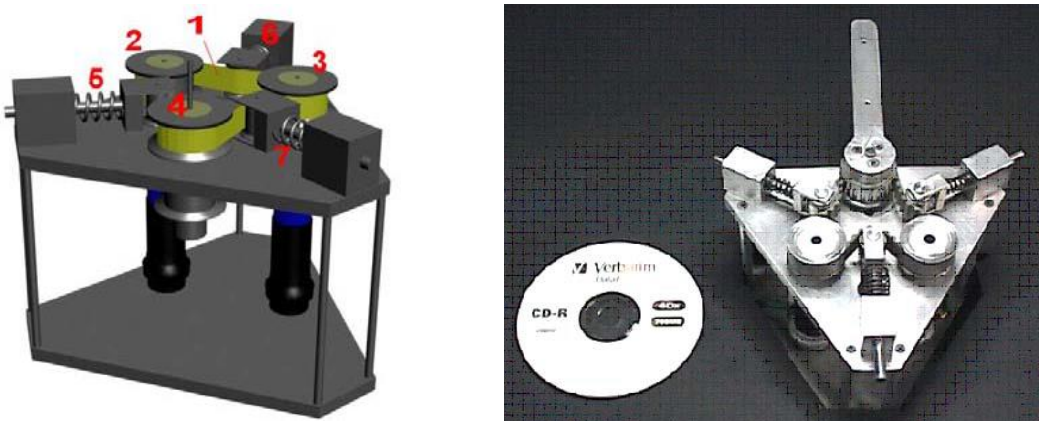

Figure 2-7: Variable Stiffness Actuator (Tonietti, G., Schiavi, R. & Bicchi, A., 2005).

The actuator's principle of operation is as follows: the pulleys of two DC motors 2-3 are connected to the actuator output shaft 4 through transfer belt 1. The whole system is tensioned by three spring mechanisms 5-6-7. To control the position, both motors rotate in the same direction. When a force is applied to the output in an anticlockwise direction, the transfer belt is forced against the upper spring mechanism, compressing it and introducing joint compliance. The actuator is constructed from heavy and large size components which increases the inertia of the system. Additionally the output torque generated by the actuator is limited.

2.3.3 Variable Stiffness Actuator for Safe and Performing Robots Interacting with Humans

The same researcher's team has constructed an improved version of the previous actuator (Schiavi, R., et al., 2008). The previous actuator is restricted in terms of the

capacity of the generated torque. This means that it is not suitable for use in real robots. However, the improved VSA has been proposed to overcome these shortcomings.

Figure (2-8) shows the improved VSA structure. A one-link robot arm using the improved VSA is also shown.

Figure 2-8: Improved VSA prototype and an experimental setup of the improved VSA in one-link robot arm (Schiavi, R., et al., 2008).

The experimental results showed a higher torque generation capability compared to the previous one. However, this actuator is unable to adjust position or reduce its stiffness quickly.

2.3.4 Mechanical Adjustable Compliance and Controllable Equilibrium Position Actuator

A rotational actuator with adaptable compliance was constructed by Van Ham and used in a walking biped robot (Van Ham, R., et al., 2007). They built a walking robot using six Mechanical Adjustable Compliance and Controllable Equilibrium Position Actuators (MACCEPA). Figure (2-9) shows both the actuator and the walking robot.

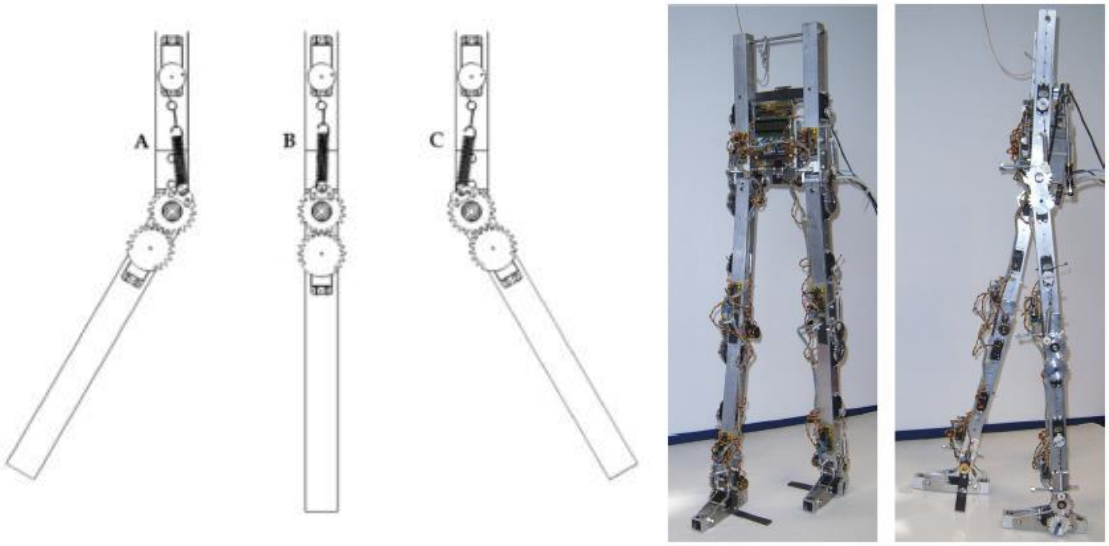

Figure 2-9: MACCEPAs in three positions (A:-30^{o}, B: 0^{o}, C: +30^{o}) and the walking robot (Van Ham, R., et al., 2007).

The compliance and equilibrium position of this actuator are controlled separately using two independent motors. The relatively complex construction and difficulty controlling the performance of this actuator are considered as a drawbacks. Also the use of two servo motors reduces the efficiency of the system.

2.3.5 Mechanical Adjustable Compliance and Controllable Equilibrium Position Actuator 2.0

An improved version of the MACCEPA adjustable compliance actuator was suggested by Vanderborght (Vanderborght, B., et al., 2009). The modifications were achieved by selecting a suitable structure for the profile disk. In the construction of this actuator, a profile disk was used instead of the lever arm in the previous version. This flexibility in the selection of the torque-angle curve leads to considerable stiffening in the spring, which is desirable for hopping robots, or in human-robot interaction. Figure (2-10) shows the shape of the MACCEPA 2.0 actuator.

Figure 2-10: MACCEPA 2.0 actuator (Vanderborght, B., et al., 2009).

MACCEPA 2.0 is an electrical actuator, which uses two dedicated servomotors to control both compliance and joint position independently. As the profile disk rotates, it creates a torque at the joint but due to the larger pre-tensioning force, the joint will be stiffer. The drawback of the actuator is that it cannot support heavy loads.

2.3.6 Variable Stiffness Based on Adaptable Pivot Point

Jafari proposed a variable stiffness actuator based on the adaptive pivot point (Jafari, A., Tsagarakis, N., & Caldwell, D., 2011). Two separate motors were used to control the equilibrium position and stiffness of the proposed actuator independently. The proposed Actuator with Stiffness Adjustable (AwSA-II) is an improved version of the old AwSA; see (Jafari, A., et al, 2010). While the old version changes the stiffness by changing the spring location and arm length, the AwSA-II adjusts the stiffness using a force amplifier that depends on the lever mechanism, which is a pivot point to change the amplification ratio of the output force starting from zero to infinity. Figure (2-11) shows a graphic of the construction of the AwSA-II.

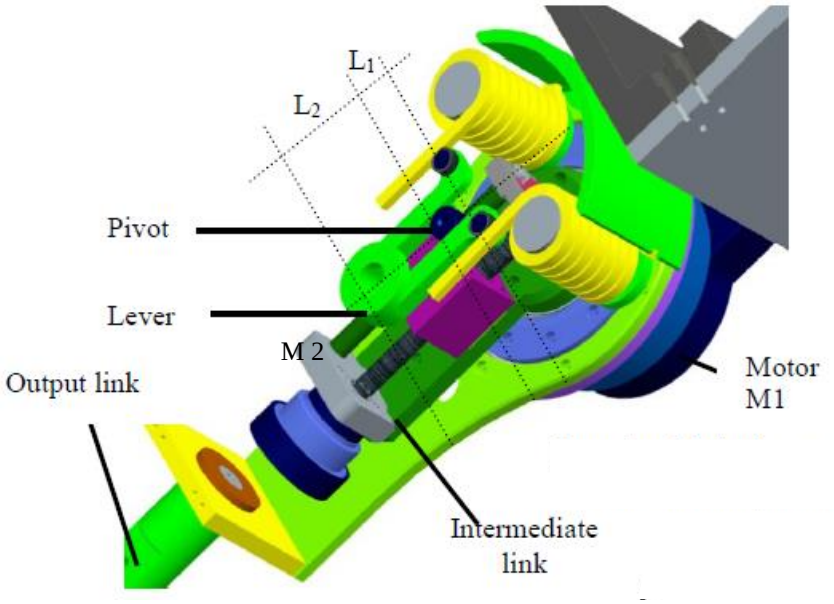

Figure 2-11: Graphical construction of the AwSA-II (Jafari, A., Tsagarakis, N., & Caldwell, D., 2011).

The stiffness of the AwSA-II does not perform against the force of the spring. The displacement of the AwSA-II is applied vertically to the spring force, and this allows

the stiffness to be changed efficiently. The range of the stiffness does not depend on the spring constant or lever length, and hence a light spring and short lever can be used, allowing the overall size of the AwSA-II to be minimised. On the other hand, minimising the lever arm will lead to a reduction in the time needed to regulate the stiffness of the actuator from soft to rigid.

Although this actuator is compact in size, use of rigid materials in the construction of this actuator make it relatively heavy.

2.3.7 Variable Stiffness Joint by Granular Jamming

Jiang proposed a high DOF variable stiffness joint, and demonstrated its use in a miniature snake-like robot (Jiang, A., et al., 2012). The variable stiffness was achieved in the proposed joint by use of granular jamming. They used a vacuum to pull the granular-filled membrane columns; hence, the joint stiffness was raised due to jamming of the granules. Figure (2-12) shows the structure of the variable stiffness elements.

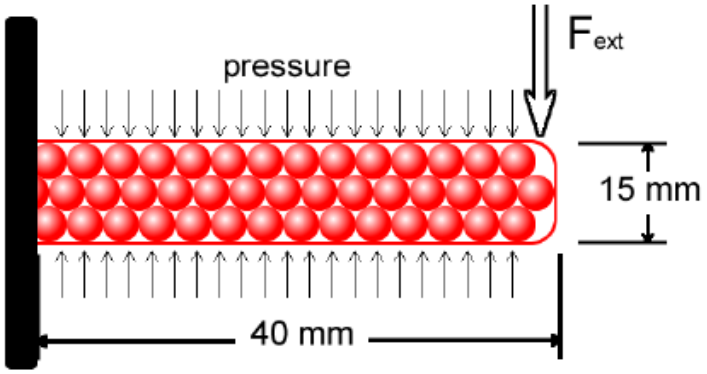

Figure 2-12: Structure of the variable stiffness element (Jiang, A., et al., 2012).

The amount of stiffness depends on the dimensions of the membrane columns, the granular element shape and the outer texture cover. As an example, thicker membranes produce a lower amount of stiffness. Nonlinearity and energy loss due to friction are two significant drawbacks in the proposed design.

2.4 Pneumatic Muscle Actuator

To gain compliance and safety in robots that interact directly with humans, a new type of actuator was developed. The pneumatic actuators can be used instead of SEAs and VSAs to construct a new generation of robots. Pneumatic Muscle Actuators (PMAs) can provide a high power-to-weight ratio (Byrvan, H., et al., 2009). In addition, PMAs can be used directly without gearboxes in robot construction. Hence, they are low cost and are lightweight compared to other actuators. PMAs are physically soft and can be used to construct soft robots, that is, which do not have rigid parts in their structures. Hence, this kind of robot can interact with humans with safety.

The most promising design for the PMA is the McKibben Muscle (Schulte, H., 1962). The McKibben muscle actuator has been widely used in the construction of a new generation of robots, the so-called soft, or continuum, robots. In the following sub-sections, PMA working principles, how they are made, how they can be used, how they may be modelled, and what control strategies are used to control their behaviour will be discussed.

2.4.1 Pneumatic Muscle Actuators Structure

A PMA can be defined as a very light and soft actuator compared to traditional stiff/rigid actuators. Furthermore, PMAs can deform their shapes during operation, thus providing high flexibility. Figure (2-13) shows the geometry of the pneumatic muscle actuator.

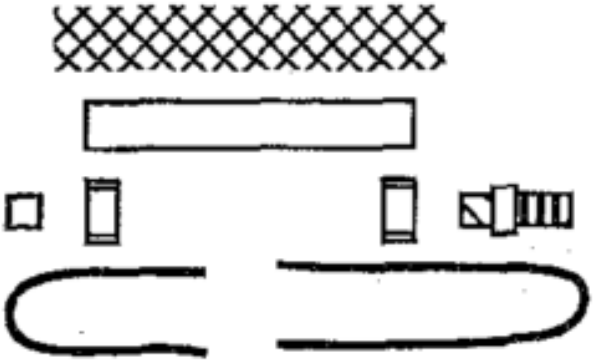

Figure 2-13: Geometry of a McKibben Pneumatic Muscle Actuator (Chou, C., & Hannaford, B., 1996).

McKibben's Muscles are made as follows: the rubber tubing in the figure (2-13) forms the inner layer of the pneumatic muscle and is used to contain the air pressure. The plug, fitting and adapter are used to close the two ends of the rubber tubing. One of the ends is also used to let air in and out of the pneumatic muscle. A woven nylon shell is used as the outer layer to the pneumatic muscle; it is this braided shell that determines the behaviour of the resultant muscle when pressurised. Depending on how the braided shell is installed, the resultant actuator will either contract in response to the air pressure (contractor muscle actuator) or extend (extensor muscle actuator). These actuators are lightweight, but can generate large forces. In addition, because air is compressible the actuators are compliant. However, the actuator is only able to produce force in one direction, meaning they may be used in an antagonistic pair. This has the advantage of allowing variable stiffness through raising or lowering the total pressure in both muscles. Figure (2-14) below shows a complete pneumatic muscle.

Figure 2-14: Left extensor and right contractors pneumatic muscle actuators.

The overall shape of the PMA after assembly resembles that of a thin cylinder. Due to the behaviour of the actuators being superficially similar, at least in appearance, to a biological muscle, these actuators have been used in biologically inspired robots.

2.4.2 Pneumatic Muscle Actuator Operation

As mentioned in the previous section, the muscle consists of an inner rubber bladder. When the muscle is pressurised, this inner bladder increases in diameter. The woven braid material placed over the inner bladder converts the change in diameter into a corresponding change in actuator length.

Depending upon how the actuator is constructed, it can operate in one of two ways. In the first method, as the actuator is pressurised its diameter increases and the braid causes a reduction in the length of the actuator. These types of muscle are commonly known as contractile muscles as they contract in length when activated. The second method of construction installs the braid in a different way. In this design, as the bladder is forced against the braid by the air pressure, the braid causes the actuator to extend in length. This type of pneumatic muscle is commonly known as an extensive muscle as it elongates when activated. In both designs, the actuator is only able to produce force in one direction – a contractile actuator only produces a tensile (pull) force and an expansive actuator only produces a compressive (push) force.

2.4.3 Pneumatic Muscle Actuator Construction

PMAs can be made in different sizes to satisfy any given required purpose. While the length of the muscle may vary from 100 mm to 4000 mm, their diameters can be between 10 mm to 70 mm (Davis, S., et al., 2003). This gives the developer the flexibility to construct effective soft robots that can satisfy a range of applications, especially in humanoid robots and human assistance robots.

2.4.4 Pneumatic Muscle Actuator Applications

The PMA can be used in many manufacturing processes. However, pneumatic muscles are yet to see widespread use in industry. In recent years, robot developers have begun to use this type of actuators extensively (Davis, S., et al., 2003). By using PMAs, a new generation of soft robots that can interact safely with a human has been produced. Due to the compliant behaviour coming from air compressibility, and the light weight of the PMA, a new range of applications can be addressed through the use of soft robots. These applications require either direct interaction with humans or must otherwise operate within an unspecified work environment.

Pneumatic muscles have been used in humanoid robots (Davis, S. & Caldwell, D., 2006), dexterous robot hands (Robinson, G., Davies, J., & Jones, J., 1998), walking robots (Zheng, T., et al., 2013), and control of a high-speed linear axis (Aschemann, H., & Schindele, D., 2008).

An alternative method for the use of PMAs is to construct soft robots made from multiple sections of actuators connected together in series and in parallel to form continuum arms.

2.4.5 Mathematical Models for Pneumatic Muscle Actuators

There are a lot of static and dynamic models, as produced by many researchers that are used to model pneumatic muscles. Each model has a different level of complexity and its associated limitations.

Chou report simplified statics as well as a quasi-static models for both the volume and pressure dynamics of pneumatic muscles, with the hysteresis represented numerically through a static friction hypothesis (Chou, C., & Hannaford, B., 1996). Tondu present a method of representing the hysteresis in the pneumatic muscle model by introducing the effect of frictional force in the suggested model (Tondu, B., & Lopez, P., 2000). Davis presented an idea to model the hysteresis statically and by considering the braid friction (Davis, S., & Caldwell, D., 2006). The above three modelling methods depend on many parameters, that are not easy to quantify, and may change under dynamic conditions and add more complexity in controlling the operation of the PMAs.

Minh suggested another solution for the pneumatic muscle hysteresis through the use of a non-local memory to store the hysteresis function represented by a lumped parameter model (Minh, T., et al., 2009). However, only static hysteresis was considered for both extension and contraction action of the pneumatic muscle. Another limitation of the above method was that all the models presented are for the contractor muscle actuator; hence, there are no models developed for the extensor actuators yet.

2.4.6 Methods of Controlling Pneumatic Muscle Actuators

To control the performance of a pneumatic muscle, the air pressure inside it must be controlled. This can be achieved by controlling the air passing through the inlet using a valve, usually an electrically driven valve, connected to a pneumatic muscle (Caldwell, D., Medrano-Cerda, G., & Goodwin, M., 1993). To keep the efficiency for the system high, the valve should be chosen to work using the minimum amount of energy possible.

Depending on the type of valve, the signal used to drive the valve will vary, but it is common to drive the valve using a Pulse Width Modulated (PWM) signal, which will allow the airflow through the valve to be controlled. By changing the duty cycle and the length of the applied signal, the air pressure in the pneumatic muscle is controlled.

The operational cycles of the system can be explained as follows: when the valve is on, the air supplied to the pneumatic muscle and the pressure are both increased. Hence, depending on the type of the muscle, the pneumatic muscle either contracts or extends. Alternatively, if the valve switches off, the pneumatic muscle will be relaxed. Again, by controlling the duty cycle of the PWM signal applied to the valve, the contraction or extension behaviour of the pneumatic muscle can thus be controlled.

It is necessary to state that the overall behaviour of the system is nonlinear. Hence, it is not easy to control the operation of such a system. Many researchers have proposed schemes to control the operation of the pneumatic muscles. For instance, Hesselroth report a controller based on a training algorithm of neural networks (Hesselroth, T., et al., 1994). An adaptive position controller has been produced by Medrano-Cerda (Medrano-Cerda, G., Bowler, C., & Caldwell, D., 1995), whilst a variable structure controller has been proposed by Repperger (Repperger, D., Johnson, K., & Phillips, C., 1998). Another idea for controlling the pneumatic muscle was suggested by Repperger, where a gain scheduling model-based controller was used (Repperger, D., Phillips, C., & Krier, M., 1999). Fuzzy controllers have also been proposed to control pneumatic muscles, as presented by (Chang, X., & Lilly, J., 2003) and (Balasubramanian, K., & Rattan, K., 2003). A nonlinear optimal predictive controller introduced by Reynolds (Reynolds, D., et al., 2003) has been used to control a pneumatic muscle. Direct Continuous-time adaptive control for pneumatic muscles has been presented by Lilly (Lilly, J., 2003). A PID controller tuned by neuro-fuzzy techniques was suggested by Chan (Chan, S., et al., 2003). Another nonlinear PID controller using neural networks techniques was produced by Ahn (Ahn, K., & Thanh, T, 2005). Van Damme, suggested a proxy sliding mode controller (Van Damme, M., et al., 2007). A sliding-mode controller was proposed by Aschemann (Aschemann, H. & Schindele, D., 2008). A hybrid distributed macro-mini-controller was provided by Shin (Shin, D., Sardellitti, I. & Khatib, O., 2008). A robust variable structure controller was introduced by Choi

(Choi, T., & Lee, J., 2010). Finally, a multi-parametric optimal controller was produced by Andrikopoulos (Andrikopoulos, G., et al., 2014).

2.5 Continuum Arms

Most traditional robots are built using discrete joints with stiff connecting links, as inspired by human limbs. Every joint in these robots has one degree of freedom whose movement can be straightforwardly controlled by manipulating the movement of these joints. The use of these stiff joints will result in a heavy overall structure because of the need to use large supporting sections in the overall system construction. While these stiff/rigid robots are a desirable part of many manufacturing operations, there are many applications that require robots with different features and modes of performance.

In contrast to traditional robots, continuum robot arms do not have discrete joints. Instead, their entire structure can be bent to achieve a required movement. Continuum robot arms can be considered to behave in a very similar way to an elephant's trunk, an octopus's legs, or a caterpillar. In addition, there are no rigid links or moving joints in the construction of these types of robots (Robinson, G., & Davies, J., 1999). The movement strategies used for continuum robots depend on continuous bending along their lengths through deformation.

As continuum arms do not have discrete joints, the way they interact with the environment is entirely distinct from that of a traditional robot. If a continuum robot is partially constrained to prevent a section of it from moving, other sections of the arm will remain free to bend. This means a continuum arm could easily operate inside a pipe, for instance, where a traditional robot would struggle. Continuum arms are also able to deform to match the shape of the object with which they are in contact. This means that if the arm is used to grasp an object, then the grasping force will be distributed over a larger area to minimise any damage to the object. Figure (2-15) shows some animals with continuum limbs.

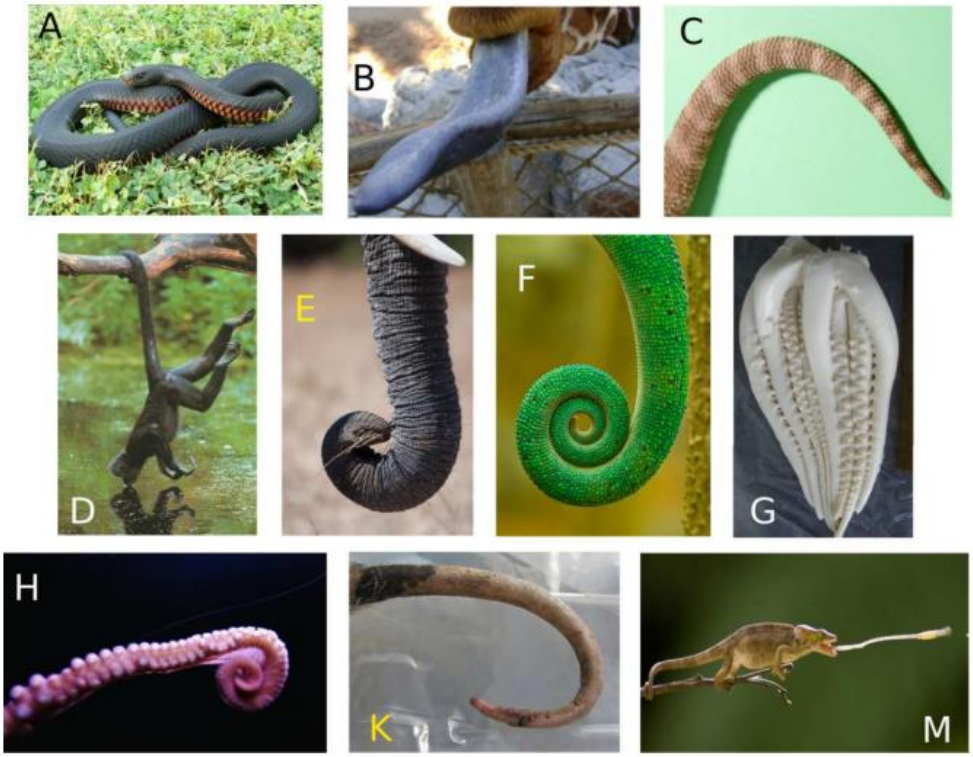

Figure 2-15: Continuum arm/appendage examples found in nature: (A) bodies of snakes; (B) giraffe tongue; (C) lizard tails; (D) tail of the spider monkey; (E) elephant trunks; (F) chameleon tails; (G) squid tentacles; (H) octopus' arms; (K) opossum tails; and (M) chameleon tongues (Godage, I., et al, 2012).

Depending on the method and location of the actuation mechanism, a number of continuum arm designs have been developed. They may be classified into three major categories: intrinsic, extrinsic and hybrid (Robinson, G., & Davies, J., 1999).

Furthermore, these three groups can be subdivided into planar or spatial systems depending on the kind of movement they produce. While planar systems can move in one plane only by bending, spatial systems have the ability to bend in all directions along their longitudinal axis. More details on all of these systems are given below.

2.5.1 Intrinsic Planar Continuum Arm

In the continuum actuator presented by Nemir, a single pressure input is used to provide bending in one plane (Nemir, D., 1989). The fluid-operated planner system shown in figure (2-16) is an example of such a system.

Figure 2-16: Intrinsic Planar Continuum Actuator (Nemir, D., 1989).

The resultant motion depends on the physical structure of the actuator walls. The axial stiffness of the actuator walls is not equally distributed around the actuator itself, and hence the elasticity of the actuator on one side differs from that of the others. Bending occurs by increasing the pressure inside this actuator. If the applied pressure is removed or decreased, the actuator motion will be changed due to the elasticity effect in straightening the actuator.

2.5.2 Intrinsic Spatial Continuum Arm

Robinson proposed the intrinsic spatial continuum actuator (Robinson, G., & Davies, J., 1998). Figure (2-17) below shows the basic structure of an intrinsic spatial continuum actuator as pressurised by fluid.

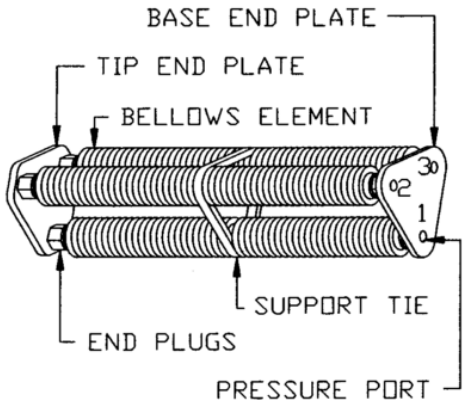

Figure 2-17: Spatial Bellows Actuator (Robinson, G., & Davies, J., 1998).

This actuator can produce motion in three dimensions. Its main characteristics lie in its simple, compact and lightweight design. Both bending direction and magnitude of movement may be straightforwardly controlled by adjusting the pressure inside each of the three parallel bellows actuators. Continuum arms with many degrees of freedom can be produced by combining several actuator sections in series.

2.5.3 Extrinsic Continuum Arm

Extrinsic continuum arms are lightweight and can provide a higher number of DOF. The actuators in this type of continuum arm are located remotely, with the motion typically transferred to the main actuator by sets of tendon cables. Various structures have been introduced with different numbers of continuum arm sections and which consist of various tendon arrangements and degrees of freedom; see, for example, (Hemami, A., 1984), (Lock, J., et al., 2010), (Mahvash, M., & Dupont, P., 2010), (Su, H., et al., 2012) and (Webster III, R., & Jones, B., 2010). Figure (2-18) shows the extrinsic actuator.

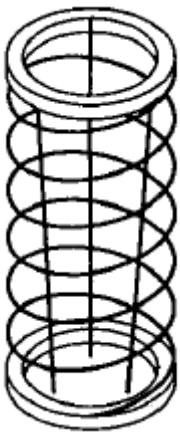

Figure 2-18: Extrinsic Actuator (Nemir, D., 1989).

It uses an extension spring with three tendons attached. Applying a force to one or more of the tendons will induce the bending of the actuator.

2.5.4 Hybrid Continuum Arm

The structure of this type of actuator has the same general appearance as the extrinsic actuator. However, it uses bellows instead of a passive spring. Figure (2-19) shows the construction of the hybrid actuator.

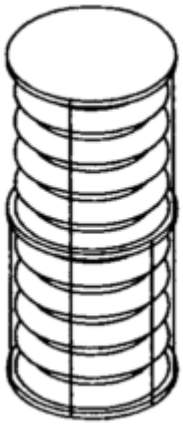

Figure 2-19: Hybrid Actuator (Nemir, D., 1989).

Actuation depends on the joint operation for both the bellows and the triads of three tendons arranged around the bellows. It is clear that, one tendon triad has to be connected to the middle of the bellows construction to control the shape of the lower half of the actuator. Similarly, another tendon triad must be connected to the far end of the actuator to control the operation of the upper half of the actuator. The internal pressure of the bellows controls the tension of the tendons, which works against the tendon operation. Hence, by changing the amount of the pressure in the bellows and by using different lengths of tendons the operation of the whole actuator can be controlled. Immega developed a commercial version of the hybrid actuator called a KSI hybrid actuator (Immega, G., & Antonelli, K., 1995).

2.6 Pneumatic Continuum Arms

As discussed earlier, there are many types of continuum arms, which can be actuated using different mechanism schemes. Pneumatic muscle continuum arms have been reported as being a promising scheme by which to build soft continuum robots (Godage,

I., et al., 2012). Using pneumatic actuation, fully compliant robots can be constructed because of the compressibility of air. Another benefit is the ability to use the whole arm to grasp objects because of the ability of such arms to easily bend in any direction. Hence, continuum arm robots have the ability to work in an unstructured work environment. In the following sub-sections, the most promising design for continuum soft robots will be illustrated.

2.6.1 Extensor Continuum Soft Robot Arm

McMahan developed the OctArm continuum soft robot arm, which uses PMAs (McMahan, W., et al., 2006). They use three or six extensor pneumatic muscles connected in parallel to construct each section. These extensor PMAs have the ability to provide both two-axis bending and extension in length. The OctArm IV is a four-section continuum soft robot arm with a total of twelve DOF, as shown in figure (2-20). In each section, mesh and plastic coupler were used to prevent extensor buckling.

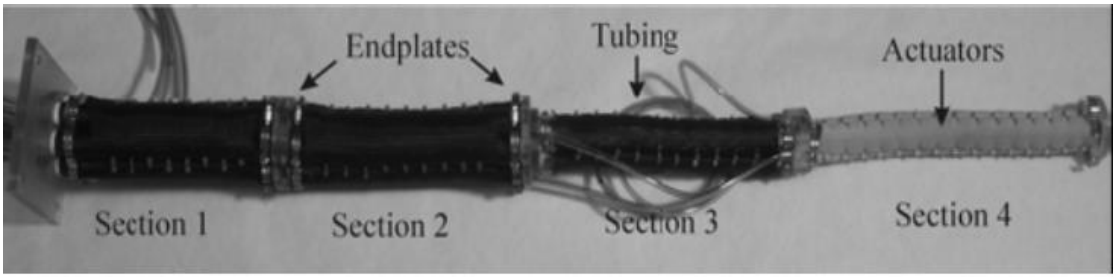

Figure 2-20: OctArm IV extensor continuum soft robot arm (McMahan, W., et al., 2006).

OctArm IV can produce up to a 66% extension and 360^{o} rotation in less than 0.5 seconds. The extensor continuum soft robot arm has the ability to use the entire arm for grasping and manipulating objects of a variety of sizes and scales.

The angle of the braid covering the muscle determines if the muscle is an extensor or contractor; if the angle is greater than 54^{o}44', the actuator can be defined as an extensor, whilst if it less than 54^{o}44' the actuator can be defined as a contractor.

The first and second sections of the OctArms have six PMAs grouped in pairs, while the third section is constructed from three PMAs in each section. At least three PMAs

in each section are required to achieve bending and extension in three directions to give three DOF.

This gives the actuators located in the first two sections a greater stiffness and load capacity. In contrast, actuators in the other sections have the ability to provide higher curvature.

Extensor pneumatic muscles are susceptible to buckling, and so the OctArms includes two mesh sleeve layers. The first layer ensures the muscles remain in contact with each other during bending and prevents individual muscles from buckling. The second mesh layer, or fabric skin, is used to protect the whole arm against abrasion and wear.

The OctArm sections are connected mechanically together using 16 mm thick endplates. These endplates provide the holes used to fit the actuators, and the central hole is used as a pass-through for the pneumatic tube.

Evaluation tests for the proposed continuum soft robot arms showed their ability to work in air and under water successfully, and to grasp objects by wrapping the body of the continuum manipulator around them.

The main drawback in terms of grasping for this arm was due to a lack of object-shape sensing, especially during remote teleoperation. Sometimes objects were dropped because of the lack of grip strength/grasp stability and difficulties on the part of the teleoperator in visually determining the shape of the robot.

2.6.2 Contractor Continuum Soft Robot Arm

Bartow developed a continuum trunk robot based on contractor PMAs (Bartow, A., Kapadia, A., & Walker, I., 2013). Biological trunks and tentacles have inspired the design of the proposed robot. It is constructed from three sections, which are controlled independently. Each section has three DOF, the whole continuum soft robot arm has nine DOF. Sections have been constructed by three or more parallel-connected contractor PMAs. Hence, it can bend in two dimensions and contract in length as well.

Contractor PMAs become shorter when the pressure is increased, representing the opposite behaviour to extensor PMAs. Hence, the unpressurised contractor continuum

arm represents its maximum length, and it contracts through operation. Figure (2-21) shows the OctArm continuum soft robot arm was constructed by using a contractor PMA.

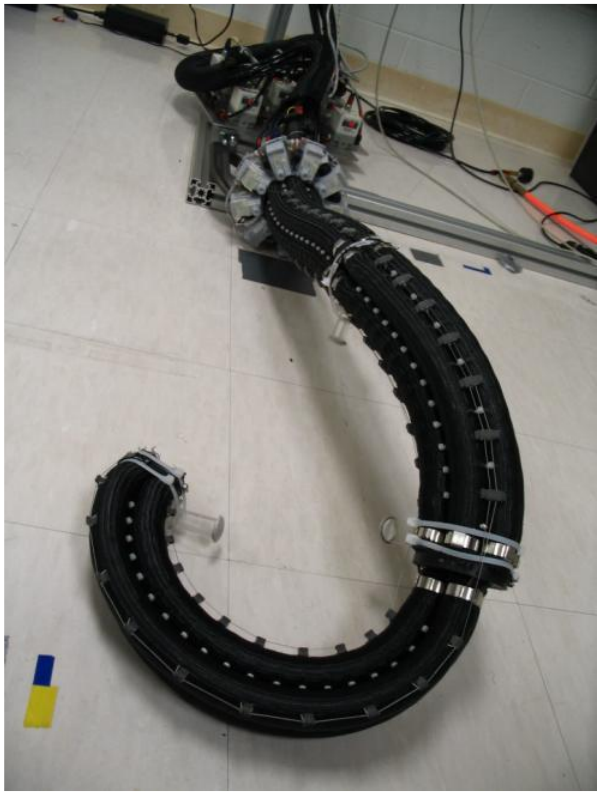

Figure 2-21: OctArm continuum soft robot arm (Bartow, A., Kapadia, A., & Walker, I., 2013).

The PMA arrangement in the structure of the contractor continuum soft robot arm was the same as in the extensor continuum soft robot arm. Hence, the muscle diameters were the same. The nylon mesh angle set was less than the threshold angle discussed in the previous sub-section. This gives the contracting property for the proposed continuum soft robot arm.

Compared to the extensor OctArm continuum soft robot arm, the curvature capability of the contractor continuum soft robot arm is smaller. However, the extension properties matched those of the extensor OctArm.

The proposed contractor continuum arm can grasp along the entire length of its arm; however, the range of graspable objects is limited to those of relatively large size due to the low curvatures that can be achieved compared to the extensor OctArm.

2.6.3 Air-Octor Continuum Soft Robot Arm

The Air-Octor is another continuum soft robot arm constructed from multiple pneumatic sections, as proposed by McMahan (McMahan, W., Jones, B., & Walker, I., 2005). Figure (2-22) shows a two-section Air-Octor continuum soft robot arm.

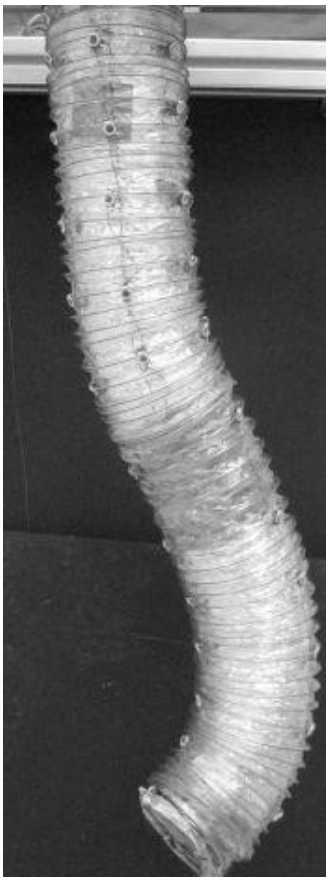

Figure 2-22: Two-section Air-Octor continuum soft robot arm (McMahan, W., Jones, B., & Walker, I., 2005).

The main difference between the Air-Octor continuum soft robot arm and the other two pneumatic continuum soft robot arms discussed previously lies in the construction of the Air-Octor continuum soft robot arm itself. While extensor and contractor continuum arms use McKibben pneumatic muscles, the Air-Octor is constructed using a "hose-in-hose" concept. It combines pneumatic and electric (tendon-driven) actuation attached to an internal and external hose structure. Hence, there are other differences in controlling the stiffness, extension and bending in each section of the arm between the

Air-Octor and the previous two continuum soft robot arms. The operation of the actuator may be achieved by a combination of tendon motion and internal pressure regulation.

The implementation of the Air-Octor continuum soft robot arm consists of a central air chamber that is pressurised pneumatically. The chamber is in the form of hose ducting which is sealed at both ends by end caps. The chamber is constructed from a soft air-tight fabric that is supported using a metal spring around it to form a bellows structure. Hence, the central chamber can extend and retract easily in a controlled manner as air is added to or removed from the bellows. However, the softness of the central chamber also makes it relatively fragile. Therefore, another bellows type hose was added to form an outer protection shell, allowing the arm to perform whole arm grasping without damaging the internal airtight chamber. The outer layer can also be used as a surface to which cables and sensors can be attached.

DC motors and an air pressure regulator were used to control the operation of the Air-Octor continuum arm. The DC motors were used to spool the three cables, which were used to control bending. These were mounted 120^{o} apart around the outer layer of the arm.

One of the main benefits gained from the design of the Air-Octor continuum soft robot arm is in the use of only one actuator per tendon. As the Air-Octor's compliance is controlled pneumatically (higher pressure in the central chamber leads to higher stiffness).

The experimental result shows the ability to use the whole arm for grasping, picking up objects or dealing with obstacles. The payload capability of the Air-Octor arm is comparatively small when bending the trunk to pick up an object due to the pneumatic pressure used. On the other hand, the low weight of the Air-Octor allows it to bend and respond quickly to input as compared to the large payload designs, which gives it good behavioural operation for a soft, continuum manipulator.

The developed manipulator has many degrees of freedom: four in bending and two in controllable compliances.

2.6.4 Single Latex Rubber Tube Continuum Soft Robot Arm

Neppalli studded the previous Air-Octor and Oct-Arm continuum soft robot arms (Neppalli, S., & Jones, B., 2007). They then proposed a new design for the continuum soft robot arm, which uses a central main member constructed by a single latex rubber tube. The new design's structure was similar to that of the Air-Octor continuum arm, but is considerably more robust. Figure (2-23) shows the single latex rubber tube continuum arm.

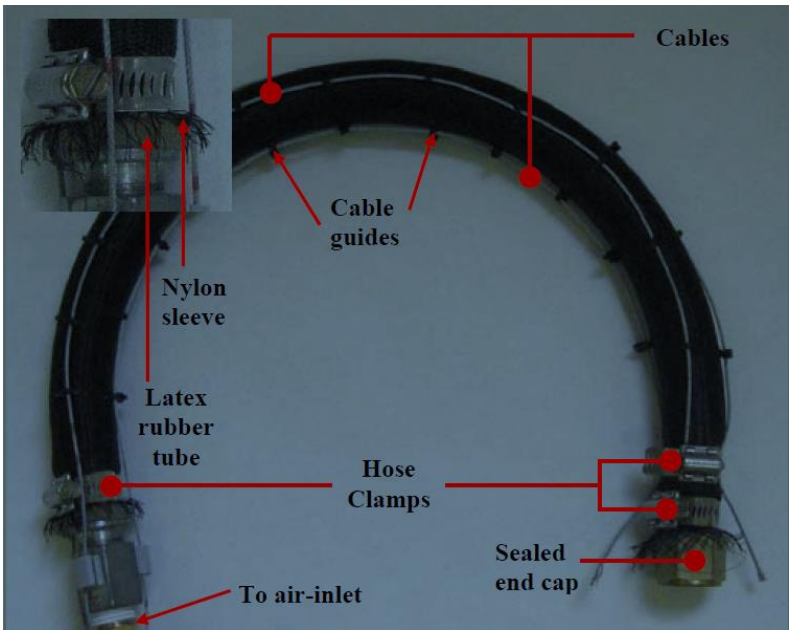

Figure 2-23: Single latex rubber tube continuum soft robot arm (Neppalli, S., & Jones, B., 2007).

Three tendon cables, equally spaced and secured using cable ties around the central member, were used as a bending mechanism for the proposed arm. Groups of electrical motors were used to spool these cables according to the required direction of bending.

While the Oct-Arm continuum arm uses a number of pressurised elements, the proposed trunk uses just one, reducing the complexity of the design considerably. However, the complicated control strategy is one of the main drawbacks of the proposed continuum trunk. Also, the use of a single pneumatic section reduces the deforming capabilities of the trunk, and further limits its range of applications. Hence, the low-cost mechanical

design of the continuum trunk property is lost because of the need to use a complicated and expansive two-level control strategy. Finally, use of electrical motors reduces the compliance of the arm.

2.6.5 Granular Jamming Continuum Soft Robot Arm

Cheng proposed a new structure for a continuum soft robot arm based on the use of the granular jamming technique to construct the arm (Cheng, N., et al., 2012). Tension cables and spooling motors are used to control the bending of the continuum arm. Use of granular jamming allows for stiffness tuning capability. To increase the stiffness in the proposed continuum arm, a vacuum is applied to the sealed manipulator sections. Figure (2-24) shows the structure of the two granular jamming soft robot manipulators developed during this work.

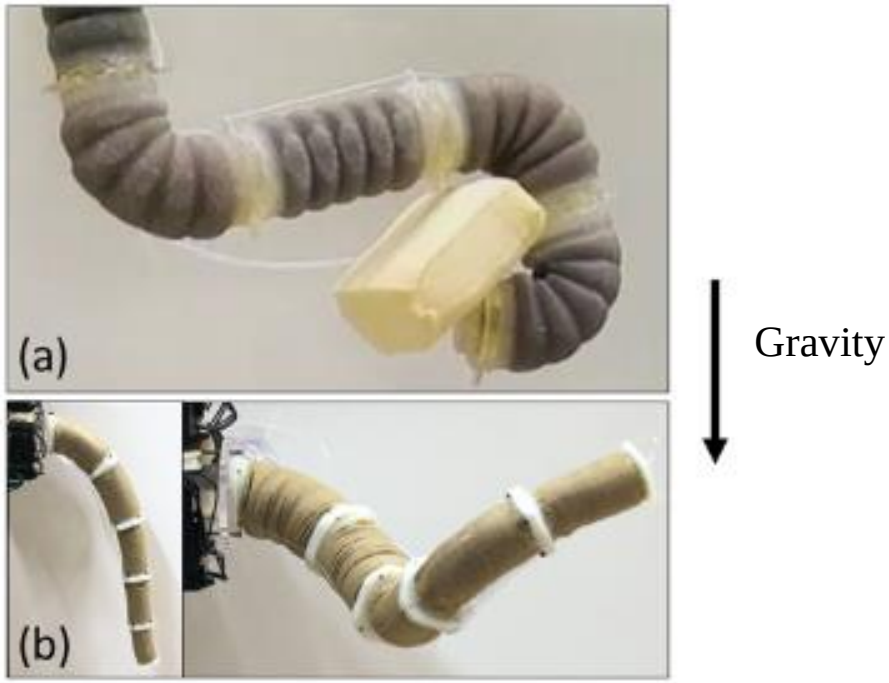

Figure 2-24: Jammable manipulator. (a) First prototype of the jammable manipulator. (b) The second prototype of jammable manipulator: (left) in the unjammed state, and (right) jammed in a corkscrew configuration (Cheng, N., et al., 2012).

Two manipulators have been developed during this work. Both have been constructed of five sections, as shown in figure (2-24). All sections in the first prototype are

constructed in an identical manner, each being 50 mm in length. The total length of the manipulator is 355mm. The second prototype, constructed with a 380mm length, was designed to improve the strength-to-weight and load capacity compared to the first prototype. In addition, the diameter of the sections connected in series become sequentially smaller between sections, except the first two sections which retain the same diameter

Four spooler motors were used to spool the tension cables. The tension cables were fitted along the entire length of the manipulator. Both were used together to control the bending of the manipulator. Latex membranes were used as an outer cover for the granules. Low stiffness-compression inner springs were used to form the shape of each section during operation and, additionally, to constrain the bending motion. Sections were connected by rigid tube fittings and end caps at the end of each section. A coarsely ground coffee was used as the granular medium. One air vacuum pump, connected to the fluid lines of all sections, was used to jam the granules inside each section. Thus, the stiffness of the entire manipulator was increased. The fluid lines were also connected to a solenoid valve located separately to the arm, giving the capability of controlling the stiffness/jamming of each section independently.

Achieving position control for the proposed manipulator requires both jamming/unjamming of different sections and length control of the tensioning cable. Clearly, the use of all this hardware will increase the cost of the manipulator construction and increase the complexity of the controller. Although motors were allocated off-board, the compliance of the overall manipulator was reduced. The use of five sections in the manipulator structure will increase the number of DOF. However, it is not easy to control the movement of each section independently to achieve the required task according to pre-specified paths. Finally, the bending strength for the proposed manipulator will be limited to the jamming pressure for all sections.

2.6.6 Mathematical Models for the Pneumatic Continuum Arms

The mathematical models developed for the pneumatic muscles are discussed in section (2.4.5). Usually, a group of three or more pneumatic muscles actuators are combined to

construct the continuum arm section. Many researchers have investigated kinematics models for the continuum arm sections.

Jones proposed a model to describe the kinematics of a continuum arm (Jones, B., & Walker, I., 2006). This model enables real-time control and shape control in response to the actuator inputs for the Air-Octor continuum arm. However, it does not give a precise dynamic analysis because of the highly non-linear behaviour of the continuum arm. To overcome this limitation, a new 2D dynamic model proposed by Tatlicioglu was employed (Tatlicioglu, E., Walker, I., & Dawson, D., 2007). These authors reported the details of this model along with simulated results for a multi-section continuum arm that depended on both the section length and its curvature as parameters. Both these parameters, length and curvature, are geometrically correlated. However, they are used separately in the model, and this will introduce unacceptable or impossible curve-length combinations. Another drawback of this model is that it does not consider the dynamics of the actuator.

Recently, Godage investigated a 3D dynamic model that depends on the shape function as applied to continuum arms with variable lengths (Godage, I., et al., 2011). This model overcomes the length and curvature problem of the 2D model. The contraction and extension behaviour of the continuum arm are considered in this model. However, the specific actuator dynamics are not considered. Godage proposed an improved 3D dynamic model technique by considering the Bouc-Wen hysteresis model, which is used to describe non-linear hysteretic systems (Godage, I., et al., 2012). The new model has been extensively investigated and experimentally validated. This new model can be used with both extensor and contractor pneumatic continuum actuators.

2.7 Soft Robot End-Effectors

Soft robots are highly deformable and can conform to surfaces they come into contact with. If this technology is applied to grippers, it provides two potential benefits. From a safety point of view, this means that in the event of a collision with a person, contact stresses are distributed over a larger area, meaning localised forces are lower and injuries are potentially less serious (Laschi, C., et al., 2012). It can also provide for the ability to distribute forces over a larger area of the object being grasped, again

minimising localised forces and reducing the chance of damaging the object being held. The larger grasp contact area can also result in a more secure grasp compared to a grip that uses point contacts.

Grasping, handling or processing objects are desirable capabilities required from such robots. For many industrial applications, a “pick and place strategy” is a fundamental requirement (Giri, N., & Walker, I., 2011). Hence, researchers have dedicated a considerable amount of work in developing robot end effectors.

One of these approaches has been influenced by the human hand and has attempted to imitate its behaviour. Hence, many prototypes have been developed to study the construction of multi-fingered hands and analyse their behaviour (Bicchi A., 2000). However, to date industrial robots still use the parallel jaw gripper because of the inherent complexity of the human hand and the clear difficulties in emulating its behaviour.

To deal with the above challenges, researchers have reported many solutions in terms of both construction and strategies to achieve grasping. Hence, there have been a number of soft robot end effectors developed that have been used in a range of different actuation methods. In the following sub-sections, different approaches to grasping techniques and end effector design will be examined.

2.7.1 Whole Arm Grasping Using Continuum Soft Robot

This technique is inspired by the octopus’s arm which involves wrapping the arm around the object to grasp instead of using a hand. This method of grasping was demonstrated using the Oct-Arm continuum soft robot arm. Figure (2-25) shows different-shaped objects that can be grasped using the Oct-Arm.

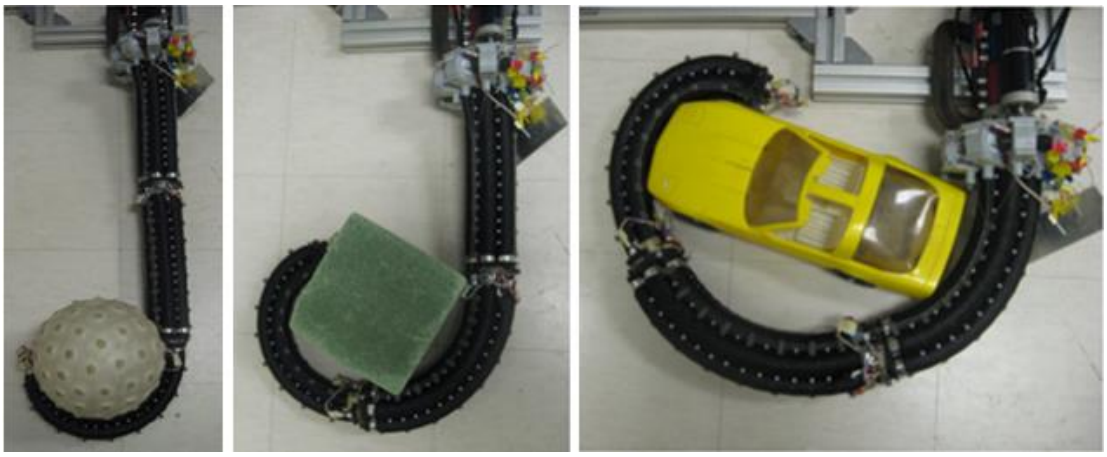

Figure 2-25: Grasping capabilities of the Oct-Arm continuum soft robot arm (Bartow, A., Kapadia, A., & Walker, I., 2013).

Increasing the pneumatic pressure in the actuators will increase the stiffness of each section. This will reduce the compliance of the arm, but make object grasping more secure. While the objects differ in size and shape, one or more sections are required to achieve grasping.

Another whole arm grasping technique, as inspired by the elephant trunk, is the Air-Octor continuum soft robot arm. This continuum soft robot is constructed from only two sections. Figure (2-26) shows the grasping capability of the Air-Octor continuum soft robot arm.

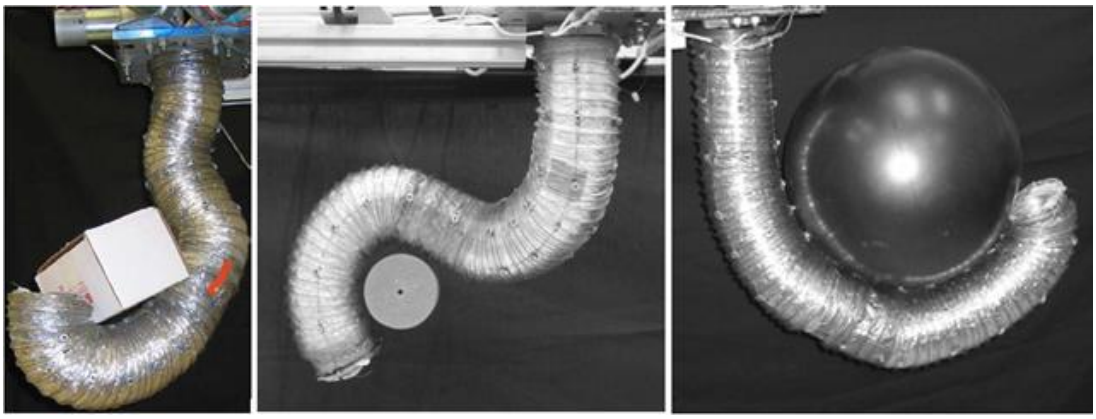

Figure 2-26: Grasping capabilities of the Air-Octor continuum soft robot arm (McMahan, W., Jones, B., & Walker, I., 2005).

Giannaccini proposed a variable stiffness continuum soft arm (Giannaccini, M., et al., 2013). The proposed soft arm can grasp and hold cylindrical objects. It is constructed from an elastic outer shell filled with an incompressible liquid, and is actuated by two cables fitted on the side of the soft arm as shown in figure (2-27), which also shows the grasping capability of this arm.

Figure 2-27: Variable compliance soft arm grasping capabilities (Giannaccini, M., et al., 2013).

All these continuum soft arms are constructed to have a large contact area with any object being grasped. Hence, they have good capability in grasping large-sized objects. On the other hand, it is very hard to grasp small-sized objects using any of the above continuum soft robot arms. Finally, controlling the performance of the gripper is especially difficult as it deforms and bends in the working space whilst in contact with the grasped object.

Stilli introduced a hybrid actuation strategy to control the stiffness of soft manipulators by combining pneumatics and tendons in actuation (Stilli, A., Wurdemann, H., & Althoefer, K., 2014). The idea underpinning this type of actuation mechanism was inspired by nature, where one group of muscles works in opposition to another in order to change stiffness. Figure (2-28) shows the structure of the proposed pneumatic manipulator.

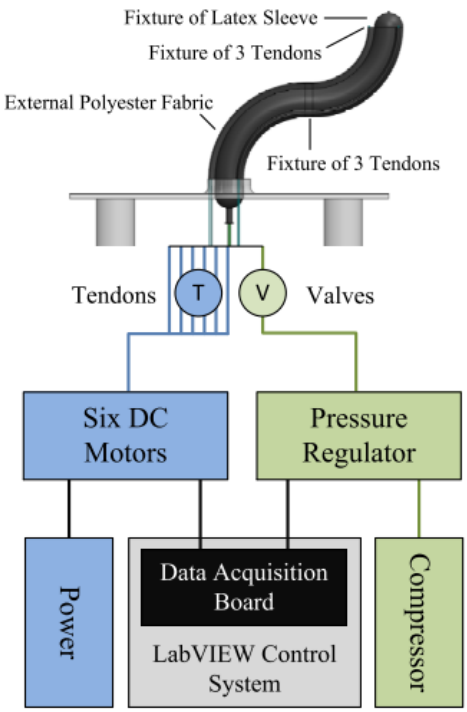

Figure 2-28: The structure of the pneumatic manipulator (Stilli, A., Wurdemann, H., & Althoefer, K., 2014).

This manipulator consists of inner airtight bladder covered by a stretchable latex bladder and then a polyester fabric sleeve. When pressure is applied to the manipulator, it will extend in length. The six surrounding tendons are used to control the bending, as well as the stiffness, of the manipulator by tightening the tendons while pressure is applied. Three of these tendons were fitted half way down the pneumatic manipulator whilst the other three were fitted to the end. The tendons will thus need six DC motors to actuate them. The resultant pneumatic actuator looks as though it has six DOF. The variable stiffness capability of the proposed arm was not investigated. As well as the use of six DC motors decreasing the efficiency of the manipulator, they will also add complications in controlling the performance of the proposed manipulator. Finally, the shape and the size of the objects to be grasped using the proposed manipulator are limited.

Maghooa proposed a soft robot arm actuated by a combination of pneumatic and tendon actuation, each one in opposition to the other (Maghooa, F., et al., 2015). The design imitates the structure of an octopus arm. By controlling the amount of pressure in the

inflatable manipulator and the tendon's length, the stiffness of the entire arm can be controlled. Tendons are also used to control the bending of the inflatable manipulator by powering them in the opposite direction to that of the pneumatic pressure. Figure (2-29) shows the conceptual system architecture of the manipulator.

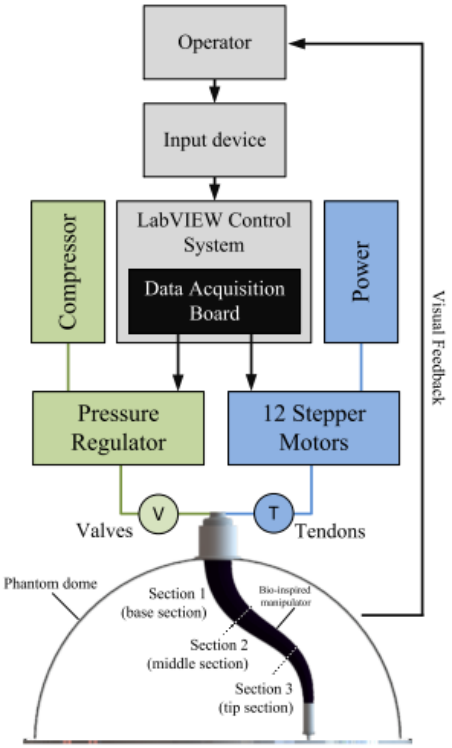

Figure 2-29: Conceptual system architecture of the bio-inspired manipulator (Maghooa, F., et al., 2015).

It is clear from figure (2-29) that the manipulator is constructed from three pneumatic inflatable manipulator sections and 12 tendons. Hence, 12 stepper motors were required to spool the tendons to control the bending of the inflatable manipulator. Even though there is a variable stiffness capability in this manipulator, the use of a huge number of stepper motors in the construction of the proposed manipulator will decrease its efficiency. In addition to the complicated structure, it is not easy to control the performance of the proposed inflatable manipulator. Finally, using this sort of structure reduces the ability of the inflatable manipulator to grasp objects of different shapes and sizes.

Katzschmann introduced a soft planar grasping manipulator (Katzschmann, R., Marchese, A., & Rus, D., 2015). The soft manipulator is fabricated as one piece using soft materials and has a continuum bending ability. It is constructed as a homogeneous soft segment with fluidic cavities, which allows fluid to be pumped in and out during operation to control the bending of the manipulator during object grasping. Figure (2-30) shows the proposed manipulator and the soft arm under actuation.

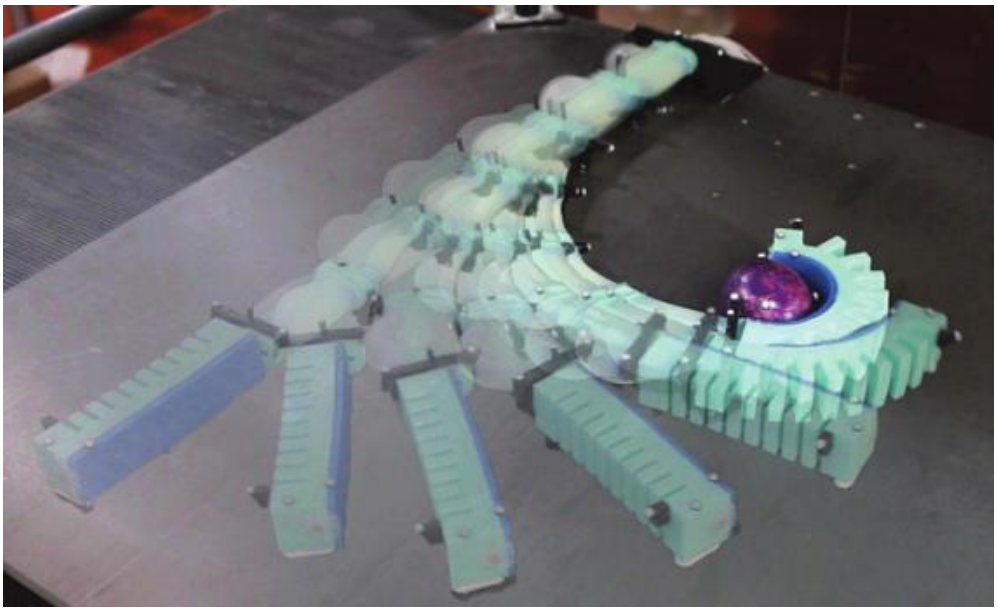

Figure 2-30: Soft planar grasping manipulator (Katzschmann, R., Marchese, A., & Rus, D., 2015).

The main characteristics of this manipulator are its complete compliance and the ability to interact safely with humans. However, this manipulator has a low payload. In addition, the objects being grasped must not be squeezed or broken easily. Finally, there are no sensors attached to this manipulator to give any feedback signal.

Mosadegh, introduced elastomeric actuators powered pneumatically (Mosadegh, B., et al., 2014). The basic idea underpinning the design of this actuator is to use a number of chambers and small air channels fabricated within the elastomeric materials and silicon to allow air pressure actuation. Applying a specific pressure to these small channels will produce sophisticated motions. These motions will result in a bending behaviour in the proposed actuator whose form is dependent on the design features of the air channels. The speed and range of bending depends on the actuation pressure. If the applied

pressure is removed, the actuator will return to its unactuated initial state. Figure (2-31) shows the shape and operation of the proposed elastomeric actuator.

Figure 2-31: Elastomeric actuator (Mosadegh, B., et al., 2014).

One of the main drawbacks of this actuator is that gravity itself can affect its ability to bend when the actuator's bottom layer faces the ground. In addition, chambers can expand randomly in response to the applied pressure when the actuator is at its full deflection, fully actuated. Thus, the force applied to the grasped object by the actuator will not be equally distributed around the object. Finally, there is no possibility of being able to change the stiffness of the actuator, and it can only be used to grasp small or cylindrically shaped objects.

2.7.2 Multi-fingered Soft Robot End Effectors

This approach uses bio-inspired techniques to construct the gripper. However, instead of using a whole arm grasping with the above-mentioned limitations and drawbacks, fingers were constructed and attached to the robot as an end effector and subsequently used to achieve object grasping.

Suzumori developed a Flexible Micro-Actuator (FMA) which used an electro-pneumatic actuation system (Suzumori, K., Iikura, S., & Tanaka, H., 1991). This actuator has three degrees of freedom, and is constructed as shown in figure (2-32).

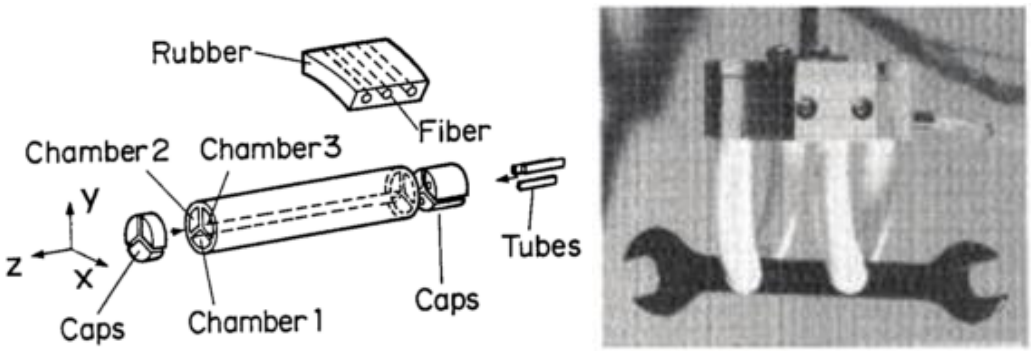

Figure 2-32: Structure and final shape of the FMA gripper (Suzumori, K., Iikura, S., & Tanaka, H., 1991).

The FMA is made from a fibre-reinforced rubber, which consists of three internal chambers. The internal pressure for each of these three chambers is individually controlled. Hence, if the pressure in one of these chambers is increased, then the FMA bends in the opposite direction about the pressurised chamber. A group of four of these actuators are used to construct a gripper for grasping objects, as shown in figure (2-32) above.

Although the fingers are soft, they are attached to a stiff base to construct the end effector. Hence, this combination may be unsuitable for application where human safety is a desirable requirement.

Robinson developed the Advanced MAnipulator for DEep Underwater Sampling (AMADEUS) dextrous robot end-effector (Robinson, G., & Davies, J., 1998). It is a three-fingered hydraulic hand that uses a continuum finger structure. Each finger is constructed by use of three bellows and actuated by hydraulic fluid. According to which one of the actuators is pressurised, the finger will bend in a particular direction. The construction of the finger and the overall shape of the proposed gripper are shown in figure (2-33).

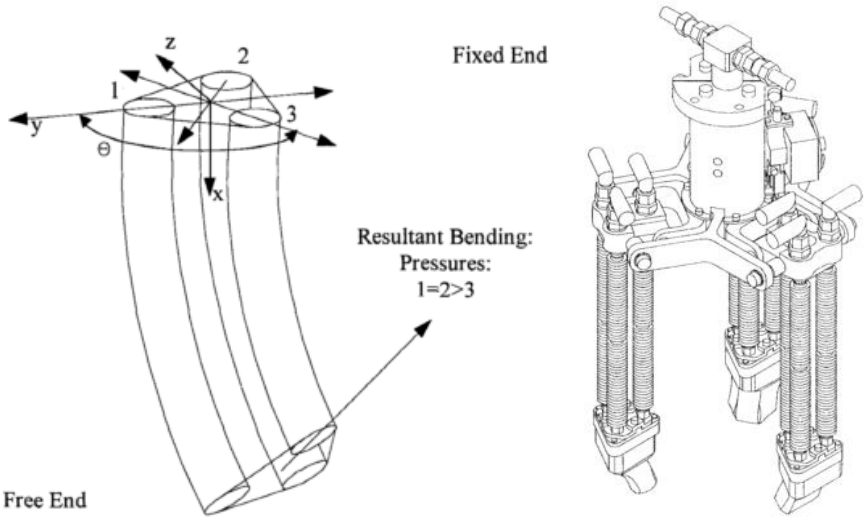

Figure 2-33: AMADEUS dexterous robot end-effectors (Robinson, G., & Davies, J., 1998).

In addition to the complexity of the design of this hand, there is also considerable difficulty in controlling its operation. The overall system is heavy due to the use of hydraulic fluid for finger actuation. Another drawback of this system is the size of the hand, which makes it impractical for human scale operational applications.

Tavakoli proposed a Flexirigid gripper that works by a caging and force closure technique when grasping an object (Tavakoli, M., Marques, L., & De Almeida, A., 2013). This design has only two degrees of freedom and uses two pairs of tendons to control grasping, one pair for each finger. Figure (2-34) shows a model of the gripper.

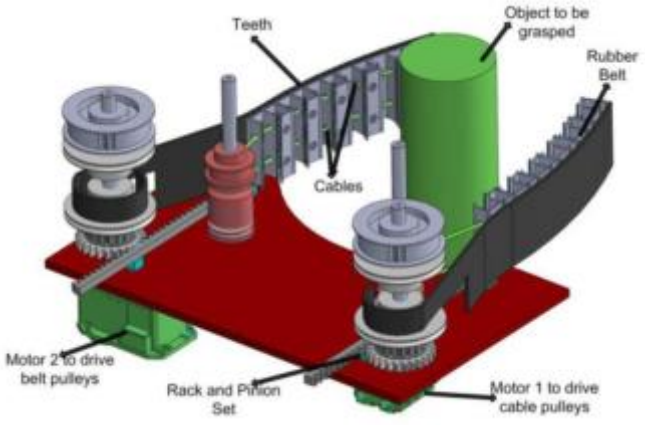

Figure 2-34: Flexirigid gripper model (Tavakoli, M., Marques, L., & De Almeida, A., 2013).

The Flixirigid gripper is simple, flexible, with a low degree of freedom, and with good ability to grasp differently shaped objects. On the other hand, there are no variable stiffness capabilities and limited compliance. The efficiency of the proposed gripper is low because of the use of motors and gearboxes in its construction to actuate the tendons.

Wakimoto proposed a fibreless flexible micro actuator as a soft hand (Wakimoto, S., et al., 2009). This actuator is constructed from reinforced rubber, which contains a number of air chambers that are actuated pneumatically. The soft hand was constructed by three curling actuators attached to a base. Figure (2-35) shows the basic structure, shape parameters and the complete soft hand.

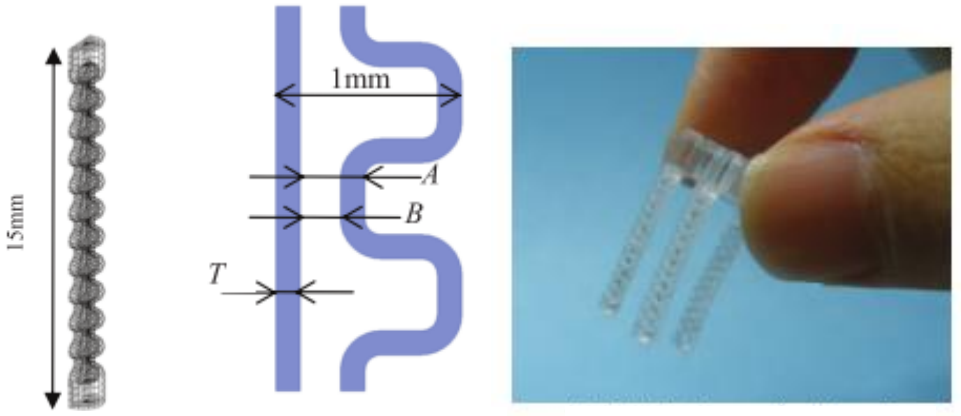

(a) Basic structure (b) Shape parameters (c) Finished state of soft hand

Figure 2-35: Basic structure, shape parameters and soft hand construction (Wakimoto, S., et al., 2009).

The soft hand fingers can bend in both directions when a positive or negative pressure is applied. However, both position and force characteristics have not been investigated in any practical sense. Also, due to the size of the proposed hand being extremely small, only a limited range of object sizes and shapes can be grasped successfully. Moreover, there is no variable stiffness capability in the proposed soft hand, and hence it is difficult to control its performance.

Manti presented a bio-inspired general-purpose gripper constructed from a combination of soft materials (Manti, M., et al., 2015). The gripper structure is formed from three fingers fitted to a base to give the shape of the gripper. The actuation mechanism of the

proposed soft gripper depends on the tension in a single cable used to control the grasping of the gripper. A DC motor located in the base is used to control the tension in the cable. Figure (2-36) shows the overall shape of the general-purpose gripper.

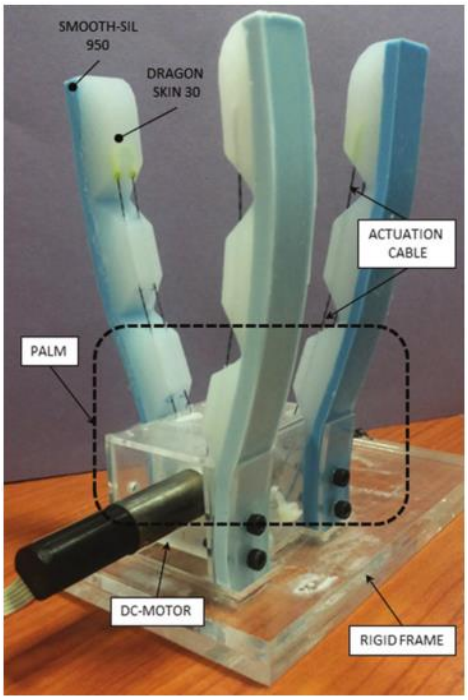

Figure 2-36: General-purpose gripper (Manti, M., et al., 2015).

While this gripper has a simple structure and only needs a simple control strategy to achieve grasping of objects, the limited degree of freedom is one of the main drawbacks of this design. Also, the use of a DC motor to actuate the cable reduces the compliance of the gripper. Finally, there is no capability to control the stiffness of the proposed gripper.

Rateni developed a soft robotic gripper using an elastomeric material (Rateni, G., et al., 2015). The soft gripper is constructed of three soft finger-like segments arranged around a frame, all produced by a 3D printer. Figure (2-37) shows a drawing of the proposed soft gripper.

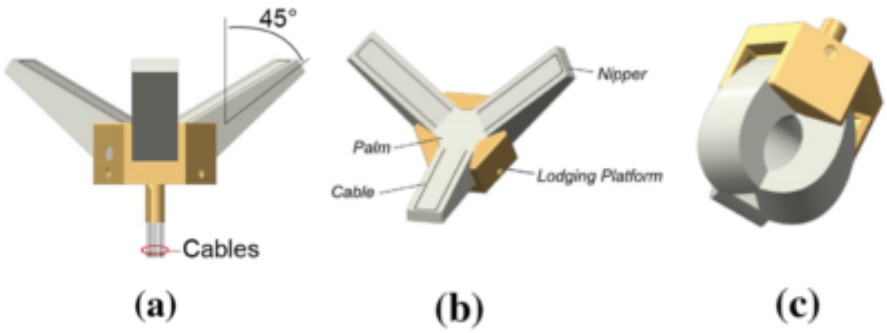

Figure 2-37: Elastomeric soft gripper. (a) Front and (b) isometric view in open configuration; (c) isometric view in close (Rateni, G., et al., 2015).

A pair of tendons is used in each finger to close the gripper or to control the amount of bending of each finger during grasping operations. A servomotor is needed to actuate all the tendons at the same time to achieve grasping. Force sensors are placed in the fingertips to measure the force during grasping.

Only small-sized objects can be grasped using this soft gripper. The stiffness of the gripper is constant and depends on the characteristics of the materials used in fabrication. Finally, the use of servo motors to actuate tendons affects the compliance of the proposed soft gripper.

Homberg presented a soft gripper that is constructed from three identically sized fingers that are actuated pneumatically. Each one of these three fingers is fabricated with a resistive bend sensor (Homberg, B., et al., 2015). The bending of the fingers was achieved by a pneumatic piston controlled by a linear actuator driven by a motor. Figure (2-38) shows the proposed soft gripper.

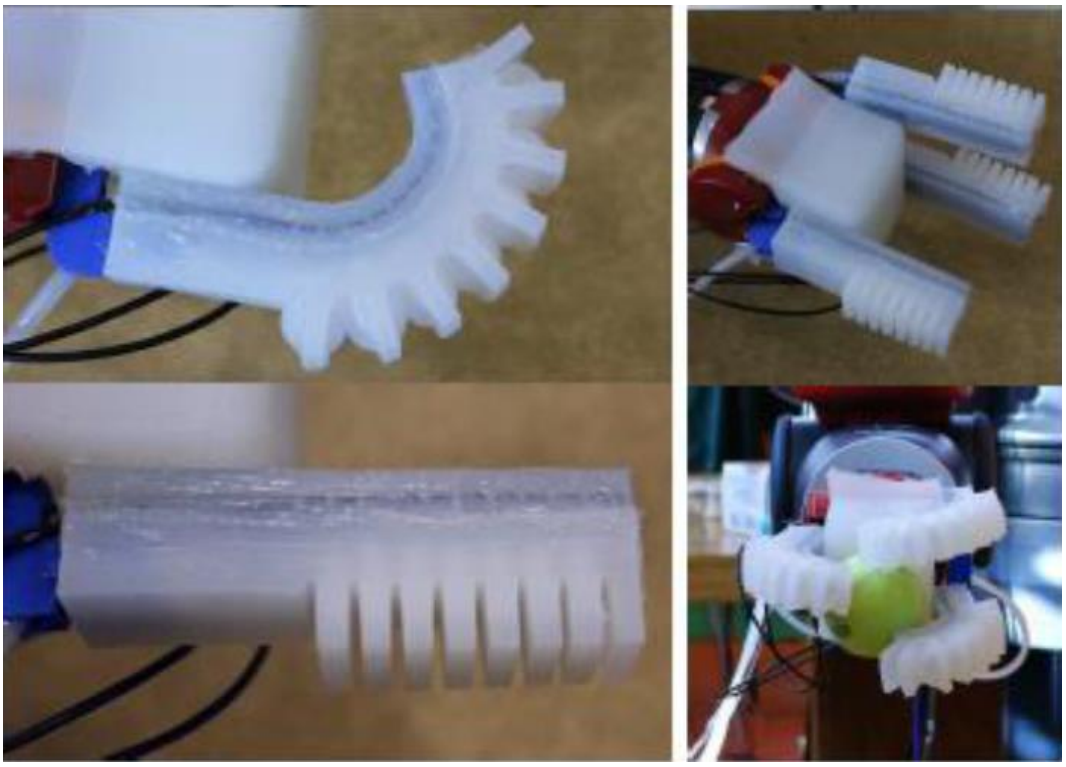

Figure 2-38: Homberg Soft Gripper (Homberg, B., et al., 2015).

While it is a compliant, the capability of grasping uncertain objects, the gripper and the specific object configuration are not well known. In addition, the proposed soft gripper needs a motor and pneumatic piston to control the bending of the fingers; this will reduce the operational efficiency of the gripper. Finally, there is no capability to change the stiffness of the proposed gripper during operation.

Galloway developed an underwater soft gripper whose design is based on soft robotics fundamentals (Galloway, K., et al., 2016). As it is constructed from compliant materials, the proposed gripper can manipulate deep reef fragile species gently. The gripper consists of four fingers actuated by hydraulic pressure. Figure (2-39) shows the structure of the gripper as well as the grasping techniques under pressure.

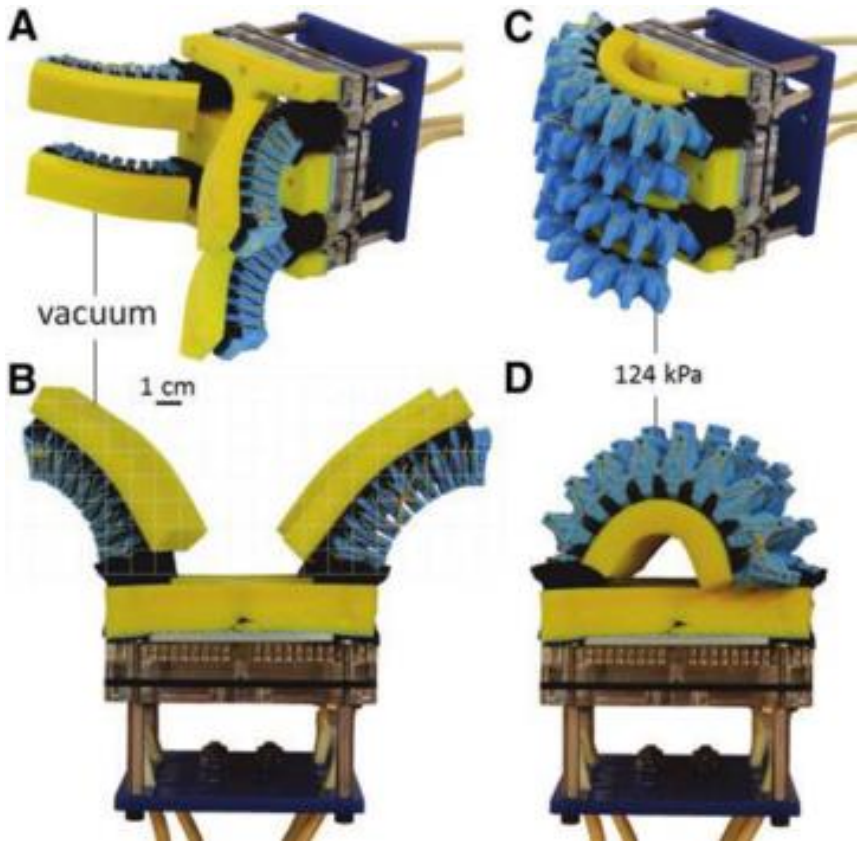

Figure 2-39: Underwater soft gripper. (A, B) Isometric and top view, respectively, of the bellows-type soft actuators under vacuum in the open pose state. (C, D) Isometric and top view of the bellows-type soft actuators (Galloway, K., et al., 2016).

The construction of the gripper is complicated and requires a precise, high-performance controller to control the flow of the hydraulic fluid used to actuate the gripper. The objects that can be grasped are relatively restricted in their size, being of medium or large size only. In addition, there is no ability to change the stiffness in this gripper during operation. Compliance is limited due to the use of rigid parts as a base to which to attach the soft gripper's fingers.

Niiyama developed a printable soft actuator that contains gas-tight bladders fabricated by heat bonding on sheet materials (Niiyama, R., et al., 2015). It is an easily produced, pneumatically driven actuator with a low-cost construction. The actuator is constructed to simulate the human hand in size and has five fingers with air channels actuated by 12 pouch motors. Figure (2-40) shows the printable soft actuator.

Figure 2-40: Printable soft hand (Niiyama, R., et al., 2015).

A simple controller with no feedback signal to improve the performance of the soft hand is used to control the operation of this hand. The weight and the size of the objects that can be grasped using this hand is very limited because it is easy to break. The stiffness of the proposed soft hand is constant and is dependent on the design specification.

Tavakoli proposed the ISR-Softhand, which is constructed from soft fingers with flexible joints (Tavakoli, M., & De Almeida, A., 2014). The ISR-Softhand can achieve 31 out of the 33 grasping forms of the human hand. A single actuator was used to control the movement of the thumb, whilst another was used to control the movement of the index finger, and a third was used to control the movement of the remaining three fingers. Figure (2-41) below shows the construction of the ISR-Softhand.

Figure 2-41: ISR-Softhand (Tavakoli, M., & De Almeida, A., 2014).

The ISR-Softhand uses electromechanical actuators constructed using gears, linkages and belts. Hence, the compliance and the efficiency of the proposed hand is significantly reduced. The motors were back-drivable, and continuous power must be applied during grasping, thus the overall system efficiency is reduced. Finally, the ISR-Softhand has no variable stiffness capability.

Wall (Wall, V., Deimel, R., & Brock, O., 2015) presented five PneuFlex actuators which could form the fingers of a multi finger gripper. The actuators use different methods of jamming to allow them to vary their stiffness and position. Two methods to change the stiffness of the proposed soft continuum actuator are tested, granular jamming and layer jamming. Figure (2-42) shows the proposed actuators.

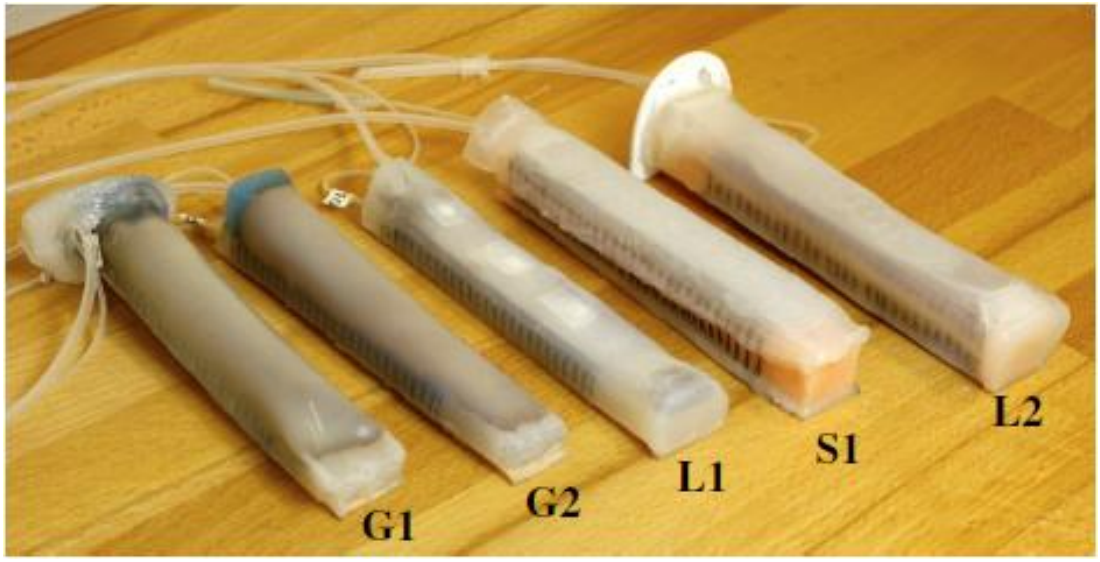

Figure 2-42: PneuFlex actuators with different jamming design (Wall, V., Deimel, R., & Brock, O., 2015).

The first two continuum actuators, G1 and G2, are based on the granular jamming concept described earlier and use metal alloys as the granular material. The other three actuators L1, S1 and L2 use a novel layer jamming method to change the stiffness. It was found that the use of layer jamming gave better performance, achieving twice the increase in stiffness compared to the granular jamming actuators.

The proposed actuator is compliant, low cost and easy to implement. However, the ability to change the stiffness of this actuator is limited compared to other granular jamming continuum actuators reported.

2.7.3 Granular Jamming Universal Grippers

Brown proposed a universal gripper constructed from a granular material placed in a nonporous elastic bag as a single mass instead of individual fingers (Brown, E., et al.,

2010). The gripper achieves gripping by attaching and deforming around the object to be grasped. A vacuum is activated to reduce the pressure inside the single mass, thus 'jamming' the granular material. By jamming and unjamming the granular material, the gripper status can be adjusted between soft and solid. Thus, the object will hold, without the need for any kind of feedback to ensure grasping. Figure (2-43) shows the proposed universal, unlimited DOF gripper attached to a fixed robot arm and its ability to grasp objects with a variety of types and shapes easily.

Figure 2-43: Universal unlimited DOF gripper. (A) Jamming-based universal gripper attached to a fixed-base robot arm. (B) Picking up a shock absorber coil. (C) View from the underside (Brown, E., et al., 2010).

As an application, the proposed gripper can be used to securely grip unknown-shaped objects. However, it is difficult to have a feedback signal to confirm grasping.

Amend introduced a simple passive granular jamming universal gripper that uses positive and negative pressures to achieve object grasping (Amend, J., et al., 2012). It is constructed from a single mass of granular material enclosed in an elastic membrane. It can successfully pick and place a range of differently shaped and sized objects, such as flat, soft or complex geometry objects, which are normally not easy to achieve using a universal gripper. To pick up an item, the gripper is passively applied to the target object shape. The vacuum is used to harden the granular jamming universal gripper from its liquid-like (mobile state) to solid state (Amend, J., et al., 2012). As a result, it will grip the object. To place or release the item, a positive pressure must be applied to the universal gripper.

The positive pressure universal gripper can be used to pick more than one object simultaneously. Figure (2-44) shows the proposed gripper gripping two objects.

Figure 2-44: Positive pressure universal gripper capabilities (Amend, J., et al., 2012).

A wide and varied range of object shapes can be grasped successfully by the proposed gripper. However, researchers state that the use of crushed coffee as a granular material limits the gripping performance of the proposed universal jamming gripper at this scale of construction because it cannot allow for a sufficient amount of force to grip objects. Adding positive pressure will improve the gripping performance of the proposed robotic system.

2.8 Conclusion

The SEA is an excellent step forward in developing compliant actuators. However, SEAs suffer from a backlash, friction, limited performance at low output impedance and high positional error. The main reason for the high error is motor saturation. This

amount of error is unacceptable in a practical sense as well as in terms of safety, especially in the latter case when the robot is interacting directly with humans. In addition, the selection of a spring constant that satisfies the requirements of the design is very hard to achieve, while a low spring constant is required at low output impedance to minimise the effects of nonlinear friction, a high spring constant is required with large output impedance bandwidth. Hence, the use of a linear spring can simplify the design of the controller, but at the same time reduces the efficiency of the SEA.

The VSA overcomes many of the SEA drawbacks. However, there are still many limitations in the use of variable stiffness actuators, especially in unspecified and in joint work environments where safe human-robot interaction is a desirable concept. One of the limitations of VSAs is their inability to adjust their position quickly. A robot constructed by VSAs still can cause serious injury if it interacts directly with humans because it will be unable to reduce its stiffness quickly enough should an incident occur. Other limitations of VSAs are the size and weight of the actuators. The reason for this increased weight is due to the use of two motors in the actuator construction (one motor to control the position and another motor to adjust the stiffness). Furthermore, there are still notable power losses in variable stiffness actuators due to friction and the use of two electric motors in their construction.

To gain compliance and safety in robots that interact with humans directly, another type of actuator which is compliant has been proposed as an alternative to using SEAs and VSAs. PMA can provide these characteristics whilst still delivering a high power-to-weight ratio. They use only soft materials in their construction, and can be used directly without gearboxes. The most popular design of PMA is based on the McKibben Muscle structure. PMAs have been widely used in the construction of a new generation of robots called soft, or continuum, robots. The overall behaviour of the PMA is similar to a variable stiffness spring. Hence, compliance can be achieved in robots that use this type of actuator. Robots constructed from PMAs and from soft materials have the potential to allow for much safer systems, as compared to the traditional robot, when interacting directly with humans.

One of the main concepts discussed in this chapter is the use of soft continuum structures in the design of robot systems. A human-robot joint working environment

without any barrier between them is a potential benefit of the use of continuum soft robots. This provides for the possibility of another kind of application, that of a safe human assistive robot for elderly or disabled people.

The main, and common, drawback to the continuum soft arms discussed is the weaknesses inherent to the various control strategies that may be used to control the behaviours of these types of robot. One cause of these weaknesses lies with their highly non-linear behaviour. Another weakness is that there is no currently available precise/exact mathematical model that can describe the kinematics of continuum soft arms, which places additional limitations on the control of this kind of robot.

Another drawback arises from the limited capability to change the stiffness of the proposed continuum soft arms during operation, with the exception of the granular jamming case. The importance of variable stiffness can be simply stated as the reality that a stiff robot's performance can be controlled easily; however, to directly interact in a safe manner with a human requires the stiffness of the robot to be reduced. Hence, developing a continuum soft robot arm with the ability to change its stiffness during operation will be a huge step forward in the development of future robots.

Different approaches to grasping techniques and end effector design have been illustrated. The whole arm grasping technique uses continuum soft robot arms constructed to have a large contact area with a grasped object. Hence, they have a good capability to grasp large-sized objects. On the other hand, it is very hard to grasp small-sized objects. Finally, controlling the performance of the gripper is particularly difficult because it deforms and bends in the working space while in contact with the grasped object.

Due to the range of size and shapes of objects, a multi-fingered soft hand was found to be a better choice to achieve grasping in robot end effectors. Although the fingers themselves are soft, they are attached to a stiff base to construct the end effector. Hence, this combination may be unsuitable for applications where human safety is a desirable requirement. In most cases, there are no sensors attached to these manipulators to give any feedback signal that can be used to control the performance of the multi-fingered soft hand during grasping operations. Furthermore, these grippers are unable to change

their stiffness. While highly compliant fingers may be desirable for grasping certain products, at other times stiffer fingers may be desirable.

The ability to change the stiffness in the granular jamming universal gripper plays a desirable role in the ability to effectively pick and place a wide variety of objects that are not otherwise easy to pick, such as flat and soft objects. The use of crushed coffee as a granular material limits the gripping performance of the proposed universal jamming gripper. As a result of the conclusions of this literature review a multi-fingered, variable stiffness, continuum soft robot end effector was chosen for development in the remainder of this research.

Chapter Three

3 Actuator Modelling and Variable Stiffness Investigations

3.1 Introduction

Based on the literature review, it was decided that this work would develop a soft robot end effector based on continuum-type manipulators. The proposed design uses contractor muscles to bend the fingers, with the fingers themselves constructed from extensor muscles. The end effector should have the ability to vary its stiffness. Two methods to vary the stiffness will be explored, one based on the antagonistic operation of pneumatic muscle actuators, and the other based on granular jamming.

This chapter focuses on the practical characteristics of the contractor and extensor PMAs in order to find a suitable mathematical model for use in designing a proper controller to control the behaviour of the PMAs.

In order to model the behaviour of the soft robot end effector mathematically, it is important to characterise the behaviour of the PMAs experimentally. Force/displacement and pressure/displacement characteristics will be investigated experimentally for the contractor and the extensor PMAs individually. The results of these experiments will be used in determining a mathematical model that is suitable for both the contractor and extensor PMAs.

The variable stiffness capabilities of PMAs and the granular jamming continuum finger are investigated experimentally in this chapter. Groups of experiments will be conducted to investigate the compliance capabilities of the two types of PMA when arranged in a particular configuration. Compliance, or the variable stiffness property for the proposed system configuration, which is the combination of the contractor and the extensor PMAs, is determined experimentally. The experimental results are obtained by measuring the displacement of the extensor PMA in response to the attached force under different combinations of pressures as applied to both the contractor and extensor PMAs.

Other experiments are conducted to calculate the force/displacement characteristics of the granular jamming continuum finger. The results of these experiments are used to determine the bending stiffness characteristics.

In the following sections of this chapter, an illustration of the experiments conducted and the experimental results found for each type of PMA will be given. A graphical illustration of the results, in addition to a description of the procedure used to determine the mathematical model, will be shown. Claims as to the novelty of the proposed configuration and how it can be used to produce a new, variable stiffness, pneumatic and granular soft continuum hand will be discussed at the end of this chapter.

3.2 Contractor Pneumatic Muscle Actuator Modelling

The total length for the unpressurised contractor PMA used in this experiment is designed to be 240 mm and 15 mm is chosen as the diameter. This length can be contracted by up to 67% of the original length to approximately 180 mm (as a shorter length) if pressure is applied to the contractor PMA. The main function of the contractor PMAs is to provide bending capabilities to the extensor PMAs as fingers in the proposed continuum soft robot hand. The actuation force is transferred from the contractor PMAs to the extensor PMAs through a group of tendon cables. By calculating the combined pressures in both extensor PMAs and contractor PMAs, the compliance can be determined for the soft robot end effector. Figure (3-1) shows a graphical setting for the experiment used to observe the force/displacement and pressure/displacement characteristics for the contractor PMAs.

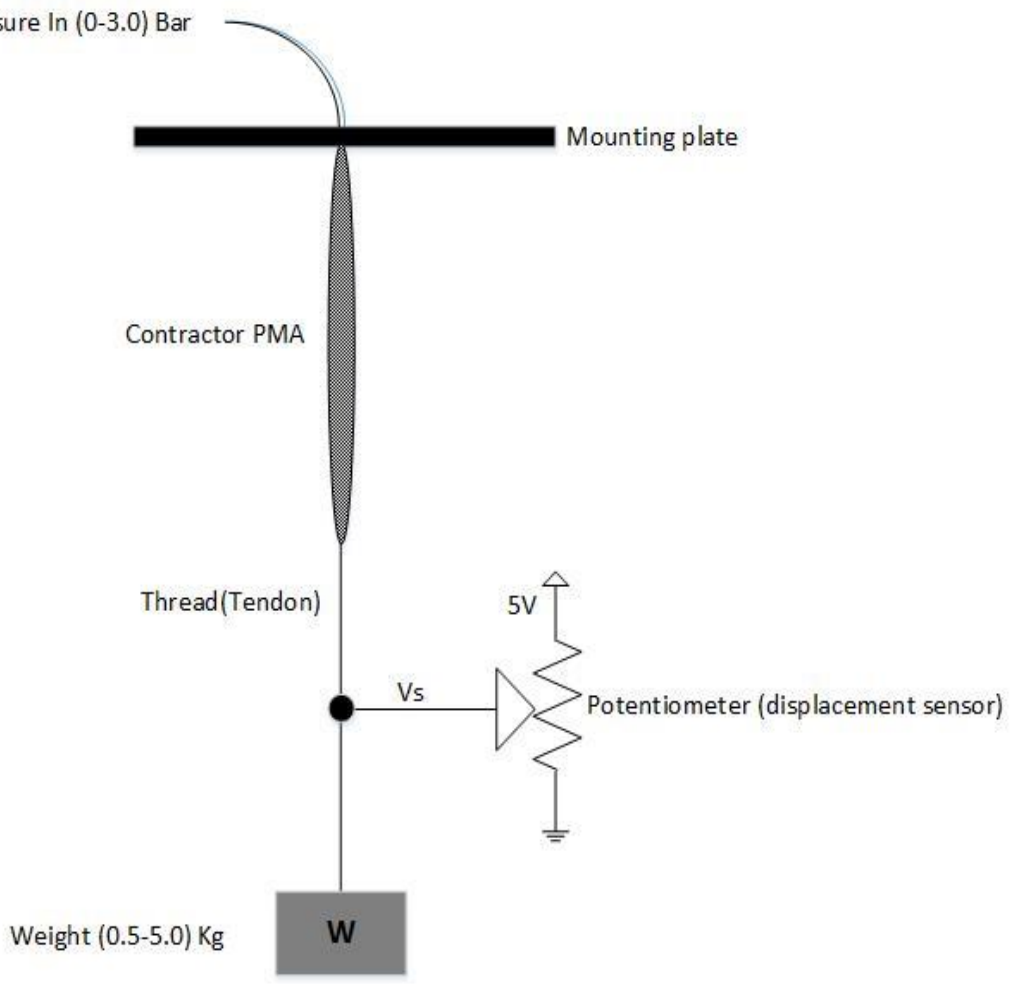

Figure 3-1: Contractor PMA observation experiment setting.

An experiment will be conducted to determine the amount of force produced by the contractor PMA with pressure. Tendon cables are used in this experiment to attach a weight (which is applying a downward force) to the contractor PMA as a load. Tendon cables are also spooled around the central terminals of the 10 kΩ linear potentiometers, which are used as displacement sensors. Once the contractile muscle is actuated, the tendon is pulled and the potentiometer identifies the amount of displacement that has occurred. An Arduino microcontroller is used as a data acquisition device to read the displacement as a voltage signal produced by the linear potentiometers. The other two main terminals of the 10 kΩ linear potentiometers are connected to the +5 V and GND pins on the Arduino microcontroller board.

3.2.1 Force/Displacement Characteristics of the Contractor PMA

During the experiment, constant pressure was applied to the contractor PMA and the displacement measured whenever the attached weight changed throughout the experiment. In the first experiment, the contractor muscle is pressurised to 3 bar and the displacement measured for each incremental step of the weight attached as a load. The attached weight (load) started at 0.5 kg and was increased to 5 kg in increments of 0.5 kg. These loads will generate load forces of approximately 5, 10, 15… 50 N respectively.

Further measurements are then taken while sequentially reducing the weight in decrements of 0.5 kg until the initial, zero load condition is again reached. The same experiment was repeated five times with different pressures applied to the contractor PMA. The experiment was repeated with pressures of between 2.5 bar to 0.5 bar in decrements of 0.5 bar for each successive trial.

In this work, the behaviour of the pneumatic muscle will be modelled as a variable stiffness spring.

The linear representation for the displacement of the contractor PMA can be determined using a linear equation:

$$Y = m * X + c \qquad (3.1)$$

Where:

Y (=Vs): The voltage measured on the central terminal of the linear potentiometer, whose value ranges between 0 and +5 Volts.

X: The displacement in mm, which is a measurement of the change in length in either the contractor or extensor PMA.

c (= 0.55): A constant representing the initial value of the voltage in the central terminal of the linear potentiometer, as measured when there is no pressure applied to the PMA and a 5.0 kg load is attached (50N of force, approximately).

m (= 0.05): A scaling factor which is calculated as the ratio of the voltage difference between the two main terminals of the linear potentiometer (+5 Volts) to the maximum displacement in the linear potentiometer (100 mm).

Hence:

$$Disp.(mm) = \frac{Vs - c}{m} = \frac{Vs - 0.55}{0.05} \qquad (3.2)$$

Equation (3.2) is used to calculate the displacement in all conducted experiments.

A graphical representation of the experimental results is shown in figure (3-2). This graph shows the force/displacement characteristics of the contractor PMA when actuated by different pressures and under different attached load forces.

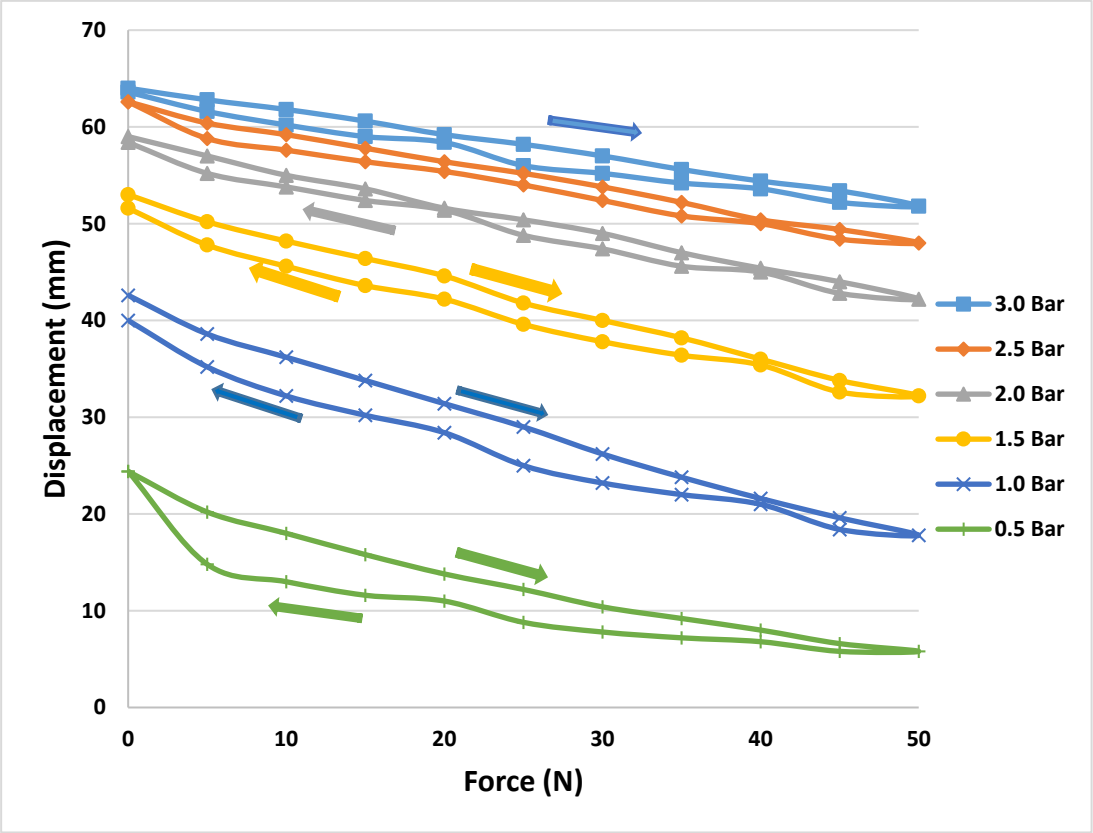

Figure 3-2: Force/displacement characteristics for the contractor PMAs.

It is clear that there is a hysteretic behaviour in the performance of the contractor PMA, with the arrows indicating if force is increasing or decreasing. This hysteresis arises during the operation of the pneumatic muscle due to the friction between the inner tube and the surrounding sleeve mesh of the pneumatic muscle (Chou, C., & Hannaford, B., 1996) and between adjacent mesh strands. To account for the effect of friction in the mathematical model of the PMA, a constant force offset should be added; see, for example Davis (Davis, S., & Caldwell, D., 2006) or Tondu (Tondu, B., & Lopez, P., 2000).

Next, the contractor PMA will be mathematically modelled as a variable stiffness spring, which is considered as the best simplified representation of its behaviour. The spring model was chosen due to its simplicity and because it shows the same behaviour as the pressurised PMAs. For the contractor PMA, the behaviour is similar to that of an extending spring. Hence, the extension of the contractor PMAs when a load is applied is taken into consideration. The displacement of the actuator is converted to extension by subtracting the measured contraction from the maximum possible contraction. The

maximum possible contraction has determined experimentally at no load and a pressure of 5 bar, which is the maximum pressure that can be applied to the contractor PMA and the displacement was found to be 72 mm.

Figure (3-3) shows the extension in the contractor PMA calculated according to the force/displacement characteristics, which are shown in figure (3-2), and with 72 mm as the maximum contraction of the muscle. Note that the extension values for increasing/decreasing load are averaged to remove the effect of the hysteresis.

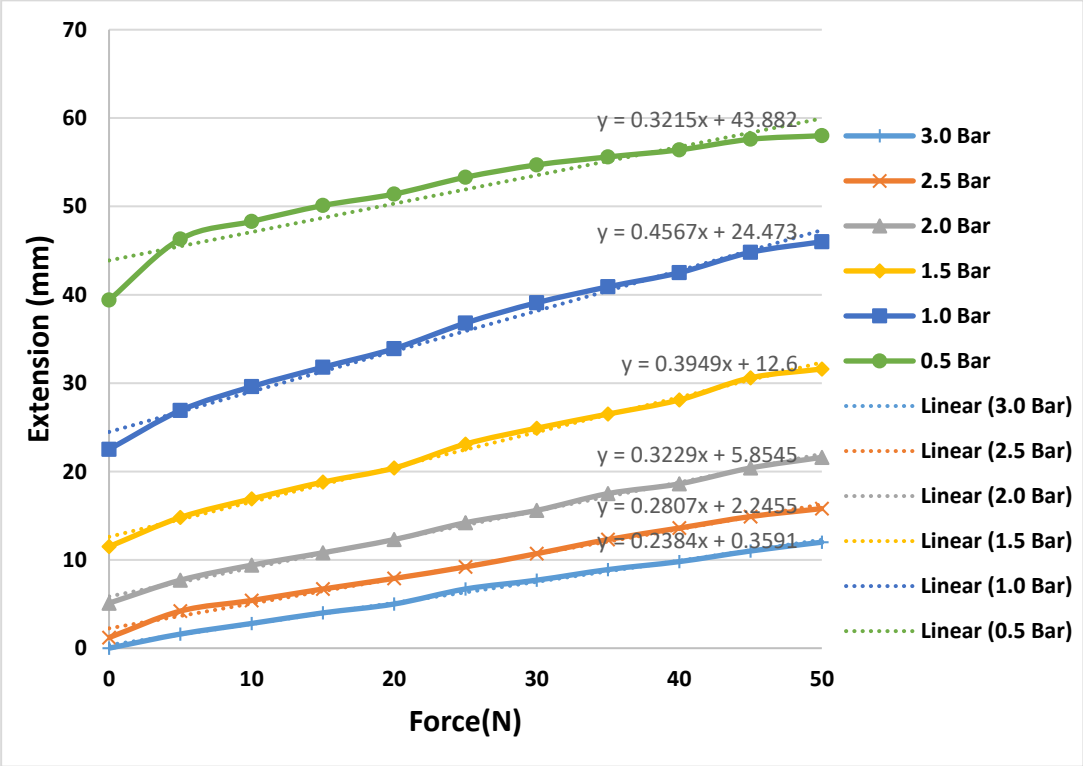

Figure 3-3: Force/displacement extensions for the contractor PMAs.

The dotted lines in figure (3-3) represent the linear approximation of the force/pressure characteristics of the contractor PMA. These lines are automatically generated using the Excel software application as a trend line, and they represent the best linear approximations to these nonlinear experimentally measured extensions. The gradients of the trend lines versus applied pressure are shown in figure (3-4).

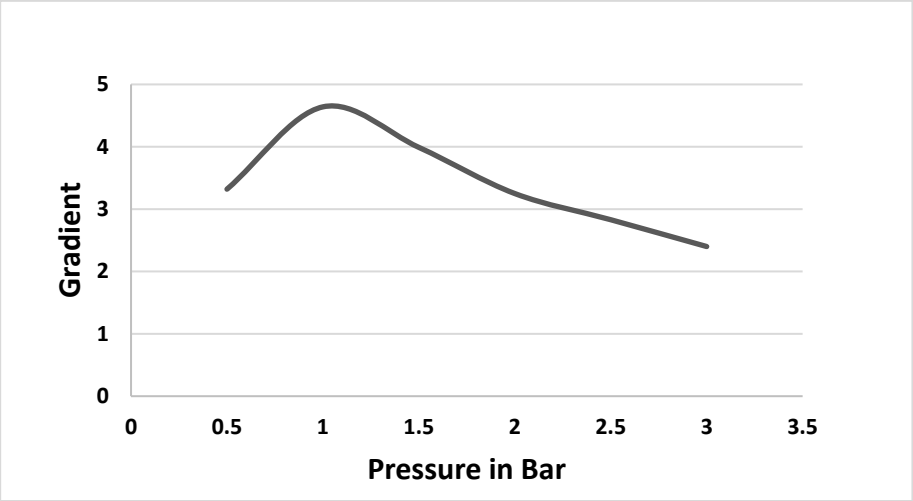

Figure 3-4: Gradient Vs. pressure for the contractor PMAs.

For the moment, we will ignore the value of slope at 0.5 bar as it is known that pneumatic muscles behave differently at low pressures. The reason for this is that a certain amount of pressure is required to inflate the rubber bladder. This is pressure that does not contribute to the actuator force. The gradient of the force to displacement lines appear to have an approximately linear relationship with pressure (except at 0.5 bars). Hence, the contractor PMAs can be modelled as springs according to Hook's low (Tsagarakis, N., & Caldwell, D., 2000):

$$F = k * X \qquad (3.3)$$

Where $\boldsymbol{F}$ represents the pneumatic muscle force, $\boldsymbol{k}$ is the spring constant and $\boldsymbol{X}$ represents the extension of the pneumatic muscle. In this case, the spring constant depends on the pressure, so equation (3.3) can be modified to:

$$F = P * \ kf * X \qquad (3.4)$$

Where P is the applied pressure, and kf is the actuator spring constant, which is a function of P. This constant will be selected (later) to obtain the best fit to the original force/displacement characteristics.

Therefore:

$$X = \frac{F}{P * kf} \qquad (3.5)$$

By using equation (3.5), the extension can be calculated for different applied pressures to the muscle, a graphical representation of which is shown in figure (3-5).

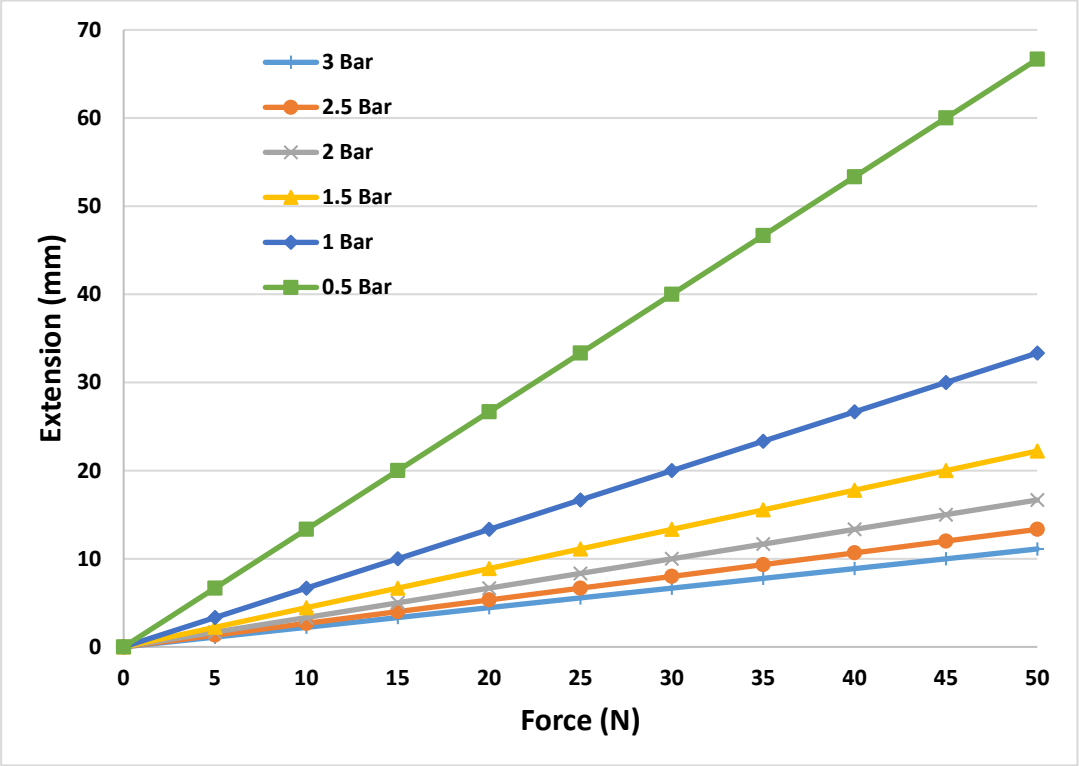

Figure 3-5: Calculated force/displacement characteristics for the extension of the contractor PMAs.

This basic model shows that the spring constant is higher at higher pressures. This basic model was good for Tsagarakis (Tsagarakis, N., & Caldwell, D., 2000) as they used large muscles. In large muscles, the frictional losses are low compared to the force the muscle generates. The reason for this is that the friction forces are low in comparison to the muscle force which is high. When they have no load, large muscles tend to reach their equilibrium point (54.7^{o}) in the braid angle at all pressures. However, in small muscles, like the one tested, the friction is more significant (meaning an unloaded muscle will not reach its equilibrium point at all pressures). This new model includes the offset from the equilibrium (54.7^{o}) in the braid angle point seen in small muscles as they are pressurised. This offset can be seen as the *Y*-intercept on the force/displacement plots in figure (3-3).

Although the lines in figure (3-5) have different gradients, unlike the real results, there is no offset on the *Y*-axis (which represents the displacement). This is because the model suggests that when there is no load on the muscle, it will reach maximum contraction at any positive pressure. Actual results show that this is not the case. Hence, the equation of the model is modified in order to account for this effect. Figure (3-6) shows the force offset according to the values of the *Y*-intercept from figure (3-3).

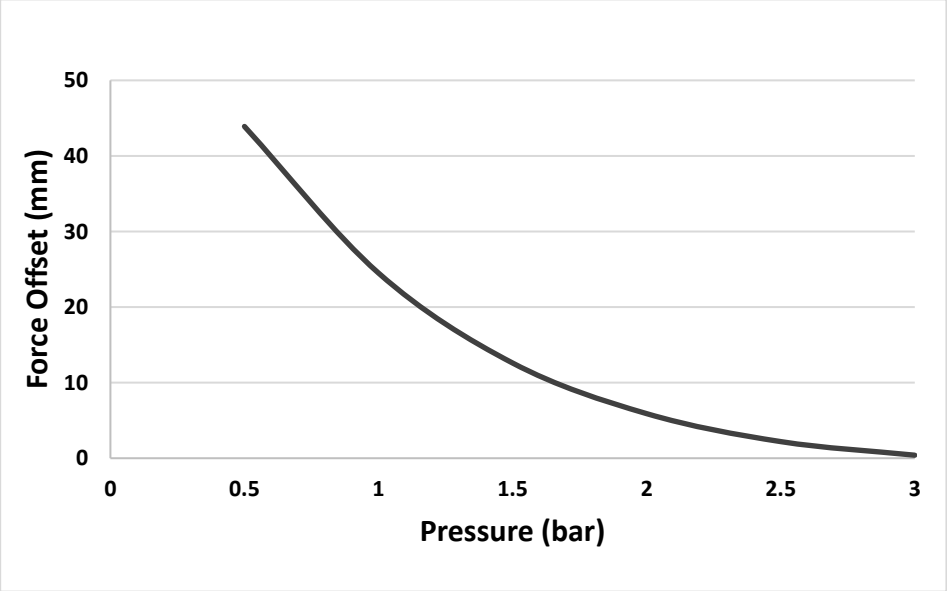

Figure 3-6: The force offset for the contractor PMA.

It is clear that there appears to be an inverse relationship between the pressure and the force offset, which can be modelled as:

$$Force\ Offset = \frac{1}{Ko * P} \qquad (3.6)$$

Where *P* is pressure and *Ko* is a constant.

However, the force offset is zero at 3 bar. Therefore, another constant (*XminPmax*) is added to the previous equation to become as follows:

$$Force\ Offset = \frac{1}{Ko * P} - XminPmax \qquad (3.7)$$

Appropriate values of *Ko* and *XminPmax* constants were selected to give the best match between experimental and modelled results, as shown in figure (3-7).

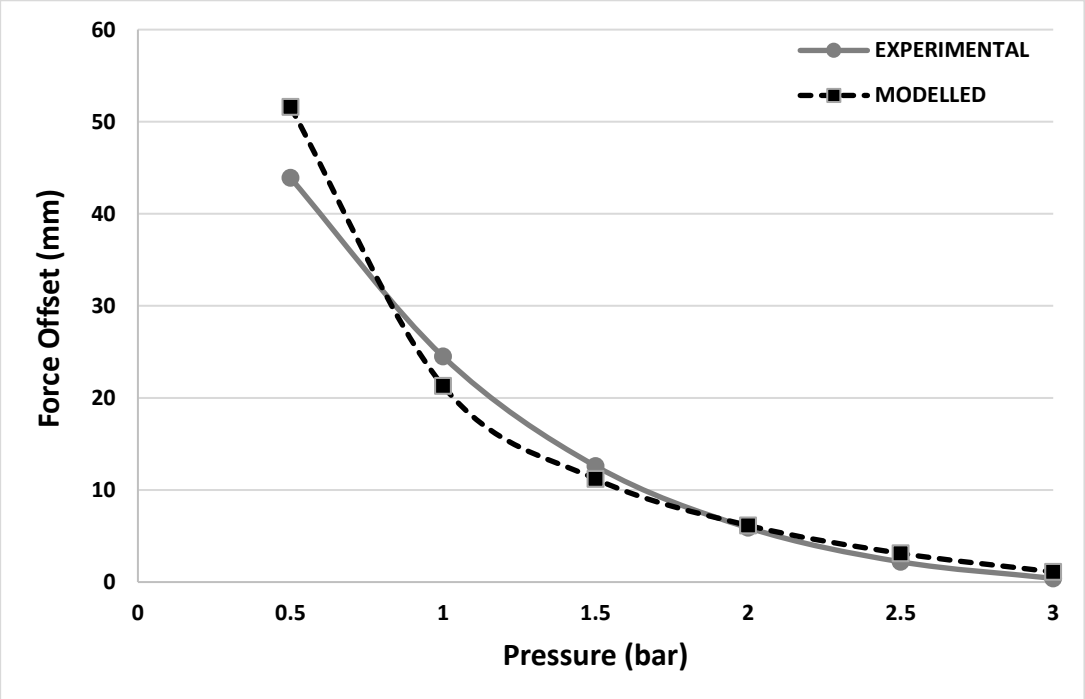

Figure 3-7: The modelled and the experimental force offset for contractor PMA.

Hence, to get a better model for the contractor PMA, the force offset must be included in the extension in equation (3.5).

The extension equation becomes:

$$X = \frac{F}{P * kf} + Force\ offeset \qquad (3.8)$$

The force offset and the extension of the contractor PMA are recalculated according to equations (3.7) and (3.8) for each pressure used in the experiment. Hence, by selecting ***kf*** = 1.5, ***ko*** = 0.033 and ***XminPmax*** = 9, the following modified calculated extension in the contractor PMA is as shown in figure (3-8).

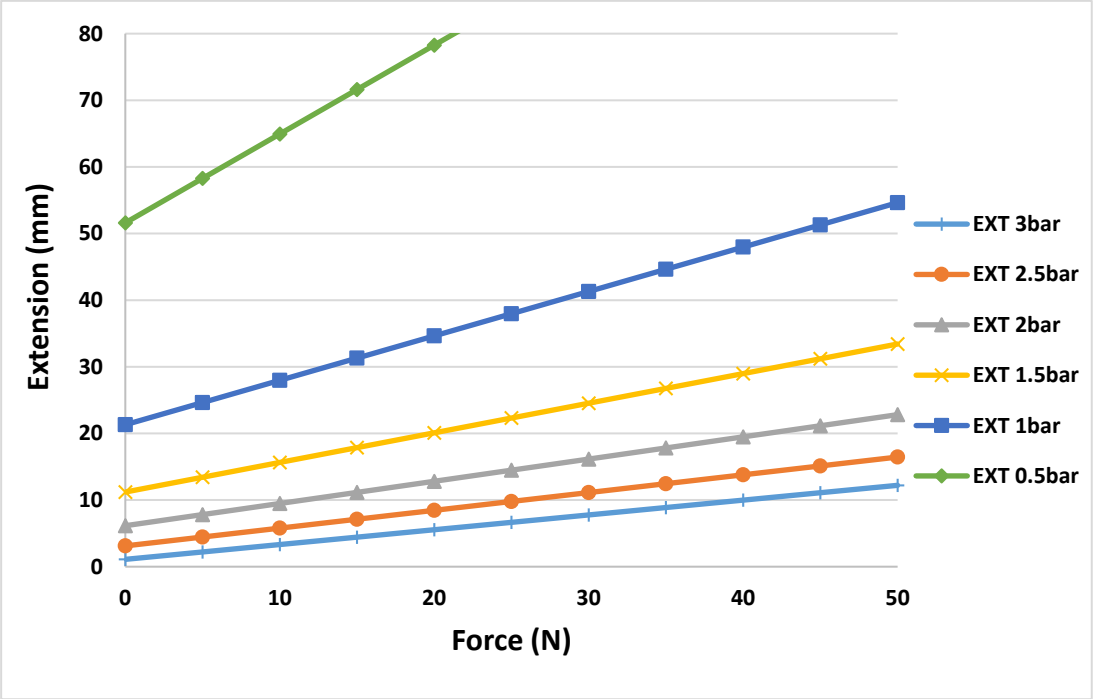

Figure 3-8: Calculated force/displacement extension for the contractor PMAs.

It is clear that this looks more like the trend line of the experimental extension of the contractor PMA, as per figure (3-3). Figure (3-9) shows the calculated (theoretical) and the actual (experimental) results when constants are adjusted to gain the best fit.

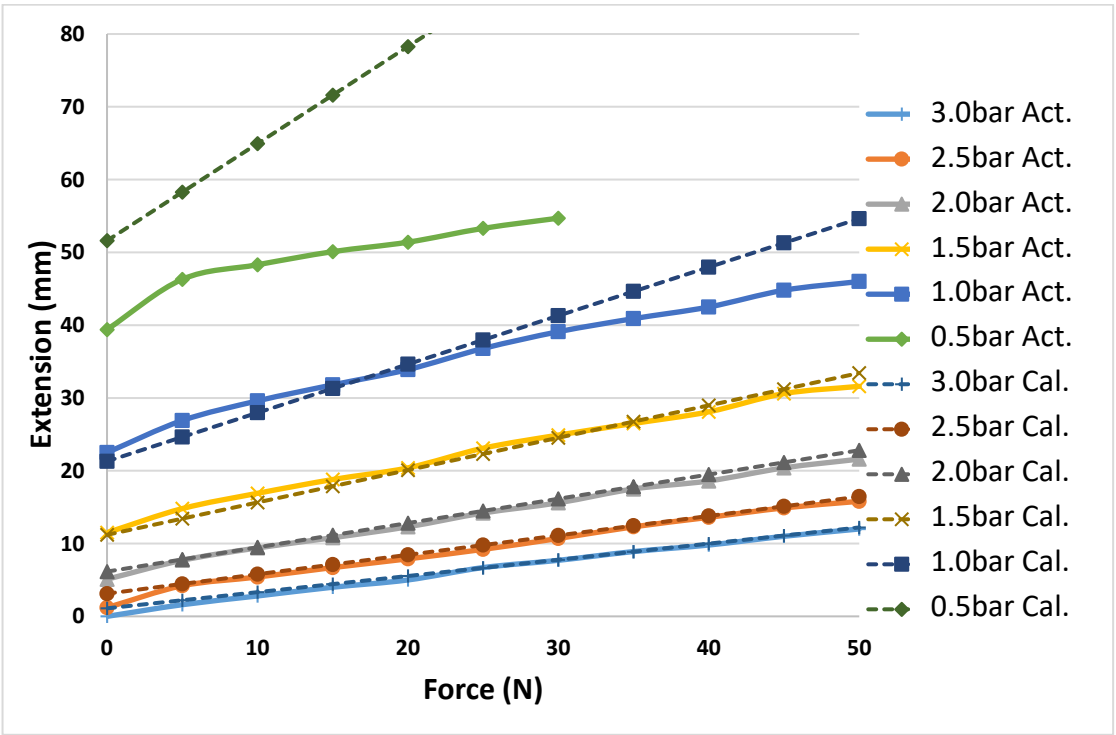

Figure 3-9: Actual and calculated models for the contractor PMA.

While the solid curves represent the experimental force/pressure characteristics of the contractor PMA, the dashed lines represent the calculated extension of the contractor PMA. The calculation was achieved according to the developed mathematical model of contractor PMA in equations (3.7) and (3.8). Hence, the mathematical model described by these equations provides a good representation to the experimental model of the contractor PMA at a pressure of 1.5 bar and greater, and can be used to predict the behaviour of the contractor PMA. Figure (3-5) shows the results using Tsagarakis's model comparing this to figure (3-9) it can be seen that the new model fits the experimental results much more precisely.

3.2.2 Pressure/Displacement Characteristics of the Contractor PMA

Another experiment was conducted for the contractor PMA to determine its pressure/displacement characteristics. This time, the attached weight (as a load) is kept constant and the applied pressure is adjusted during the test. The displacement characteristics of the contractor PMA also can be determined using equation (3.2). In the experiment a 1kg load was applied to the muscle. The displacement was then measured as the pressure was increased from zero to three bar and then reduced back to zero in 0.5 bar increments/decrements. This experiment was then repeated with a load of 2, 3, 4 and 5 kg respectively. The hysteresis behaviour also appeared in this experiment due to the same reasons of the previous experiment (friction between the rubber tube and the sleeve shell).

In the first experiment, the pressure is kept constant during each test and the attached weight (as force) is changed. In this experiment, the attached weight (force) is kept constant and the applied pressure is changed during each test. Figure (3-10) shows the resultant pressure/displacement characteristics for the contractor PMA when 1, 2, 3, 4 and 5 kg loads are attached, respectively. These loads will generate load forces of approximately 10, 20, 30, 40 and 50 N, respectively.

It is clear that there is no change in the overall behaviour of the contractor PMA in the two experiments. The extension is raised by increasing the applied pressure (first experiment) or reducing the attached load to the contractor PMA (second experiment).

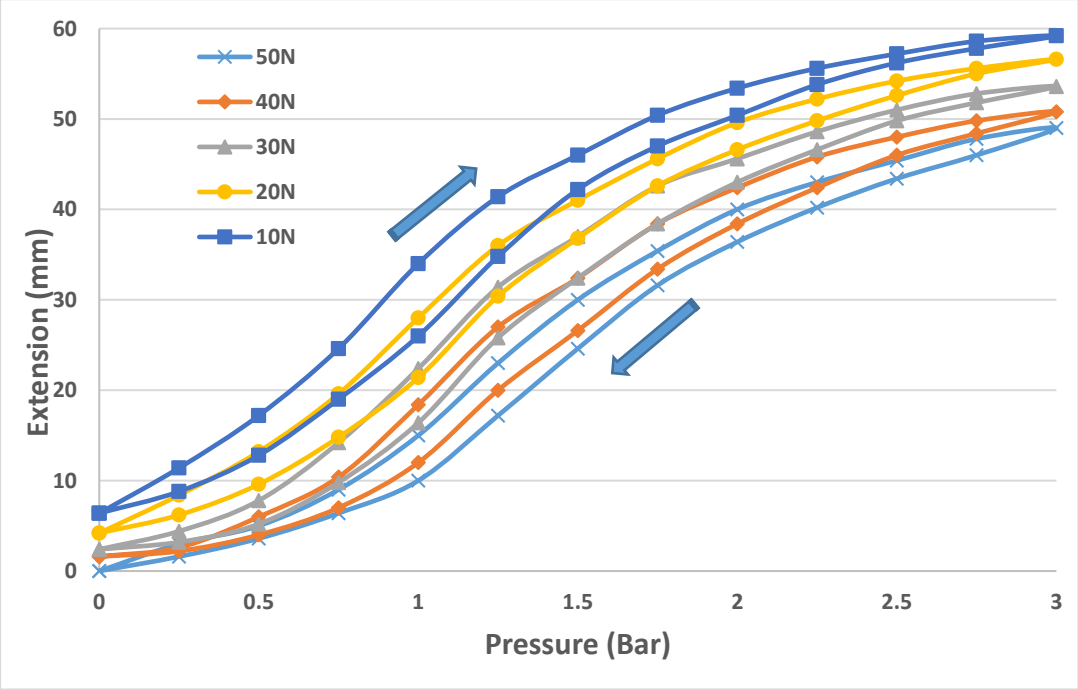

Figure 3-10: Pressure/displacement characteristics for the contractor PMAs.

Figure (3-10) shows the experimental results and the hysteresis is clear as described in (Davis, S., et al, 2006). Figure (3-11) shows the modelled results for this experiment with averaged extension values determined whilst increasing and decreasing the pressure to remove the associated hysteresis effect.

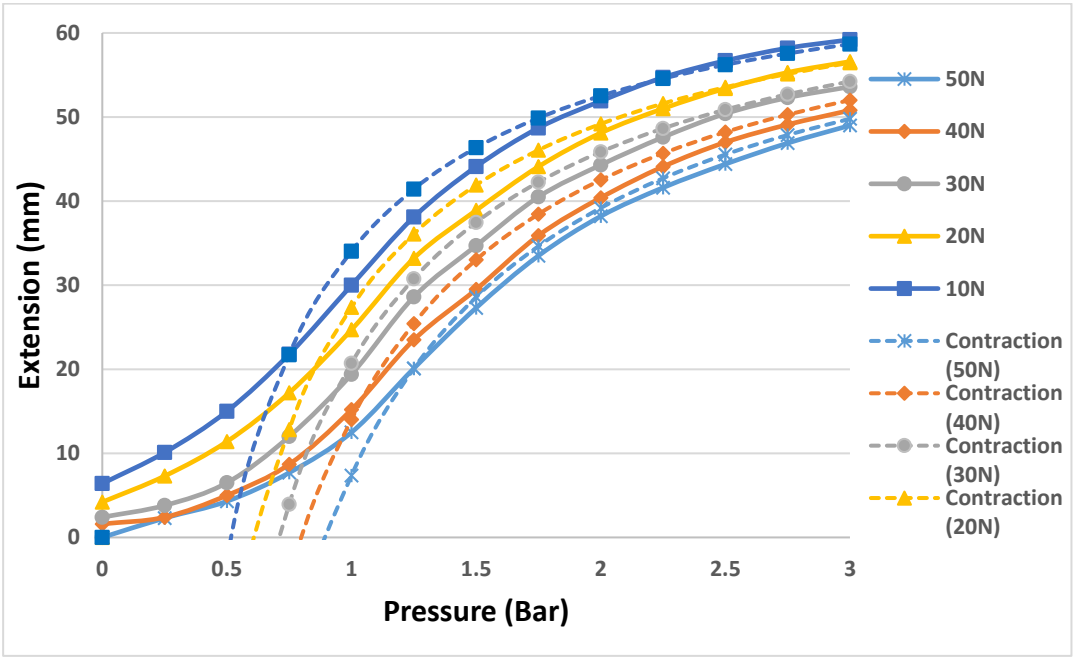

Figure 3-11: Actual and determined model for the contractor PMAs.

Figure (3-11) also demonstrates the suitability of the mathematical model developed in equations (3.7) and (3.8) to represent the behaviour of the contractor PMAs at pressures of 1.5 bar and above. Below 1.5 bar the pressure losses inflating the bladder means the model does not fit the data.

In the next section, the behaviour of the extensor PMA will be investigated using the same experimental techniques that used with the contractor PMA. Hence, two further experiments will be conducted to investigate the characteristics of, and to determine a mathematical model for, the extensor PMA.

3.3 Extensor Pneumatic Muscle Actuator Modelling

The relaxed length of the extensor PMA used in this section is designed as 160 mm, and the diameter is 30 mm. This length can be elongated to 200 mm, approximately, when 3 bar or greater pressure is applied, the diameter will reduced to about 20 mm in that pressure. To construct the pneumatic muscle as an extensor PMA, the angle of the braided cover shell when unpressurised must be greater than 54.7^o ($\Phi > 54^o44'$), as explained previously in section (2.4.1).

To determine the force/displacement and pressure/displacement characteristics for the extensor PMA, a group of experiments are conducted. During these experiments, tendon cables are used to attach a weight (force) to the extensor PMA. Three tendon cables were fitted (using cable ties) to the extensor PMA and used to attach the load force. These tendons were equally spaced around the muscle and attached to the free end. This meant that when a force was applied to the tendons it would compress the extensor muscle. These tendon cables are spooled, as well, around central terminals of three 10 kΩ linear potentiometers (displacement sensors) to give an indication of how far the extensor PMA extends/compresses during the experiment. The average of these three voltages, from three potentiometers, was considered to be the displacement of the extensor PMA. This is done to account for any buckling of the muscle during the experiment.

An Arduino microcontroller is used to measure the 10 kΩ linear potentiometers output voltage signals. The other two terminals of each 10 kΩ linear potentiometer are connected to +5 V and GND pins of the Arduino microcontroller board.

Figure (3-12) shows the experimental setup used to observe the force/displacement and pressure/displacement characteristics of the extensor PMA.

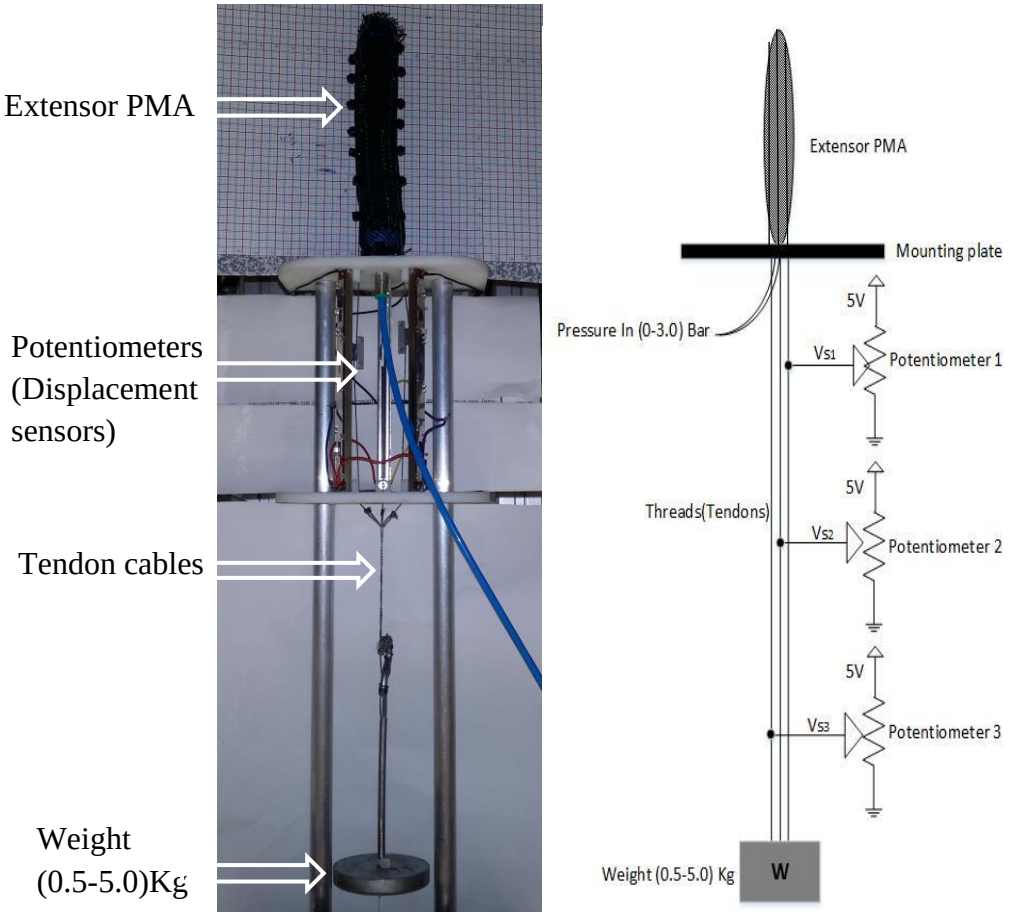

Figure 3-12: Extensor PMA observation experiment setup.

3.3.1 Force/Displacement Characteristics of the Extensor PMA

Constant pressure was applied to the extensor PMA, and the resultant displacement measured during the experiment for each change in the attached load (force). Initially, the extensor PMA was pressurised to 3 bar and the attached weight increased from 0 up to 5 kg in increments of 0.5 kg. These loads will generate load forces of approximately

0 up to 50 N, respectively. The displacement was measured at each step. Then, the attached weight was reduced to 0.0 kg in 0.5 kg decrements. The same experiment was conducted five more times by applying a different pressure to the extensor PMA in each instance, namely 2.5, 2, 1.5, 1 and 0.5 bar, respectively.

The displacement of the extensor PMA was calculated according to equation (3.2), as illustrated in section (3.2.1). The constant, *c*, in the equation represents the average of the initial values for the 10 kΩ linear potentiometer (sensors) voltages. To estimate a specific value for the constant *c*, a measurement has been performed without load and with 6.0 bar of pressure applied to the extensor PMA. Under these conditions, the value of the constant found as $c = 1.32$.

A graphical representation of the results is shown in figure (3-13). This graph shows the relationship between displacement and force when different pressures are applied to the contractor PMA. Again, to remove the effect of the hysteresis, the results obtained for the increasing and decreasing force experiments are averaged. The irregularities in the data for 0.5 and 1.0 bar are a result of the fact soft robots do not behave consistently. It is not felt that these are a feature of the system.

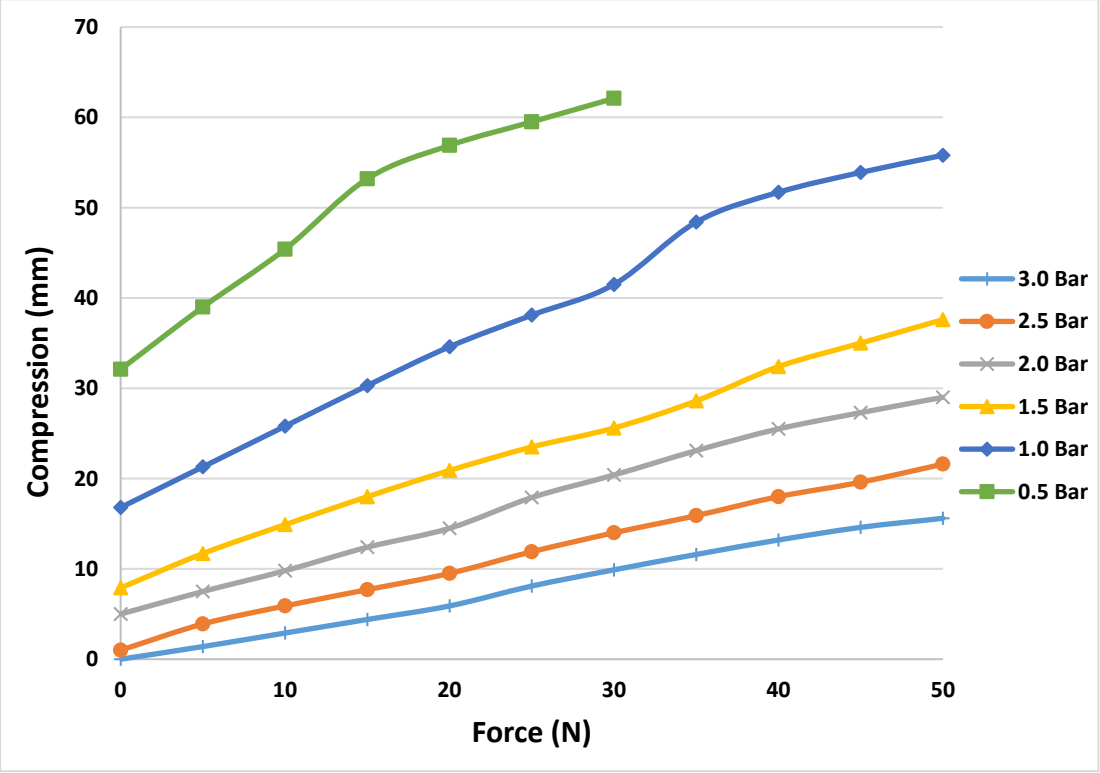

Figure 3-13: Force/displacement characteristics for the extensor PMAs.

The missing data for the 0.5 bar curve arose because when a low pressure is applied to the extensor PMA with a high load attached, there is not enough force to support the attached load.

Given the similarities between the contractile and extensor muscles, a variable stiffness spring mathematical model will again be considered to describe the behaviour of the extensor PMAs, as has already been done for the contractile muscles.

The above result represents a compression of the extensor PMA when a force is applied. For the extensor PMA, the behaviour is similar to that of a compression spring when a force is applied. Hence, the contraction of the extensor PMAs when the force applied is taken into consideration. The maximum possible extension was calculated at no load and at a pressure of 6.0 bar applied to the extensor PMA.

Figure (3-14) shows both the lines of best fit and the actual behaviour of the extensor PMA during the experiment. The same procedure as used in section (3.2.1) is used again to develop a mathematical model for the extensor PMA.

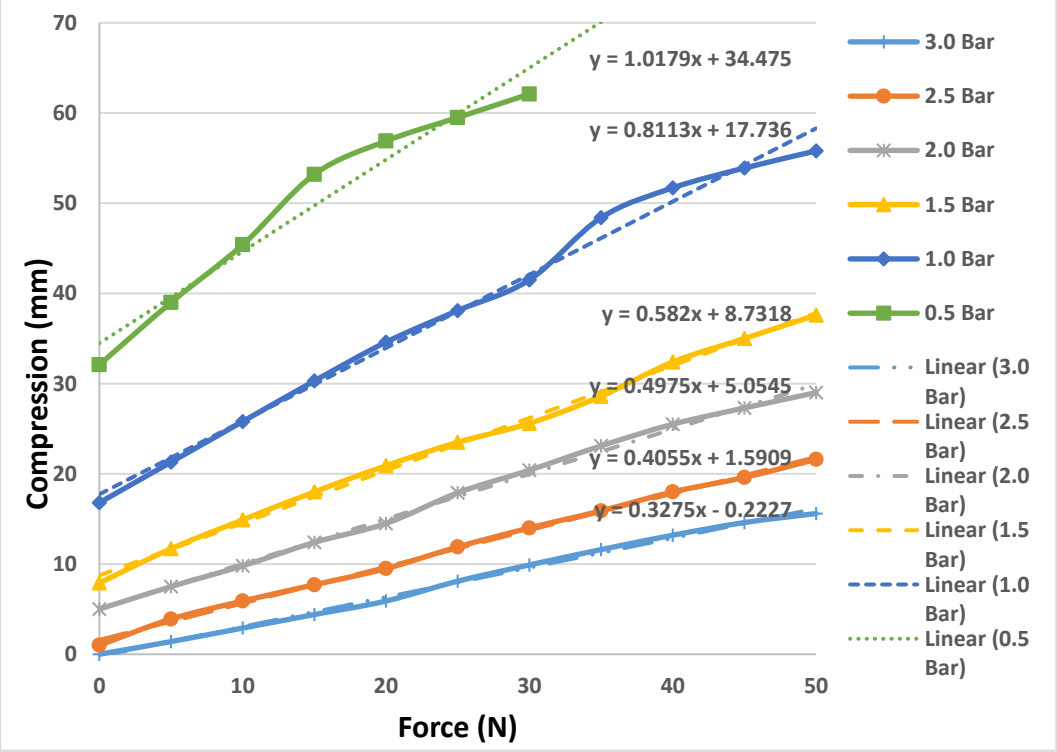

Figure 3-14: Linear fit and actual force/displacement characteristics for the extensor PMAs.

Figure (3-15) shows a combination of the calculated mathematical model representation and the actual force/displacement characteristics.

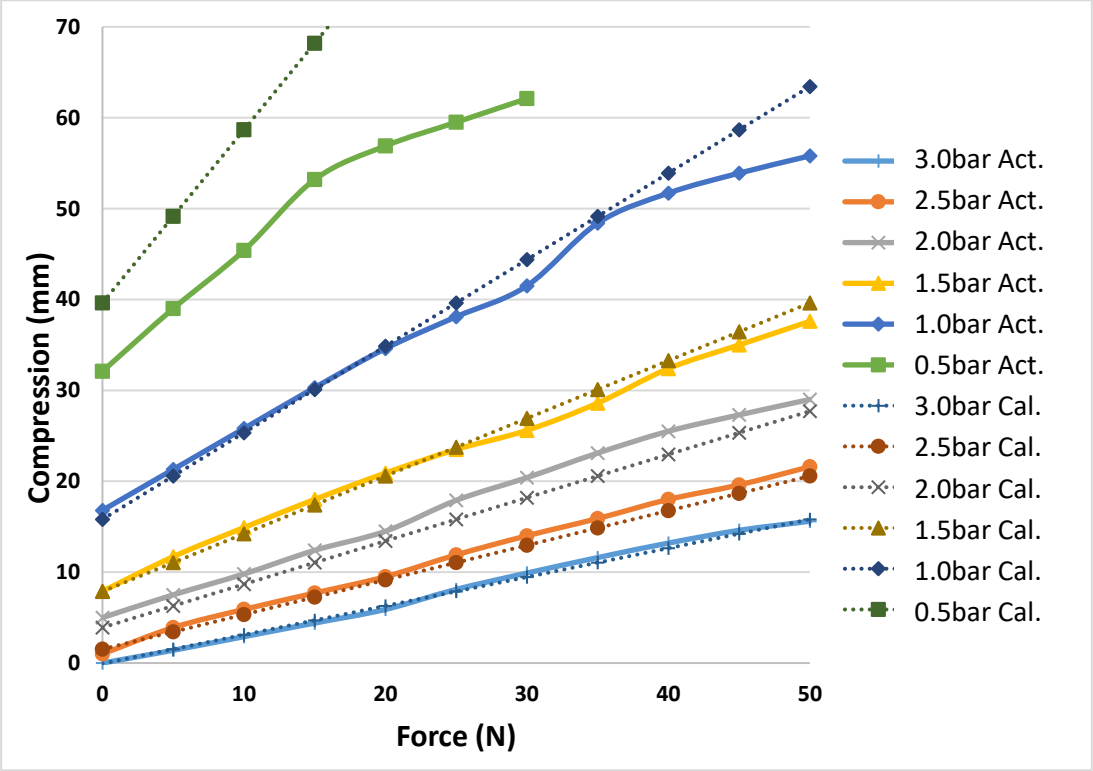

Figure 3-15: Actual and calculated model for the extensor PMA.

The solid curves in figure (3-15) represent the experimental force/pressure characteristics for the extensor PMA. The dotted lines represent the calculated model for the extensor PMA. Hence, the mathematical model described in equations (3.7) and (3.8) provide good fits to the behaviour of the extensor PMA at pressures of 1.0 bar and greater due to pressure loss in inflating bladder. Then, the developed model can be used to predict the behaviour of the extensor PMA. The parameter values in equations (3.7) and (3.8) are selected as ***kf*** = 1.05, ***ko*** = 0.042 and ***XminPmax*** = 8 to provide a good fit between the proposed mathematical model and the actual behaviour of the extension PMA.

3.3.2 Pressure/Displacement Characteristics of the Extensor PMA

Another experiment was conducted to determine the pressure/displacement characteristics of the extensor PMA. During this experiment, the load (force) was kept constant, and the applied pressure adjusted in each of six tests. The displacement of the

extensor PMA was determined using equation (3.2). The experiment was repeated for loads of 1.0 kg to 5.0 kg in increments of 1.0 kg. These loads will generate load forces of approximately 10, 20, 30, 40 and 50 N, respectively. The pressure applied to the extensor PMA was changed from 0.0 up to 3.0 bar then back to 0.0 bar in 0.5 bar increments/decrements during each test.

Note that there is no change in the overall behaviour of the extensor PMA in either experiment. The extension is augmented by increasing the applied pressure or by reducing the load attached to the extensor PMA. While the mathematical model can be developed using either of these two experimental results, using the force/displacement data from the first experiment is more accurate because there is a possibility of human error during manual selection of the applied pressure in the second experiment. A manual pressure regulator was used during the second experiment to change the applied pressure to the extensor PMA. In addition, in this case hysteresis behaviour can be observed.

Figure (3-16) shows the resultant pressure/displacement characteristics of the extensor PMA. To remove the effect of the hysteresis, the results for increasing and decreasing pressure are averaged.

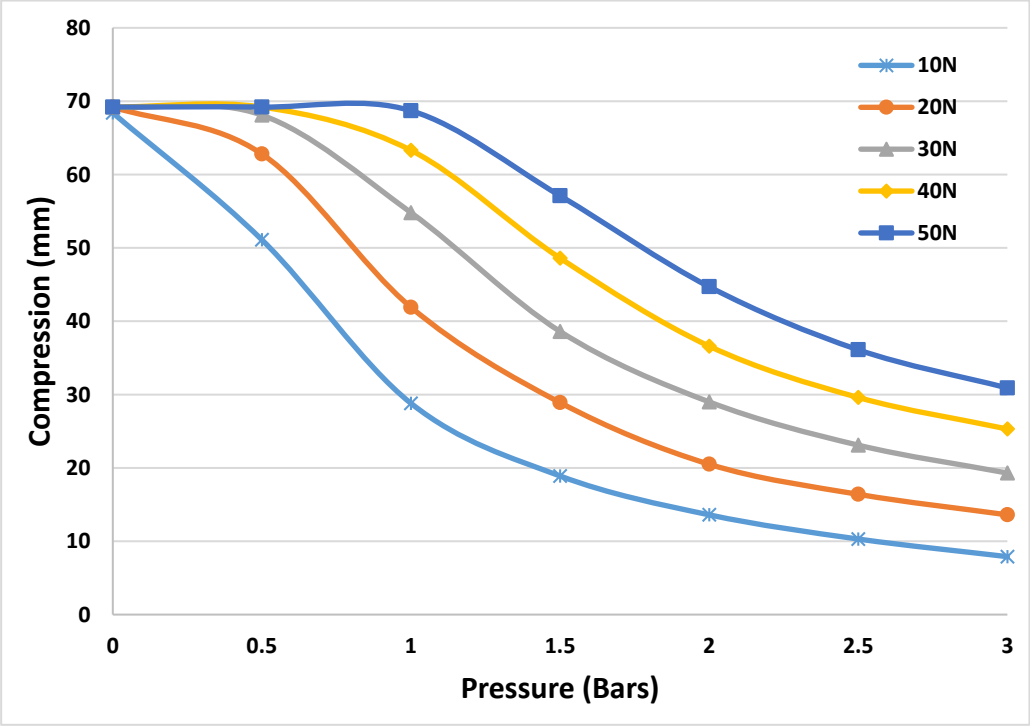

Figure 3-16: Pressure/displacement characteristics for the extensor PMAs.

3.4 Variable Stiffness Characteristics Investigation for the Pneumatic Muscle Actuators

The importance of variable stiffness can be simply stated as the reality that a stiff robot's performance can be controlled easily; however, to directly interact in a safe manner with a human requires the stiffness of the robot be reduced. Hence, developing a continuum soft robot arm with the ability to change its stiffness during operation will be a huge step forward in the development of future robots.

The fingers of the proposed pneumatic muscle-based continuum soft robot end effector consists of three contractor muscles and a single extensor muscle, as shown in figure (3-17).

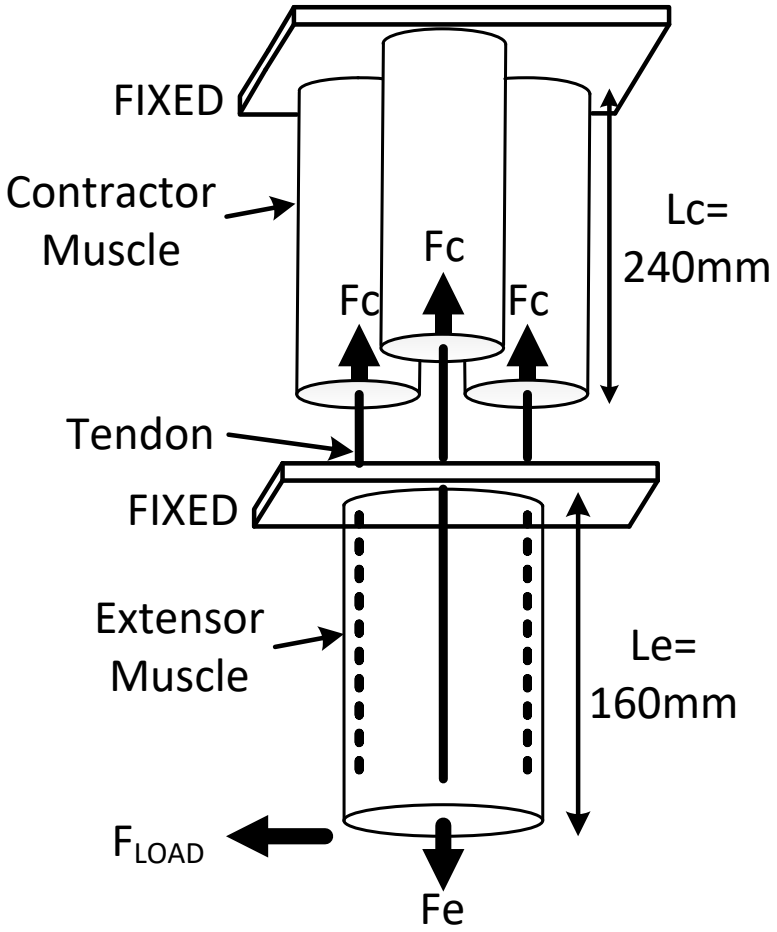

Figure 3-17: Bending stiffness experimental configuration.

These fingers take their shape when pressure is applied, and bend in proportion to the actuation magnitude of the contractor PMAs. The stiffness of a pneumatic muscle is directly proportional to the air pressure inside it. In the proposed end effector, the contractor PMAs constantly act in an antagonistic manner against the extensor PMAs. That is, if the pressure in the extensor muscle is increased then to maintain the same finger position the pressure in the contractor muscles must also be increased. The higher pressure in both the contractor and extensor PMAs will increase the overall stiffness of the finger. This section explores the variable stiffness capability of the PMAs.

Low pressure in both the extensor and contractor PMAs allows for a very soft robot end effector. On the other hand, if high pressure is applied to both extensor and the contractor PMAs then the end effector becomes much stiffer. The stiffer end effector is desirable when precise control is required. Theoretically, there are infinite arrangements of the pressures that may be used in the proposed soft robot end effector to vary its stiffness.

While the length of the extensor PMA is increased by raising the input pressure, increasing the pressure in the contractor PMA will reduce its length. This contraction will affect the elongation of the extensor PMA because the two muscles are connected by tendon cables. These tendons are used to control the bending of the fingers as well. Due to this interplay between the muscles, the maximum length that the extensor PMA can reach is 195 mm. This length can be achieved by applying 1.0 bar or more of pressure to the extensor PMA with the contractor PMA either completely unpressurised or at a very low pressure.

The test rig used to analyse the bending stiffness of the extensor PMA can be seen in figure (3-18). The soft robot end effector was suspended vertically so the finger is pointing downwards. A tendon was then attached to the fingertip, which was passed over a pulley to a load. As the load is increased, the horizontal force applied to the fingertip increases and this results in a lateral displacement of the fingertip. This displacement could then be measured and lateral finger bending stiffness calculated for a range of extensor muscle pressures. A moveable aluminium pulley was used to control the direction of the cable and thus the applied force. The pulley's height was adjusted

in each step. A laser pointer fitted to the end of the extensor PMA is used to give an indication of the displacement by directing the beam onto a piece of graph paper.

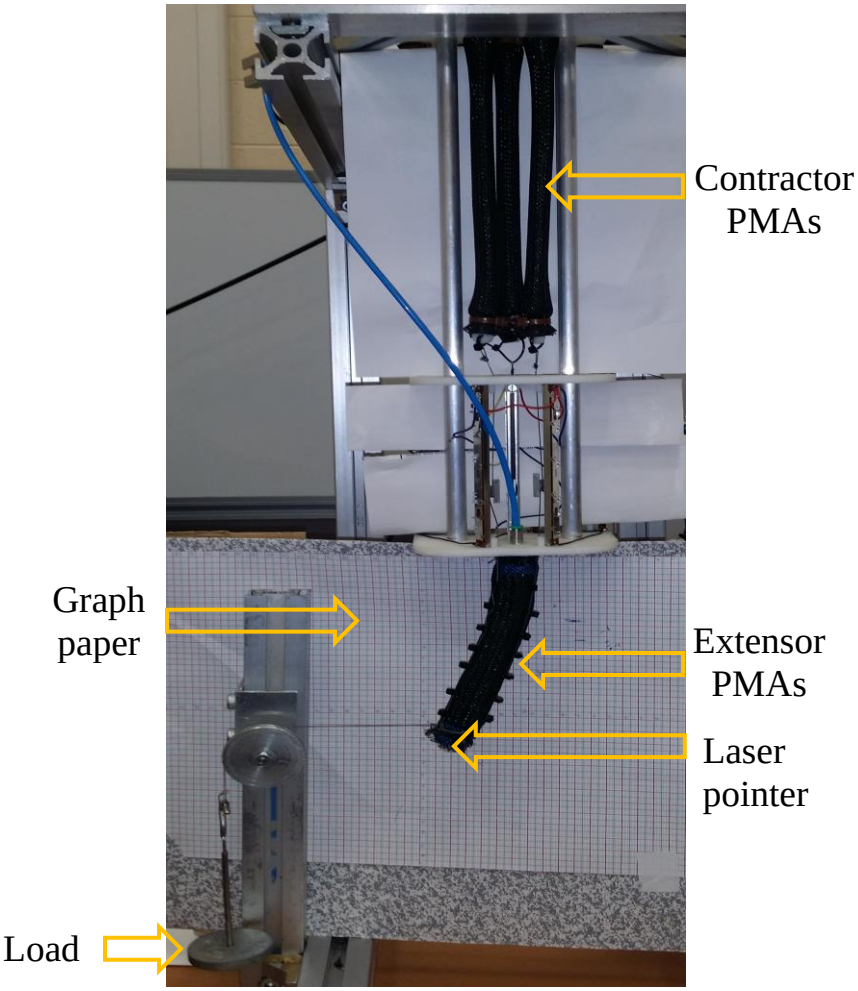

Figure 3-18: Stiffness determination experimental rig.

The experimental procedure was started by venting all air from the contractor muscles and then using the manual pressure regulator to set the pressure in the extensor muscle to the required test pressure. This will generate a force, Fe, and result in the extensor muscle, finger, increasing in length. A second pressure regulator was then used to increase the pressure in the three contractor muscles. All three contractor muscles were connected to the same regulator and so produced the same contractile force, Fc, as shown in figure (3-17). These forces acted, via the tendons, antagonistically against Fe and resulted in a reduction in the length of the extensor muscle, Le. The pressure in the contractor muscles was increased so that the finger length, Le, was equal to that required for the specific bending stiffness experiments described below.

The first bending stiffness experiment was conducted with a finger length of 190 mm. The pressure in the extensor muscle was set to 1 bar, and the pressure in the contractor muscles was then raised to 0.5 bar until the finger reduced in length to 190 mm. Lateral loads (F_{LOAD}) were then applied to the fingertip in 0.98 N increments up to a maximum of 9.8 N, and the lateral displacement of the finger was then recorded. The experiment was then repeated with extensor muscle pressures of 2, 3 and 4 bar and the contractor muscles pressures of 0.6, 0.9 and 1.0 bar respectively to keep the length of the finger at 190 mm. Each experiment was repeated multiple times and an average value determined. Figure (3-19) shows the experimental results. As might be expected, as the force is increased the lateral displacement of the finger also increases. It can also be seen that when the extensor muscle is at higher pressures, the lateral force needed to displace the fingertip is higher than that when a lower pressure is used.

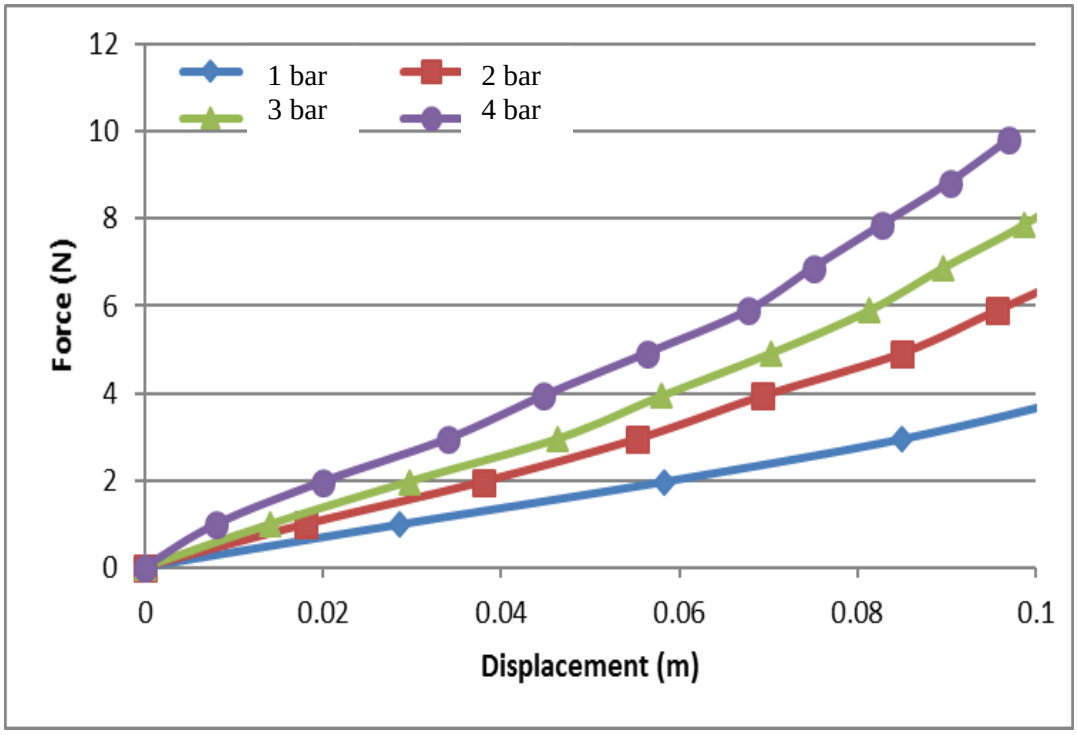

Figure 3-19: Lateral finger displacement as load increases at a finger length (Le) of 190 mm at increasing extensor pressures.

To determine if the length of the finger had an effect on its bending stiffness the experiment was repeated with an extensor muscle/finger length of 180 mm. The results of this experiment are shown in figure (3-20).

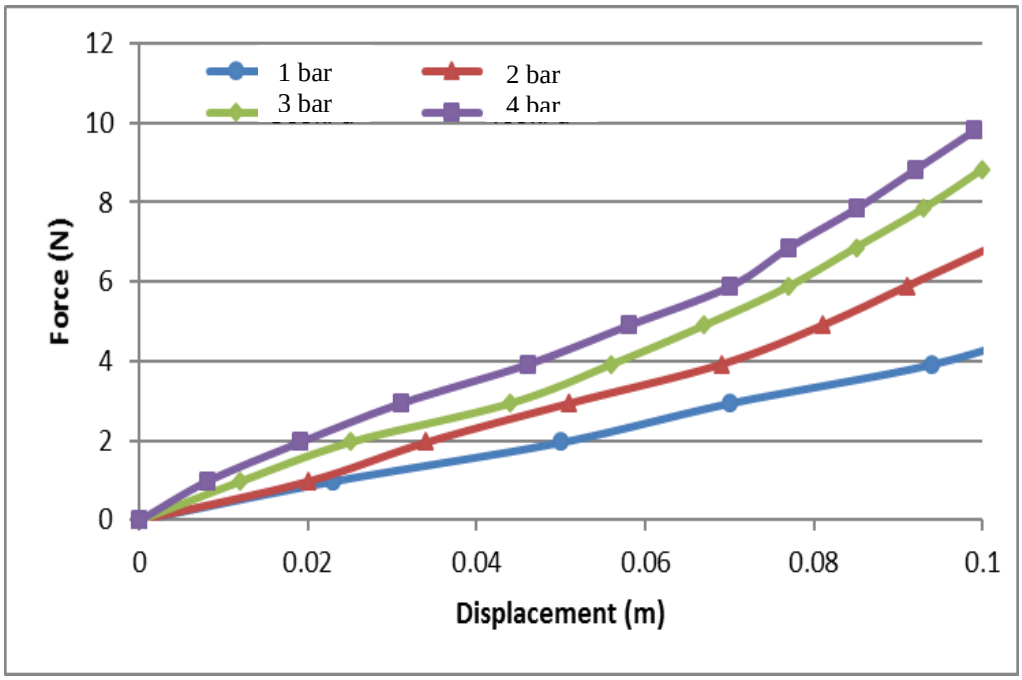

Figure 3-20: Lateral finger displacement as load increases at a finger length (Le) of 180 mm at increasing extensor pressures.

From the experimental results described above, it is possible to determine a bending stiffness value for each of the experiments. This was achieved by producing a linear approximation for the experimental results. The stiffness is calculated according to the following equation:

The compliance of the system is:

$$Compliance = \frac{Displacement}{Force} \qquad (3.9)$$

Moreover, the stiffness is:

$$Stiffness = \frac{1}{Compliance} \qquad (3.10)$$

At a finger length of 190 mm, the bending stiffness of the finger is increased from 36 N/m at an extensor/contractor pressures of 1.0/0.5 bar to 96.9 N/m at a pressure of 4.0/1.0 bar respectively. For a finger length of 180 mm, the stiffness increased from 43 N/m at an extensor/contractor pressure of 1.0/0.8 bar to 93 N/m at a pressure of 4.0/1.6 bar respectively. Figure (3-21) shows the bending stiffness of the extensor PMA/finger.

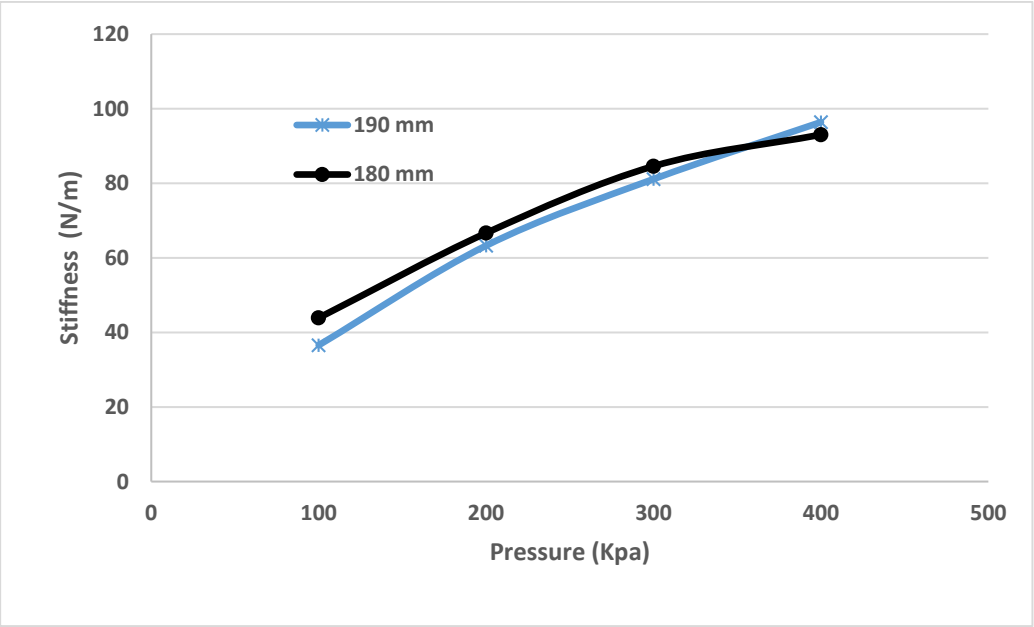

Figure 3-21: Bending stiffness for the finger at lengths of 190 mm and 180 mm.

Figure (3-22) shows the percentage increase in finger bending stiffness as the pressure in the extensor muscle was increased. It can be seen that increasing the extensor pressure to 4 bar results in an increase in stiffness of 163% for a 190 mm finger and 112% for a 180 mm finger.

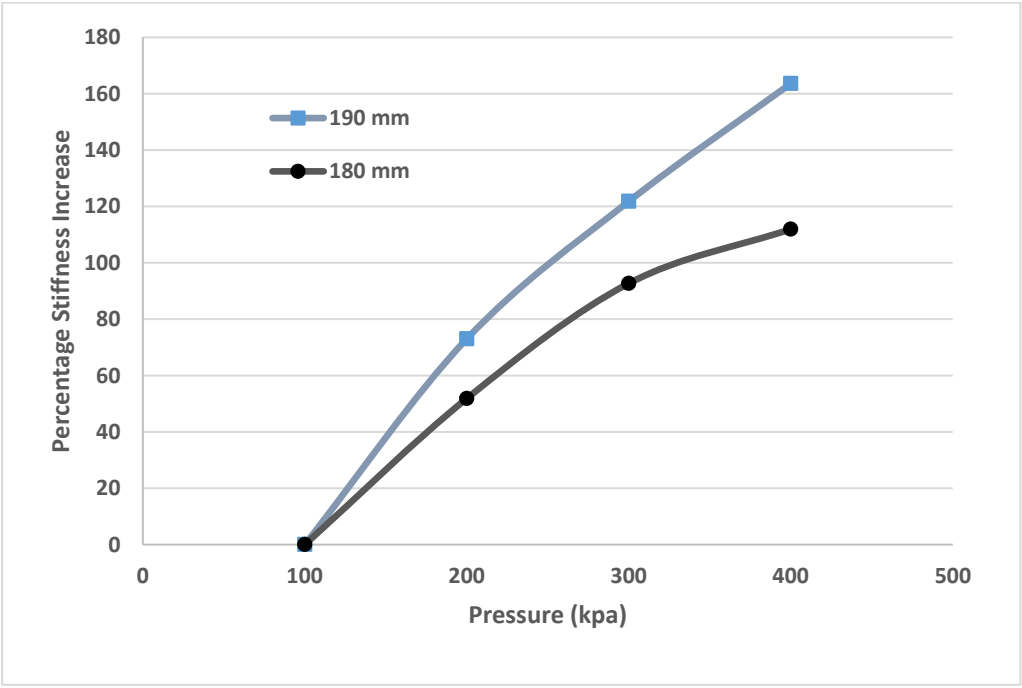

Figure 3-22: Percentage increase in finger bending stiffness as extensor muscle pressure increased.

It can be seen that the results are broadly similar for both finger lengths. However, the bending stiffness of the finger was fractionally higher at a finger length of 180 mm than a finger length of 190 mm. This result is not, however, unexpected. The force generated by a pneumatic muscle is a function of both pressure and contraction. For a contractor muscle, the force is proportional to muscle pressure and inversely proportional to muscle contraction. For an extensor muscle, force is proportional to muscle pressure and inversely proportional to muscle extension. This means that in the second experiment, for the same pressure, the extensor muscle will generate a higher force (as it will extend less). This means that the contractor muscles acting antagonistically will need to generate a larger force, requiring them to have a higher pressure than in the first experiment. Indeed, this was observed during the experiment. A pneumatic muscle can be considered to be a variable stiffness spring with the spring constant being proportional to the pressure inside the muscle. Therefore, in the second experiment, the contractor muscles would be stiffer. When a lateral force was applied to the finger, this pulled the tendons and extended the contractor muscle. As the muscle was stiffer than that in the first experiment, the displacement would be expected to be less (as, in fact, was observed). Although not tested experimentally, the axial stiffness of the finger will also increase. This is due to the higher pressures in all the muscles and the fact they are all producing a high force. Displacing these muscles would therefore require a greater force.

3.5 Granular Jamming Variable Stiffness Characteristics Investigation

The second proposed method to allow the soft robot end effector to change its stiffness is the use of granular jamming. Variable stiffness joints based on the use of granular jamming materials are discussed in section (2.3.7) of this thesis. In addition, the implementation and performance evaluation of the granular jamming continuum soft robot arm is illustrated in detail in section (2.6.5). Furthermore, granular jamming universal grippers' construction and operational characteristics are reported in section (2.7.3). It was found that the continuum soft robots that use granular jamming materials have the capability to change their stiffness during operation.

A granular jamming continuum finger was constructed to investigate the variable stiffness capabilities experimentally. Figure (3-23) shows the materials used to construct the granular jamming continuum finger.

Figure 3-23: The parts of the granular jamming finger's prototype.

The rubber bladder in figure (3-23) formed the cover of the granular jamming continuum finger and was used to contain all the granular materials. The granular material used in this prototype is rice. The plug, fitting and adapter were used to close the two ends of the plastic tubing. One of the ends was also used to admit air in and out of the granular jamming continuum finger. A foam plug was used in the air inlet plug to prevent granular materials leaking out during operation of the vacuum valve. A woven nylon shell was used as the outer layer of the granular jamming continuum finger; it is the braided shell, which is not needed in this finger construction. However, it is added here to allow tendon cables to be attached, as will be discussed further in later chapters of this thesis, it does not add any force to the actuator.

The system is compliant because the granular materials are able to move. However, when vacuum is applied, the grains are pressed together and friction makes it harder for them to move so the finger becomes stiffer; see figure (3-24).

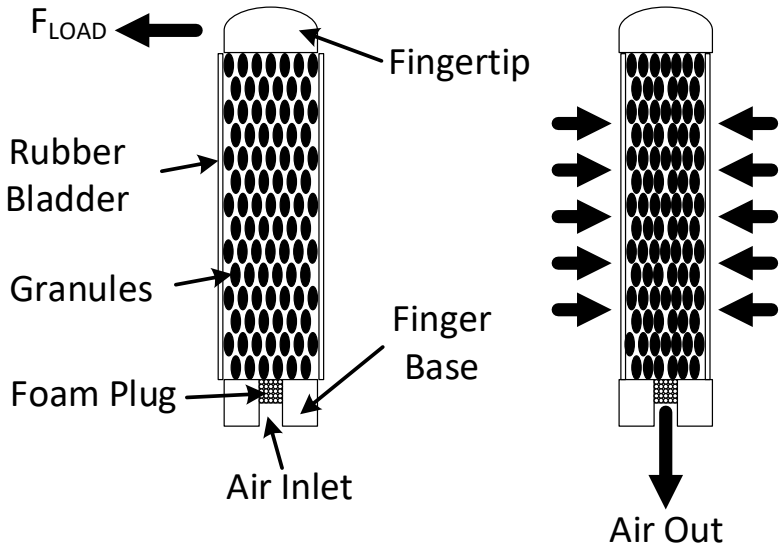

Figure 3-24: Bending stiffness experimental procedure for the granular jamming continuum finger.

Figure (3-25) shows an image of the complete granular jamming continuum finger.

Figure 3-25: The developed granular jamming continuum finger.

The test rig used to analyse the bending stiffness of the fingers can be seen in figure (3-26). The granular jamming continuum finger was suspended vertically to the desk, pointing upwards. A tendon cable was then attached to the fingertip which passed over a pulley to a load. As the load increased, the horizontal force applied to the fingertip is increased, resulting in a lateral displacement of the fingertip. This displacement could then be measured and lateral finger bending stiffness calculated for a range of granular

jamming continuum finger pressures. An aluminium pulley was used to control the direction of the tendon cable and thus the applied force. The pulley's height was adjusted in each step to minimise the effect of vertical component of the force. The displacement of the fingertip was measured manually, using callipers, by measuring the movement of the tendon relative to a fixed point on the test rig which is shown in figure (3-26).

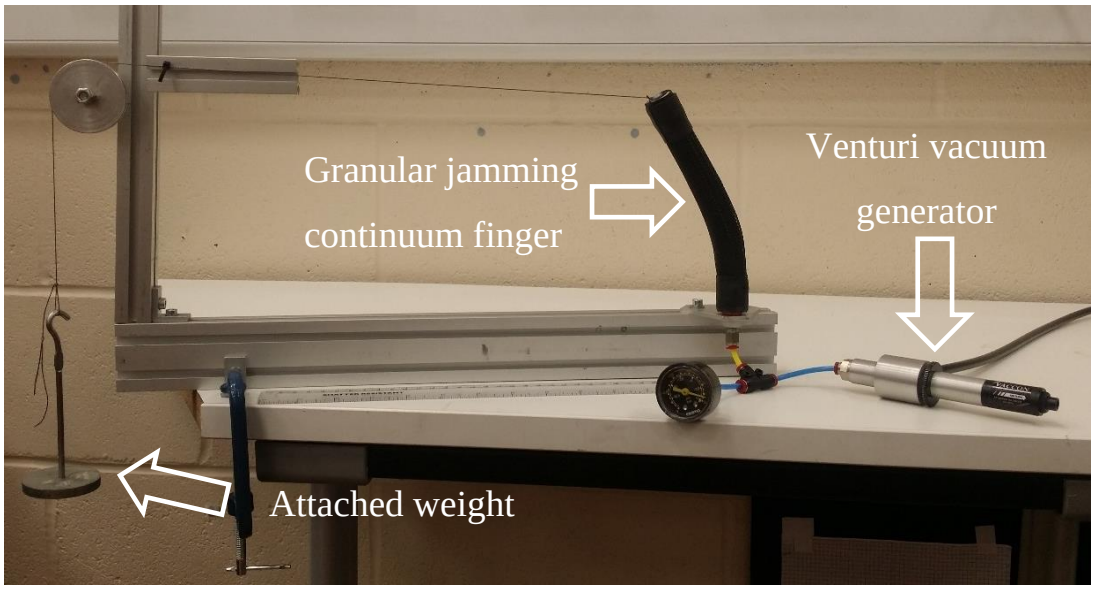

Figure 3-26: The granular jamming continuum finger experimental rig.

The experimental procedure began by venting air from the granular jamming continuum finger using the venturi vacuum generator shown in figure (3-26) to increase the stiffness of the granular jamming continuum finger. The pressure inside the granular jamming continuum finger was set to be 0.0 bar down to -0.8 bar in decrements of -0.2 bar in each experiment.

The attached weight, which is applied horizontally to the granular jamming continuum finger, started from 25 grams and was increased to 150 grams in increments of 25 grams in each step of the experiment. This will generate a force, F_{Load}, applied horizontally to the granular jamming continuum finger to force it to bend. The experiment was repeated five times to increase the reliability of the results; an average was then taken over these results. Figure (5-27) shows the force/displacement characteristics for the granular jamming continuum finger.

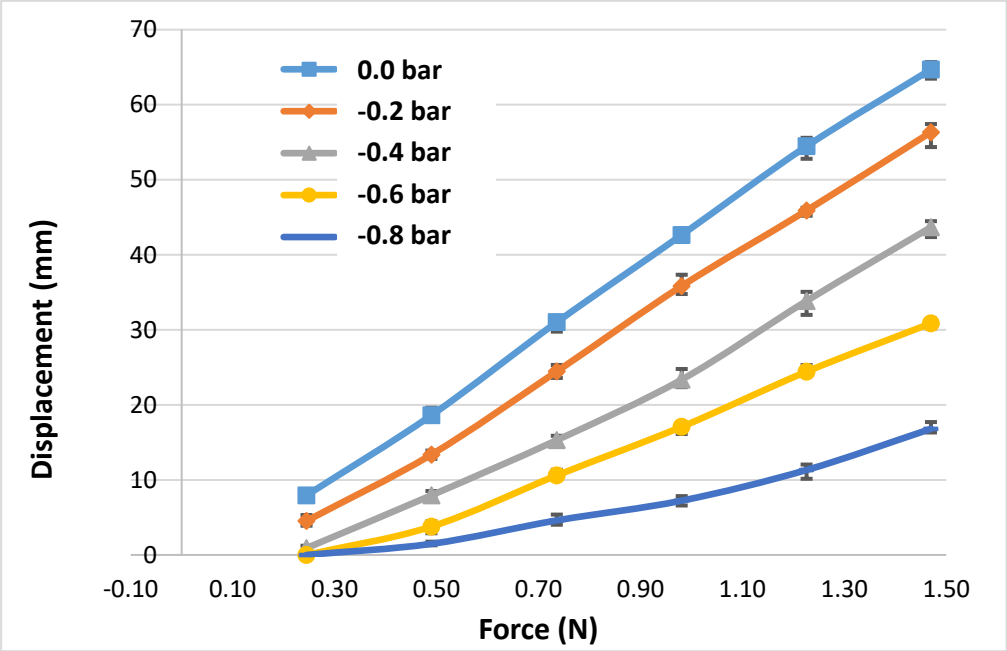

Figure 3-27: Force/displacement characteristics for the granular jamming continuum finger.

Lines of best fit were found for the above curves in order to calculate the bending stiffness of the granular jamming continuum finger experimentally. The bending stiffness for the granular jamming continuum finger can be calculated by taking the gradient of each best fit according to equations (3.9) and (3.10). Figure (3-28) shows the bending stiffness of the granular jamming continuum finger.

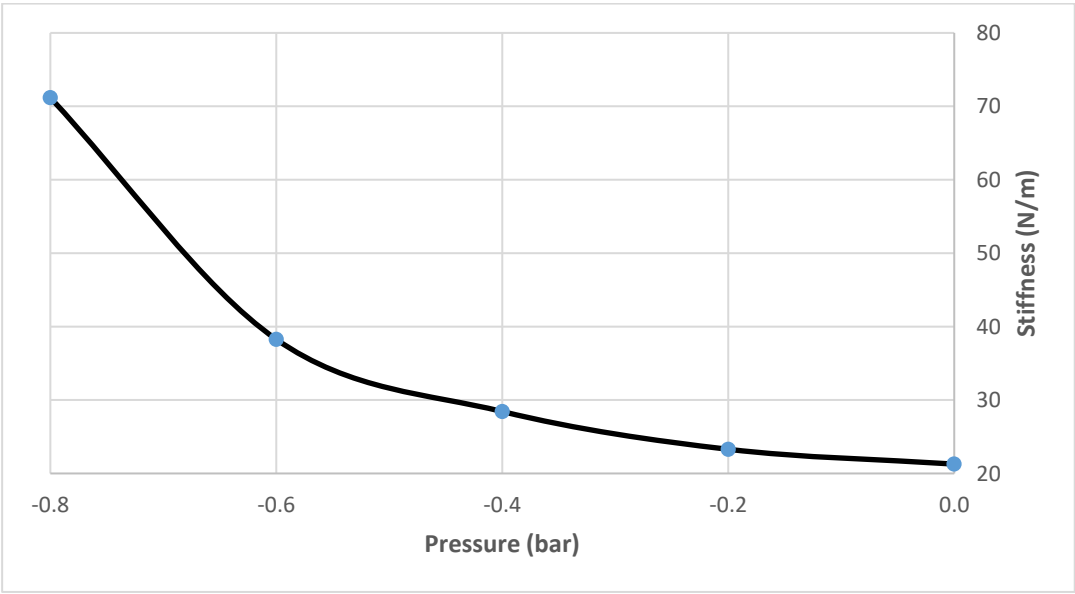

Figure 3-28: Bending stiffness for the granular jamming continuum finger.

Figure (3-29) shows the percentage increase in the granular jamming continuum finger bending stiffness as the pressure in the continuum actuator is decreased. It can be seen that decreasing the granular jamming continuum finger pressure to -0.8 bar results in an increase in stiffness of 235%.

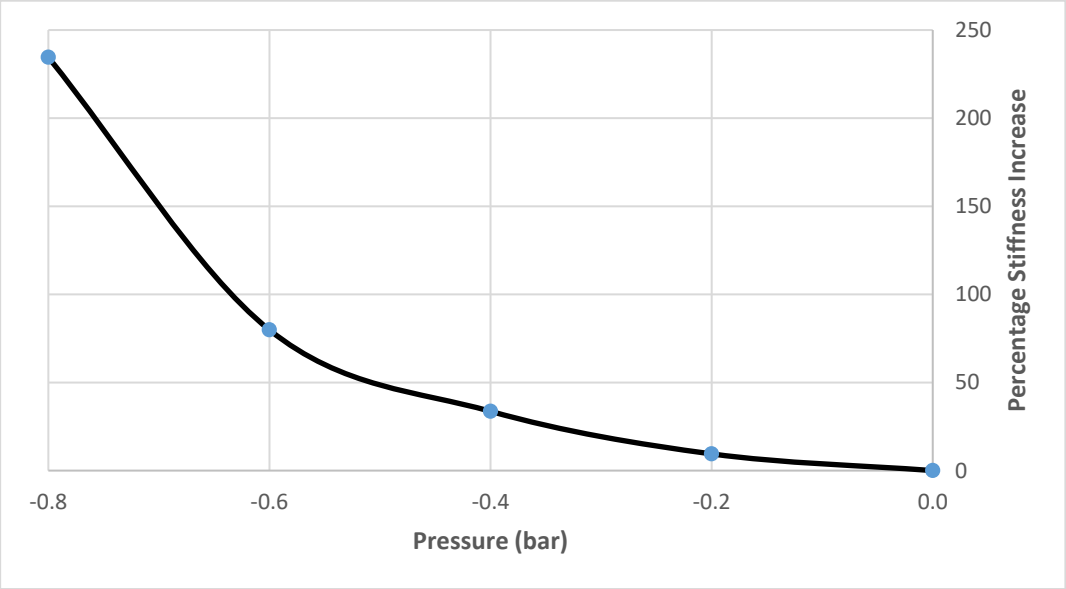

Figure 3-29: Percentage increase in the continuum granular jamming finger bending stiffness.

3.6 Conclusion

In this chapter, the practical characteristics of the contractor and extensor PMAs were investigated experimentally to develop a mathematical model of their behaviour. In order to model the behaviour of the pneumatic actuators mathematically, it is important to characterise their behaviour fully. Force/displacement and pressure/displacement characteristics have been investigated experimentally for both of the contractor and the extensor PMAs individually. The results found for these experiments were used to determine appropriate mathematical models. The variable stiffness spring mathematical model was found to be suitable to represent the behaviour of the PMAs. This model will be taken into consideration when a proper controller is designed to control the operation of the PMAs.

The variable stiffness capabilities of the pneumatic and granular jamming continuum fingers were also investigated experimentally in this chapter. A group of experiments were conducted to investigate the compliance capabilities for the two types of PMAs when arranged in a particular configuration. Compliance, and the variable stiffness property for the proposed system configuration, which is a combination of both the contractor and extensor PMAs, was determined experimentally. The experimental results were obtained by measuring the displacement of the extensor PMA in response to the attached force under different combination of pressures, which was applied to both contractor and extensor PMAs. It was found that increasing the extensor pressure to 4 bar results in a stiffness percentage increase of 163% for a 190 mm finger length and 112% for a 180 mm finger length, respectively.

Another group of experiments were conducted to calculate the force/displacement characteristics of the granular jamming continuum finger. The results of these experiments were used to determine the bending stiffness characteristics of the granular jamming continuum finger. It was found that decreasing the granular jamming continuum finger pressure to -0.8 bar resulted in an increase in stiffness of 235%.

As a result, both these techniques would appear to be suitable to develop a variable stiffness soft robot and an end effector. This soft robot and end effector should have the capability to work in a low stiffness, compliant mode to interact safely with humans; in addition, they should have the capability to change their stiffness during operation so as to be stiff, similar to a rigid robot, in order to control their behaviour more accurately. It is well proven in literature that the more compliant a system is the more difficult it is to control accurately.

In the next chapter, the implementation and a performance evaluation for the variable stiffness soft robot end effectors will be illustrated in detail.

Chapter Four

4 Design and Implementing, Variable Stiffness, Soft Robot End-Effectors

4.1 Introduction

There have been a number of soft robot grippers developed that use a range of different actuation methods. Manti (Manti, M., et al., 2015) and Rateni (Rateni, et al., 2015) developed a tendon-actuated soft three-finger gripper formed from soft deformable materials. Shintake developed a soft gripper based on electro-adhesion (Shintake, J., et al., 2016).

Several soft grippers have been developed that are fluid powered, such as pneumatically and hydraulically powered. Katzschmann (Katzschmann, R., Marchese, A., & Rus, D.,

2015), Mosadegh (Mosadegh, B., et al., 2014) and Homberg (Homberg, B., 2015) developed soft continuum fingers consisting of an expanding pneumatic layer sandwiched to a non-extensible flexible layer, which when pressurised flexes. Wakimoto demonstrated a similar actuation method in a microgripper that flexed in different directions depending on which of its internal chambers where pressurised (Wakimoto, S., et al., 2009). Galloway developed a gripper with a similar principle of operation for subsea applications that used hydraulic power (Galloway, K., et al., 2016). A very different design of pneumatic soft hand was demonstrated by Niiyama (Niiyama, R., et al., 2015), whose gripper used recently developed hinged pouch motors which, when pressurised, caused the joints of the hand to bend.

In most cases, these grippers are unable to change their stiffness. Whilst highly compliant fingers may be desirable for grasping some products, at other times stiffer fingers may be desirable. Stilli (Stilli, A., Wurdemann, H., & Althoefer, K., 2014) and Maghooa (Maghooa, F., et al., 2015) explored methods of controlling the stiffness of a soft manipulator that used DC motors to apply forces to tendons located along the outer surface of a reinforced pneumatic bladder. The pneumatic system generated an antagonistic force acting against that of the tendon cables. This allowed stiffness to be increased as increasing pressure in the pneumatic actuator resulted in higher stiffness.

The main contribution of the chapter is the design and testing of a pneumatic variable stiffness, three-fingered, soft robot end effector. The chapter details the development, testing and control of the end effector. The chapter describes the theory behind the proposed end effector and its capability to vary its stiffness. The chapter then describes the design of the variable stiffness soft robot end effector before analysing the associated kinematics. A series of experiments are then conducted to assess the control characteristics of the end effector at a number of different gripper stiffnesses before giving a set of concluding remarks. In addition, the chapter details the development, testing and control of the granular jamming end effector.

4.2 Continuum Actuator

The end effector developed in this work is based on the concept of continuum manipulators. Each of the three fingers is composed of a three DOF continuum

manipulator based on McKibben muscles. Jones demonstrated a continuum manipulator arm based on three parallel pneumatic muscles (Jones, B., & Walker, I., 2006) where differential pressurisation of each muscle resulted in the motion of the end of the manipulator.

The fingers in this end effector take their inspiration from Jones' design but include an additional actuator to allow the stiffness of the continuum fingers to be adjusted independently of the fingers' positions. Each finger is formed from four parallel pneumatic muscles as shown in figure (4-1). They consist of one central expansive (i.e., increases in length when pressurised) pneumatic muscle surrounded by three equally spaced contractile (i.e., contract when pressurised) pneumatic muscles. This configuration does not have a direct biological inspiration, although it is superficially similar to a simplified elephant's trunk where the muscular hydrostat is replaced by an expanding muscle.

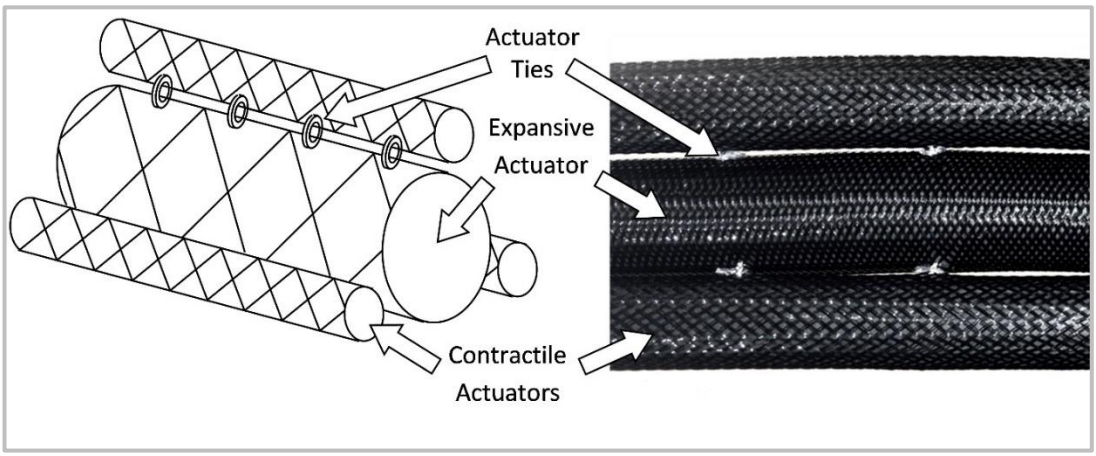

Figure 4-1: Variable stiffness continuum manipulator.

The four actuators used to create each finger are secured to mounting plates at both ends of the finger. Ties are used as shown in figure (4-1) to ensure that all the contractile actuators remain equidistantly spaced along the entire length of the finger and further remain in constant contact with the central actuator at all times. The ties are made from flexible nylon cables and are looped through adjacent openings in the central and outer muscles as shown.

The stiffness of a pneumatic muscle is proportional to the air pressure inside it. However, for a fixed load, the displacement is also proportional to pressure – this means position and stiffness cannot be controlled independently. In this novel design, when pressurised, the central actuator creates a force that opposes the motion of the outer muscles. Therefore, by increasing the pressure in both the extensor and contractor muscles the stiffness of the finger can be increased without a resulting change in position. Therefore, there are an infinite number of actuator pressure combinations that will result in the same fingertip position but also in a different stiffness.

A variable stiffness continuum finger could be created by using a soft incompressible central spine surrounded by contracting muscles. However, in such a design there is potential for the spine to buckle when the stiffness increases. Having an actuated central section prevents the finger from compressing as it applies a force to resist compression. The combined use of both expanding and contractile muscles means that the length of the finger can also be controlled if desired, a feature that would not be possible if a spine was used.

The other benefit of using a continuum design rather than a system consisting of discrete joints and flexible coverings is that the fingers can conform to any shape and operate when partially constrained. This is not possible with a traditional serial manipulator. A redundant manipulator would offer greater flexibility but would still only be able to flex at the individual joint locations.

4.3 Continuum Soft Robot End Effector's Basic Prototypes

Initial testing of a four-parallel pneumatic muscle continuum link shows it has the potential to allow variable stiffness. The construction of the continuum link is that of one central expansive pneumatic muscle actuator surrounded by three equally spaced contractile pneumatic muscle actuators, as shown in figure (4-1).

Figure (4-2) shows a first prototype variable stiffness continuum end effector. Each muscle is 150 mm long when unpressurised. The unpressurised diameters of the contactor and extensor muscles are 10 mm and 15 mm, respectively. Pressurising each contractor muscle, in turn, causes the finger to bend in one of three directions.

Activation of multiple contractors extends the workspace of the finger to a cylinder as it allows for bending of the finger in all directions, and also a reduction in finger length if all contractors are simultaneously activated.

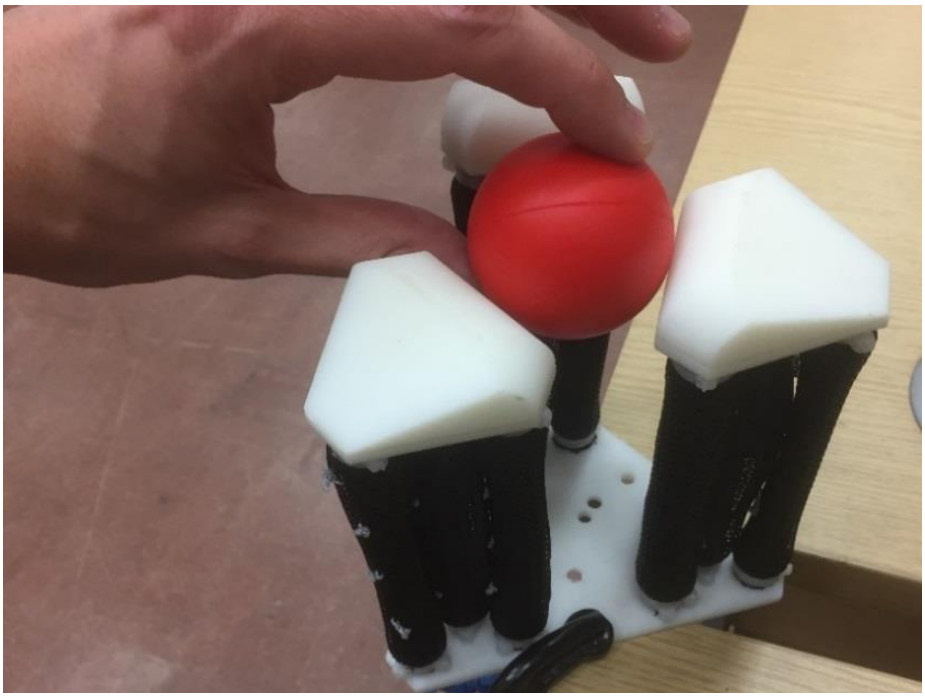

Figure 4-2: Variable stiffness continuum end effector.

The three-finger gripper was tested in an open loop manner using matrix solenoid valves (described in more detail later) to control the flow of air to the muscles. This experiment showed that the fingers could be moved and used to grasp objects as seen in figure (4-2).

Manual testing also showed that the gripper appeared to continue to operate when the pressure in the extensor muscle was increased. The antagonistic force produced by the extensor muscle is what gives the system its variable stiffness capability. It was therefore vital to demonstrate that the fingers could still be bent at high extensor pressures.

Although the gripper worked as expected, as can be seen in figure (4-2), the size of the fingers in this first prototype are much larger than that in the human hand. This significantly limits the possible applications of the gripper. Whilst the actuators could all be made smaller, because the force they generate is proportional to their cross-sectional area this would reduce the grasping strength of the hand. Also smaller muscles proved much more difficult to fabricate.

To overcome this problem, a second prototype has been produced. This second prototype uses the same type of muscles as the first prototype but, by relocating the contractor muscles and transmitting their force to the finger via tendons, the overall size of the fingers can be reduced to approximately human scale.

Hence, during this research, an alternative continuum actuator-based finger design was developed, as seen in figure (4-3). Simple experiments on this pneumatic finger with tendons shows good potential for the development of a new multi-fingered continuum soft robot end effector. One tendon is connected to the top and another one to the middle of the finger in order to manually explore different types of finger bending.

Figure 4-3: Continuum finger using pneumatic muscle actuator and tendon cables.

This finger design is smaller than that shown in the figure (4-2) and has the potential to be used to grasp objects of many shapes. Figure (4-4) shows a basic prototype consisting of three tendon driven fingers. This prototype allowed the motion of the fingers to be explored; for example, the approximate amount of tendon motion required to achieve a desired range of finger motion. The prototype also allowed different methods of construction and assembly to be compared.

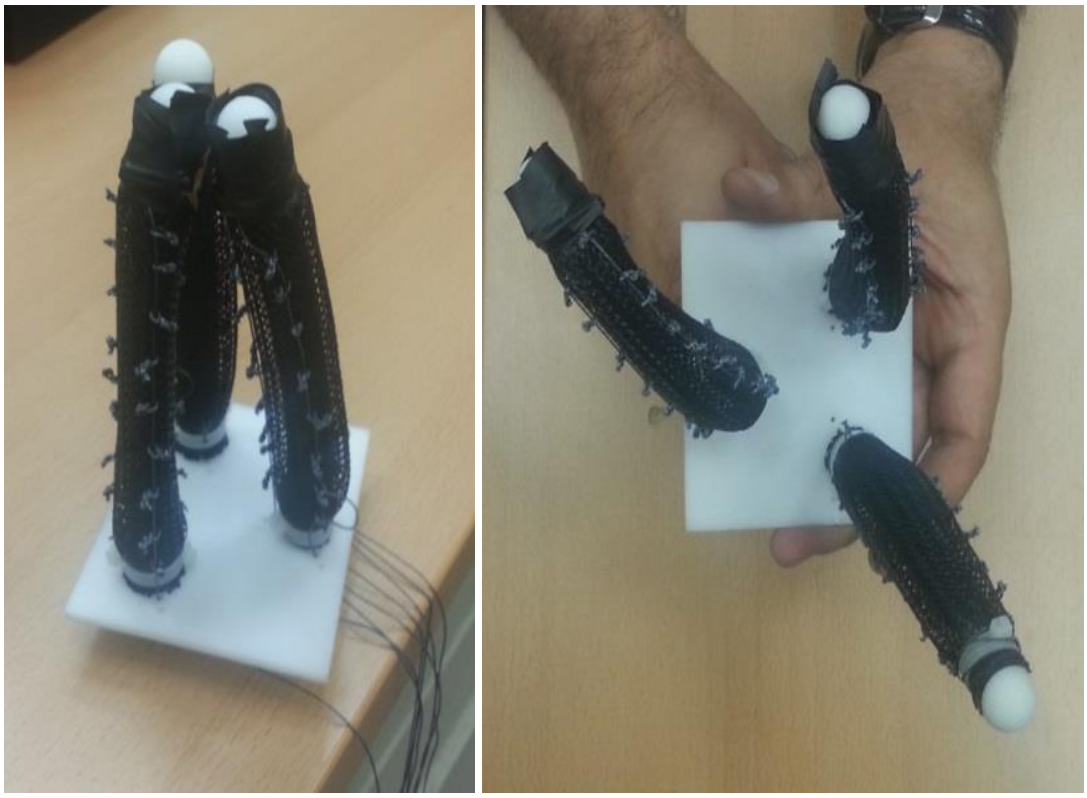

Figure 4-4: Basic prototype for the new three fingered hand.

4.4 Design and Implementation of Continuum Soft Robot End Effector

Based on the previous basic design of the three fingers gripper, a new continuum soft robot end effector has been designed and constructed. Several continuum actuators (fingers) have been designed. Use of the new continuum actuators means fingers can change their stiffness. SolidWorks CAD software was used to design the three mounting plates subsequently produced by a 3D printer to form the end effector frame. The dimensions of the mounting plates are chosen to be (125 x 125 x 6) mm. The first plate sketch diagram is shown in figure (4-5).

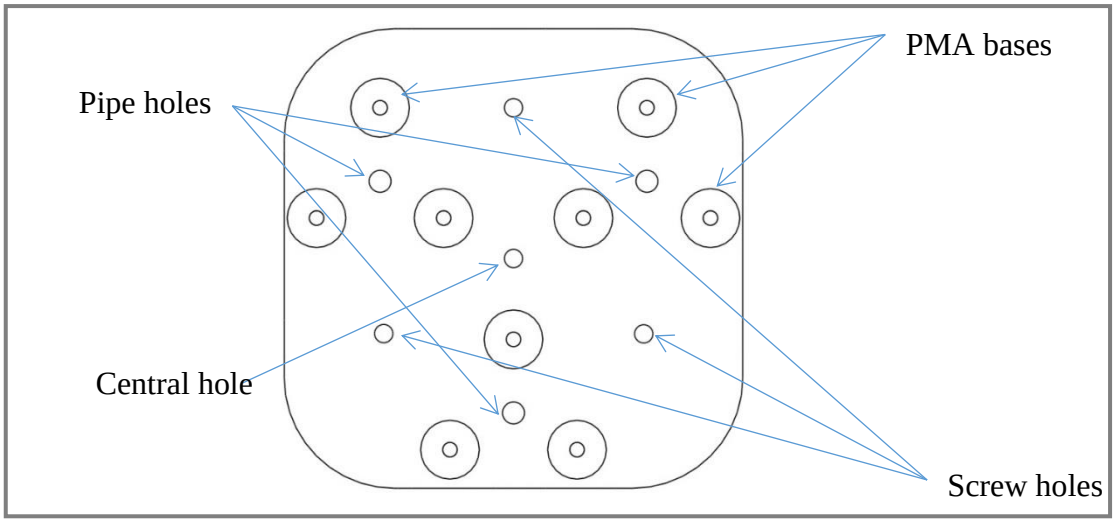

Figure 4-5: First mounting plate sketch diagram.

Pipe holes were used as paths for the pneumatic pipes to the three fingers, which are secured to the third mounting plate (see below). The PMA bases are used to mount the contractor PMAs, which were used to control the bending of the fingers, themselves secured to another base on the third mounting plate. In the centre of each PMA mounting base there is a hole to allow air pressure in and out. The central hole is used as a route for potentiometer connection cables. Finally, screw holes were used to assemble the aluminium beams with plates to form the structure of the end effector. The shape and the actual construction of the first mounting plate are shown in figure (4-6).

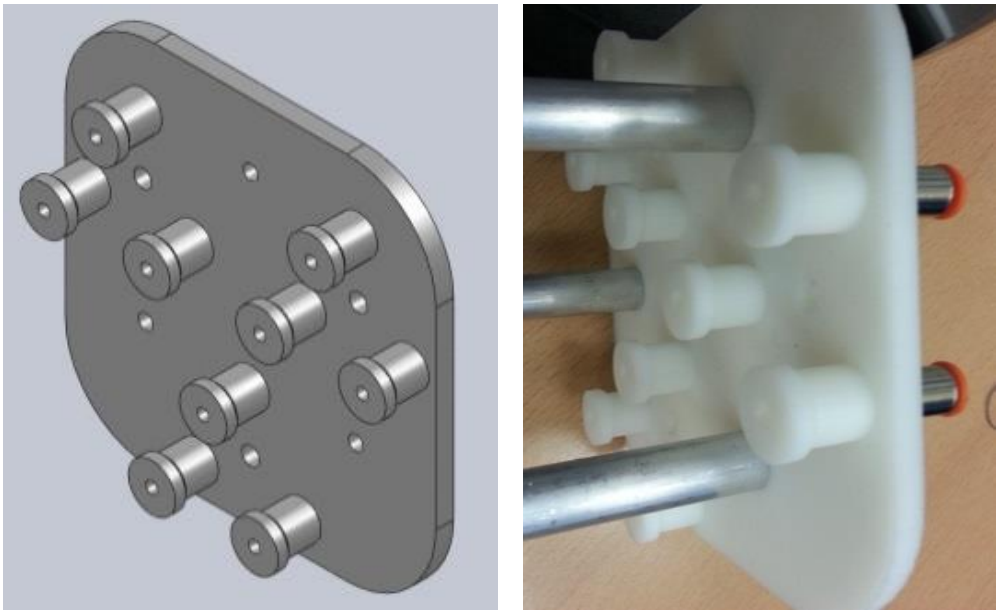

Figure 4-6: First mounting plate details.

The second mounting plate was also designed and inspected using SolidWorks CAD software application. Figure (4-7) shows the sketch diagram for the second mounting plate.

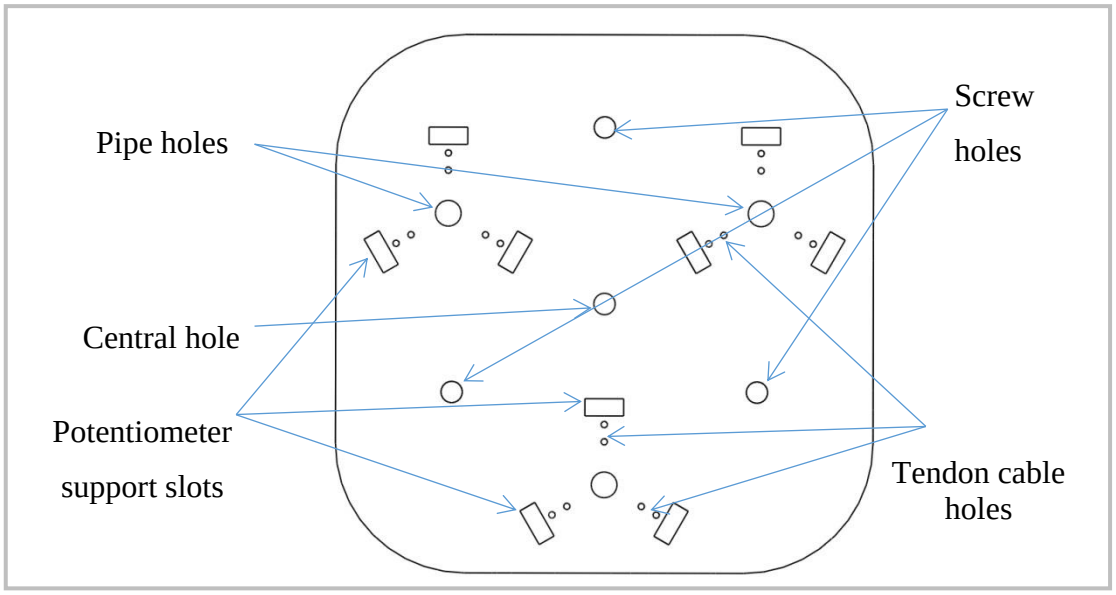

Figure 4-7: Second mounting plate sketch diagram.

Pipes, screws and central holes all have the same functions as described for the design of the first mounting plate. Potentiometer supporter slots were constructed with side screw holes and are used to secure the nine potentiometers used as displacement sensors. The tendon cable holes are used as a route for the tendon cables that connect extensor muscles (fingers) to the contractor muscles in order to control the bending of the fingers. Three tendons are fitted around each finger separated by angles of 120^{o} (i.e., equally spaced). The tendon cables were connected to the three contractor muscles which are used to control the bending of the finger in any direction. The tendon cables are also spooled around the central terminal of the three potentiometers located between the finger and the three contractor muscles. The shape and the construction of the second mounting plate is shown in figure (4-8).

Finally, the third mounting plate was designed using SolidWorks. One of its two faces is exactly the same as that used in the second mounting plates, except there is no central hole. Figure (4-9) shows the sketch diagram for the third mounting plate from another side of view.

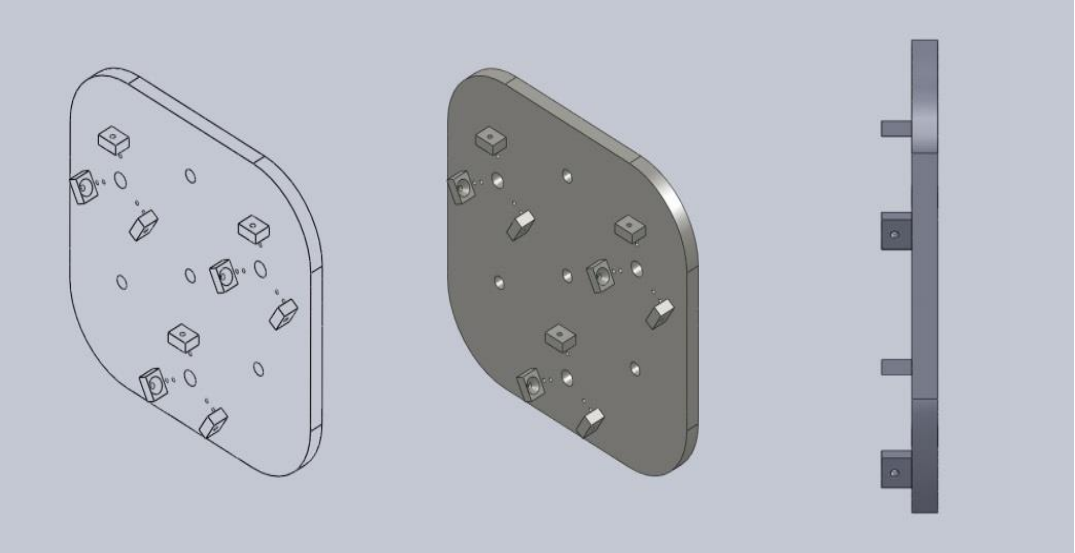

Figure 4-8: Second mounting plate details.

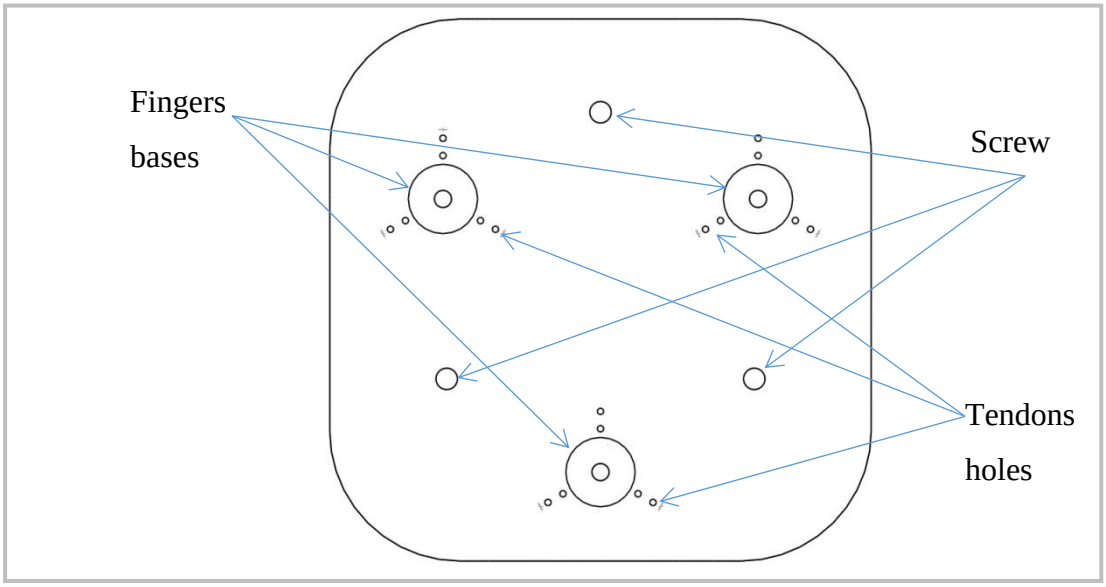

Figure 4-9: Third mounting plate sketch diagram.

The shape and the actual construction of the third mounting plate are shown in figure (4-10). This side of the plate is used to secure three fingers to the three fingers bases. Also, there are three screw holes to secure the other three aluminium beams and give the final shape for the end effector.

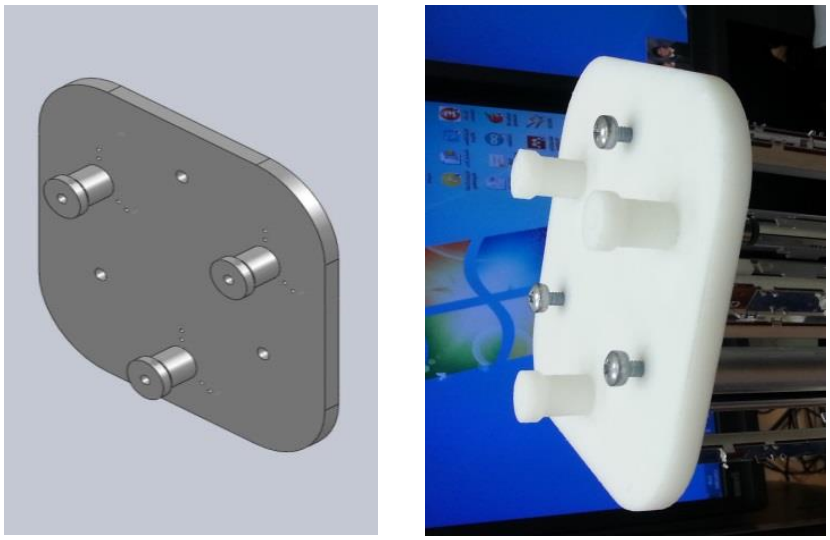

Figure 4-10: Third mounting plate details.

Figure (4-11) shows the final design of the end effector frame excluding the extensor and the contractor PMAs.

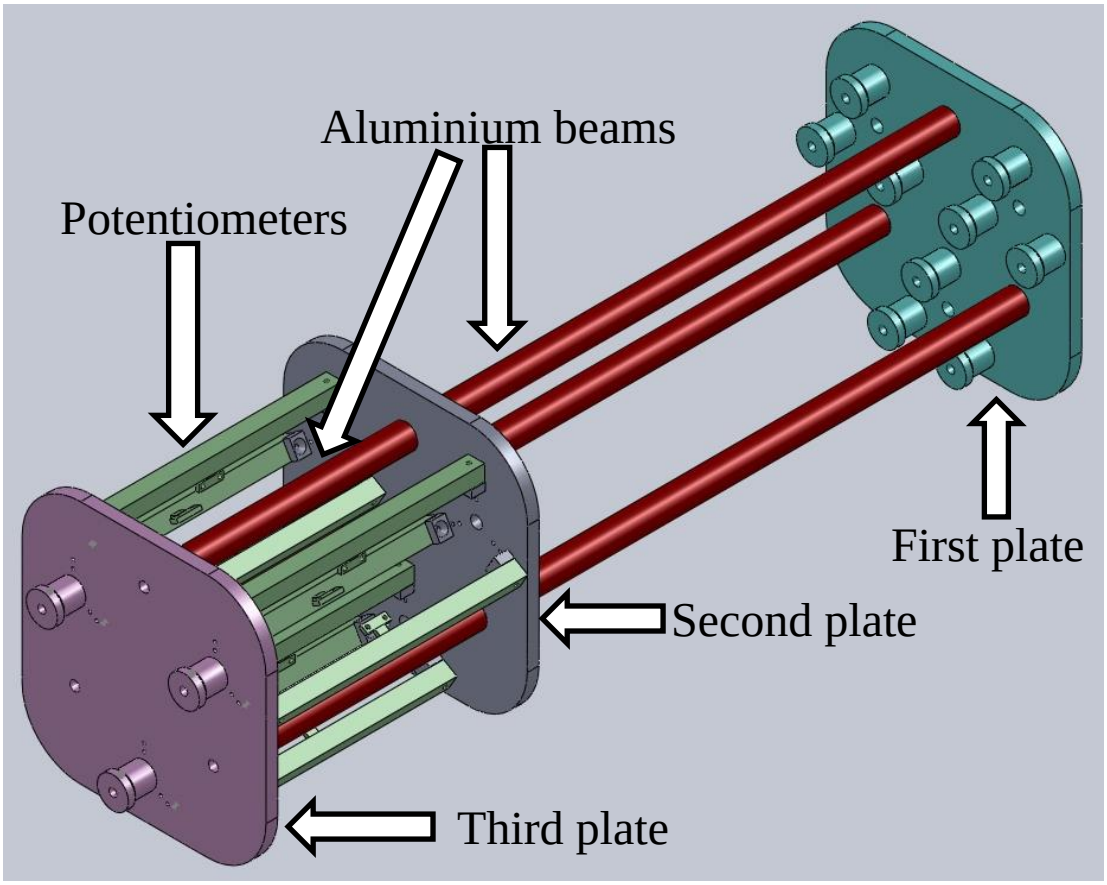

Figure 4-11: The soft end effector frame, structural design.

Six aluminium beams are inserted between the three mounting plates to give the required frame structure. The length of the longest three aluminium beams is 270 mm, which allows enough space for the contractor muscle actuators to operate. However, the length of the shortest three aluminium beams is 127 mm, which is selected to be at the same length as the potentiometers. Hence, a suitable space is available to mount all the nine contractor PMAs between the first and the second mounting plates. In addition, all the nine potentiometers are located between the second and the third mounting plates. These potentiometers are used to measure the displacement produced by powering the contractor muscle actuators. Tendon cables are used to connect the contractor PMAs to the extensor PMAs (fingers) through the potentiometers (displacement sensors).

The PMA mounting bases are designed to be 16 mm in length, 11 mm in body diameter and 15 mm in cap diameter. All these bases have a hole of 4 mm in diameter to allow the air in and out of the muscle. The total length of the hand frame shown in the figure (4-11) is 431 mm.

In summary, the prototype gripper was designed and analysed using SolidWorks CAD software and then produced by a 3D printer. The design includes three fingers, formed by three extensor PMAs and nine contractor PMAs, which are used in a combined manner to power the three fingers.

Figure (4-12) shows the conceptual design of the second prototype, three-fingered soft gripper. Each one of the fingers is constructed of an expanding pneumatic muscle with a length of 160 mm and a diameter of 20 mm when unpressurised, and a length of 200 mm and a diameter of 15 mm at the maximum operating pressure of 4 bar. The fingers are attached to a forearm-like structure consisting of nine contractor pneumatic muscles, each with a maximum length of 240 mm and a diameter of 15 mm which has a contracted length at 4 bar of 180 mm. These muscles have a maximum force output of approximately 200 N at 4 bar. Each finger can vary its length from 160 mm to 200 mm depending on the relative pressures in the expanding and contracting muscles.

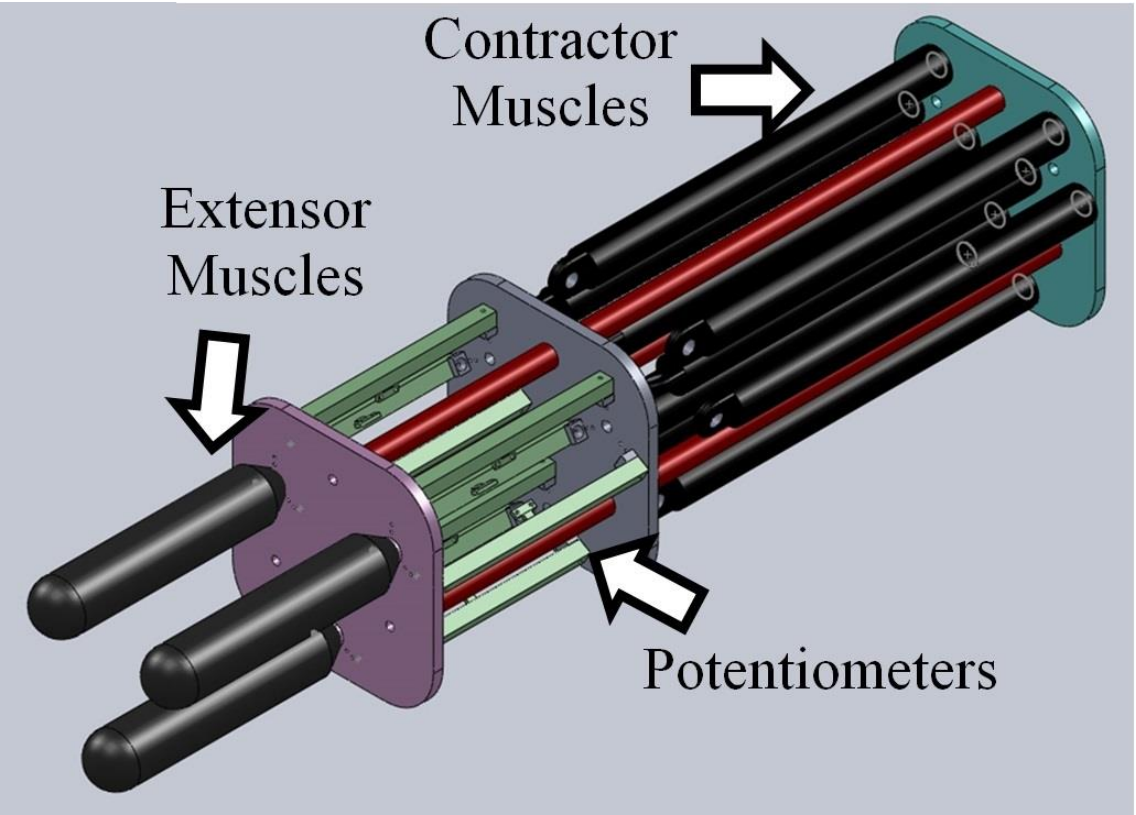

Figure 4-12: The overall structure of the fingered soft robot end effector.

As the contractor muscles are in the forearm, they do not come into contact with the object to be grasped. Therefore, on first consideration it follows that the actuators applying tension to the tendons do not need to be soft and an electric series elastic actuator could instead be used. However, the gripper is intended to be used on a fully soft manipulator and it is, therefore, vital that the entire gripper, including its actuators, is soft. Although the fingers and actuators are soft the design still includes some rigid parts (the plates and beams).

The contractor PMAs are arranged in three groups, each consisting of three actuators, with each group of three providing power to one finger. The contractor PMAs determine how the fingers bend. The combined pressure in the extensor and the contractor PMAs determines the stiffness of the fingers. Nylon tendon cables are attached to the free end of the contractor muscles and to the other end of the fingertip (i.e., the free end of the extensor muscle). These tendon cables are used to transfer the actuation power from the contractor PMAs in order to bend the fingers in a direction according to the location of tendon around the finger. To ensure the tendons remain correctly located along the

length of the finger, nylon loops are added to the outside of each finger through which the tendon passes, as can be seen in figure (4-13). These loops ensure that as the fingers bend, the tendons remain in contact with the outer edge of the finger. Figure (4-13) shows the overall construction of the proposed three-fingered soft robot end effector with all the contractor and extensor PMAs in place.

Figure 4-13: The overall actual construction of the three-fingered soft robot end effector.

As can be seen, linear potentiometers (sensors) are located between the extensor and contractor muscles. Each tendon is attached to a single potentiometer, which is used to measure the displacement of the contractor muscles. These sensors allow the position of the fingertip to be determined using kinematic analysis (introduced later) to achieve the closed-loop control of the end effector. As the sensors are remote, they will not be as accurate as if they were located directly on the fingers. However, as the tendons have a high elastic modules they do not extend significantly during operation and so the accuracy of the sensing is maintained.

Overall control of the continuum soft robot end effector is provided by an Arduino microcontroller linked to MATLAB to allow the Arduino to generate the necessary PWM signals to drive all the pneumatic valves. Two Adafruit 16-channel PWM/Servo Shields were used to expand the PWM output capability of the Arduino microcontroller. Driving circuits were also required as the Arduino is not capable of providing sufficient current to power the valves directly. Figure (4-14) shows a block diagram structure of the system configuration for the proposed soft robot end effector.

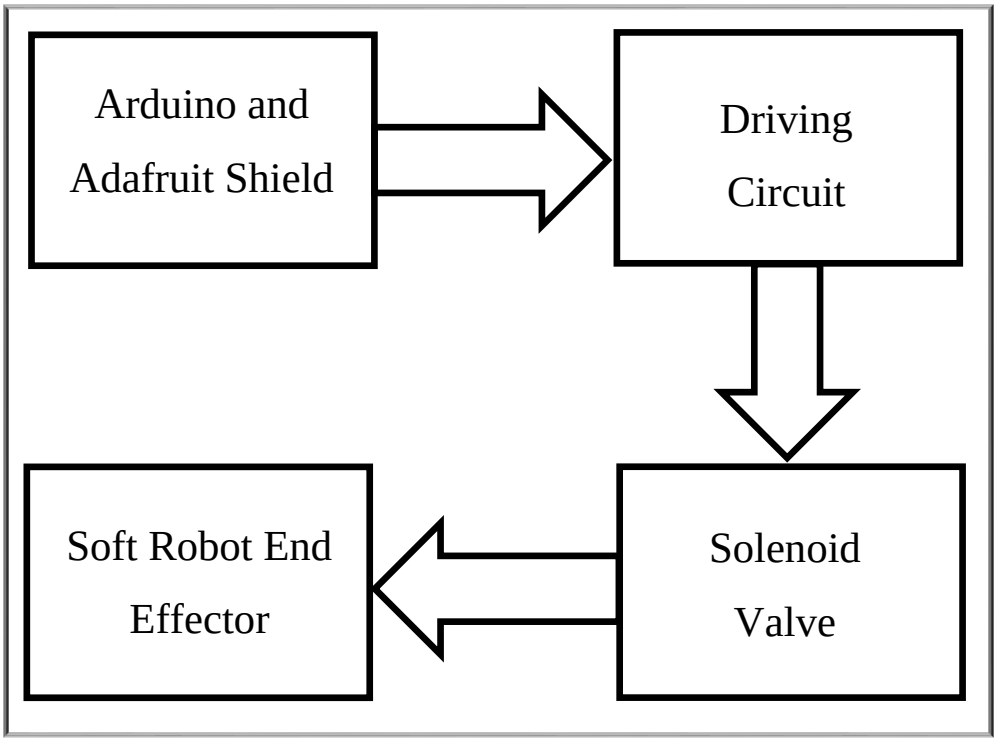

Figure 4-14: The system lock diagram.

In total, there are twelve PMAs, composed of three extensor and nine contractor PMAs, which are used to control the bending of the three extensor PMAs, as fingers. All of the extensor muscles, fingers, are attached to a single air pressure regulator, allowing the pressure in the fingers to be varied manually. All the contractor muscles are, however, attached to individual MATRIX 3-3 solenoid valve, which allow air to be supplied to, or vented from, individual muscles when required. The valve's control signals are PWM signals to allow control over the flowrate of air into and out of the muscle. Hence, nine pneumatic valves are required to power the contractor PMAs. Three of the pneumatic compact solenoid multi-valves are used in this soft robot end effector, each of which has a total of four (3-3) pneumatic valves. Figure (4-15) shows an image of the compact solenoid multi-valves used in the construction of this project.

Figure 4-15: Four-port pneumatic compact solenoid multi-valve.

In each valve of the pneumatic compact solenoid multi-valve, there are three wires that can be used to control its operation. Table (4-1) below illustrates the colour and the function of all wires in the pneumatic compact solenoid multi-valves used in this project.

Wire colour	Port No.	Function
Black	All	Common
Brown	1	Vent
Red	1	Fill
Orange	2	Vent
Yellow	2	Fill
Green	3	Vent
Blue	3	Fill
Violet	4	Vent
Grey	4	Fill

Table 4-1: The wire colours/functions for the pneumatic compact solenoid multi-valve.

While 24 VDC is required to power the pneumatic compact solenoid multi-vales, only 5 VDC is required for the Arduino microcontroller. Hence, a driving circuit is needed to drive the pneumatic valves to control the operation of the soft robot end effector through the Arduino microcontroller. Figure (4-16) shows the circuit diagram used to control filling or venting in each valve, as a driving circuit.

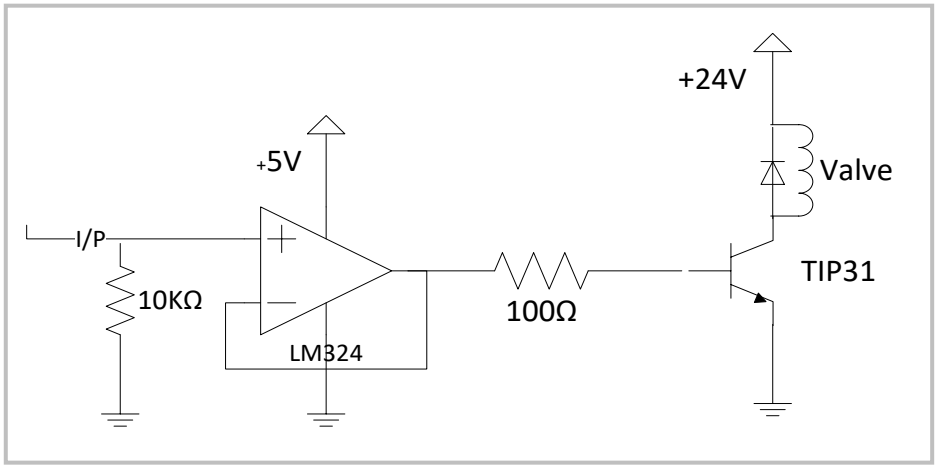

Figure 4-16: Driving circuit (one section).

There are nine PMAs pressurised by nine pneumatic valves. However, eighteen driving circuit sections are required to drive all valves: nine for filling and nine for venting. Figure (4-17) shows a photo of the assembled driving circuit.

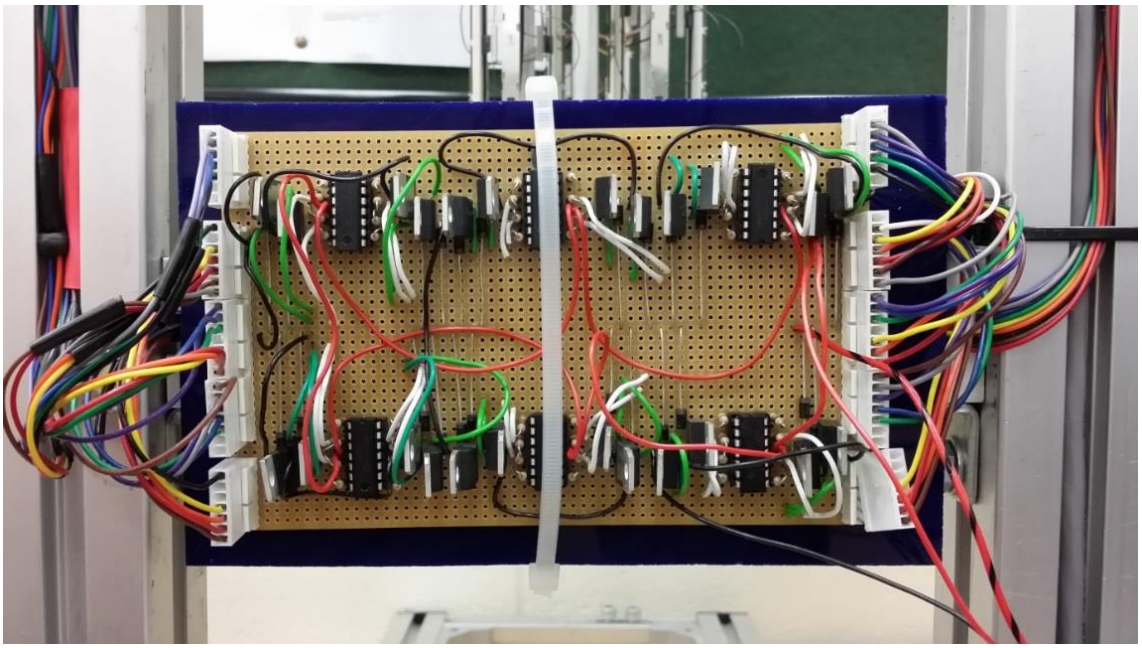

Figure 4-17: The driving circuit construction.

Six LM324 operational amplifier integrated circuits are used in the construction of the driving circuit, each of which contains four operational amplifiers. Diodes are used to protect the TIP31 power transistor from the reverse bias that may occur due to the coils inside the valves. The main function of the transistor is to switch on and off in response to the applied PWM signal as input to the base of each transistor. The 100 Ω resistor is used to limit the current passed to the base of the transistor. The 10 kΩ resistors are used as overcurrent protection for the operational amplifiers. Figure (4-18) shows two images for the Arduino UNO microcontroller and two Adafruit PWM/Servo shield boards coupled together.

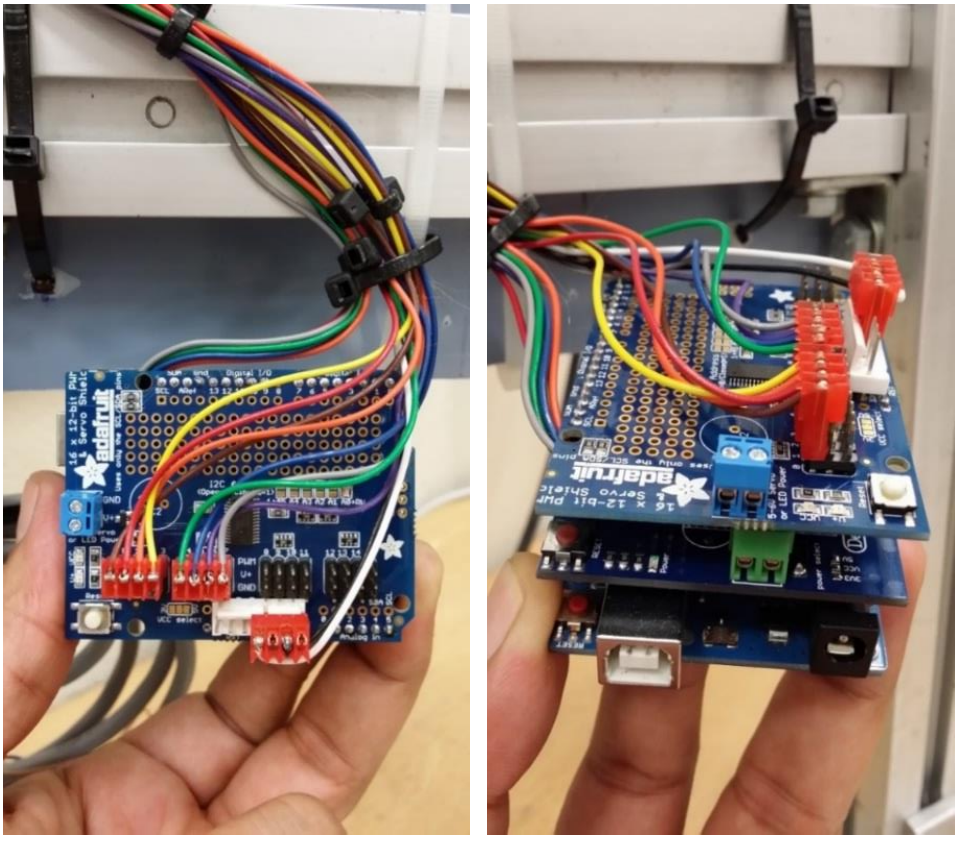

Figure 4-18: The Arduino UNO microcontroller with Adafruit PWM/Servo shield.

A dual-output power supply was used to provide the required DC voltage to power the Arduino microcontroller, Adafruit expansion boards, driving circuit and the solenoid valves.

4.5 The Finger Kinematics in the Continuum Soft Robot End Effector

To determine the position of each fingertip of the soft robot end effector, it is necessary to analyse the kinematics of the finger. The position of the fingertip relative to the base is determined by the length of the three contractor actuators that are equally spaced around the circumference of the central extensor pneumatic muscle. When the contractor PMAs are activated they will shorten, and as they are attached (via tendons) to the side of the central extensor PMA they will cause it to flex and form a constant radius curve with an arc. The length of the arc is determined by the angular displacement between the two ends of the finger, as can be seen in figure (4-19).

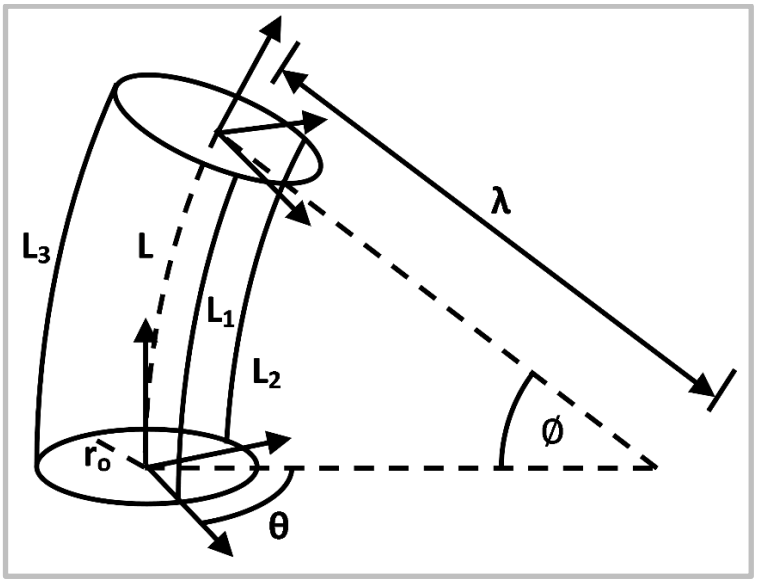

Figure 4-19: The kinematics of the continuum finger.

Godage analysed the kinematics of a continuum manipulator based on three expanding actuators (Godage, I., et al., 2011), and the same general approach can be used to determine the behaviour of the pneumatic finger. Four properties are used to describe the position of the free end of the continuum element relative to the base. The radius of the curve formed is defined as λ, ∅ is used to describe the angular displacement between the two ends of the finger, L is the length of the arc formed and θ is the angle between the end of the element point relative to the base coordinate frame.

The kinematics of the four-actuator continuum finger described in this research are given by the following four equations:

$$\lambda = \frac{(L_1+L_2+L_3)r_o}{2\sqrt{{L_1}^2+{L_2}^2+{L_3}^2-L_1L_2-L_1L_3-L_2L_3}} \quad (4.1)$$

$$\emptyset = \frac{2\sqrt{{L_1}^2+{L_2}^2+{L_3}^2-L_1L_2-L_1L_3-L_2L_3}}{3r_o} \quad (4.2)$$

$$\theta = \tan^{-1}\left(\frac{\sqrt{3}(L_3-L_2)}{L_2+L_3-2L_1}\right) \quad (4.3)$$

$$L = \lambda\emptyset \quad (4.4)$$

By combining equations (4.1), (4.2) and (4.4), one can determine the length of the finger as:

$$L = \frac{L_1+L_2+L_3}{3} \quad (4.5)$$

Where L is the length of the extensor PMA used to form the finger and L_1, L_2 and L_3 are the respective contractions of the three contractor muscles, (and r_o is the radial distance from the finger's central axis to the contractile actuators, though this value is not required for the actual determination of $\boldsymbol{L}$.

Up to this point the analysis has been based on previous work; see (Godage, I., et al., 2011). However, in this work as the finger is formed from an extensor PMA, its diameter is not constant, as it extends as its diameter reduces. Therefore, the radial distance of the tendons from the central axis of the finger is equal to the radius of the extensor muscle used to form the finger, which varies with the actuator length. The length (L) and radius (r_o) of a pneumatic muscle are determined using the following equations:

$$L = \cos\theta_B \quad (4.6)$$

$$r_o = \frac{b\sin\theta_B}{2n\pi} \quad (4.7)$$

Where Θ_B is the angle of the braid with respect to the central axis of the muscle, b is the length of a single fibre used to form the muscle, and n is the number of times each braid

fibre loops around the circumference of the muscle. Combining these two equations with respect to Θ_B and substituting into equation (4.5) gives the following equation, which relates muscle radius to the length of the three tendons:

$$r_o = \frac{\sqrt{b^2 - L^2}}{2n\pi}$$

$$r_o = \frac{\sqrt{b^2 - \left(\frac{L_1 + L_2 + L_3}{3}\right)^2}}{2n\pi}$$

$$r_o = \frac{\sqrt{9b^2 - (L_1 + L_2 + L_3)^2}}{6n\pi} \qquad (4.8)$$

Equation (4.8) can then be combined with equations (4.1), (4.2) and (4.3) to determine the position of the fingertip relative to the base, and is dependent upon the contraction of the three contractile actuators (L_1, L_2 and L_3).

It should be noted that this analysis only holds true when there are no external forces acting on the finger, for example when the gripper is not holding an object. The soft nature of the fingers means they would deform in a highly complex manner in response to the application of external forces, and a more advanced kinematic/dynamic analysis would then be required.

4.6 Control and Performance Evaluation of the Continuum, Variable Stiffness, Soft Robot End Effector

To be of practical use, the proposed soft robot end effector needs to be controllable in a closed-loop manner. A PID controller was programmed to control the displacement (length) of each of the contractor muscles. PID controllers have successfully been used in the past to control pneumatic muscles as the force/displacement/pressure characteristics can be approximated to linear relationships; see (Davis, S., et al., 2003) and chapter three of this thesis. As explained in section (4.5), the position of each fingertip is determined by the relative length of the three contractor muscles used to power it. The controller reads the displacement from the potentiometer (displacement sensor) and then generates the necessary PWM control signals to control the flow of air

in and out of the muscles. The PID controller was tuned using the Ziegler-Nichols method; see (Ziegler, J., & Nichols, N., 1942).

To assess the performance of the proposed PID controller, the response to a step position change was tested along with the ability to track a sinusoidal input. Figure (4-20) shows the experimental rig used in the control investigation experiment.

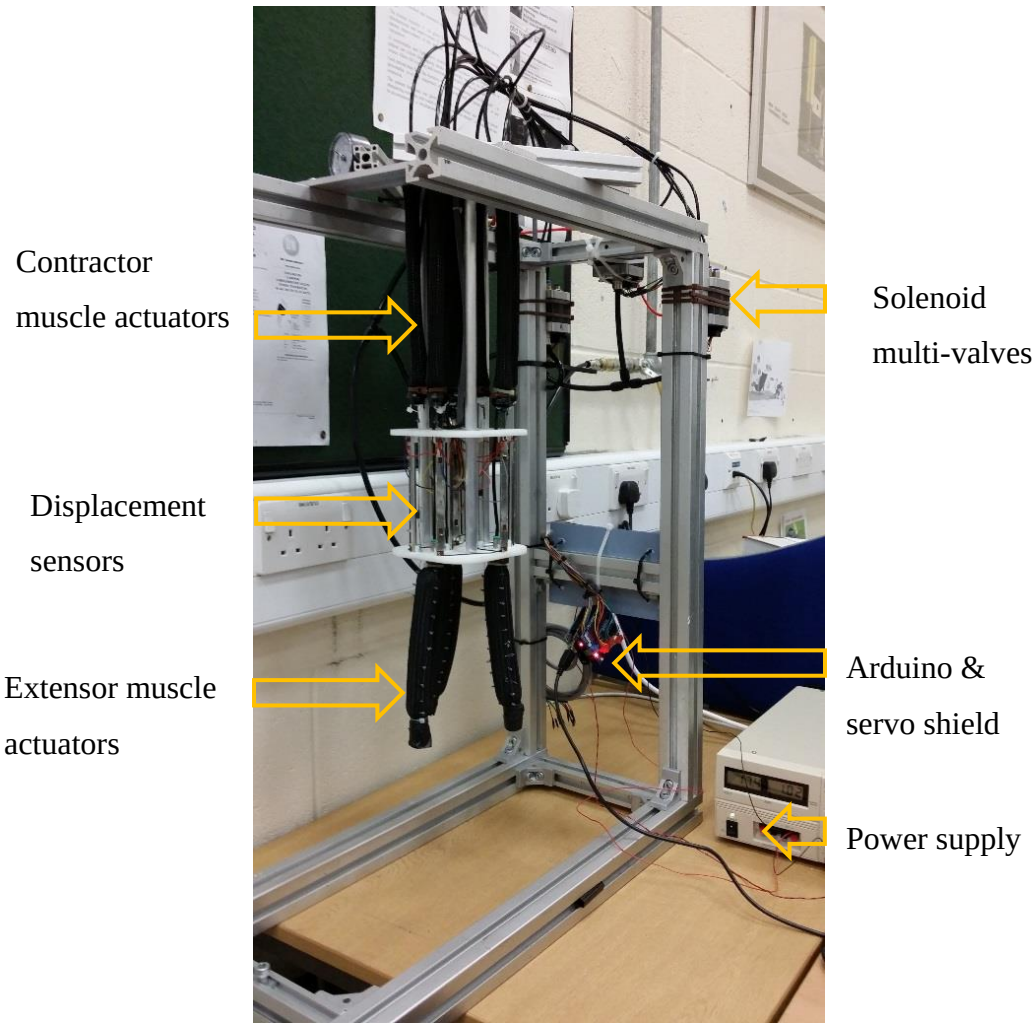

Figure 4-20: Experimental rig for the soft robot end effector.

The experimental procedure followed for the control experiments was as follows: the soft robot end effector was suspended in a test rig with the fingers pointing vertically downwards. The pressure in the extensor muscle was manually set to a fixed pressure. The controller was instructed to keep the length of the two contractor muscles on the rear of the finger (furthest away from the centre of the palm) at a constant length by putting a specific amount of pressure into the two contractor muscles. The single muscle on the front of the finger was then instructed to contract, which caused the finger to flex.

When this muscle relaxed, the two contractor muscles on the rear of the finger caused it to extend again.

Figure (4-21) shows the controller response to a series of step inputs that caused the muscle on the front of the finger to contract by (a) 20 mm, (b) 30 mm, and (c) 40 mm from an initial starting position. This caused the fingers to flex from an initially straight configuration to a point where the fingertip had displaced approximately 50 mm, 65 mm and 80 mm, respectively, in the horizontal plane. The blue curve represents the required target response and the red curve represents the actual controller response in the following figures.

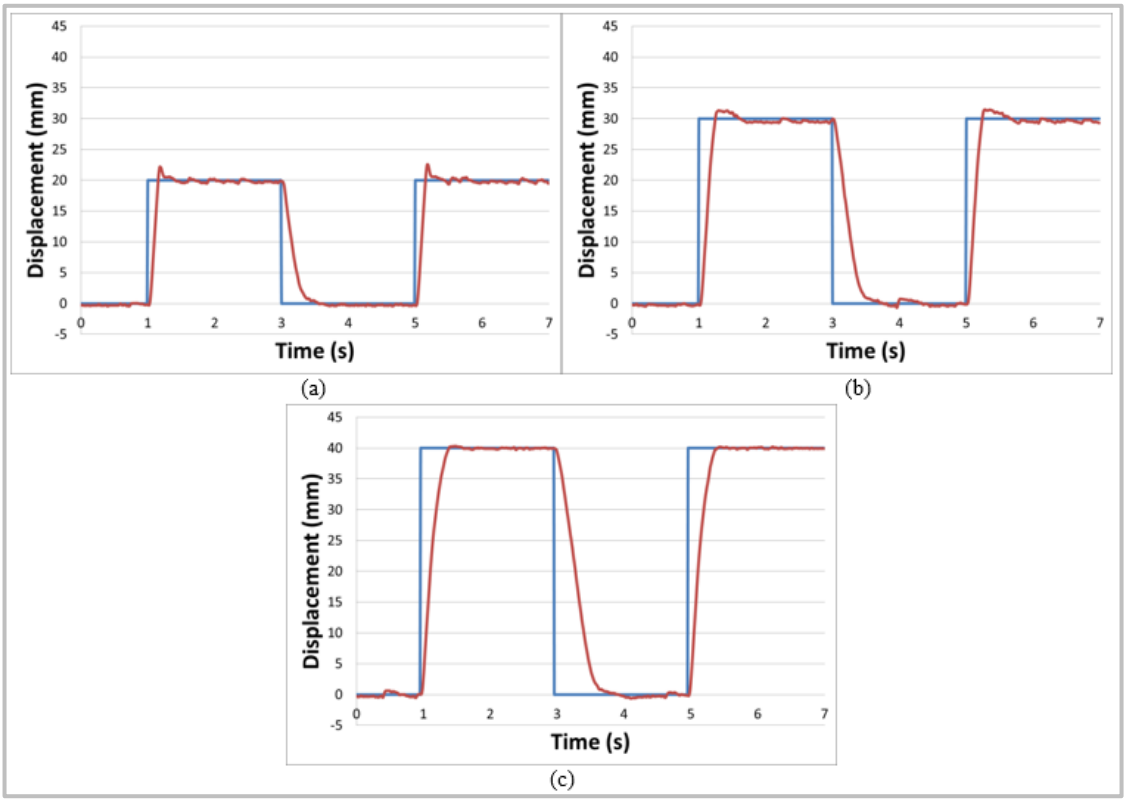

Figure 4-21: Response to (a) 20 mm, (b) 30 mm and (c) 40 mm step displacements of the contractor PMA.

It can be seen that in all cases the controller overshoots slightly (2.5 mm for the 20 mm step, 2.0 mm for the 30 mm step and 0.5 mm for the 40 mm step) before returning to the target position. For all three steps, the controller reaches a point where it is within an error range of ± 0.5 mm within 0.46 seconds for finger flexion and 0.6 seconds for finger extension.

Figure (4-22) shows the ability of the controller to track a sinusoidal input signal. The range of motion was the same as in the step response experiment with the contractor PMA, causing flexion moving through (a) 20 mm, (b) 30 mm and (c) 40 mm peak to peak displacement from the initial position. The experiment was individually conducted at frequencies of 0.25 and 0.50 Hz. At 0.25 Hz, the maximum position error was found to be 2 mm and the Root Mean Square (RMS) error was 1.1 mm. At 0.5 Hz the maximum error was 2.5 mm with an RMS error of 2 mm.

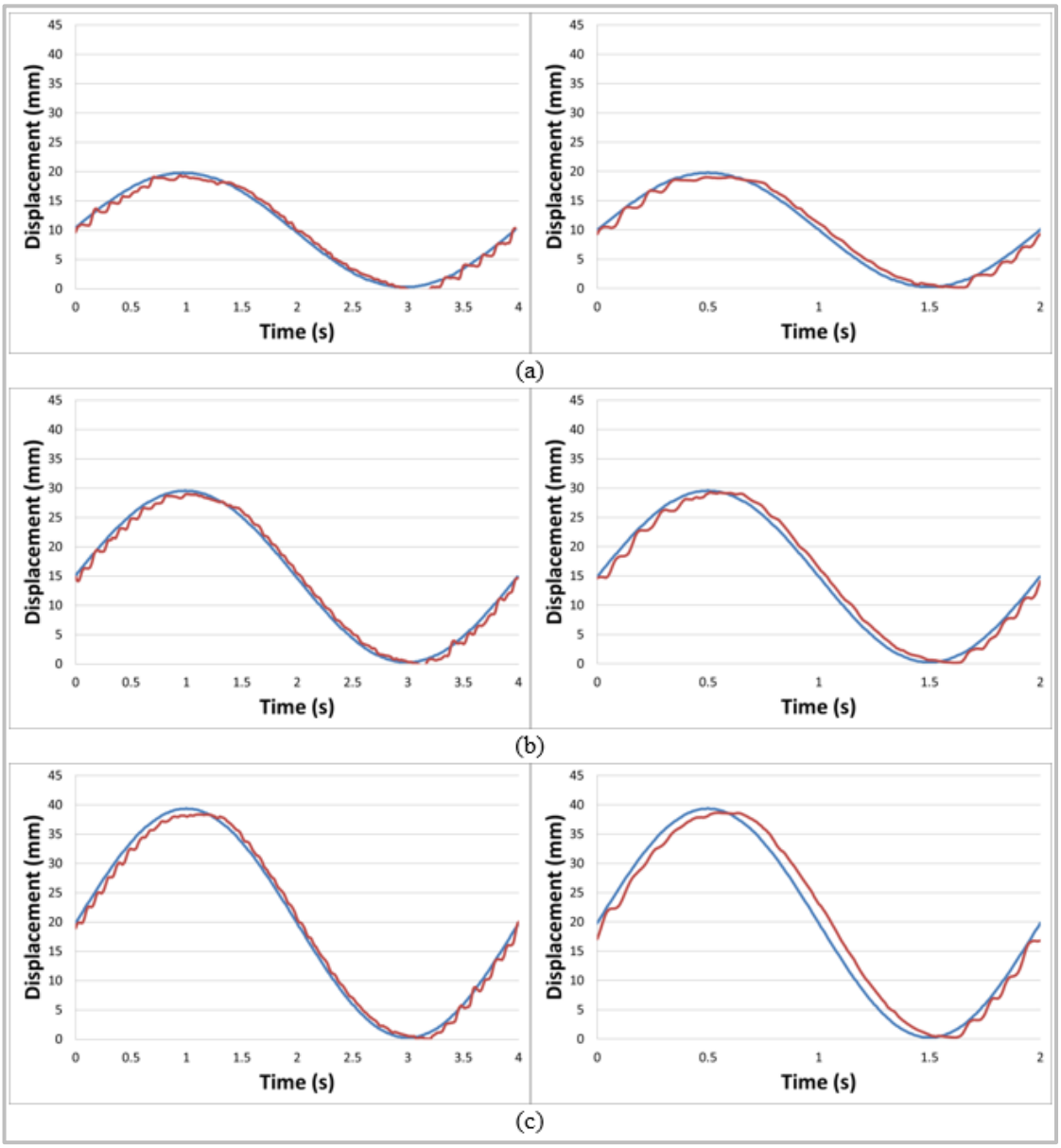

Figure 4-22: Response to (a) 20 mm, (b) 30 mm and (c) 40 mm sinusoidal displacements of the contractor PMA at 0.25 Hz and 0.5 Hz.

As discussed in previous sections, the proposed soft robot end effector has the ability to vary the stiffness of its fingers. This is achieved by increasing the pressure in the extensor PMAs, which increases the force acting antagonistically against the contractor PMAs. This means the pressure in the contractors needs to be increased to counteract the extensor force and maintain finger position. Actuator stiffness is a function of pressure, meaning the stiffness of the end effector increases.

For the proposed end effector to operate in various stiffness modes, it is vital that it can be controlled irrespective of the pressure in the extensor PMAs. To determine if this was possible, step and sinusoidal response experiments were conducted over a range of different extensor pressures. Figure (4-23) shows the finger tracking a 40 mm peak to peak signal with extensor muscle pressures of (a) 1 bar, (b) 2 bar and (c) 3 bar.

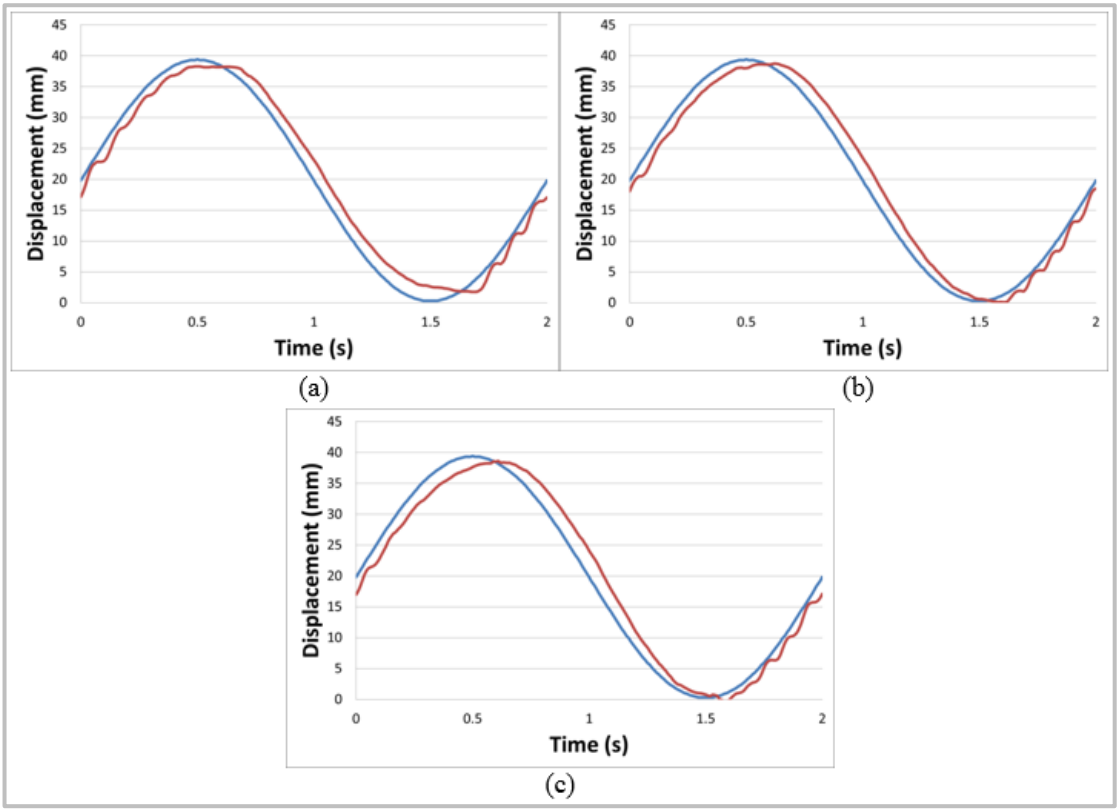

Figure 4-23: Contractor PMA response in tracking 40 mm sinusoidal displacements signal with extensor pressure of (a) 1 bar, (b) 2 bar and (c) 3 bar.

The controller gains were kept the same in each case, and it can be seen that the finger is able to track the input signal in all cases. By observing the response when an extensor

pressure of 1 bar was used, the finger does not return to the zero-displacement position as effectively as when higher pressures are used. The likely reason for this is that when the contractor PMA relaxes, it requires a force to extend it. This force is provided as the result of a combination of forces generated by the extensor and the contractor PMAs on the back of the finger. As the pressures, and therefore force generated by these muscles, is reduced, the restoring force is reduced and the finger does not extend as rapidly.

This problem can be overcome by increasing the gain of the controller used to vent the contractor PMAs. However, this then creates other problems with regards to the accuracy of the tracking when higher extensor pressures are used. This is not an altogether unexpected result as a PID controller is not able to tolerate the non-linearity that are likely to be present in this system, particularly when the stiffness of the soft robot end effector is changed.

In the experiments described above, the two contractor PMAs on the rear of the finger were required to maintain a fixed length. However, in some applications, it may be necessary for the controller to change the length of all three contractor PMAs simultaneously. To demonstrate if the controller is able to achieve this, and also to demonstrate the gripper's ability to adjust its finger length, a further control experiment was conducted. The experiment involved instructing all three independently controlled contractor PMAs to move back and forth in a step between target lengths of 200 and 230 mm. This caused the finger to expand and contract in length across a range of 30 mm. From the results, as shown in figure (4-24), it can be seen that when all three contractor PMAs are being controlled simultaneously, the displacement is broadly as accurate as when two of the extensors were kept at a fixed length.

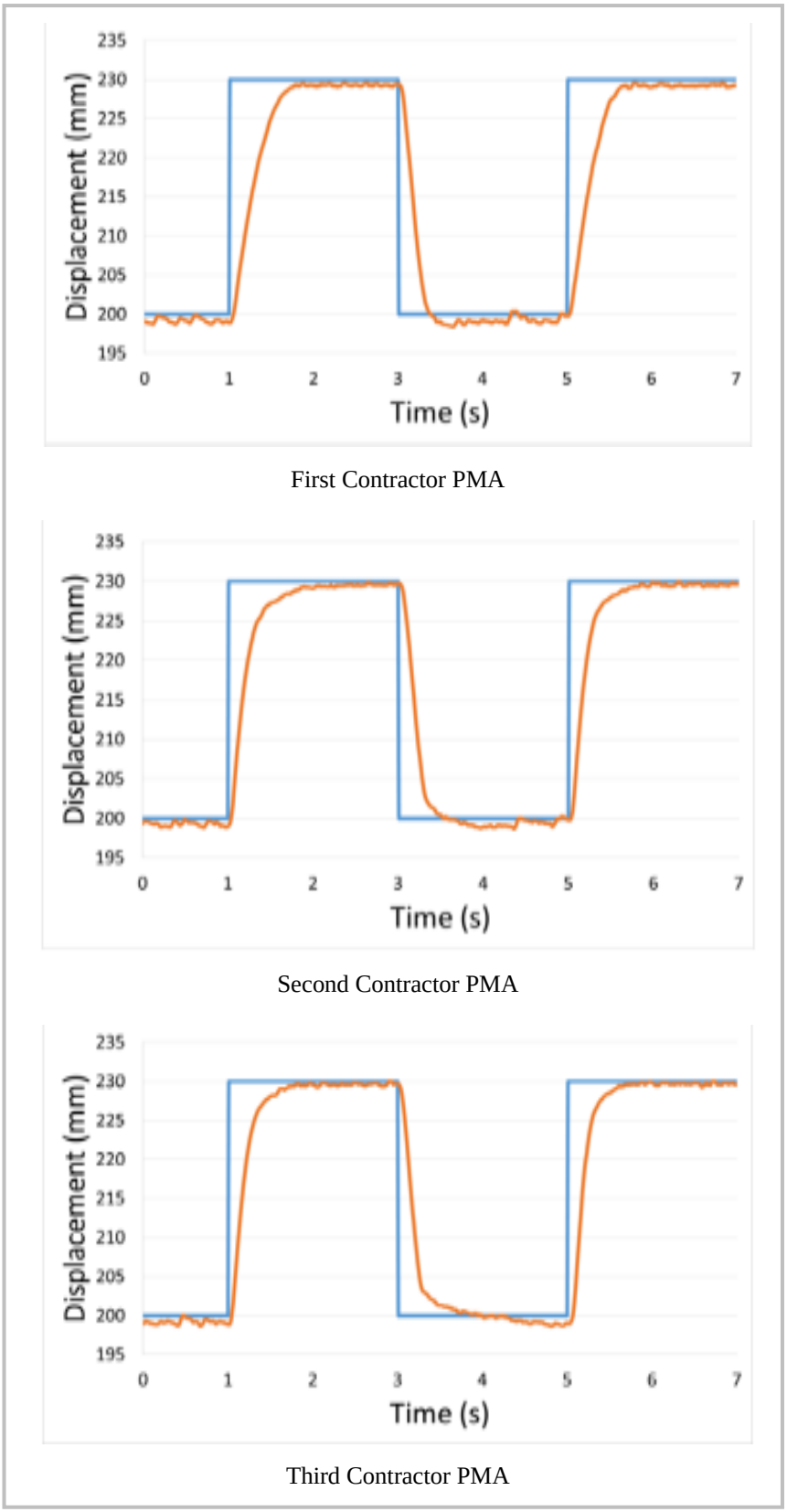

First Contractor PMA

Second Contractor PMA

Third Contractor PMA

Figure 4-24: The response of the three contractor muscles when producing a step change in finger length.

The results previously discussed illustrate the closed-loop position control of just one finger, although the same results were observed for each of the three fingers. In order to be of any practical use, the three fingers of the gripper need to be used simultaneously. Figure (4-25) shows the results of grasping experiments. The soft robot end effector was demonstrated grasping a (a) rigid tin can and (b) a soft deformable piece of fruit.

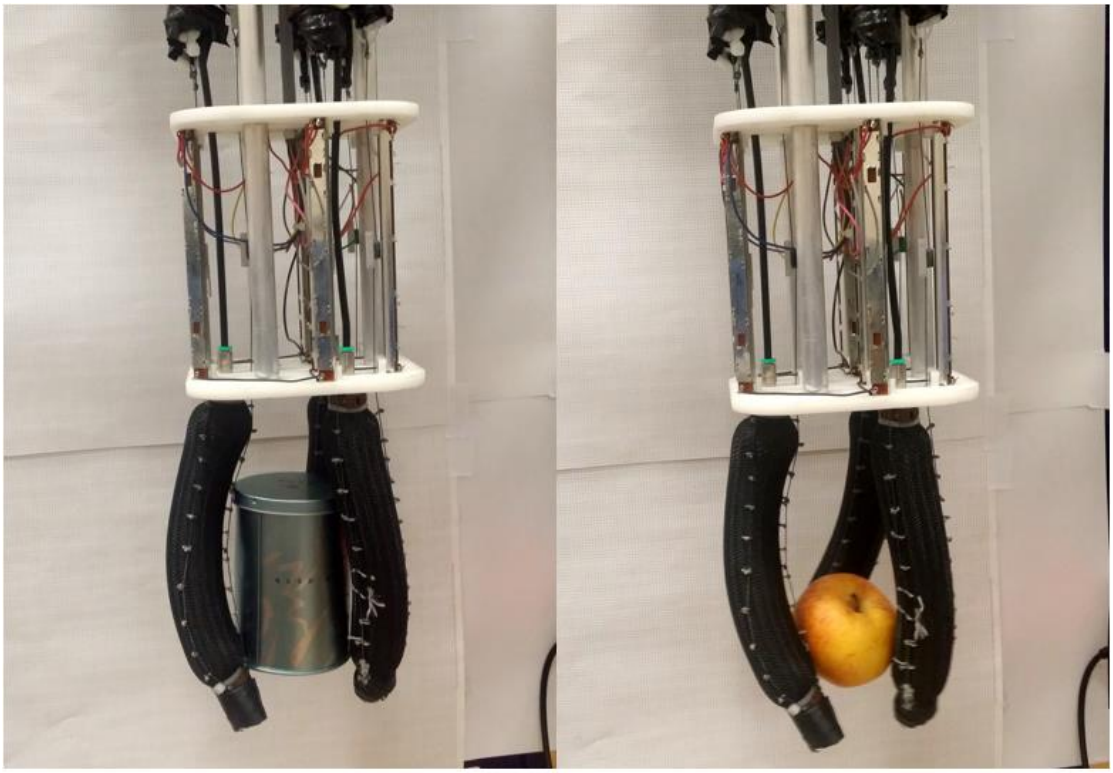

(a) (b)

Figure 4-25: The soft robot end effector grasping sample products.

Whilst the grasps were successful, the gripper currently only has position sensors, meaning there was no force control during the grasp. This meant that the finger positions necessary to achieve a secure grasp needed to be determined beforehand. The addition of force sensors would remove this requirement and will be explored in next chapter.

To investigate the system bandwidth, a 20 mm peak to peak sinusoidal signal was applied as a required target for the antagonistic system. By increasing the frequency of the signal until the finger was only able to achieve 70.7% of the required displacement the bandwidth of the system could be determined. Figure (4-26) shows the actual response of the antagonistic system when reach 70.7% of the required target.

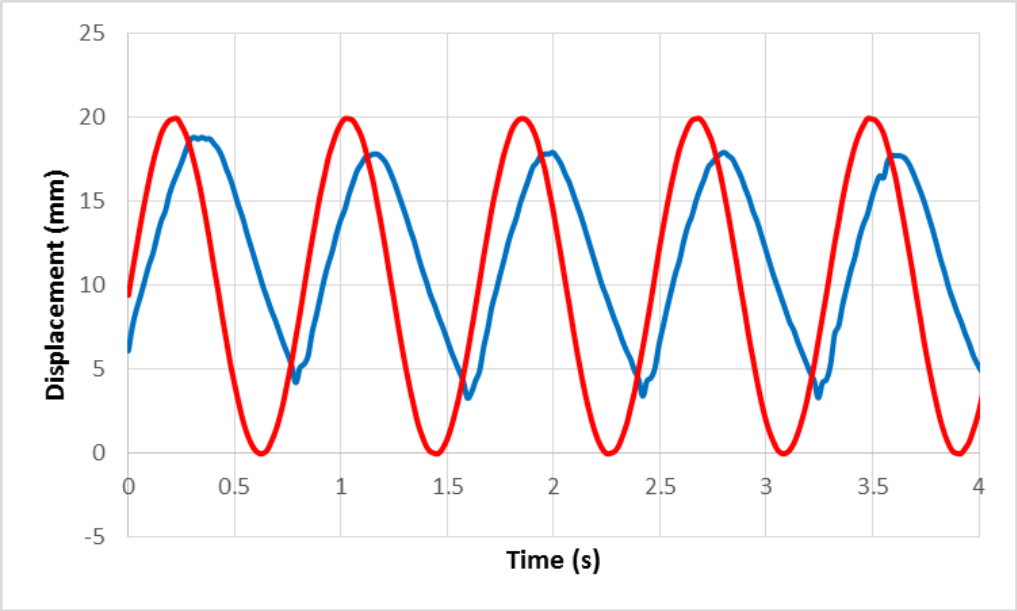

Figure 4-26: Bandwidth measurement for the antagonistic system.

From this experiment it is found that the bandwidth of the system is 1.177 Hz.

4.7 Design and Implementation of Continuum Soft Robot End Effector with Granular Jamming

To further assess the performance of granular jamming as a method of varying the stiffness of a gripper, a three-fingered variable stiffness end effector prototype was developed using granular jamming continuum fingers. The new granular jamming-based variable stiffness soft robot end effector uses the same frame design explored previously in section (4.4). However, extensor PMAs, which were used to form fingers in the previous end effector, are replaced by granular jamming continuum fingers. The granular jamming continuum fingers are designed similarly to that shown in figure (3.25). Hence, the resultant structure of the new granular jamming soft robot end effector is the same as that shown in figure (4-12). Figure (4-27) shows the actual construction of the proposed variable stiffness granular jamming soft robot end effector.

Figure 4-27: Variable stiffness granular jamming soft robot end effector.

It should be noted that cable ties are used to route three tendon cables fitted around each finger. These tendon cables, in addition to contractor PMAs, are used to control the bending of the fingers as in the previous pneumatic variable stiffness soft robot end effector. Potentiometers are also used in this granular jamming-based variable stiffness end effector to give an indication of displacement, which is used as a feedback signal to the PID controller. The ability to change the stiffness in the granular jamming-based variable stiffness soft robot end effector arises from the frictional force between granular materials when a vacuum is applied instead of an antagonistic force, as in the previous pneumatic variable stiffness soft robot end effector.

4.8 Control and Performance Evaluation of Variable Stiffness Granular Jamming End Effector

To evaluate the performance of the granular jamming-based variable stiffness soft robot end effector and to compare it directly to the pneumatic variable stiffness soft robot end

effector, the same experimental rig shown in figure (4-20) is used. The same PID controller and experimental settings are used to assess the performance and control for the new end effector. For the proposed end effector to operate in various stiffness modes, it is vital that it can be controlled irrespective of the pressure in the granular jamming continuum fingers. To determine if this was possible, step and sinusoidal response tracking experiments were conducted over a range of different granular jamming continuum finger pressures.

Figure (4-28) shows the system response when a step input is applied to each contractor muscle. The first contractor muscle causes flexion of the finger whilst the other two muscles cause extension. The step signal applied to the first muscle was 180^{o} out of phase to the signal applied to the second and third muscles. This caused the finger to repeatedly flex and extend. These first results were obtained with a granular jamming pressure of 0.0 bar.

While the dashed-blue curve represents the required target response, the red curve represents the actual controller response in all the following figures.

The experiment was repeated with a -0.4 bar pressure applied to the granular jamming continuum fingers (fingers) using a vacuum. Figure (4-29) shows the step response for all three fingers when their stiffness was increased by 34% (as determined by the stiffness experiment in section 3.5) compared to figure (4-28).

Figure (4.30) shows the controller step response for fingers when a -0.8 bar pressure is applied to the granular jamming continuum fingers. This represents an increase in stiffness compared to a jamming pressure of 0.0 bar of 235%.

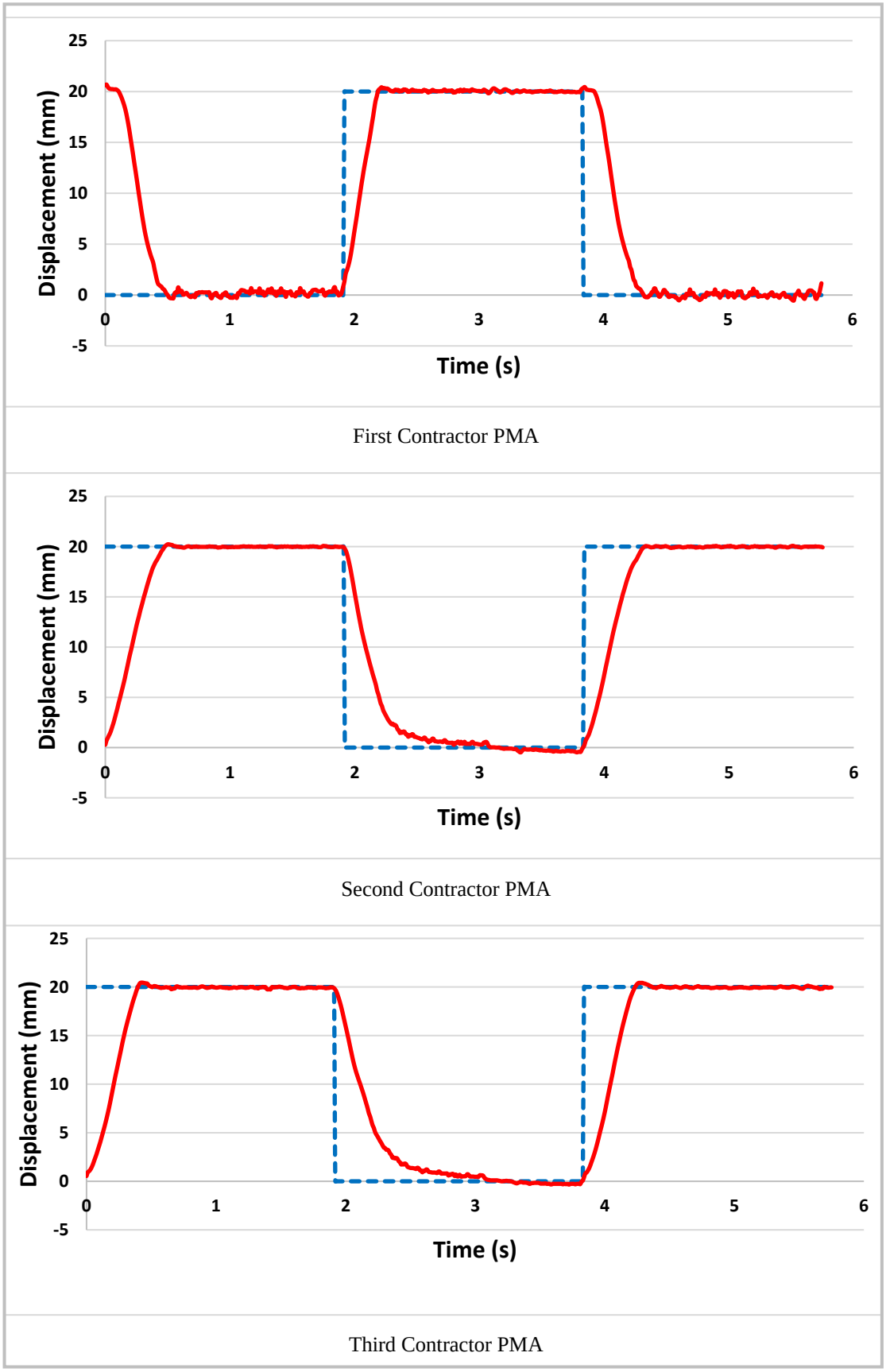

Figure 4-28: The response of the three contractor muscles when producing a step change in the finger displacement with a 0.0 bar pressure.

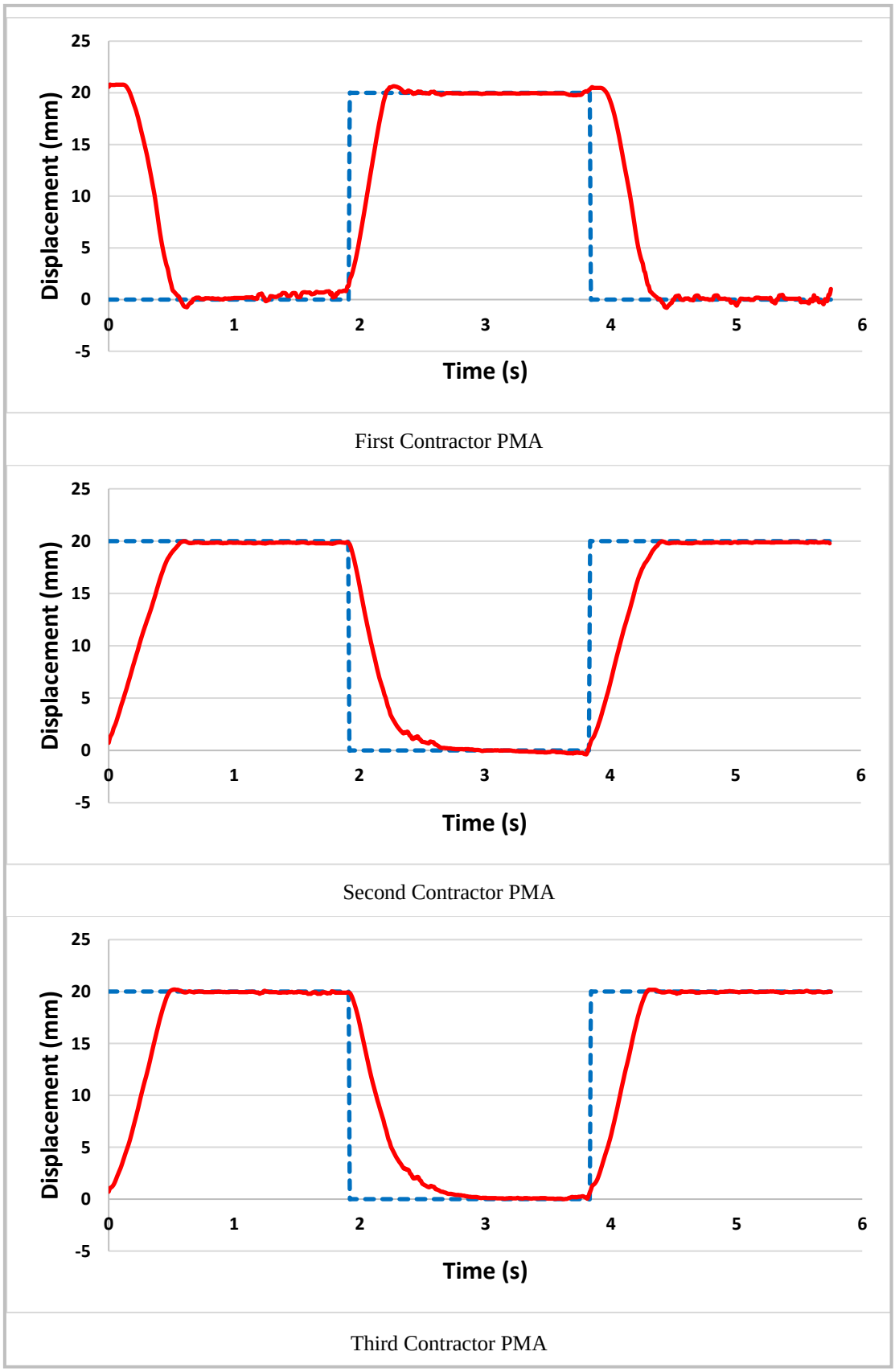

Figure 4-29: The response of the three contractor muscles when producing a step change in the finger displacement with a -0.4 bar pressure (34%) stiffness increase.

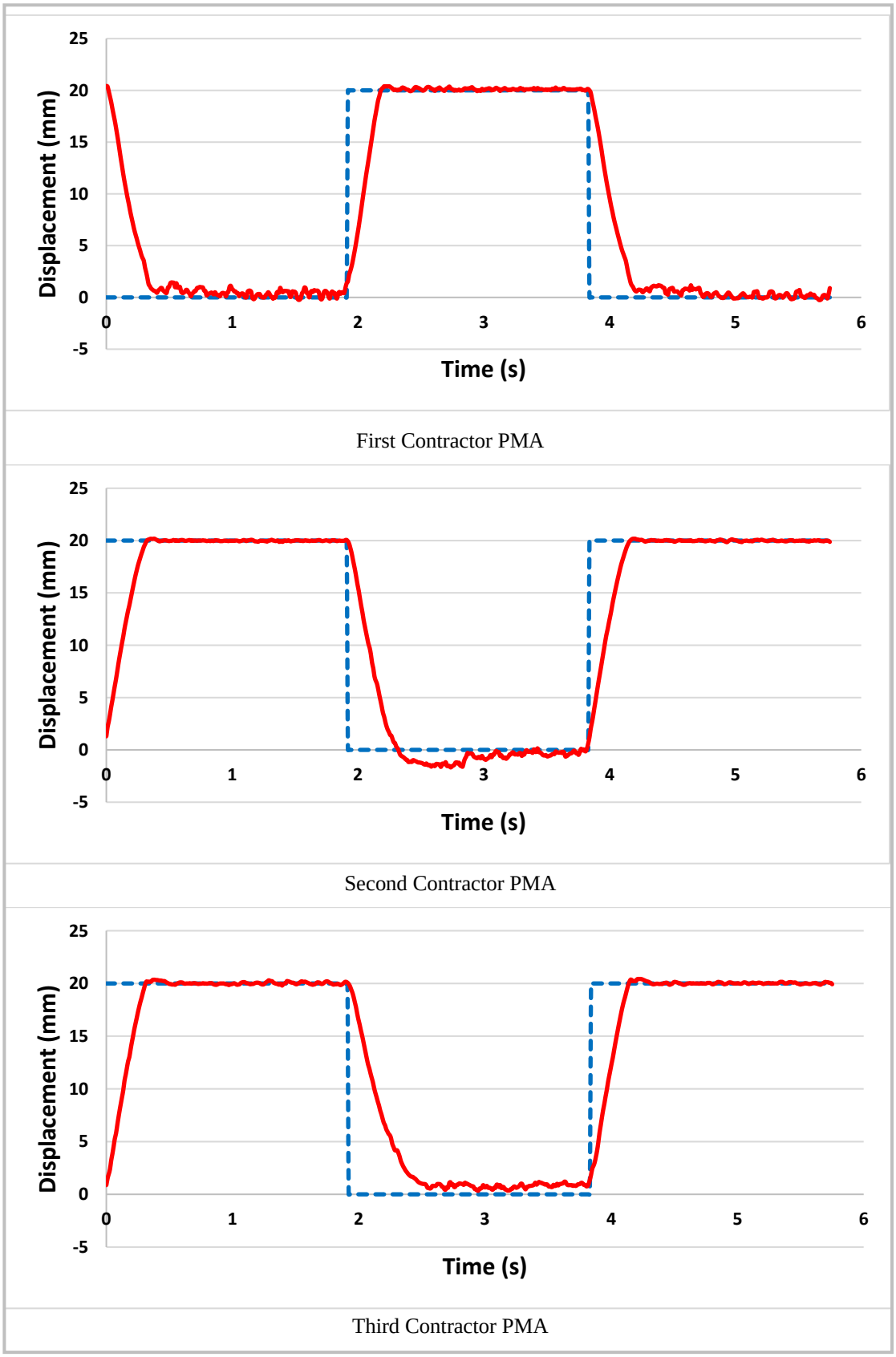

Figure 4-30: The response of the three contractor muscles when producing a step change in the finger displacement with a -0.8 bar pressure (235%) stiffness increase.

It can be seen that the performance of the end effector is similar at 0.0 bar and -0.4 bar. In both these cases, the finger reaches the target position in 0.5 seconds. The average error is 0.158 mm. However, when the pressure in the granular jamming finger is reduced to -0.8 bar, the performance of the controller reduces. The controller for the two muscles that extend the finger are still accurate; however, the contractor muscle used to flex the finger is much less accurate than that at 0.0 bar and -0.4 bar. This is not an unexpected result as if the finger is stiffer, the force the contractor muscle must apply to it to make it bend will be higher. The PID controller gains, which were selected for the lower stiffness setting, are not appropriate at higher stiffness values. This problem could likely be overcome through the use of a non-linear control method or gain scheduling.

The following figures show the ability of the controller to track a sinusoidal input signal. The range of motion was the same as in the step response experiment, with the contractor PMA causing flexion moving through an 18 mm peak-to-peak displacement from the initial position. This caused the finger tips to move by approximately 80 mm. The experiment was conducted at a frequency of 0.33 Hz.

Figure (4-31) shows the ability of the controller to track a sinusoidal input signal that induced movement in the contractor PMAs on the front of the finger when no vacuum actuation was applied (0.0 bar) to the fingers. An 180^{o} phase shift was introduced in the first contractor PMA because it was used to bend the finger in one direction and the other two bend the finger in the reverse direction.

The dashed-blue curve represents the required target response, and the red curve the actual controller response in the following figures.

The experiment was repeated with -0.4 bar applied to the granular jamming continuum fingers using the venturi. Figure (4-32) shows the sinusoidal tracking response for all three fingers when the stiffness of the fingers was increased by 34% compared to figure (4-31).

Figure (4.33) shows the controller sinusoidal tracking response for the fingers when a -0.8 bar pressure is applied. This will result in an increase in stiffness of 235%.

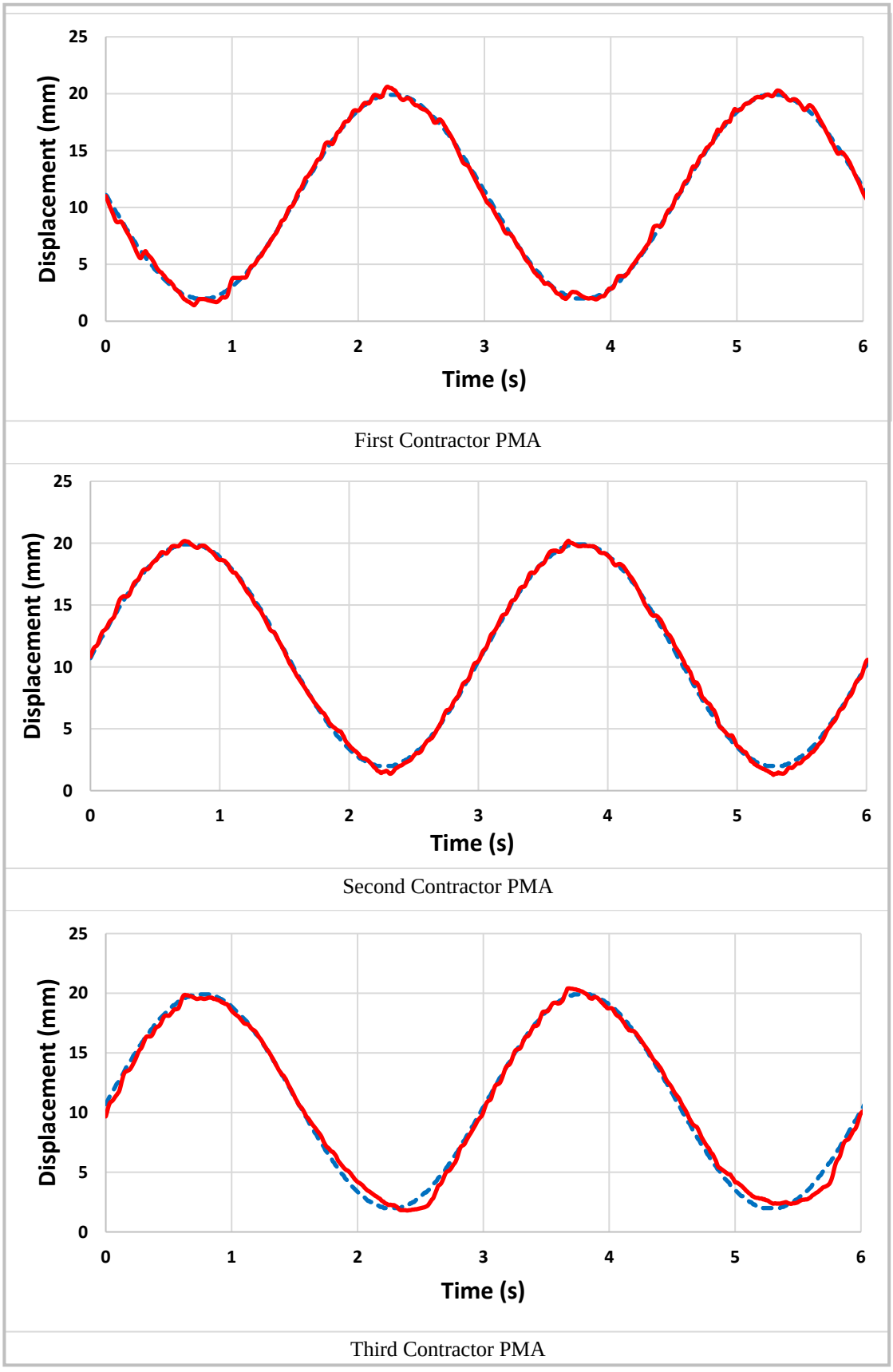

Figure 4-31: The response of the three contractor muscles when producing a sinusoidal change in the finger displacement with a 0.0 bar pressure.

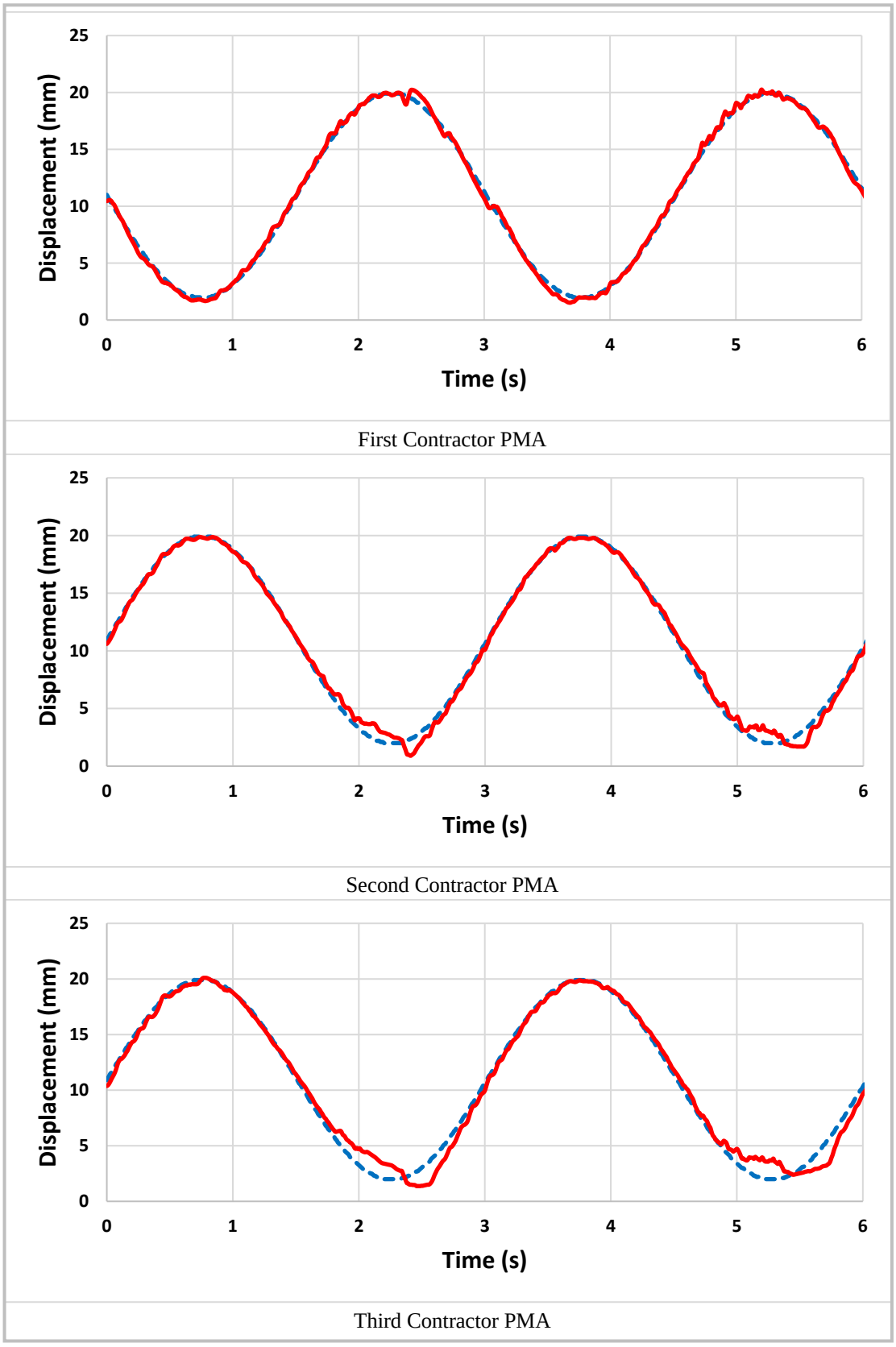

Figure 4-32: The response of the three contractor muscles when producing a sinusoidal change in the finger displacement with a -0.4 bar pressure (34%) stiffness increase.

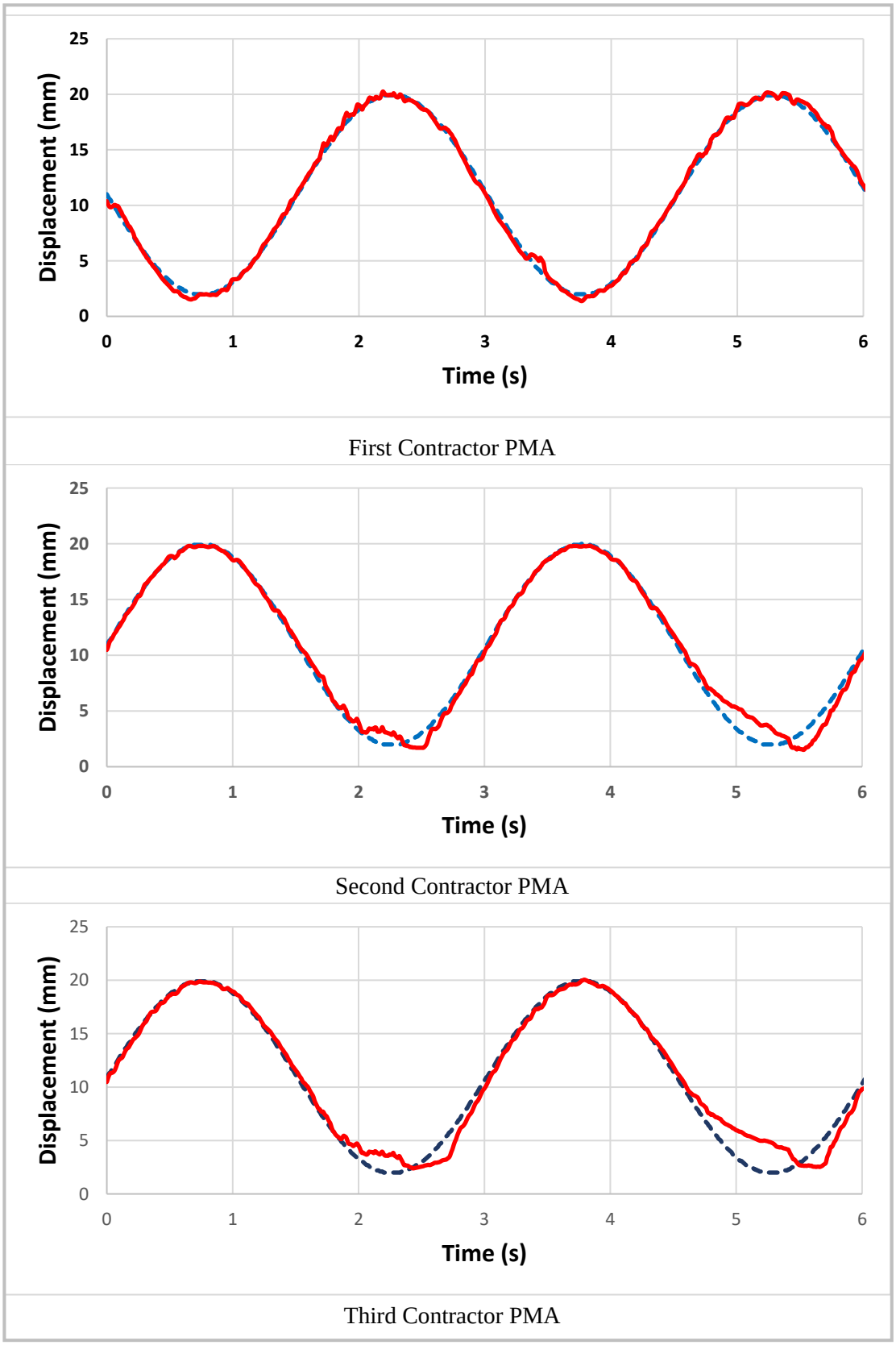

Figure 4-33: The response of the three contractor muscles when producing a sinusoidal change in the finger displacement with a -0.8 bar pressure (235%) stiffness increase.

Again, it is clear that results of the sinusoidal tracking are similar to those found in the unit step response. For both the 0.0 bar and -0.4 bar cases, the average error is 0.278 mm. In the -0.8 bar finger pressure case, the performance of the controller is reduced. The controller for the two muscles that extend the finger are still accurate. However, the contractor muscle used to flex the finger is much less accurate than at 0.0 bar and -0.4 bar. This is because the finger is stiffer and the force the contractor muscle must apply to it to make it bend will be higher. Similarly, the PID controller gains, which were selected for lower stiffness settings, are not appropriate at higher stiffness values.

Finally, the bandwidth of the granular jamming end effector was found to be the same as that for the antagonistic pneumatic end effector. As the same contractor muscles and solenoid valves are used this is an expected result.

It should be noted that whilst the use of rice as the granular material was sufficient during these experiments it is not considered a good choice of material for long term use. The reason for this is as the granules move against each other friction will cause them to experience wear. Therefore after extended use large amounts of the rice will have become a power and the performance will likely change significantly. For this reason if granular jamming is to be used in a commercial gripper other materials, which experience less frictional wear, should be investigated.

4.9 Conclusion

This chapter presents the design of two variable stiffness three-fingered soft dexterous robot end effectors. The end effectors use pneumatic muscles, which are soft and inherently compliant. In the first design, the pneumatic muscles were used to form the actual fingers of the gripper, as well as providing the force to power them. The design uniquely uses a combination of both contracting and extending pneumatic muscles that operate antagonistically. This means that by raising the pressure in all of the actuators, the stiffness of the end effector can be increased without the position of the fingers changing. This gives the proposed gripper the ability to change the position and stiffness of the fingers independently, a supposition that has been proven experimentally.

The forward kinematics of the continuum finger have been developed. These are based on kinematic analysis of previous continuum robots that have then been modified to

account for the fact that the distance of the contractor muscles from the central axis varies as the extensor is pressurised.

It has been shown that the fingers can be controlled using a PID controller and are able to respond to a step position change, track a sinusoidal inputs of different frequencies, and grasp objects. It has also been shown that the same controller can continue to position the fingers even when the stiffness of the fingers is varied.

The PID controller is widely accepted as not being the best technique by which to control soft robots, which are likely to be highly non-linear. Whilst the experimental results have shown that the fingers can be controlled, the accuracy is likely to be greatly improved if other control techniques are used.

A second variable stiffness soft robot end effector was designed and evaluated in this chapter. Three granular jamming-based variable stiffness continuum fingers replaced the extensor PMAs (fingers) in the previous end effector design. In this end effector, the stiffness was increased by increasing the friction between the granular material due to use of a pneumatic vacuum to apply a negative pressure to the granular jamming continuum fingers. The same frame, experimental rig and the PID controller were used to investigate the performance of the granular jamming variable stiffness end effector.

Stiffness was increased by 235% in the granular jamming design, compared to only 163% in the antagonistic muscle design. However, when comparing the actual stiffness of the two grippers, the antagonistic design is able to achieve a higher maximum stiffness of 96.94 N/m compared to 71 N/m for the granular jamming design. It can also be seen that the antagonistic design is easier to control than the granular jamming design, with performance being broadly the same at all stiffness values. The reason for this is likely due to the high amount of friction in the granular jamming gripper, which is likely to have highly non-linear behaviour. This is in contrast to the antagonistic design, where it was shown in chapter three that the behaviour of the extensor muscle can be approximated with a linear relationship.

A further advantage of the antagonistic design is that the length of the fingers can be controlled, allowing them to extend and contract, thus increasing the dexterity of the fingers. This is not possible in the granular jamming design where the finger length is fixed.

From a control point of view, both end effectors are capable of controlling the end effector stiffness and position independently. The use of a PID controller to control the operation of the proposed soft robot end effector is sufficient for the purposes of this research to evaluate performance. However, a PID controller is not the best choice to control granular jamming continuum fingers due to the non-linear behaviour.

Control experimental results for the granular jamming variable stiffness end effector show that when -0.8 bar is used, the end effector becomes very stiff (235% stiffer than with no vacuum) and more force or pressure in the contractor PMAs is required to achieve bending. During the testing of both types of end effector, the same pressures are used to actuate the contractor PMAs. Hence, a comparison between the performances of end effectors becomes more accurate and meaningful.

Both the pneumatic and granular jamming variable stiffness soft robot end effectors used contractor PMAs and tendon cables to manage the bending of their fingers. Hence, both are compliant and safe in any close interactions with humans.

Chapter Five

5 Controlling the Operation of Pneumatic Variable Stiffness Soft Robot Manipulator and End Effectors

5.1 Introduction

During this research, two techniques have been used to develop variable stiffness soft robot end effectors, one based on the antagonistic operation of pneumatic muscle actuators and the other on granular jamming. In the first system, pneumatic pressure generates an antagonistic force acting against that of the tendon cables used to move the finger. This method is explored and investigated for the first time in this research and a

novel structure for a soft robot end effector is constructed. A second variable stiffness soft robot end effector was designed and evaluated using the granular jamming method.

Contractor PMAs and tendon cables are used to manage the bending of fingers in the pneumatic and granular jamming variable stiffness soft robot end effectors. Hence, this will give a compliant and safe end effector that can be used in any close interactions with humans by both design methods.

While a 235% stiffness increase is achieved in the granular jamming design, only a 160% stiffness increase is achieved in the antagonistic design. However, the antagonistic design is able to produce a higher maximum stiffness of 96.94 N/m compared to 71 N/m for the granular jamming design. In addition, it is easier to control the antagonistic design than the granular jamming design, with performance being broadly the same at all stiffness values. The complicity in controlling the granular jamming continuum finger arises because of the large amount of friction force between granular materials, this will lead to highly non-linear behaviour. In contrast, in the antagonistic design, the behaviour of the extensor muscle can be approximated with a linear relationship, as shown in chapter three.

One more advantage to the use of an antagonistic design is that the length of the fingers can be controlled during operation by allowing them to extend and contract. This property is not available in the granular jamming design, where the finger length is fixed. In summary, it was found that the use of an antagonistic design gives better performance and a less complicated control strategy in the development of variable stiffness soft robot end effectors.

In this chapter, a modified variable stiffness four-fingered soft dexterous robot end effector design will be presented. The end effector uses pneumatic muscle actuators, which are soft and inherently compliant. In this design, pneumatic muscles were used to form the actual fingers of the gripper and provide the force to power it. The operation of the proposed four-fingered soft robot end effector is controlled by two different methods. A position controller was used in the first evaluation of the performance and the controller uses the same structure as that used in chapter four. Then, a force sensor is added to the tip of a finger in order to provide a feedback signal to the force controller when the grasping of an object is achieved.

Moreover, a pneumatic continuum arm is designed, explored and investigated for the first time in this chapter. The pneumatic continuum arm is constructed by using two types of PMAs (Extractor and Contractor), which are connected together in a novel structure. The performance of the proposed continuum soft robot arm is examined and pressure sensors are used to give a feedback signals to the arm's controller. Hence, a pressure control strategy is used in controlling the operation of the proposed continuum soft robot arm.

To be useful when employed, a simplified four-fingered soft robot end effector is attached to the end of the soft robot arm. It is constructed of four extensor PMAs as fingers, whilst another four contractors PMAs are used to manage the bending of the fingers through the use of tendon cables. A force controller is used to control the operation of the end effector. Pressure and force controllers are used to control the operation of the proposed soft robot manipulator.

This chapter details the design, implementation, testing and control of all of the new end effectors and the soft continuum arm. A series of experiments are then used to assess the control characteristics of the continuum arm and the end effectors at a number of different stiffnesses before a set of concluding remarks are given.

5.2 Design and Implementation of a Pneumatic Four-Fingered Continuum Variable Stiffness Soft Robot End Effector

The design and the implementation strategy used to develop the new four-fingered pneumatic variable stiffness soft robot end effector is based on the same previous design of the three-fingered end effectors. However, the number of contractor muscle actuators per finger are reduced to two instead of three, as per the previous design. A modified tendon cable arrangement is used to enhance the bending direction of the finger in this end effector. This will reduce the complexities inherent to the construction and control of the performance of the end effector. Two, four or eight pneumatic valve channels can be used to actuate this end effector. Hence, three control design options can be used. Either the end effector achieves object grasping by controlling all the fingers together

(to open or close) simultaneously, which will require only two valve channels; alternatively, each oppositely located pair of fingers are controlled together (to open or close), which will require four pneumatic valve channels. Otherwise, the use of two pneumatic valve channels for each finger, and hence eight pneumatic valve channels, are required to control the performance of all four fingers of the end effector. The number of PID control sections depends on the number of pneumatic valve channels in either configuration.

SolidWorks was used to design three mounting plates which are produced by the (Dimension Elite) 3D printer to form the end effector frame. The dimensions of the mounting plates are chosen to be (100 x 100 x 5) mm, which will reduce the amount of material and production time required for the 3D printer compared to the previous three-fingered end effector. The function of each plate is the same as that used in the end effectors developed in chapter four. However, cross-like shaped plates are used instead of the square shape employed for the previous plates. This will again reduce the material used by the 3D printer and reduce production time. Figure (5-1) shows the first plate with four extensor PMA fingers attached.

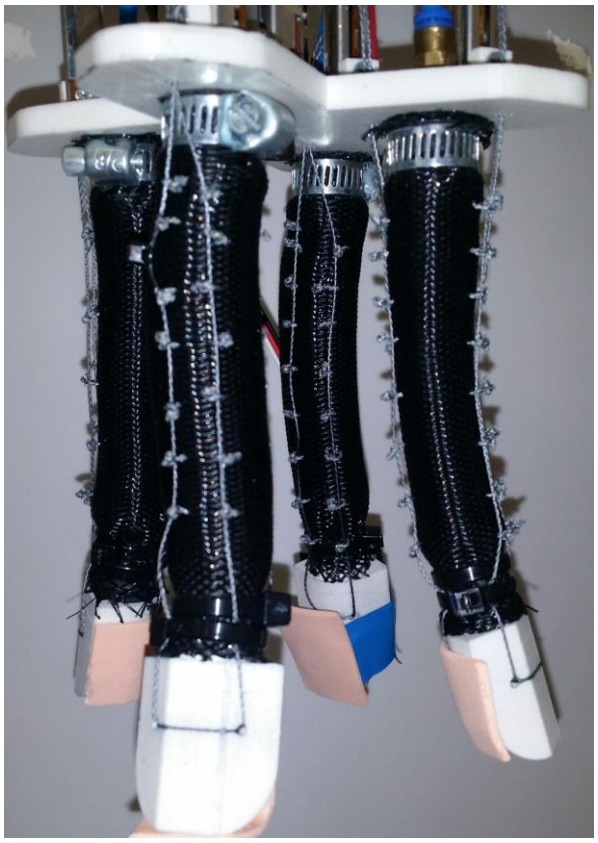

Figure 5-1: First plate with four extensor PMA fingers.

Figure (5-2) shows the complete four-fingered pneumatic variable stiffness soft robot end effector.

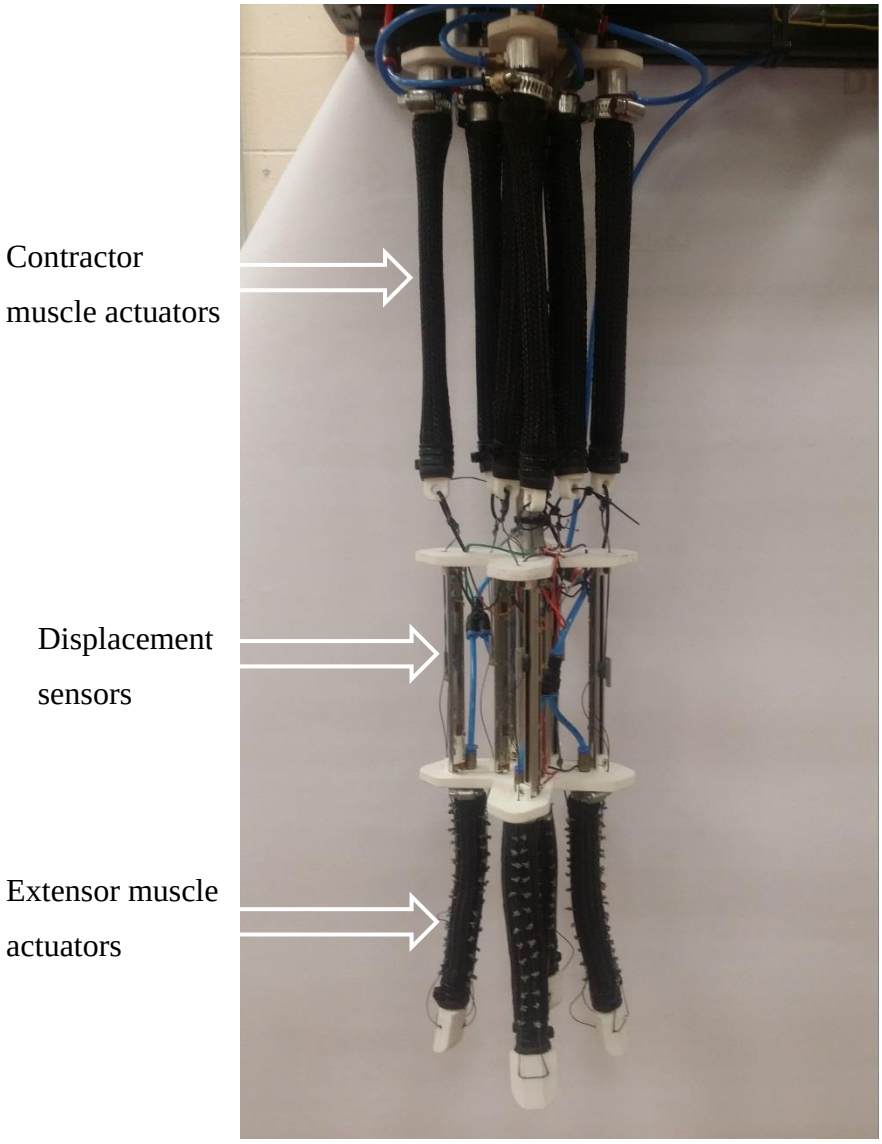

Figure 5-2: Four-fingered pneumatic variable stiffness soft robot end effector.

The unpressurised length of each finger was 120 mm, whilst the length of each of unpressurised contractor PMA was 240 mm; the length of the potentiometers used was 127 mm and the total length of the developed soft robot end effector was 560 mm. While the diameter of the unpressurised contractor PMAs is 18 mm, the same as that used in the previous design, the unpressurised new fingers diameter is reduced to 20 mm in this design.

Two tendon cables are used on each side of the finger, instead of one in the previous design (see figure 5-1), to enhance the finger bending direction (either to close or to open the gripper) during grasping. These tendon cables are used to transfer the actuation power from contractor PMAs in order to bend the fingers in any given direction according to the location of the tendon around either of these fingers. To ensure the tendons remain correctly located along the length of the finger, nylon loops are added to the outside of each finger through which the tendon passes, as can be seen in figure (5-1). These loops ensure that as the fingers bend the tendons remain in contact with the outer edge of the finger.

The tendon cable holes in the first and second mounting plates are used as a path for the tendon cables which are used to connect each side of the extensor muscles (fingers) to one contractor muscle. Hence, two contractor muscles are used to control the bending of each finger in two directions (flex and extend). A total of eight contractor muscles are used to control the bending of the entire end effector and they are divided into four groups for a total of four fingers. The tendon cables are also spooled around the central terminal of the potentiometers located between the fingers and the contractor muscles to indicate the displacement of the fingers in either direction. Potentiometer support slots in the first and second mounting plates are constructed with side screw holes and they are used to secure the eight potentiometers which are used as displacement sensors. While one terminal of all the potentiometers is connected to the +5V, the other terminals are connected to the GND. The third central terminals of all the eight potentiometers are connected to the analogue inputs of the Arduino microcontroller. These output voltage signals of the potentiometers are used as a feedback signal for the position controller which is used to control the operation of the end effector.

The four fingers are attached to a forearm like structure consisting of eight contractor pneumatic muscles, each with a maximum length of 240 mm and a contracted length at 4 bar of 180 mm, the unpressurised diameter of these contractor muscles is 18 mm. These muscles have a maximum force output of approximately 200N at 4 bar. Each finger can vary its length from 120 mm to 160 mm depending on the relative pressures in the expanding and contracting muscles, the unpressurised diameter of these fingers is 20 mm.

A single pipe is used to feed all the fingers with the same amount of pressure to all fingers of the end effector during operation. Two aluminium beams (270 mm and 127 mm in length) are used in the construction of the four-fingered, soft robot, end effector's frame compared to six in the previous design. This doesn't affect the overall frame rigidity. However, this will reduce the total weight of the end effector and, additionally, reduce the production cost of the proposed end effector.

An Arduino microcontroller linked to MATLAB was again used to control the soft robot end effector. An Adafruit 16-channel PWM/Servo Shield was used to expand the PWM output capability for the Arduino microcontroller. Two printed driving circuits were developed as the Arduino could not provide sufficient current to power the valves directly. Each printed circuit consisted of eight sections of the circuit, as shown in figure (4-16). The system configuration block diagram of the proposed four-fingered soft robot end effector is the same as that shown in figure (4-14).

In total, there were twelve PMAs, four extensors and eight contractors PMAs. All the extensor muscles, fingers, were attached to a single air pressure regulator allowing the pressure in the fingers to be varied manually. The eight contractor muscles were, however, attached to eight individual solenoid valves which allowed air to be supplied to, or vented from, a single muscle when required. The valves were controlled by PWM signals to allow the flow rate of air into and out of the muscle to be controlled. Hence, eight pneumatic valves (MATRIX 3-3 solenoid valve) are needed to power the contractor PMAs. Two of the pneumatic compact solenoid multi-valves were used in this soft robot end effector, each of which had a total of four pneumatic valves. Figure (5-3) shows a photograph of two compact solenoid multi-valves, two amplification (driving) circuits, an Arduino Mega 2560 microcontroller and an Adafruit 16-channel PWM/Servo Shield, which are all used in the construction of this four-fingered soft robot end effector.

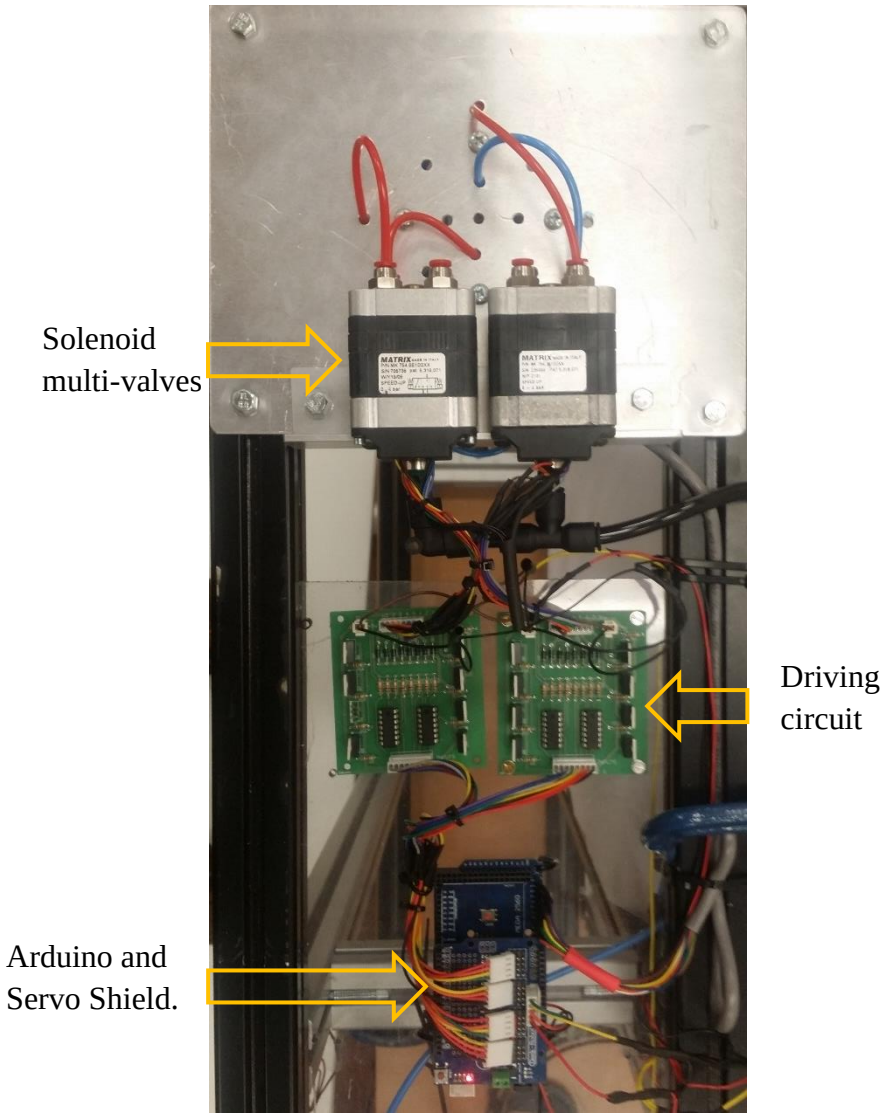

Figure 5-3: Two compact solenoid multi-valves, two amplification circuits, Arduino Mega 2560 microcontroller and Adafruit 16-channel PWM/Servo Shield.

There were eight contractors PMAs pressurised by eight solenoid valves. However, sixteen driving circuit sections are required to drive all valves, eight for filling and eight for venting the contractor PMAs.

A dual output power supply was used to provide the required DC voltages to power the Arduino microcontroller, Adafruit expansion boards, driving circuit and the solenoid valves.

5.3 Position Control for the Pneumatic Four-Fingered Continuum Variable Stiffness Soft Robot End Effector

To assess the performance of the proposed four-fingered end effector, a positional PID controller with the same configuration as that used in the previous two end effectors was again used. Figure (5-4) shows the experimental rig used in the performance investigation experiment.

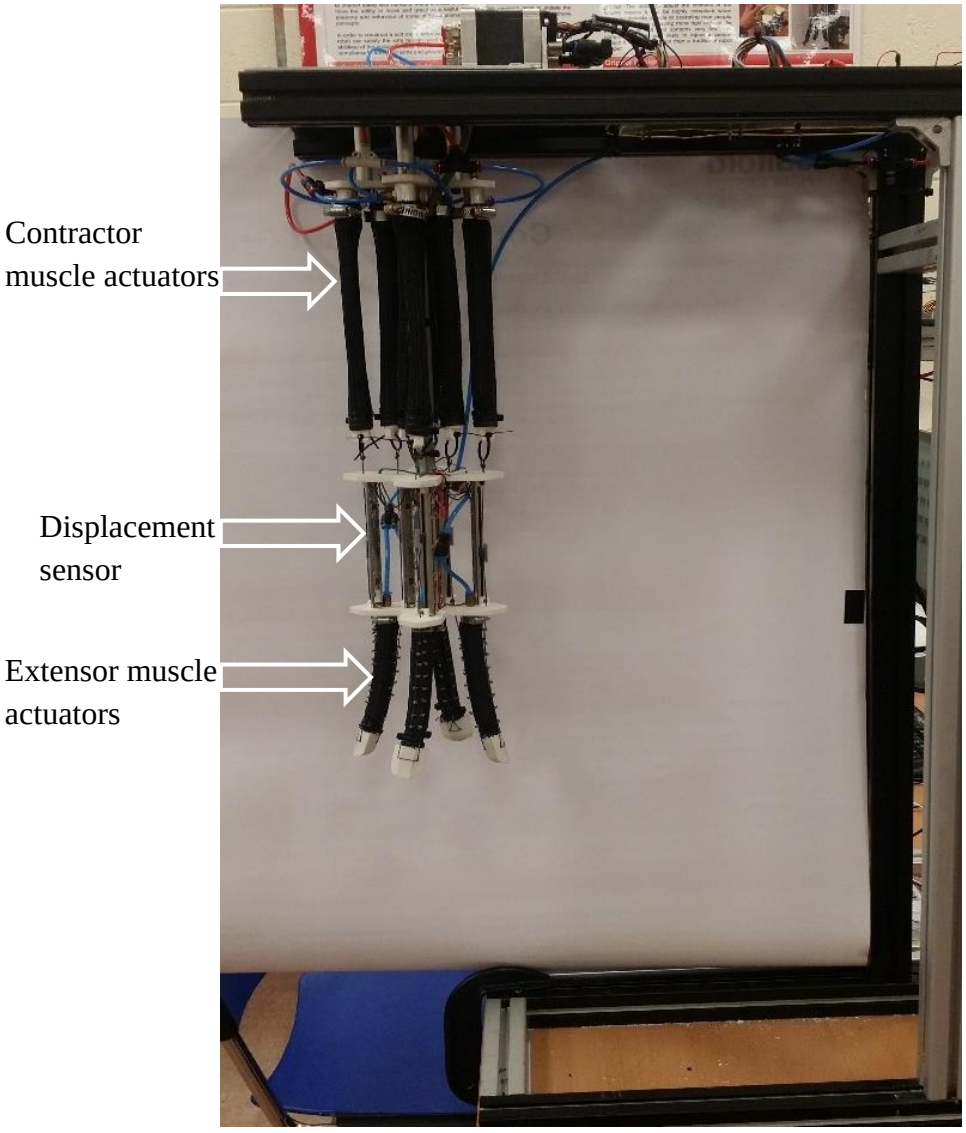

Figure 5-4: Four-fingered end effector fitted to the experimental rig.

Figure (5-5) shows the results of the grasping experiments. The soft robot end effector was demonstrated grasping numerous items with different shapes, weights and sizes.

Figure 5-5: Four-fingered soft robot end effector grasping sample products.

It was found that the four-fingered soft robot end effector is capable of grasping a wide range of items with different shapes, weights and sizes, as shown in figure (5-5). However, where the gripping was successful, the gripper currently only has displacement sensors, meaning there was no force control during the grasping operation.

5.4 Force Control for the Pneumatic Four-Fingered Continuum Variable Stiffness Soft Robot End Effector

To assess the force PID controlling suitability in controlling the gripping operation of the four-fingered continuum variable stiffness soft robot end effector, a force-sensitive resistor sensor was attached to the tip of one finger of the proposed end effector. Figure (5-6) shows the pneumatic four-fingered variable stiffness soft robot end effector with the force sensor attached.

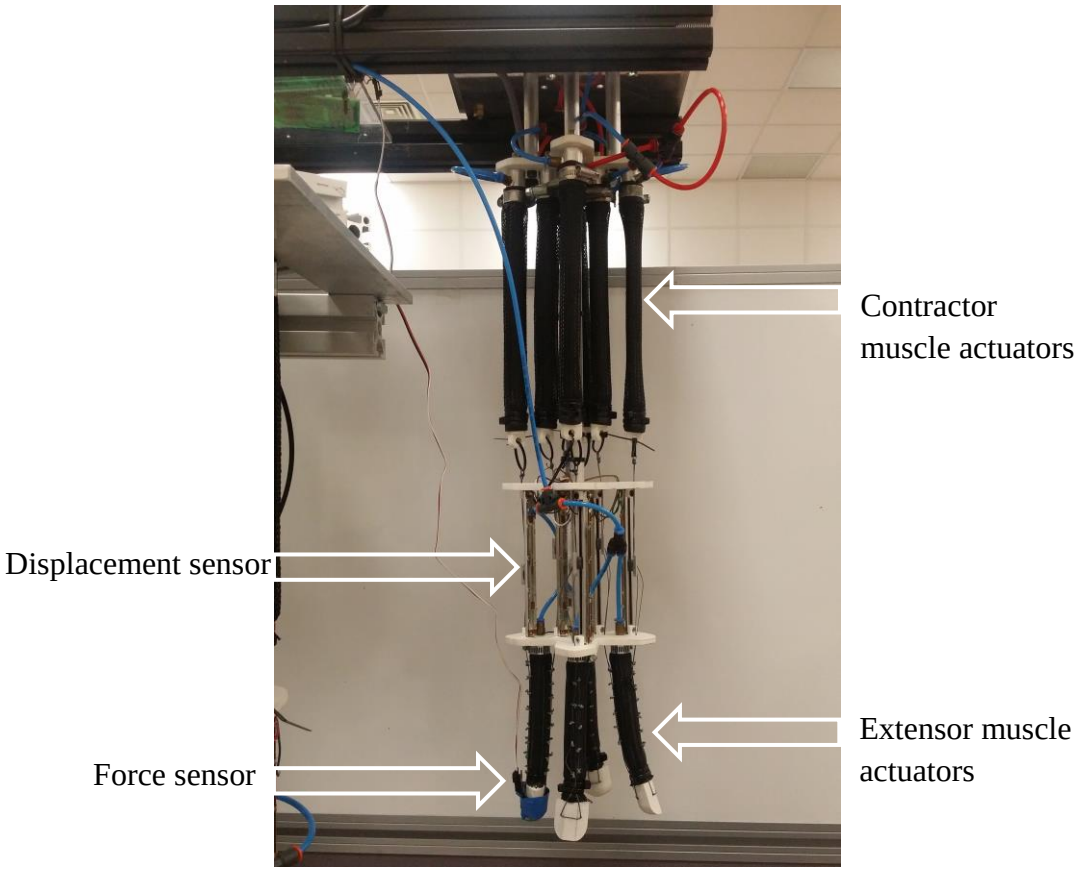

Figure 5-6: Force control experimental rig for the four-fingered end effector.

The GND and +5 V terminals of the force sensor were supplied from the Arduino microcontroller board; the output voltage signal of the sensor was also determined

through the Arduino microcontroller. The voltage signal from the force sensor was used as a feedback signal to drive the PID controller. In the following experiment, the end effector will be used to grip a ball. The finger flexing is controlled in response to the force sensor feedback signal. For the object to be released, or to open the gripper, the potentiometer voltage signal was used as a feedback signal to the PID controller. That is to say, force control was used during grasping but position control was used to open the fingers and release an object. If force control was used to release the object, there is no guarantee that the fingers would actually spread. Using position control ensures they are opened wide before the next object is grasped. Figure (5-7) shows the response of the gripper to the control signal when a ball is being gripped. Note that the blue curve represents the required target response and the red curve represents the actual controller response.

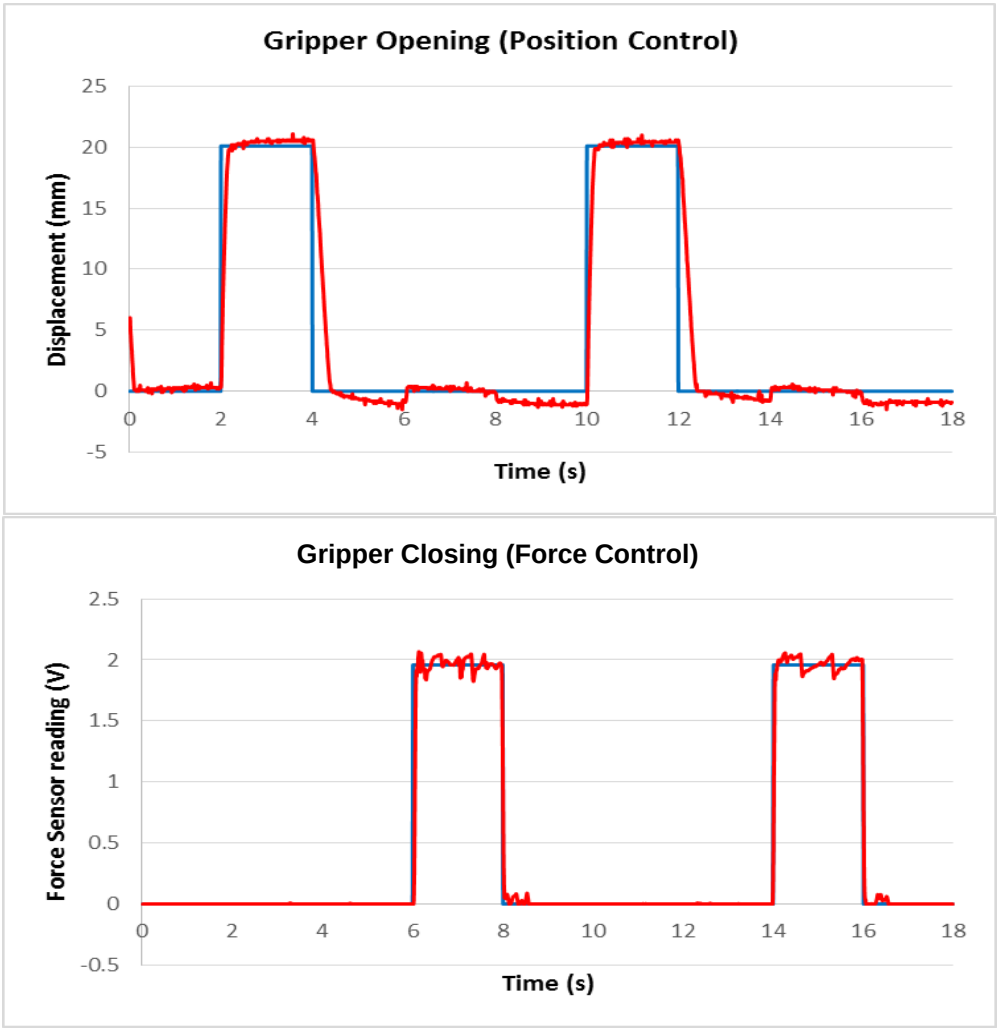

Figure 5-7: Position and Force controller's response for the pneumatic four-fingered soft robot end effector.

Figure (5-7) confirms the suitability of the force controller in controlling the operation of the pneumatic four-fingered soft robot end effector. Figure (5-8) shows examples of some objects grasped during this experiment.

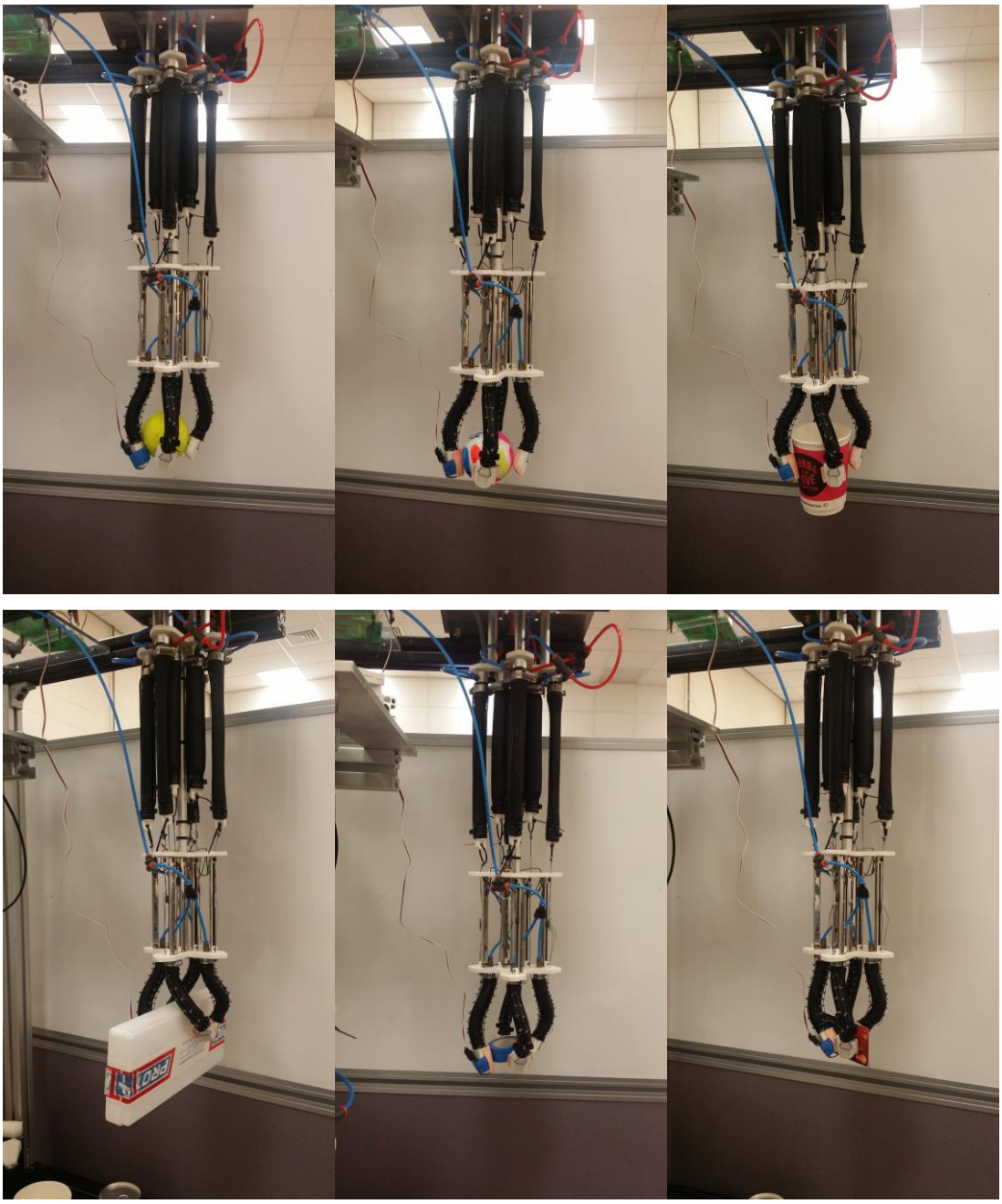

Figure 5-8: Examples of some objects grasped during force control experiment.

5.5 Design and Implementation of Pneumatic Continuum Soft Robot Arm

A pneumatic soft robot continuum arm was also developed during this work. The continuum arm was implemented using the same method as shown in figure (4-1). The continuum soft robot arm was constructed using three contractor pneumatic muscle actuators fitted around one central extensor pneumatic muscle actuator, and the group was secured together using cable ties. As the arm uses antagonistic muscles, it has the same capability to change its stiffness as the grippers previously described. During operation by proportionally increasing the pressure in all the pneumatic muscle actuators at the same time, the arm is able to change its stiffness without affecting the end effector's position.

In the design of the continuum arm, the SolidWorks CAD software application was used to design the mounting plates which are produced by the (Dimension Elite) 3D printer to form the ends of the continuum arm. The dimensions of the mounting plates were chosen to be (100 x 100 x 5) mm. Figure (5-9) shows the construction of the two plates from both sides.

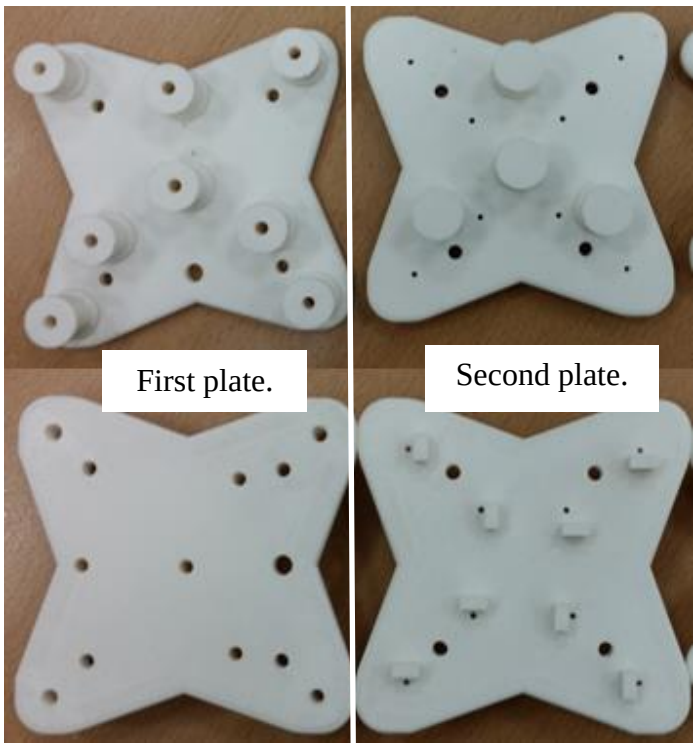

Figure 5-9: The two plate's construction for the pneumatic variable stiffness soft robot continuum arm.

From figure (5-9), the function of the first plate (left) is to mount one end of the continuum arm. The second plate (right) is used for mounting the second end of the continuum arm. Note that, there are several holes in the first mounting plate to let the air in and out of the actuators. Figure (5-10) shows the pneumatic soft robot continuum arm.

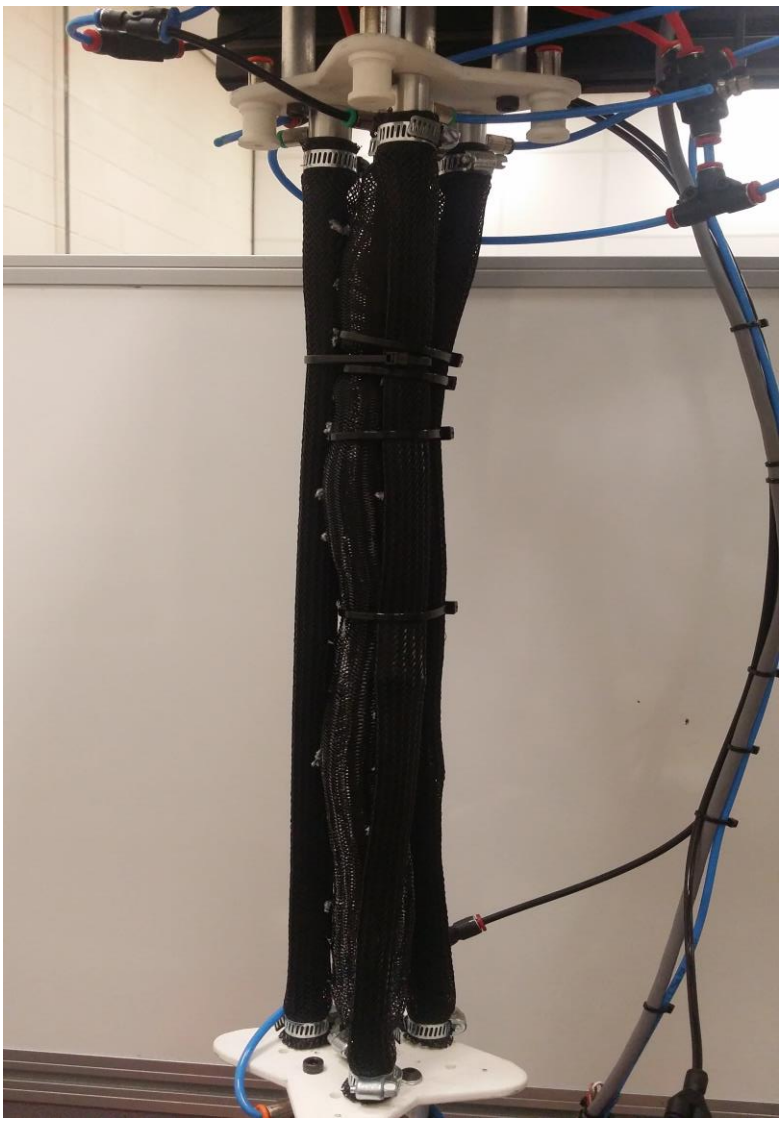

Figure 5-10: One section of pneumatic variable stiffness soft robot continuum arm.

Figure (5-11) shows a photograph of two compact solenoid multi-valves, two amplification (driving) circuits, an Arduino Mega 2560 microcontroller and an Adafruit 16-channel PWM/Servo Shield, which are all used in the construction of the continuum soft robot arm.

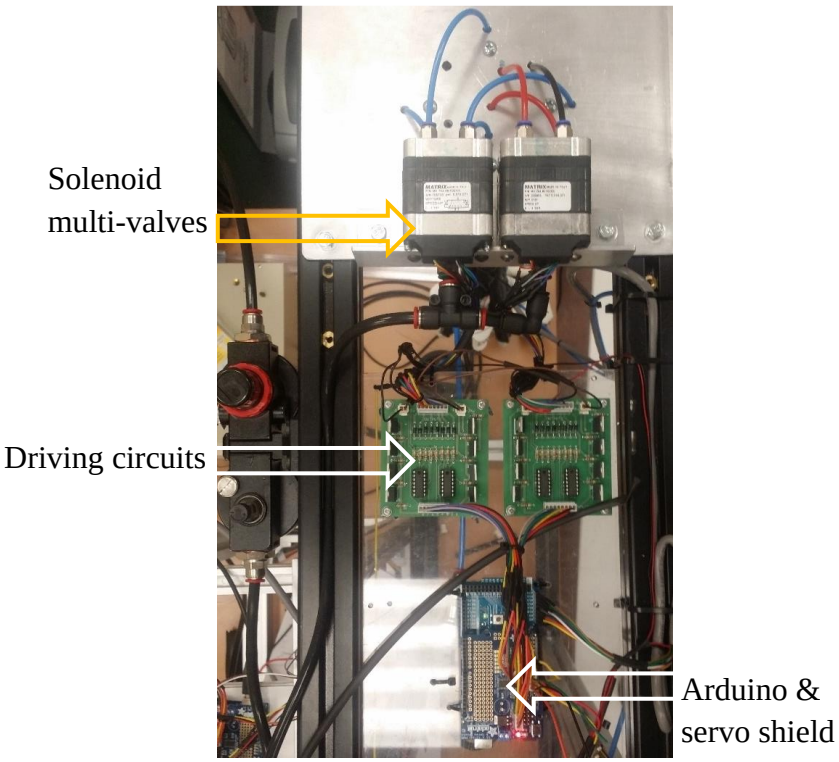

Figure 5-11: Two compact solenoid multi-valves, two driving circuits, Arduino Mega 2560 microcontroller and Adafruit 16-channel PWM/Servo Shield for the pneumatic variable stiffness continuum soft robot arm.

The unpressurised diameter for all three contractor PMAs is 20 mm, with a 35 mm diameter being used for the unpressurised extensor PMA of the continuum arm. The total length of the non-actuated continuum arm is 490 mm. Finally, the developed pneumatic soft robot continuum arm has 3-DOF, one in extension/contraction of length and two in bending in any direction around the arm.

Four MATRIX (3-3) pneumatic valves were used to control the pressurised air to be filled to or vented from either PMA in the proposed pneumatic soft robot continuum arm. One pneumatic compact solenoid multi-valve is used to actuate this continuum soft robot arm; see figure (5-11). The second solenoid multi-valve is for future use. Hence, sixteen driving circuit sections to drive all the eight MATRIX (3-3) valves are required, eight to control filling and eight to control venting the PMAs being used. Finally, a dual output power supply was used to provide the required DC voltages to power the Arduino microcontroller, Adafruit expansion boards, driving circuit and the solenoid valves.

5.6 Pressure Control of Pneumatic Continuum Soft Robot Arm

The pneumatic soft robot continuum arm developed differs from those illustrated in sections (2.6.1) to (2.6.4) of this thesis by simultaneous use of both extensor and contractor PMAs in its construction. The use of both extensor and contractor PMAs in the construction of the arm gives it the capability to change its stiffness during operation by increasing the pressure to all PMAs at the same time. This is because the actuators act antagonistically meaning a pressure increase in the contractor muscles can be counteracted by a pressure increase in the extensor muscles. This means although the pressure in the arm's actuators is increased (and as shown previously their stiffness therefore increases) the position of the arm does not change.

Four pressure transducer (0-0.5 MPa, 0.5-4.5 V) sensors were used to indicate the amount of pressure in either extensor or contractors PMAs. These indication signals are used as a feedback signal for the PID controller, which is used to control the operation of the developed pneumatic soft robot continuum arm.

Table (5-1) shows a result of a pressure sensor testing experiment, which used a manual pressure regulator and measured the output signals through an Arduino microcontroller. The input voltage for the sensor is taken from the GND and +5 V terminals of the Arduino board.

	Sensor Reading (V)	
Pressure (bar)	**Extensor PMA**	**Contractor PMA**
0	0.508	0.494
0.5	0.909	0.909
1	1.183	1.105
1.5	1.442	1.466
2	1.843	1.852
2.5	2.224	2.170
3	2.590	2.502

Table 5-1: Pressure transducer sensor testing results.

These data were used to calibrate the sensor readings in the following experiments, which were conducted to investigate the pressure control capabilities of the proposed pneumatic soft robot continuum arm.

The position of the end of the soft arm will vary depending upon the magnitude and relative ratio of the pressures inside the muscles. To demonstrate the ability of the soft arm to move between locations, three target positions were selected at random. Each position required pressures of 0.5, 1.0 and 1.5 bars, respectively, for the contractor muscle.

Figure (5-12) shows the closed-loop pressure controller response in moving the arm from an initial resting position to each target position, as mentioned above. In this first experiment the pressure in the extensor muscle was 0.5 bar.

To demonstrate that the arm could still be controlled at higher stiffnesses, the experiment was repeated with higher pressures in the extensor muscle. Figure (5-13) shows the results with an extensor pressure of 1.0 bar, and figure (5-14) shows the results with an extensor pressure of 1.5 bar.

It can be seen that the controller responds well to the step pressure change and that it can be controlled with the same amount of accuracy at all three amount of extensor muscle's pressures.

Note that the dashed blue curve represents the required target response and the red curve represents the actual controller response in all the following figures.

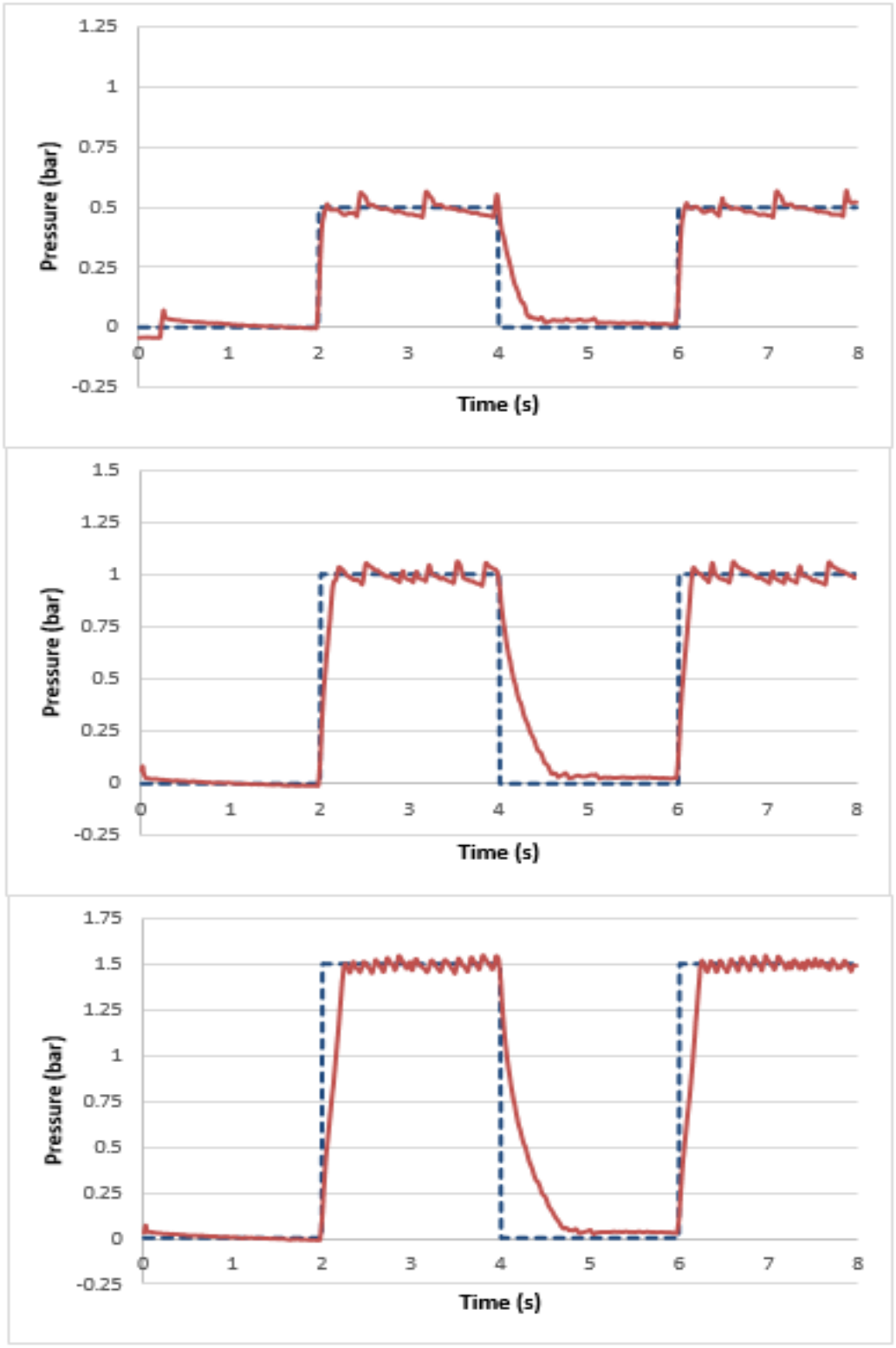

Figure 5-12: Pressure controller response for the continuum arm with 0.5 bar in the extensor PMA and 0.5, 1.0 and 1.5 bar in the contractor PMA, respectively.

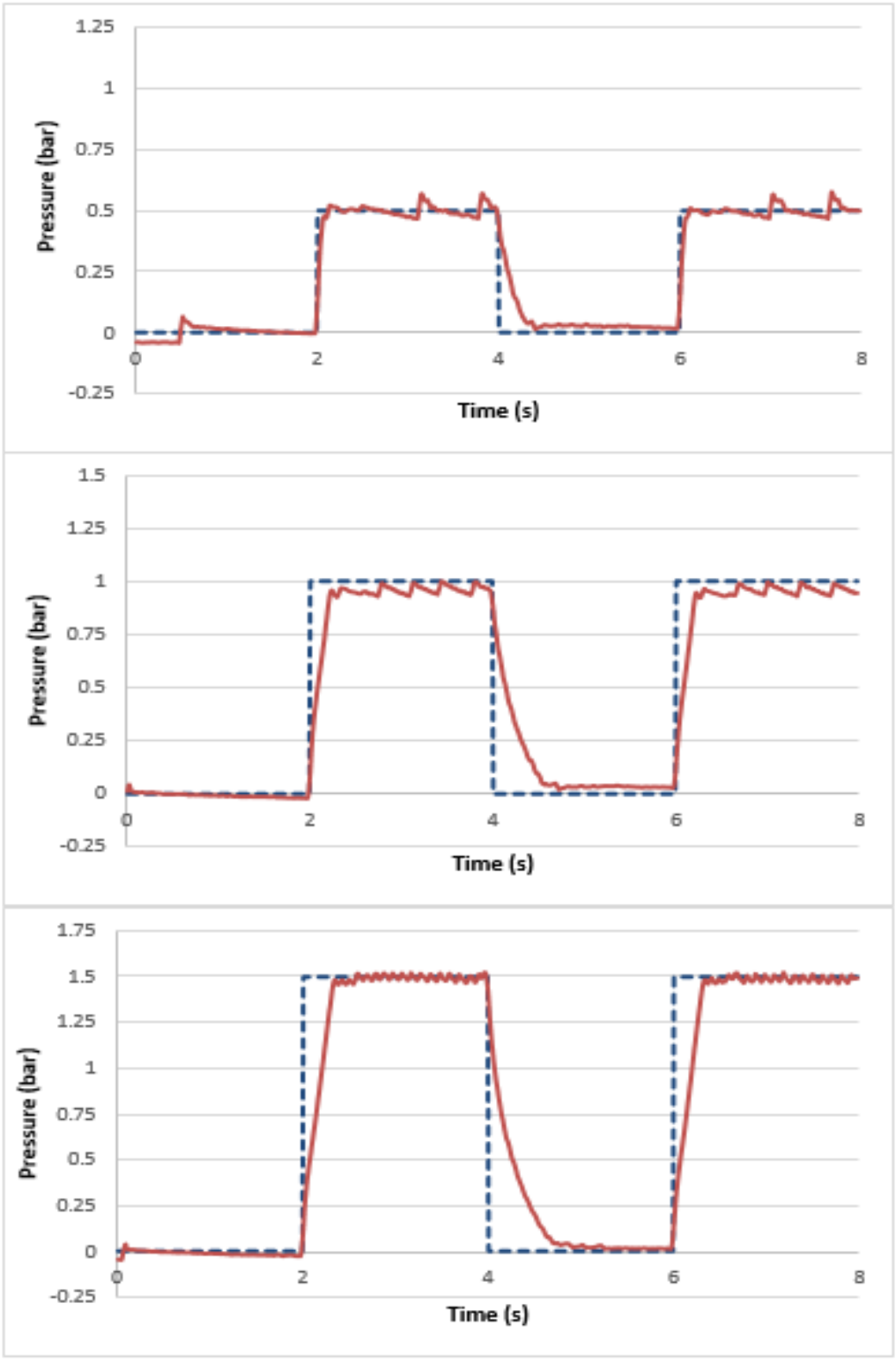

Figure 5-13: Pressure controller response for the continuum arm with 1.0 bar in the extensor PMA and 0.5, 1.0 and 1.5 bar in the contractor PMA, respectively.

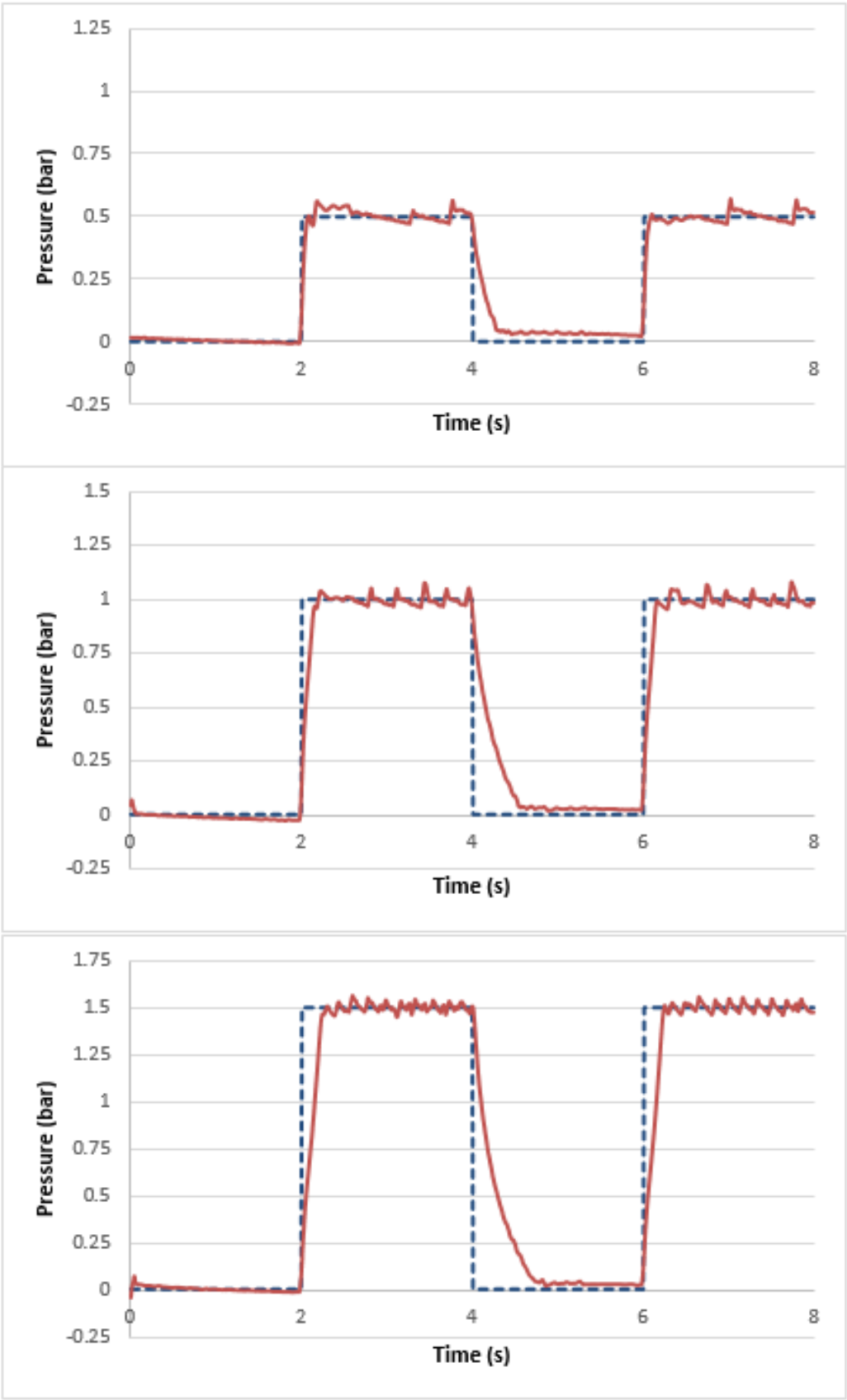

Figure 5-14: Pressure controller response for the continuum arm with 1.5 bar in the extensor PMA and 0.5, 1.0 and 1.5 bar in the contractor PMA, respectively.

Figures (5-12), (5-13) and (5-14) confirm the capabilities of the proposed pneumatic soft robot continuum arm to response to step input. It is clear that the arm has the ability to bend in the required direction whatever the pressure of the central extensor PMA.

The amount of bending of the continuum arm depends on the amount of pressure in the contractor PMA. As can be seen from all three above figures, the contractor PMA can achieve a good response at 0.5, 1.0 and 1.5 bar input pressures.

In the illustrated results of the experiment, one contractor PMA was chosen to demonstrate the pressure control capabilities of the proposed system. The control performance of the other contractor muscles was found to be broadly similar meaning the arm could move equally accurately in any direction.

The amount and the direction of the bending of the continuum arm will change if two contractor PMAs are actuated together with the extensor PMA. This also increases the payload of the proposed pneumatic soft robot continuum arm.

In order to be practical in use, a simplified pneumatic gripper was implemented and attached to the end of the proposed pneumatic soft robot continuum arm. The next section will illustrate the design and implementation of the simplified four-fingered soft robot end effector.

5.7 Simplified Four-Fingered Soft Robot End Effector

Another four-fingered variable stiffness soft robot end effector was designed and implemented during this work. The simplified design is used to save space and make it as compact as possible. The proposed end effector was fixed to the end of the pneumatic soft robot continuum arm. Figure (5-15) shows the construction of the proposed simplified four-fingered soft robot end effector.

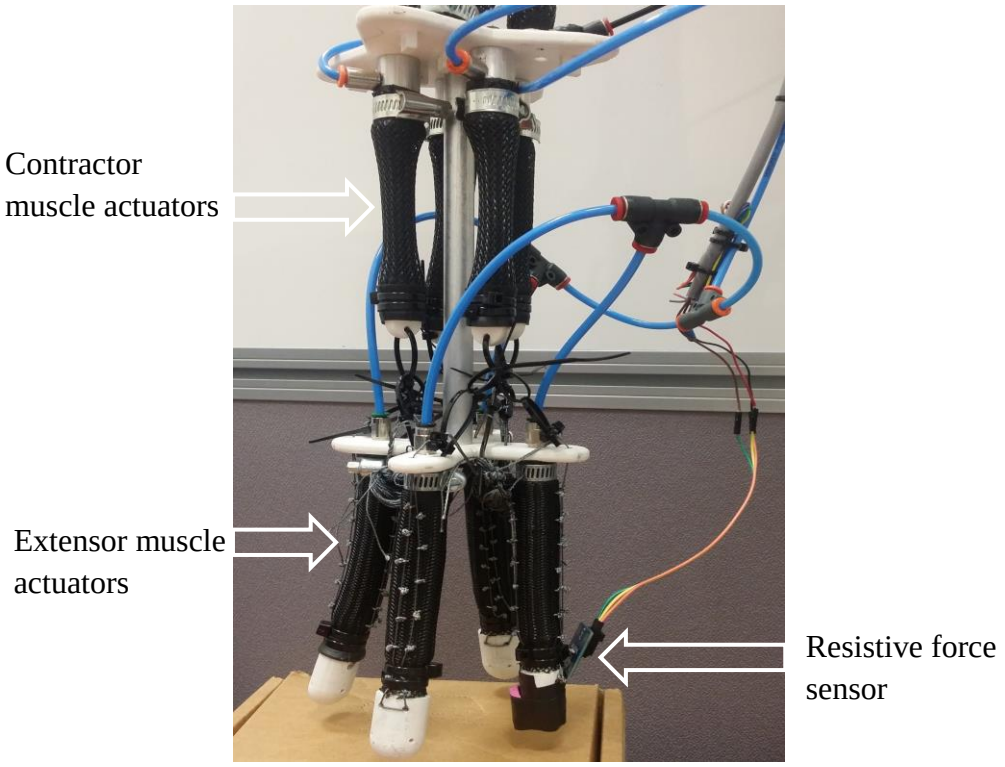

Figure 5-15: Simplified four-fingered soft robot end effector.

Four contractor PMAs were used to control the bending of the four extensor PMA fingers, compared to eight in the previous once; see section (5.2). Each pair of two opposing contractor muscles are used together either to flex or to extend all four fingers of the proposed end effector. This would reduce the cost of construction and make it simpler in terms of its design, construction and in controlling its operation compared to the previous design.

One pneumatic pipe was used to feed all the fingers so as to allow them to reach the same pneumatic pressure during operation. Two tendon cables were used on each side of the finger to ensure the bending direction during grasping. These tendon cables were used to transfer the actuation power from the four contractor PMAs in order to bend the fingers in the required direction. To ensure the tendons remained correctly located along the length of the finger, nylon loops were added to the outside of each finger through which the tendon was passed, as can be seen in figure (5-15). These loops ensure that as the fingers bend the tendons remained in contact with the outer edge of the finger.

While the diameter of the unpressurised contractor PMAs is 18 mm, the same as that used in the previous design in section (5.2), the unpressurised new finger diameter was reduced to 20 mm in the simplified four-fingered soft robot end effector. The unpressurised length of the contractor and extensor muscles is designed to be 120 mm.

A force sensor was attached to the tip of one finger to provide a feedback signal for the PID controller, which was used to control the grasping operation of the end effector. This signal was used to determine if the four-fingered end effector was achieving a proper grip on the given object by controlling the amount of pressure in the four contractor PMAs.

Only one aluminium beam (180 mm in length) was used in the construction of the simplified four-fingered end effector's frame. This was to reduce the total weight of the end effector and reduce the cost of production of the proposed pneumatic variable stiffness continuum soft robot manipulator. The unpressurised length of each finger was 120 mm and the total length of the developed pneumatic soft robot manipulator was 800 mm (including the soft arm and the simplified gripper) from the base to fingertip. A second compact solenoid multi-valve shown in figure (5-11) was used to actuate the simplified end effector.

Figures (5-16) and (5-17) show the results of grasping experiments. The pneumatic soft robot was demonstrated grasping and relocating various items of different shapes, weights and sizes. In each figure the robot can be seen to move to an object, grasp it, relocate it and then release it.

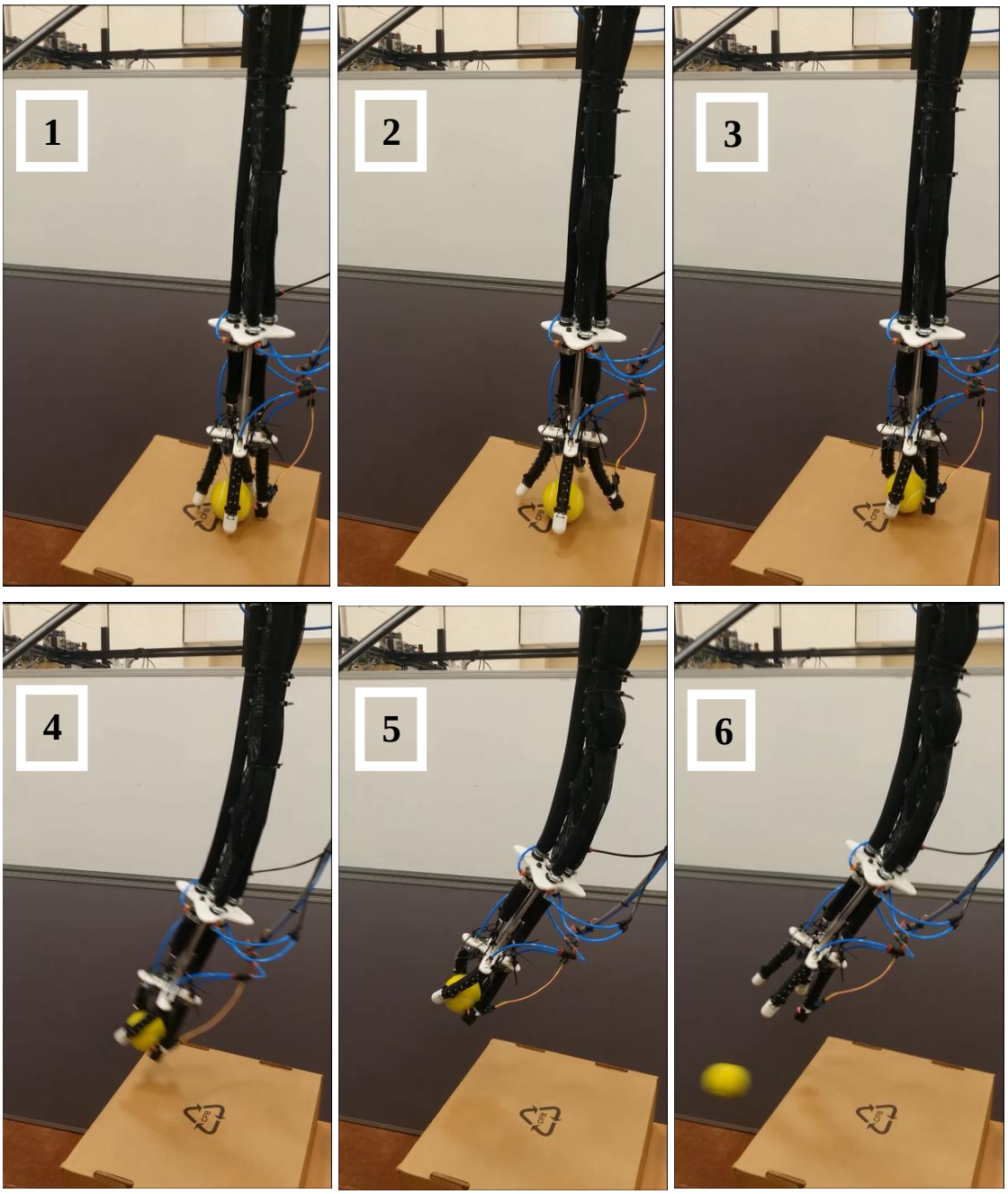

Figure 5-16: Ball grasping, relocating and releasing experiment for the proposed pneumatic continuum soft robot manipulator.

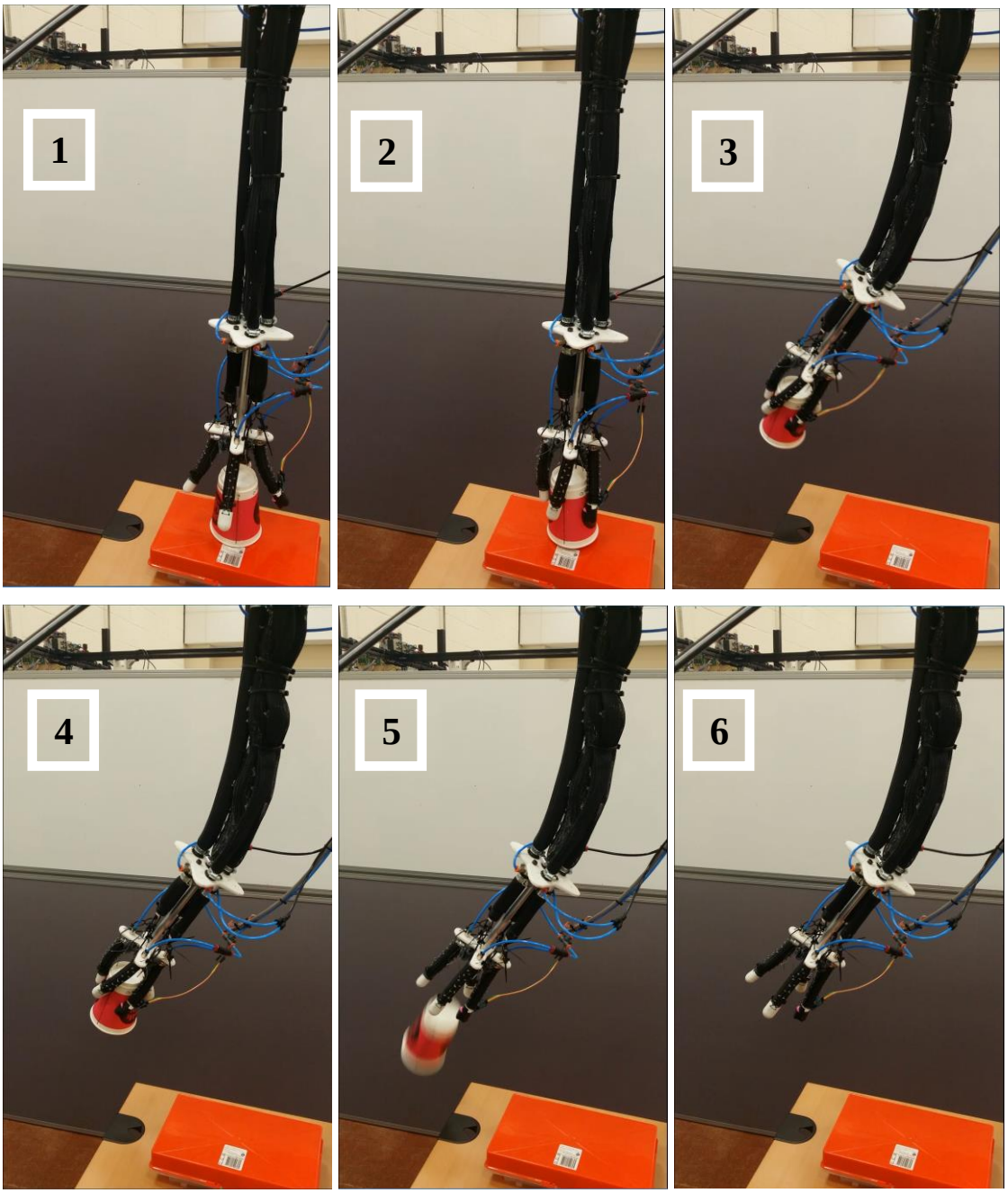

Figure 5-17: Cup grasping, relocating and releasing experiment for the proposed pneumatic continuum soft robot manipulator.

5.8 Conclusion

This chapter presented the design of two variable stiffness four-fingered soft robot end effectors in addition to a pneumatic continuum soft robot arm. The end effectors used pneumatic muscle actuators which were soft and inherently compliant and this was also the case for the continuum arm.

In the end effectors' design, pneumatic muscles are used to form the actual fingers of the gripper as well as providing the force to power them, just as for the previous three-fingered end effectors; see section (4.4). The newly designed end effectors use a combination of both contracting and extending pneumatic muscles that are operated antagonistically. Hence, by increasing the pressure in all of the actuators, the stiffness of the end effector is increased but the position of the fingers remains unchanged. So, the proposed grippers have the ability to change the position and stiffness of the fingers independently.

An enhanced design was used to form a new four-fingered variable stiffness soft robot end effector by using three pneumatic actuators per finger instead of four in the three-fingered end effector, which was examined in detail in chapter four of this thesis. This reduces the complexity of the design and the control operation of the proposed end effector, as well as reducing the time and cost of its implementation. One extensor muscle was used to form the finger, and two contractor muscles were used to create the bending of the finger. An enhanced arrangement of the tendon cables was used in the new design. This arrangement enhanced the bending of the fingers during opening and closing of the end effector. Finally, position control and force control strategies were used to evaluate the performance of the proposed end effector. Experimental results show the suitability of both types of controllers and the functionality of the proposed pneumatic four-fingered soft robot end effector.

A pneumatic soft robot arm was also implemented and investigated for the first time in this chapter. The novel design of the proposed arm uses both extensor and contractor PMAs in the construction which act antagonistically to allow the stiffness to be adjusted. One central extensor PMA surrounded by three contractor PMAs was used to implement the arm. Again, by increasing the pressure in all PMAs the overall stiffness of the arm could be increased. Four pressure sensors were used to give an indication of

the amount of pressure in each of the pneumatic muscle actuators used in the continuum arm. This gives the ability to test the suitability of pressure control schemes. The experimental results show the use of a pressure control scheme to control the stiffness and the bending of the continuum arm was successful.

In order to make the developed continuum arm useful in real applications, a simplified four-fingered soft robot end effector was also implemented during this work. The simplified four-fingered soft robot end effector used four extensor PMAs as fingers and only four contractor PMAs, the latter being used to control the bending of the fingers. Two contractor PMAs were used together to open the end effector, whilst the other two were used to close them during operation. A force control scheme was used to control the operation of the proposed simplified end effector. Experimental results show the capability of the simplified end effector to grip a range of different shape and sized objects.

Finally, the simplified pneumatic variable stiffness four-fingered soft robot end effector was fitted to the end of the soft robot continuum arm to produce a complete soft robot continuum manipulator. The developed manipulator has the ability to grasp a given object and move it to another location. This was achieved by controlling both the arm and gripper at the same time. While a pressure control scheme was used to control the operation of the continuum arm, a force control scheme was used for the end effector. Hence, both pressure and force control schemes were used simultaneously to control the operation of the developed variable stiffness soft robot continuum manipulator. The complete continuum soft robot manipulator was demonstrated grasping and relocating a number of different objects.

Chapter Six

6 Conclusions and Future Work

6.1 Conclusions

To develop soft robots that can interact safely with humans, many types of actuators have been developed. One of the earliest types of actuator investigated for this purpose was the Series Elastic Actuator. As explained previously, series elastic actuators introduced the elastic element for the first time into actuator structures. Hence, the actuator becomes more compliant. However, series elastic actuators have many drawbacks, such as backlash, friction, and limited performance. Another problem with this type of actuator lies in the selection of the spring constant used as an elastic element in the construction of series elastic actuators. While a low spring constant is required at low output impedance to minimise the effect of the nonlinear friction, a high spring constant is necessary in order to gain a large output impedance bandwidth.

To overcome some of these problems, other kinds of compliant actuators have since been introduced. Variable Stiffness Actuators began to be used instead of the series elastic actuators in constructing new types of robots, such as biped robots and humanoid robots. In variable stiffness actuators, the actuator compliance and joint position are controlled separately using two independent electric motors. However, there are many limitations in the use of variable stiffness actuators, especially in unspecified work environments and in joint work environments, where safe human-robot interaction is a desirable concept. The main limitations with variable stiffness actuators are their slow performance when adjusting their position, large actuator size, the weight of the actuator, power losses due to friction and the requirement for two electric motors in the actuator construction.

Since the 1960s a new type of actuator (pneumatic muscle actuator), as inspired by nature, has been developed. Pneumatic muscle actuators only use soft materials in their construction, and they can be used directly without gearboxes. The most popular design of pneumatic muscle actuator is based on the McKibben muscle configuration. Pneumatic muscle actuators have a high power-to-weight ratio compared to the previous rigid actuators, and are inherently soft, compliant, clean and low-cost. Hence, pneumatic muscle actuators are safe, economical and lightweight compared to other actuators.

These pneumatic muscle actuators have been widely used in constructing a new generation of robots known as soft robots. Compliance and construction from soft materials are desirable concepts in the implementation of soft robots. The development of soft robots leads to a new range of applications that would otherwise be impractical for rigid robots. Giving soft robots the ability to safely interact with humans allows for the possibility of a joint human-robot work environment. In other words, there is a clear need to develop a new category of robots that can deform their shapes and be able to adapt their behaviour to any given work environment.

One design of soft robot is the continuum robot, which has the potential to allow safe human-robot interaction. These robots do not have any rigid links or discrete joints but instead flex along their entire length. Researchers have proposed many continuum soft robot prototypes; however, these prototypes do not have the capability to change their

stiffness during operation. Variable stiffness capability is an important concept in the design and development of a dexterous soft robot manipulator and its end effectors, as variable stiffness actuation would allow continuum soft robot arms and end effectors to operate in a safe (low stiffness) mode, but with the ability to switch to a higher stiffness mode when high-precision operation is required.

From a study of the existing literature, it has been seen that grasping can be achieved using a number of different soft robotic techniques such as whole arm grasping, multi-fingered hands and a granular jamming universal gripper. The whole arm grasping technique using a continuum soft robot arms requires a large contact area with the grasped object. It has been found that they have the capability to grasp large-sized objects. However, it is not suitable for grasping small-sized objects. In addition, controlling the performance of continuum arms is a particularly challenging task as they deform and bend in the working space while in contact with the grasped object.

To deal with small-sized and unregularly shaped objects, a multi-fingered soft robot end effector has been proposed. Although fingers are soft in all the prototypes illustrated in chapter two of this thesis, they are also all attached to a stiff base in order to construct the final shape of the end effector. This combination of soft and rigid materials reduces the compliance of the system, and may be unsuitable for applications where human safety is a desirable requirement. In addition, the shape, size and weight of the objects to be grasped using the multi-fingered hands previously illustrated are limited. Moreover, most of the proposed prototypes have no sensors that can be used to give an indication of the prototype operation. Feedback signals are vital to the design of the controller to be used in controlling the operation of the multi-fingered soft hand.

In most cases, these soft grippers are unable to change their stiffness during operation. While highly compliant fingers may be desirable in order to gently grasp certain objects, stiffer fingers are required to achieve precise performance.

The ability to change the stiffness in the granular jamming universal gripper plays a desirable role in picking and placing a wide variety of objects that are not otherwise easy to pick using the universal gripper, such as certain flat and soft objects. However, the use of crushed coffee as a granular material limits the gripping performance of the universal jamming gripper. Crushed coffee in the universal gripper cannot give

sufficient force to grip an object securely. Hence, a multi-fingered, variable stiffness, continuum soft robot end effector can provide a better overall performance compared to universal grippers.

This research has demonstrated the use of pneumatic muscles in soft robotic applications. Pneumatic muscle actuator characteristics have been investigated experimentally through this research in order to develop a mathematical model to describe the behaviour of such actuators. Force/displacement characteristics have been individually investigated for both the contractor and the extensor pneumatic muscle actuators. The results found during these experiments have been used to develop the mathematical models. The variable stiffness spring model was found to be a good model to represent the behaviour of the pneumatic muscle actuators. The mathematical model developed was used to predict the pressure/displacement characteristics of the pneumatic muscle actuators, with the experimental results confirming their suitability. This mathematical model gave a good description of the behaviour of the pneumatic muscle actuators in the range of pressures starting from 1.0 bars and more.

The variable stiffness capabilities of pneumatic muscle actuators and granular jamming continuum fingers have been investigated experimentally through the development of a number of soft robot end effectors. Compliance capabilities for the pneumatic muscle actuators, both contractor and extensor, when arranged in a certain configuration, have been investigated experimentally. The experimental results were determined by measuring the lateral displacement of the extensor pneumatic muscle actuator in response to the attached force under different combinations of pressures applied to both contractor and extensor pneumatic muscle actuators. It was found that increasing the extensor pressure to 4 bar led to an increase in stiffness of up to 163% for a 190 mm extensor muscle length, and 112% for a 180 mm extensor muscle length, respectively.

The force/displacement characteristics for the granular jamming continuum finger were also investigated experimentally. The bending stiffness characteristics of the granular jamming continuum finger were determined using these experimental results. It was found that decreasing the granular jamming continuum finger pressure from zero to (-0.8) bar will result in an increase in stiffness of 235%.

Therefore, both of these two types of stiffness changing techniques were used in the development of variable stiffness soft robot end effectors. These have the capability to work in a low stiffness, compliant mode to interact safely with humans. In addition, they have the capability to change their stiffness during operation to act as stiff, rigid-like robots in order to control their behaviour more accurately.

A variable stiffness three-fingered soft dexterous robot end effector has been designed and constructed according to the findings of this research. The developed end effector uses pneumatic muscles that are soft and inherently compliant. Inside this end effector, the pneumatic muscles are used to form the actual fingers of the gripper and further to provide the force to power them. Hence, they are safe in direct interaction with humans. The design uniquely uses a combination of both contracting and extending pneumatic muscles that operate antagonistically. This means that by raising the pressure in all actuators, the stiffness of the end effector increases without changing the actual position of the fingers. This gives the developed end effector the ability to change position and the stiffness of its fingers independently, a supposition that was subsequently proved experimentally.

The forward kinematics of the continuum finger have been developed. These are based on the kinematic analysis of the previous continuum robots, which have then been modified to account for the fact that the distance of the contractor muscles from the central axis varies as the extensor is pressurised.

Granular jamming continuum fingers are used instead of the extensor muscles as fingers in the previous design. The bending of these fingers is controlled by three tendon cables equally spaced around each finger. Three contractile pneumatic muscles are used to control the spooling of these three tendon cables. Hence, the contractile muscle determines the motion of the finger, and the jamming of the granular material was used to vary the finger stiffness.

It has been shown that the fingers can be controlled using a PID controller, and can respond to a step position change, track a sinusoidal input at different frequencies and grasp objects. It has also been shown that the same controller can continue to position the fingers even when the stiffness of the fingers is varied.

Four-fingered variable stiffness pneumatic soft robot end effectors were also developed during this research. In this design, the number of contractor muscle actuators per finger is reduced to two, instead of three in the previous design. A modified tendon cable arrangement was used in this end effector to enhance the bending direction of the finger. This was to reduce the complicity in constructing and controlling the end effector. Two, four or eight pneumatic valve channels can be used to actuate this end effector. Hence, three control options are available. Either the end effector achieves object grasping by controlling all the fingers together (to open or close) simultaneously using two valve channels, or alternatively each oppositely located pair of fingers can be controlled together, with this latter option requiring four pneumatic valve channels. Otherwise, two pneumatic valve channels for each of the four fingers – and hence eight pneumatic valve channels – would be required for this design. The number of PID controllers used would depend on the number of pneumatic valve channels in each configuration.

Position control and force control strategies were used to evaluate the performance of the proposed end effector. Experimental results show the suitability of both type of controllers and the functionality of the proposed pneumatic four-fingered soft robot end effector.

Another simplified four-fingered variable stiffness soft robot end effector was developed in this work. There are two main differences in the design and construction of this end effector compared to the previous one. Firstly, four contractor muscle actuators were used to control the bending of fingers compared to eight in the previous design. Each pair of two contractor muscles either opened or closed the gripper. This would nominally reduce the cost of construction and make the design far simpler. A force control scheme was used to control the operation of the proposed simplified end effector. Experimental results show the capability of the simplified end effector to grip a range of different shapes and sized objects. Secondly, this end effector was part of a variable stiffness soft robot manipulator that consisted of a pneumatic continuum arm and the end effector. The continuum soft robot arm consisted of three contractor pneumatic muscle actuators fitted around one central extensor pneumatic muscle actuator, and was secured together using cable ties. This arm has the ability to change stiffness during operation without affecting the end effector position by increasing the pressure in all the pneumatic muscle actuators simultaneously. Four pressure sensors

were used to give an indication to the amount of pressure in either of the pneumatic muscle actuators which are used in the construction of the continuum arm. This gives the ability to test the suitability of the pressure control scheme, as well. The experimental result shows that the use of a pressure control scheme to control the bending of the continuum arm was successful.

The developed soft manipulator has the ability to grasp a given object and move it to another location. A pressure control scheme was used to control the operation of the continuum arm and a force control scheme was used for the end effector. Hence, both pressure and force control schemes were used simultaneously to control the operation of the variable stiffness continuum soft robot manipulator.

6.2 Contributions of the Work

During this research project, a number of pneumatic and granular jamming variable stiffness soft robot end effector designs were developed. The performance of the proposed end effectors was investigated in a practical sense. The overall research contributions of this research project can be illustrated as follows:

1. The development of soft robotic systems which uniquely combine both extensor and contractor pneumatic muscles to create variable stiffness soft robots.
2. Experimental development of a mathematical model for both the contractor and the extensor pneumatic muscle actuators. The developed mathematical model was verified by its use in predicting the pressure/displacement characteristics of the pneumatic muscle actuators and comparing the predicted results directly to the experimental results.
3. Analysis of the variable stiffness capabilities of both an antagonistic pneumatic muscle actuator design and a granular jamming design. It was found that the percentage increase in the stiffness of the pneumatic muscle actuators could be raised by up to 163%. On the other hand, the percentage increase in stiffness in the granular jamming continuum finger was 235%.
4. Development of a fully compliant continuum, variable stiffness, soft robot end effector using only pneumatic muscle actuators. The performance of the developed end effector has been investigated practically. In addition, the

developed end effector was found to have characteristics which may make it suited to interacting safely with humans.

5. Development of an enhanced continuum variable stiffness soft robot end effector by increasing the number of fingers whilst reducing the number of the contractor muscle actuators required to control the bending of the fingers. In the new enhanced design, the number of pneumatic channels and the controller is less than that in the previous design.
6. Development of a granular jamming variable stiffness soft robot end effector based on continuum manipulation. This end effector is representative of another method of constructing variable stiffness soft robot end effectors, and has the ability to interact safely with humans. Experimental results show that it has the capability to easily increase its stiffness during operation from a liquid-like (mobile state) to a solid-like state.
7. Development of a pneumatic continuum robot manipulator and its variable stiffness end effector using only soft materials. Both are actuated by contractor and the extensor pneumatic muscle actuators only. The experimental results show that it has the capability to grasp an object and move it to a new position with ease.
8. Positional, force and pressure control schemes are developed during this research to control the performance of the developed continuum soft robot manipulator and variable stiffness end effectors.

6.3 Limitations and suggestions for future work

During this work, all the planned aims and research objectives were successfully accomplished. However, there were a number of limitations and possibilities for future work in the proposed design. In addition, there is the possibility to enhance the performance of the developed end effectors. Some of these limitations, and a suggestion for future work, are illustrated below, and can perhaps solve the current design limitations.

i. Increase the reliability of the pneumatic muscle actuators by using more reliable materials in the construction of these actuators. This may include trying another

construction scheme instead of the McKibben muscle configuration. During the development of this work, only a single puncture occurred in one of the test muscles, however, in order to be of practical use, the material used to implement the soft robot needs to be more reliable.

ii. The PID controller is widely accepted as not being the best technique to control soft robots, which are likely to be highly nonlinear in their operational characteristics. Whilst the experimental results have shown that the fingers can be controlled, the accuracy is likely to be greatly improved if other control techniques are used, and this could well form a significant part of the future direction of the research.

iii. Using an adaptive control scheme to control the performance of the pneumatic continuum soft robot arm and its end effectors will increase the overall reliability of the system. An adaptive controller would reduce the effect of any external disturbances that might occur during the operation of the proposed soft robot end effectors. In addition, an adaptive controller would deal better with the nonlinearity of these soft robot systems.

iv. One of the adaptive control schemes that can be used in the proposed pneumatic variable stiffness soft robot arm and its end effectors is that of Neuro-Fuzzy techniques to tune the parameters of the PID controller. This will modify the performance of the PID controller to be able to deal with the nonlinearity of the systems.

v. A five-fingered soft robotics hand could be designed that can imitate the operation of the human hand. The suggested soft robotics hand could be constructed using the same soft, low cost and safe materials investigated in the course of this research. This five-fingered soft hand may be used directly by disabled people, for instance.

Bibliography

Ahn, K., & Thanh, T. (2005). Nonlinear PID control to improve the control performance of the pneumatic artificial muscle manipulator using neural network. *Journal of mechanical science and technology*, *19*(1), 106-115.

Ali, M., Kyriakopoulos, K., & Stephanou, H. (1993). The kinematics of the Anthrobot-2 dextrous hand. In *Robotics and Automation, 1993. Proceedings. 1993 IEEE International Conference on* (pp. 705-710). IEEE.

Amend, J., Brown, E., Rodenberg, N., Jaeger, H., & Lipson, H. (2012). A positive pressure universal gripper based on the jamming of granular material. *IEEE Transactions on Robotics*, *28*(2), 341-350.

Andrikopoulos, G., Nikolakopoulos, G., Arvanitakis, I., & Manesis, S. (2014). Piecewise affine modeling and constrained optimal control for a pneumatic artificial muscle. *IEEE Transactions on Industrial Electronics*, *61*(2), 904-916.

Aschemann, H., & Schindele, D. (2008). Sliding-mode control of a high-speed linear axis driven by pneumatic muscle actuators. *IEEE Transactions on Industrial Electronics*, *55*(11), 3855-3864.

Bainbridge, W., Hart, J., Kim, E., & Scassellati, B. (2008). The effect of presence on human-robot interaction. In *Robot and Human Interactive Communication, 2008. RO-MAN 2008. The 17th IEEE International Symposium on* (pp. 701-706). IEEE.

Balasubramanian, K., & Rattan, K., (2003). Fuzzy logic control of a pneumatic muscle system using a linearing control scheme. In *Fuzzy Information Processing Society, 2003. NAFIPS 2003. 22nd International Conference of the North American* (pp. 432-436). IEEE.

Bartow, A., Kapadia, A., & Walker, I. (2013). A novel continuum trunk robot based on contractor muscles. In *Proceedings of the 12th WSEAS International Conference on Signal Processing, Robotics, and Automation* (pp. 181-186).

Bicchi, A. (2000). Hands for dexterous manipulation and robust grasping: A difficult road toward simplicity. *IEEE Transactions on robotics and automation*, *16*(6), 652-662.

Bicchi, A., & Tonietti, G. (2004). Fast and" soft-arm" tactics [robot arm design]. *IEEE Robotics & Automation Magazine*, *11*(2), 22-33.

Brooks, R., & Stein, L. (1994). Building brains for bodies. *Autonomous Robots*, *1*(1), 7-25.

Brown, E., Rodenberg, N., Amend, J., Mozeika, A., Steltz, E., Zakin, M. & Jaeger, H. (2010). Universal robotic gripper based on the jamming of granular material. *Proceedings of the National Academy of Sciences*,*107*(44), 18809-18814.

Bruce, J., & Davies, C. (1991). Elephant trunks: an unforgettable alternative to rigid mechanisms. *Industrial Robot: An International Journal*, *18*(4), 29-30.

Byrvan, H., Sugar, T., Vanderborght, B., Hollander, K., & Lefeber, D. (2009). Review of Actuators with Passive Adjustable Compliance/Controllable Stiffness for Robotic Applications. *IEEE Robotics & Automation*, 81-94.

Caldwell, D., Medrano-Cerda, G., & Goodwin, M. (1993). Braided pneumatic actuator control of a multi-jointed manipulator. In*Systems, Man and Cybernetics, 1993.'Systems Engineering in the Service of Humans', Conference Proceedings., International Conference on* (Vol. 1, pp. 423-428). IEEE.

Chan, S., Lilly, J., Repperger, D., & Berlin, J. (2003). Fuzzy PD+ I learning control for a pneumatic muscle. In *Fuzzy Systems, 2003. FUZZ'03. The 12th IEEE International Conference on* (Vol. 1, pp. 278-283). IEEE.

Chang, X., & Lilly, J. (2003). Fuzzy control for pneumatic muscle tracking via evolutionary tuning. *Intelligent Automation & Soft Computing*, *9*(4), 227-244.

Cheng, N., Lobovsky, M., Keating, S., Setapen, A., Gero, K., Hosoi, A., & Iagnemma, K. (2012). Design and analysis of a robust, low-cost, highly articulated manipulator enabled by jamming of granular media. In *Robotics and Automation (ICRA), 2012 IEEE International Conference on* (pp. 4328-4333). IEEE.

Choi, T., & Lee, J. (2010). Control of manipulator using pneumatic muscles for enhanced safety. *IEEE Transactions on Industrial Electronics*,*57*(8), 2815-2825.

Chou, C., & Hannaford, B. (1996). Measurement and modelling of McKibben pneumatic artificial muscles. *IEEE Transactions on robotics and automation*, *12*(1), 90-102.

Daerden, F., & Lefeber, D. (2002). Pneumatic artificial muscles: actuators for robotics and automation. *European journal of mechanical and environmental engineering*, *47*(1), 11-21.

Davies, M. (1990). An alternative robotic proboscis. In *Traditional and non-traditional robotic sensors* (pp. 49-55). Springer Berlin Heidelberg.

Davies, J. (1994). Dextrous manipulator for complex objects. In *Proceedings Fifth World Conference on Robotics Research* (pp. 17-28).

Davies, J., Lane, D., Robinson, G., O'Brien, D., Pickett, M., Sfakiotakis, M., & Deacon, B., (1998). Subsea applications of continuum robots. In *Underwater Technology, 1998. Proceedings of the 1998 International Symposium on* (pp. 363-369). IEEE.

Davis, S., & Caldwell, D. (2006). Braid effects on contractile range and friction modeling in pneumatic muscle actuators. *The International Journal of Robotics Research*, *25*(4), 359-369.

Davis, S., & Caldwell, D. (2006). Pneumatic muscle actuators for humanoid applications-sensor and valve integration. In *Humanoid Robots, 2006 6th IEEE-RAS International Conference on* (pp. 456-461). IEEE.

Davis, S., & Caldwell, D. (2012). Biologically inspired damage tolerance in braided pneumatic muscle actuators. *Journal of intelligent material systems and structures*, *23*(3), 313-325.

Davis, S., Tsagarakis, N., Canderle, J., & Caldwell, D., (2003). Enhanced modelling and performance in braided pneumatic muscle actuators. *The International Journal of Robotics Research*, *22*(3-4), 213-227.

Diftler, M., Mehling, J., Abdallah, M., Radford, N., Bridgwater, L., Sanders, A. & Hargrave, B. (2011). Robonaut 2-the first humanoid robot in space. In *Robotics and Automation (ICRA), 2011 IEEE International Conference on* (pp. 2178-2183). IEEE.

Galloway, K., Becker, K., Phillips, B., Kirby, J., Licht, S., Tchernov, D., & Gruber, D. (2016). Soft robotic grippers for biological sampling on deep reefs. *Soft Robotics*, *3*(1), 23-33.

Gao, Z., Wei, G., & Dai, J. (2015). Inverse kinematics and workspace analysis of the metamorphic hand. *Proceedings of the Institution of Mechanical Engineers, Part C: Journal of Mechanical Engineering Science*, *229*(5), 965-975.

Giannaccini, M., Georgilas, I., Horsfield, I., Peiris, B., Lenz, A., Pipe, A., & Dogramadzi, S. (2014). A variable compliance, soft gripper. *Autonomous Robots*, *36*(1-2), 93-107.

Giri, N., & Walker, I. (2011). Continuum robots and underactuated grasping. *Mechanical Sciences*, *2*(1), 51-58.

Godage, I., Branson, D., Guglielmino, E., Medrano-Cerda, G., & Caldwell, D. (2011). Shape function-based kinematics and dynamics for variable length continuum robotic arms. In *Robotics and Automation (ICRA), 2011 IEEE International Conference on* (pp. 452-457). IEEE.

Godage, I., Branson, D., Guglielmino, E., & Caldwell, D. (2012). Pneumatic muscle actuated continuum arms: Modelling and experimental assessment. In *Robotics and Automation (ICRA), 2012 IEEE International Conference on* (pp. 4980-4985). IEEE.

Grebenstein, M., Albu-Schäffer, A., Bahls, T., Chalon, M., Eiberger, O., Friedl, W., & Höppner, H. (2011). The DLR hand arm system. In *Robotics and Automation (ICRA), 2011 IEEE International Conference on* (pp. 3175-3182). IEEE.

Haddadin, S., Albu-Schäffer, A., & Hirzinger, G. (2009). Requirements for safe robots: Measurements, analysis and new insights. The International Journal of Robotics Research, 28(11-12), 1507-1527.

Hannaford, B., & Winters, J. (1990). Actuator properties and movement control: biological and technological models. In *Multiple muscle systems* (pp. 101-120). Springer New York.

Hemami, A. (1984). Design of light weight flexible robot arm. In *Robots* (Vol. 8, pp. 1623-1640).

Hesselroth, T., Sarkar, K., Van Der Smagt, P., & Schulten, K. (1994). Neural network control of a pneumatic robot arm. *IEEE Transactions on Systems, Man, and Cybernetics*, *24*(1), 28-38.

Homberg, B., Katzschmann, R., Dogar, M., & Rus, D. (2015). Haptic identification of objects using a modular soft robotic gripper. In *Intelligent Robots and Systems (IROS), 2015 IEEE/RSJ International Conference on* (pp. 1698-1705). IEEE.

Huber, M., Rickert, M., Knoll, A., Brandt, T., & Glasauer, S. (2008). Human-robot interaction in handing-over tasks. In *Robot and Human Interactive Communication, 2008. RO-MAN 2008. The 17th IEEE International Symposium on* (pp. 107-112). IEEE.

Hurst, J., & Rizzi, A. (2008). Series compliance for an efficient running gait. *IEEE Robotics & Automation Magazine*, *15*(3).

Immega, G., & Antonelli, K. (1995). The KSI tentacle manipulator. In *Robotics and Automation, 1995. Proceedings., 1995 IEEE International Conference on* (Vol. 3, pp. 3149-3154). IEEE.

Jacobsen, S., Wood, J., Knutti, D., & Biggers, K. (1984). The UTAH/MIT dextrous hand: Work in progress. *The International Journal of Robotics Research*, *3*(4), 21-50.

Jafari, A., Tsagarakis, N., Vanderborght, B., & Caldwell, D. (2010). AwAS: a novel actuator with adjustable stiffness. In *is in the Proceeding of IEEE/RSJ International Conference on Intelligent Robots and Systems (IROS)* (pp. 4201-4206).

Jafari, A., Tsagarakis, N., & Caldwell, D. (2011). AwAS-II: A new actuator with adjustable stiffness based on the novel principle of adaptable pivot point and variable lever ratio. In *Robotics and Automation (ICRA), 2011 IEEE International Conference on* (pp. 4638-4643). IEEE.

Jafari, A., Tsagarakis, N., & Caldwell, D. (2013). A novel intrinsically energy efficient actuator with adjustable stiffness (AwAS). *IEEE/ASME Transactions on Mechatronics*, *18*(1), 355-365.

Jiang, A., Ataollahi, A., Althoefer, K., Dasgupta, P., & Nanayakkara, T. (2012). A variable stiffness joint by granular jamming. In *ASME 2012 international design engineering technical conferences and computers and information in engineering conference* (pp. 267-275). American Society of Mechanical Engineers.

Jiang, Y., Amend, J., Lipson, H., & Saxena, A. (2012). Learning hardware agnostic grasps for a universal jamming gripper. In *Robotics and Automation (ICRA), 2012 IEEE International Conference on* (pp. 2385-2391). IEEE.

Jones, B., & Walker, I. (2006). Kinematics for multisection continuum robots. *IEEE Transactions on Robotics*, *22*(1), 43-55.

Katzschmann, R., Marchese, A., & Rus, D. (2015). Autonomous object manipulation using a soft planar grasping manipulator. *Soft Robotics*, *2*(4), 155-164.

Kim, S., Laschi, C., & Trimmer, B. (2013). Soft robotics: a bioinspired evolution in robotics. *Trends in biotechnology*, *31*(5), 287-294.

Kong, K., Bae, J., & Tomizuka, M. (2012). A compact rotary series elastic actuator for human assistive systems. *IEEE/ASME transactions on mechatronics*, *17*(2), 288-297.

Kornbluh, R., Pelrine, R., Eckerle, J., & Joseph, J. (1998). Electrostrictive polymer artificial muscle actuators. In *Robotics and Automation, 1998. Proceedings. 1998 IEEE International Conference on* (Vol. 3, pp. 2147-2154). IEEE.

Lane, D., Sneddon, J., O'Brien, D., Davies, J., & Robinson, G. (1994). Aspects of the design and development of a subsea dextrous grasping system. In *OCEANS'94.'Oceans Engineering for Today's Technology and Tomorrow's Preservation.'Proceedings* (Vol. 2, pp. II-174). IEEE.

Laschi, C., Cianchetti, M., Mazzolai, B., Margheri, L., Follador, M., & Dario, P. (2012). Soft robot arm inspired by the octopus. *Advanced Robotics*, *26*(7), 709-727.

Lilly, J. (2003). Adaptive tracking for pneumatic muscle actuators in bicep and tricep configurations. *IEEE Transactions on Neural systems and rehabilitation engineering*, *11*(3), 333-339.

Lim, G., Minami, K., Yamamoto, K., Sugihara, M., Uchiyama, M., & Esashi, M. (1996). Multi-link active catheter snake-like motion. *Robotica*, *14*(05), 499-506.

Lin, H., Leisk, G., & Trimmer, B. (2011). GoQBot: a caterpillar-inspired soft-bodied rolling robot. *Bioinspiration & biomimetics*, *6*(2), 026007.

Lipson, H. (2014). Challenges and opportunities for design, simulation, and fabrication of soft robots. *Soft Robotics*, *1*(1), 21-27.

Lock, J., Laing, G., Mahvash, M., & Dupont, P. E. (2010). Quasistatic modelling of concentric tube robots with external loads. In Intelligent Robots and Systems (IROS), 2010 IEEE/RSJ International Conference on (pp. 2325-2332). IEEE.

Ma, S., Hirose, S., & Yoshinada, H. (1994). Development of a hyper-redundant multijoint manipulator for maintenance of nuclear reactors. *Advanced robotics*, *9*(3), 281-300.

Ma, S., Watanabe, M., & Kondo, H. (2001). Dynamic control of curve-constrained hyper-redundant manipulators. In *Computational Intelligence in Robotics and Automation, 2001. Proceedings 2001 IEEE International Symposium on* (pp. 83-88). IEEE.

Maghooa, F., Stilli, A., Noh, Y., Althoefer, K., & Wurdemann, H. A. (2015). Tendon and pressure actuation for a bio-inspired manipulator based on an antagonistic principle. In *Robotics and Automation (ICRA), 2015 IEEE International Conference on* (pp. 2556-2561). IEEE.

Mahvash, M., & Dupont, P. (2010). Stiffness control of a continuum manipulator in contact with a soft environment. In Intelligent Robots and Systems (IROS), 2010 IEEE/RSJ International Conference on (pp. 863-870). IEEE.

Majidi, C. (2014). Soft robotics: a perspective—current trends and prospects for the future. *Soft Robotics*, *1*(1), 5-11.

Manti, M., Hassan, T., Passetti, G., D'Elia, N., Laschi, C., & Cianchetti, M. (2015). A bioinspired soft robotic gripper for adaptable and effective grasping. *Soft Robotics*, *2*(3), 107-116.

McMahan, W., Chitrakaran, V., Csencsits, M., Dawson, D., Walker, I., Jones, B., & Rahn, C. (2006). Field trials and testing of the OctArm continuum manipulator. In *Robotics and Automation, 2006. ICRA 2006. Proceedings 2006 IEEE International Conference on* (pp. 2336-2341). IEEE.

McMahan, W., Jones, B., & Walker, I. (2005). Design and implementation of a multi-section continuum robot: Air-Octor. In *Intelligent Robots and Systems, 2005.(IROS 2005). 2005 IEEE/RSJ International Conference on* (pp. 2578-2585). IEEE.

Medrano-Cerda, G., Bowler, C., & Caldwell, D. (1995). Adaptive position control of antagonistic pneumatic muscle actuators. In *Intelligent Robots and Systems 95.'Human Robot Interaction and Cooperative Robots', Proceedings. 1995 IEEE/RSJ International Conference on* (Vol. 1, pp. 378-383). IEEE.

Minh, T., Tjahjowidodo, T., Ramon, H., & Van Brussel, H. (2009). Non-local memory hysteresis in a pneumatic artificial muscle (PAM). In *Control and Automation, 2009. MED'09. 17th Mediterranean Conference on* (pp. 640-645). IEEE.

Mosadegh, B., Polygerinos, P., Keplinger, C., Wennstedt, S., Shepherd, R. F., Gupta, U., & Whitesides, G. (2014). Pneumatic networks for soft robotics that actuate rapidly. *Advanced Functional Materials*, *24*(15), 2163-2170.

Nemir, D. (1989). Preliminary results on the design of a robotic tentacle end effector. In *American Control Conference, 1989* (pp. 2374-2376). IEEE.

Neppalli, S., & Jones, B. (2007). Design, construction, and analysis of a continuum robot. In *Intelligent Robots and Systems, 2007. IROS 2007. IEEE/RSJ International Conference on* (pp. 1503-1507). IEEE.

Niiyama, R., Sun, X., Sung, C., An, B., Rus, D., & Kim, S. (2015). Pouch motors: Printable soft actuators integrated with computational design. *Soft Robotics*, *2*(2), 59-70.

Pfeifer, R., Marques, H., & Iida, F. (2013). Soft robotics: the next generation of intelligent machines. In *Proceedings of the Twenty-Third international joint conference on Artificial Intelligence* (pp. 5-11). AAAI Press.

Pratt, G., & Williamson, M. (1995). Series elastic actuators. *In Intelligent Robots and Systems 95.'Human Robot Interaction and Cooperative Robots', Proceedings. 1995 IEEE/RSJ International Conference on* (Vol. 1, pp. 399-406). IEEE.

Rateni, G., Cianchetti, M., Ciuti, G., Menciassi, A., & Laschi, C. (2015). Design and development of a soft robotic gripper for manipulation in minimally invasive surgery: a proof of concept. *Meccanica*, *50*(11), 2855-2863.

Repperger, D., Johnson, K., & Phillips, C. (1998). A VSC position tracking system involving a large scale pneumatic muscle actuator. In *Decision and Control, 1998. Proceedings of the 37th IEEE Conference on* (Vol. 4, pp. 4302-4307). IEEE.

Repperger, D., Phillips, C., & Krier, M. (1999). Controller design involving gain scheduling for a large scale pneumatic muscle actuator. In *Control Applications, 1999. Proceedings of the 1999 IEEE International Conference on* (Vol. 1, pp. 285-290). IEEE.

Reynolds, D., Repperger, D., Phillips, C., & Bandry, G. (2003). Modeling the dynamic characteristics of pneumatic muscle. *Annals of biomedical engineering*, *31*(3), 310-317.

Robinson, D., & Pratt, G. (2000). Force controllable hydro-elastic actuator. In *Robotics and Automation, 2000. Proceedings. ICRA'00. IEEE International Conference on* (Vol. 2, pp. 1321-1327). IEEE.

Robinson, D., Pratt, J., Paluska, D., & Pratt, G. (1999). Series elastic actuator development for a biomimetic walking robot. In *Advanced Intelligent Mechatronics, 1999. Proceedings. 1999 IEEE/ASME International Conference on* (pp. 561-568). IEEE.

Robinson, G., & Davies, J. (1998). The parallel bellows actuator. *Proc. Robotica*, *98*, 195-200.

Robinson, G., & Davies, J. (1999). Continuum robots-a state of the art. In *Robotics and Automation, 1999. Proceedings. 1999 IEEE International Conference on* (Vol. 4, pp. 2849-2854). IEEE.

Robinson, G., Davies, J., & Jones, J. (1998). Development of the Amadeus dextrous robot end-effectors. In *OCEANS'98 Conference Proceedings* (Vol. 2, pp. 703-707). IEEE.

Schiavi, R., Grioli, G., Sen, S., & Bicchi, A. (2008). VSA-II: A novel prototype of variable stiffness actuator for safe and performing robots interacting with humans. In *Robotics and Automation, 2008. ICRA 2008. IEEE International Conference on* (pp. 2171-2176). IEEE.

Schulte, H. (1962). The characteristic of the McKibben artificial muscle. The application of external power in prosthetics and orthotics, 94-115.

Seok, S., Onal, C., Wood, R., Rus, D., & Kim, S. (2010). Peristaltic locomotion with antagonistic actuators in soft robotics. In *Robotics and Automation (ICRA), 2010 IEEE International Conference on* (pp. 1228-1233). IEEE.

Sergi, F., Accoto, D., Carpino, G., Tagliamonte, N., & Guglielmelli, E. (2012). Design and characterization of a compact rotary series elastic actuator for knee assistance during overground walking. In *Biomedical Robotics and Biomechatronics (BioRob), 2012 4th IEEE RAS & EMBS International Conference on* (pp. 1931-1936). IEEE.

Shadow Robot Company LTD (2015). *Shadow Dexterous Hand*. Retrieved from https://www.shadowrobot.com/products/dexterous-hand/

Shin, D., Sardellitti, I., & Khatib, O. (2008). A hybrid actuation approach for human-friendly robot design. In *Robotics and Automation, 2008. ICRA 2008. IEEE International Conference on* (pp. 1747-1752). IEEE.

Shintake, J., Rosset, S., Schubert, B., Floreano, D., & Shea, H. (2016). Versatile soft grippers with intrinsic electroadhesion based on multifunctional polymer actuators. *Advanced Materials*, *28*(2), 231-238.

Stilli, A., Wurdemann, H., & Althoefer, K. (2014). Shrinkable, stiffness-controllable soft manipulator based on a bio-inspired antagonistic actuation principle. In *Intelligent Robots and Systems (IROS 2014), 2014 IEEE/RSJ International Conference on* (pp. 2476-2481). IEEE.

Su, H., Cardona, D., Shang, W., Camilo, A., Cole, G., Rucker, D., & Fischer, G. (2012). A MRI-guided concentric tube continuum robot with piezoelectric actuation: a

feasibility study. In Robotics and Automation (ICRA), 2012 IEEE International Conference on (pp. 1939-1945). IEEE.

Sugar, T. (2002). A novel selective compliant actuator. *Mechatronics*, *12*(9), 1157-1171.

Suzuki, M., Shiller, D., Gribble, P., & Ostry, D. (2001). Relationship between cocontraction, movement kinematics and phasic muscle activity in single-joint arm movement. *Experimental Brain Research*, *140*(2), 171-181.

Suzumori, K., Iikura, S., & Tanaka, H. (1991). Development of flexible microactuator and its applications to robotic mechanisms. In *Robotics and Automation, 1991. Proceedings., 1991 IEEE International Conference on* (pp. 1622-1627). IEEE.

Tatlicioglu, E., Walker, I., & Dawson, D. (2007). New dynamic models for planar extensible continuum robot manipulators. In *Intelligent Robots and Systems, 2007. IROS 2007. IEEE/RSJ International Conference on* (pp. 1485-1490). IEEE.

Tavakoli, M., & De Almeida, A. (2014). Adaptive under-actuated anthropomorphic hand: Isr-softhand. In *Intelligent Robots and Systems (IROS 2014), 2014 IEEE/RSJ International Conference on* (pp. 1629-1634). IEEE.

Tavakoli, M., Marques, L., & de Almeida, A. (2013). Flexirigid, a novel two phase flexible gripper. In *Intelligent Robots and Systems (IROS), 2013 IEEE/RSJ International Conference on* (pp. 5046-5051). IEEE.

Tondu, B., & Lopez, P. (2000). Modeling and control of McKibben artificial muscle robot actuators. *IEEE control systems*, *20*(2), 15-38.

Tonietti, G., Schiavi, R., & Bicchi, A. (2005). Design and control of a variable stiffness actuator for safe and fast physical human/robot interaction. In *Robotics and Automation, 2005. ICRA 2005. Proceedings of the 2005 IEEE International Conference on* (pp. 526-531). IEEE.

Trivedi, D., Rahn, C., Kier, W., & Walker, I. (2008). Soft robotics: Biological inspiration, state of the art, and future research. *Applied Bionics and Biomechanics*, *5*(3), 99-117.

Tsagarakis, N., & Caldwell, D. (2000). Improved modelling and assessment of pneumatic muscle actuators. In *Robotics and Automation, 2000. Proceedings. ICRA'00. IEEE International Conference on* (Vol. 4, pp. 3641-3646). IEEE.

Tsagarakis, N., Laffranchi, M., Vanderborght, B., & Caldwell, D. (2009). A compact soft actuator unit for small scale human friendly robots. In *Robotics and Automation, 2009. ICRA'09. IEEE International Conference on* (pp. 4356-4362). IEEE.

Valenzuela-Coloma, H., Lau-Cortes, Y., Fuentes-Romero, R., Zagal, J., & Mendoza-Garcia, R. (2015). Mentaca: An universal jamming gripper on wheels. In

Electrical, Electronics Engineering, Information and Communication Technologies (CHILECON), 2015 CHILEAN Conference on (pp. 817-823). IEEE.

Van Damme, M., Vanderborght, B., Van Ham, R., Verrelst, B., Daerden, F., & Lefeber, D. (2007). Proxy-based sliding mode control of a manipulator actuated by pleated pneumatic artificial muscles. In *Robotics and Automation, 2007 IEEE International Conference on* (pp. 4355-4360). IEEE.

Van Ham, R., Vanderborght, B., Van Damme, M., Verrelst, B., & Lefeber, D. (2007). MACCEPA, the mechanically adjustable compliance and controllable equilibrium position actuator: Design and implementation in a biped robot. *Robotics and Autonomous Systems*, *55*(10), 761-768.

Van Derborght, B., Tsagarakis, N., Semini, C., Van Ham, R., & Caldwell, D. (2009). MACCEPA 2.0: Adjustable compliant actuator with stiffening characteristic for energy efficient hopping. In *Robotics and Automation, 2009. ICRA'09. IEEE International Conference on* (pp. 544-549). IEEE.

Wakimoto, S., Ogura, K., Suzumori, K., & Nishioka, Y. (2009). Miniature soft hand with curling rubber pneumatic actuators. In *Robotics and Automation, 2009. ICRA'09. IEEE International Conference on* (pp. 556-561). IEEE.

Wall, V., Deimel, R., & Brock, O. (2015). Selective stiffening of soft actuators based on jamming. In Robotics and Automation (ICRA), 2015 IEEE International Conference on (pp. 252-257). IEEE.

Webster III, R., & Jones, B. (2010). Design and kinematic modeling of constant curvature continuum robots: A review. The International Journal of Robotics Research, 29(13), 1661-1683.

Zheng, T., Godage, I., Branson, D., Kang, R., Guglielmino, E., Medrano-Cerda, G., & Caldwell, D. (2013). Octopus inspired walking robot: Design, control and experimental validation. In *Robotics and Automation (ICRA), 2013 IEEE International Conference on* (pp. 816-821). IEEE.

Ziegler, J., & Nichols, N. (1942). Optimum settings for automatic controllers. *trans. ASME*, *64*(11).